The Skeletal Environment Mediates *Staphylococcus aureus* Virulence Responses and Metabolic Processes *in Vivo*

By

Aimee Potter

Dissertation

submitted to the Faculty of the

Graduate School of Vanderbilt University

in partial fulfillment of the requirements

for the degree of

DOCTOR OF PHILOSOPHY

in

Microbiology and Immunology

September 30, 2019

Nashville, Tennessee

Committee:

Maria Hadjifrangiskou, Ph.D.

Eric Skaar, Ph.D., M.P.H.

Timothy Cover, M.D.

Scott Guelcher, Ph.D.

James Cassat, M.D., Ph.D.

ACKNOWLEDGEMENTS

To Vanderbilt, VI4, and the microbiology and immunology department: Thank you for giving me the opportunity to become a scientist at this amazing institution. I have been given more opportunities than I could have ever hoped for.

To Jim Cassat: Thank you for allowing me the privilege of being one of your first graduate students. I knew, from the first time I saw you present to the IGP students, that you were a scientist worth working with. Thank you for teaching me everything I know about experimental design, scientific writing, and mentoring. I am incredibly grateful for your insight – it has been a privilege.

To my lab-mates: Thank you for joining me on this journey. To Niki – for being the fellow first student. To Caleb –for being almost as invested in my project as I am. To Chris – for joining the lab even after rotating with me. To Jenna – for your humor. To Casey – for taking over as bacteriology guru. And to Jacob, Laura, and Andrew – for helping me do *literally* everything.

To my committee: Thank you for your advice over the past five years – I am a better scientist because of your mentorship. Dr. Eric Skaar – you have served as a pseudo-mentor to me since my very first interview. Despite having no obligation to me, you have always been willing to meet for coffee and advice- thank you. Particular thanks to Dr. Maria Hadjifrangiskou, my chair – you have taught me what it means to be an amazing female scientist. Thank you for being on my team.

To my undergraduate mentors: I would never have entered microbiology without the inspiration, support, and guidance of Dr. Lorie Cramer and Dr. Anthony Richardson. Thank you for showing me my passion.

To Drs. Neal Hammer and Nicholas Vitko: Thank you for being the first people to make me feel like I was someone worth listening to. Your encouragement of students has not gone unnoticed.

To my friends, the family we choose: Destiny, Nicki, Kyla, Ashley, Sam, Nick, and Joey – there has never been a better support team. Even though we are separated by state, I know you are only a phone call (or letter) away. I love you all.

To Sam Potter, my husband and my hero: You have supported my ambitions and taught me the meaning of loyalty. Across ten years and multiple states, you have stood by my side – even when work kept us apart. Thank you for serving as an example of dedication, work-ethic, responsibility, and accountability – I am a better person because of you.

To Tonya and Scott Wilde, my parents and biggest supporters: you encouraged my love of science and were brave enough to let ten-year-old me blood type you with my forensic science kit. You have soothed every frustration and celebrated every triumph. Thank you – for everything.

TABLE OF CONTENTS

LIST OF FIGURES

Figure **Page**

Portions of this dissertation were originally published in *PLoS Pathogens* (December 2015).

Wilde AD, Snyder DJ, Putnam NE, Valentino MD, Hammer ND, Lonergan ZR, et al. (2015) Bacterial Hypoxic Responses Revealed as Critical Determinants of the Host-Pathogen Outcome by TnSeq Analysis of *Staphylococcus aureus* Invasive Infection. *PLoS Pathog* 11(12): e1005341.

doi: 10.1371/journal.ppat.100534

CHAPTER I: BACKGROUND AND LITERATURE REVIEW

Introduction

Staphylococcus aureus is a prominent human pathogen that causes life-threatening, invasive disease and is a significant healthcare burden in the United States and globally. The prominence of *S. aureus* as a public health concern reflects the pathogen's prevalence in the general population and widespread antimicrobial resistance (1). The success of *S. aureus* demonstrates its ability to replicate and survive within a variety of host environments. *S. aureus* is capable of proliferation in nearly every human tissue, including the heart, lungs, kidneys, liver, and bone. Yet *S. aureus* also innocuously colonizes the skin and nares of one-third to one-half of the population (1). These facts suggest a remarkable flexibility in terms of metabolic and virulence programs, allowing staphylococci to adapt to diverse and changing host environments during invasive infection, while also enabling a commensal lifestyle characterized by low virulence and immunotolerance.

Infection of bone, or osteomyelitis, is one of the most common sequelae following invasive staphylococcal infection, and *S. aureus* is responsible for over 80% of all cases of osteomyelitis (2). Osteomyelitis arises as a consequence of hematogenous dissemination following bacteremia, secondarily to soft-tissue infection, following trauma, or contamination of surgical sites (3). Treatment of osteomyelitis requires extensive antibiotic therapy for several weeks to months, and despite appropriate medical maintenance, many patients fail therapy and require surgical debridement to remove infected and necrotic bone. The incidence of osteomyelitis has increased concomitantly with increased incidence of invasive staphylococcal infection due to the prevalence of community-acquired methicillin resistant *S. aureus* (MRSA) (4-7). An understanding of the factors that influence successful *S. aureus* colonization of bone is therefore

essential for designing the next generation of anti-staphylococcal therapeutics, particularly in the notoriously recalcitrant infectious setting of osteomyelitis.

Based on this foundational knowledge, this thesis examines the central hypothesis that *S. aureus* has distinct genetic and metabolic programs that facilitate survival during osteomyelitis. Chapter I discusses the necessary background to understand staphylococcal pathogenesis, the skeletal environment, and the metabolic pathways available for acquisition of nutrients during infection. Chapter II evaluates the broad genetic requirements for staphylococcal survival during osteomyelitis using an unbiased, high-throughput sequencing technique. Chapter II also characterizes the availability of a critical environmental factor, oxygen, as well as staphylococcal regulation in response to oxygen availability. Chapter III features an in-depth evaluation of the central metabolic pathways required for staphylococcal survival *in vivo* and characterizes the nutrient milieu of bone. Lastly, Chapter IV describes the significance of our results in the context of staphylococcal biology and details future directions and outstanding questions in the field of *S. aureus* metabolism and regulation during infection.

Osteomyelitis is a paradigm for invasive *S. aureus* infection

As one of the most common manifestations of invasive infection following *S. aureus* bacteremia, osteomyelitis is an excellent paradigm for invasive staphylococcal disease (4). Skeletal infections further cause significant morbidity including fracture, septicemia, and dissemination despite appropriate therapeutic management (3, 8, 9). This morbidity is driven in part due to the widespread toxin induced destruction of the bone matrix and vasculature (3). Disruption of the vascular architecture of bone inhibits both delivery of systemically administered therapeutics to the site of infection and delivery of nutrients and oxygen to host and bacterial cells within the infectious focus. The propensity of *S. aureus* to develop organized bacterial communities

surrounded by a dense organic matrix, or biofilms, in skeletal tissues and orthopedic implants further complicates treatment options (10). A biofilm lifestyle is linked to increased antimicrobial resistance and persistence, potentially due to decreased antibiotic penetrance or altered bacterial metabolism *in vivo* (10).

Despite the known role of staphylococcal toxins in bone destruction during osteomyelitis, toxins are not the sole mediator of tissue destruction. Skeletal remodeling is coordinated by the opposing action of osteoclasts, bone resorbing cells, and osteoblasts, bone depositing cells (11). These cells are responsible for breaking down and depositing the amino-acid-rich matrix that makes up the structural component of bone. Skeletal cells participate in osteo-immunologic cross talk in the presence of invading pathogens, which dramatically alters the kinetics of bone remodeling as well as skeletal homeostasis due to stimulation of skeletal cell differentiation (12, 13). Changes in skeletal cell dynamics may induce significant alterations of host substrates available for pathogen nutrient acquisition (14-16). Furthermore, osteoclasts and osteoblasts exhibit a highly glycolytic metabolism, even in the presence of sufficient oxygen for respiration (17-21). The stimulation of osteoclast and osteoblast differentiation thus significantly alters the carbon source demands of skeletal tissues. The dynamic changes in the nutrient environment of skeletal tissue during infection therefore makes osteomyelitis an ideal model for the study of fundamental processes in bacteria nutrient acquisition and central metabolism.

Staphylococcal metabolism in infectious settings

All organisms require metabolism for the generation of energy and macromolecules within the cell including carbohydrates, proteins, nucleic acids, lipids, and cofactors. Estimations of the exact composition of these metabolites for an *S. aureus* cell have been previously published (22). *S. aureus* is capable of generating all of its metabolic intermediates from 12 precursor metabolites

derived from three major central metabolic pathways: glycolysis/gluconeogenesis, the pentose phosphate pathway, and the TCA cycle (23). The rise of genome sequencing technology in the past 20 years has facilitated the development of extensive metabolic maps of *S. aureus* reconstructed from genome annotation databases (22, 24). These maps represent relatively accurate representations of staphylococcal metabolism; however, several key differences arise, which likely represent control by unknown metabolic regulatory pathways and gaps in genome annotations. Despite these limitations, metabolic databases like the Kyoto Encyclopedia of Genes and Genomes (KEGG), represent the most comprehensive resources for preliminary interrogation of metabolic data. Simplified schematics of staphylococcal metabolism adapted from the KEGG database can be found in the subsequent figures. The following section serves as an introduction for the current knowledge on staphylococcal metabolism, with an emphasis on pathways impacting staphylococcal virulence.

Respiration/Fermentation. Generally, in order to produce ATP for energy production to fuel cellular processes, the most energetically efficient pathway is respiration. This process is performed by the electron transport chain, in which electrons are transported successively along molecules with increasing electron potentials through a series of oxidation-reduction reactions. The transport of electrons across the cell membrane generates an electrical or chemical gradient that is collectively referred to as proton motive force. The proton motive force facilitates substrate transport or ATP generation through ATPase enzymes. In this way, catabolism of organic substrates during respiration can be converted to energy.

In *S. aureus* specifically, soluble NADH, generated from central metabolism shuttles electrons to the electron transport chain (**Figure 1**). The membrane bound NADH: quinone oxidoreductase, NDH2, then transfers NADH bound electrons to menaquinone (MQ), generating

NAD+ and reduced menaquinone (25). Alternatively, substrate-specific quinone oxidoreductases, called flavoproteins, can also liberate electrons to reduce quinones, many of which are implicated in staphylococcal survival *in vivo* (CidC, SdhCAB, Lqo, Mqo, and GlpD) (26-29). In the presence of oxygen, reduced menaquinone then transfers electrons to one of two terminal oxidases, Qox or Cyd (30). These terminal oxidases, or cytochromes, oxidize menaquinone and donate electrons to oxygen, the terminal electron acceptor. Both Qox and Cyd are required for full virulence during sepsis, however this phenotype is tissue dependent, suggesting that *S. aureus* utilizes different cytochrome oxidases at different infectious niches (30). *S. aureus* contains a *bo* and *ba3* type cytochrome – distinguished by the spectral signature which is dictated by the bound heme cofactor – however Qox is annotated as a cytochrome *aa3* and Cyd is annotated at cytochrome *bd*, suggesting that these cytochromes are misannotated (31-34). Alternatively, *S. aureus* can reduce nitrate and respire anaerobically, through the predicted terminal oxidase NarGH (35). In order to generate proton motive force, Qox can act as a proton pump, or protons can be translocated via Q-loops, where reduced quinones release protons on the extracellular face following oxidation (36). The resulting proton motive force drives the production of ATP by the F_1F_0 ATPase (36).

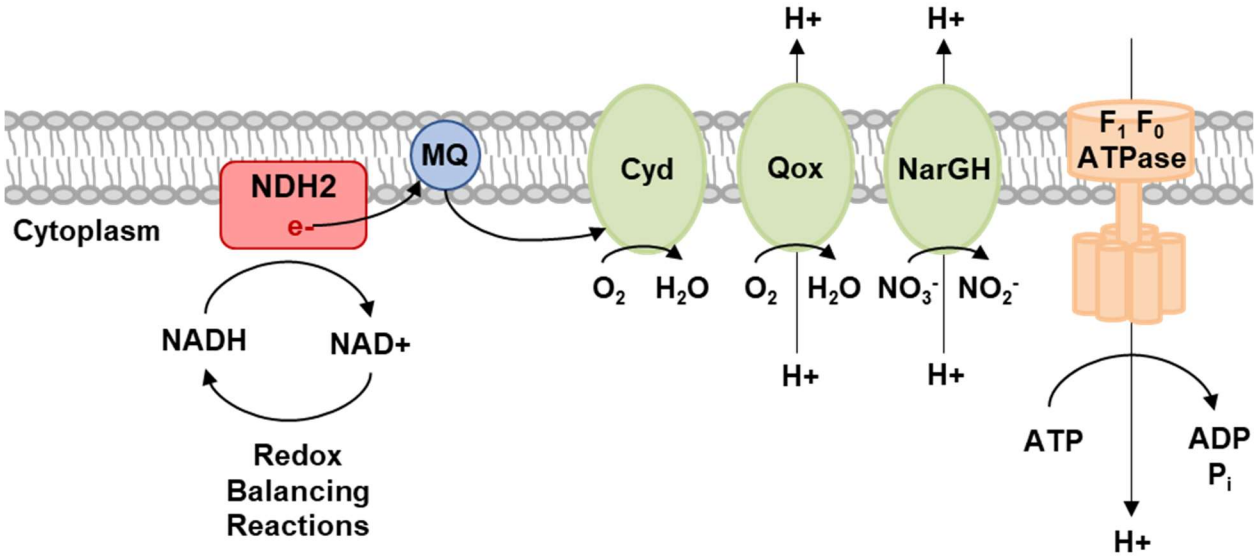

Figure 1. Schematic of the electron transport chain.

In the absence of respiration, *S. aureus* can maintain the balance of oxidation-reduction reactions (redox balance) through oxidation of organic metabolites. These reactions are less energetically favorable than respiration due to the low electron potential of catabolic end products. *S. aureus* primarily maintains redox balance through the synthesis of L-lactate, which is catalyzed by the constitutively produced Ldh2 and the respiration responsive Ldh1 (37). Ldh1 is required for resistance to nitrosative stress for the maintenance of redox balance and its regulation represents a unique adaptation of *S. aureus* to respiration limitation by nitric oxide (37). Fermentation can also produce D-lactate through D-lactate dehydrogenase (Ddh), formate through pyruvate formate lyase (PFL), and ethanol through alcohol dehydrogenase (ADH), all of which reduce NAD+ to regenerate NADH and balance the redox state of the cell (**Figure 2**). During fermentative conditions, due to the absence of respiration and a functional electron transport chain, ATP is generated by substrate level phosphorylation. However, in the absence of respiration, proton motive force must be maintained for function of essential cellular processes. Under fermentative conditions, the F_1F_0 ATPase may function in reverse, in which cation export occurs at the cost of ATP hydrolysis. Mutation of this ATPase results in elevated intracellular pH and limits the activity of staphylococcal lactate dehydrogenases, destabilizing redox balance and inhibiting growth in the absence of respiration (36). These studies suggest that the F_1F_0 ATPase enables the function of staphylococcal virulence factor, Ldh1 to maintain redox balance under nitric oxide stress derived from the host innate immune system.

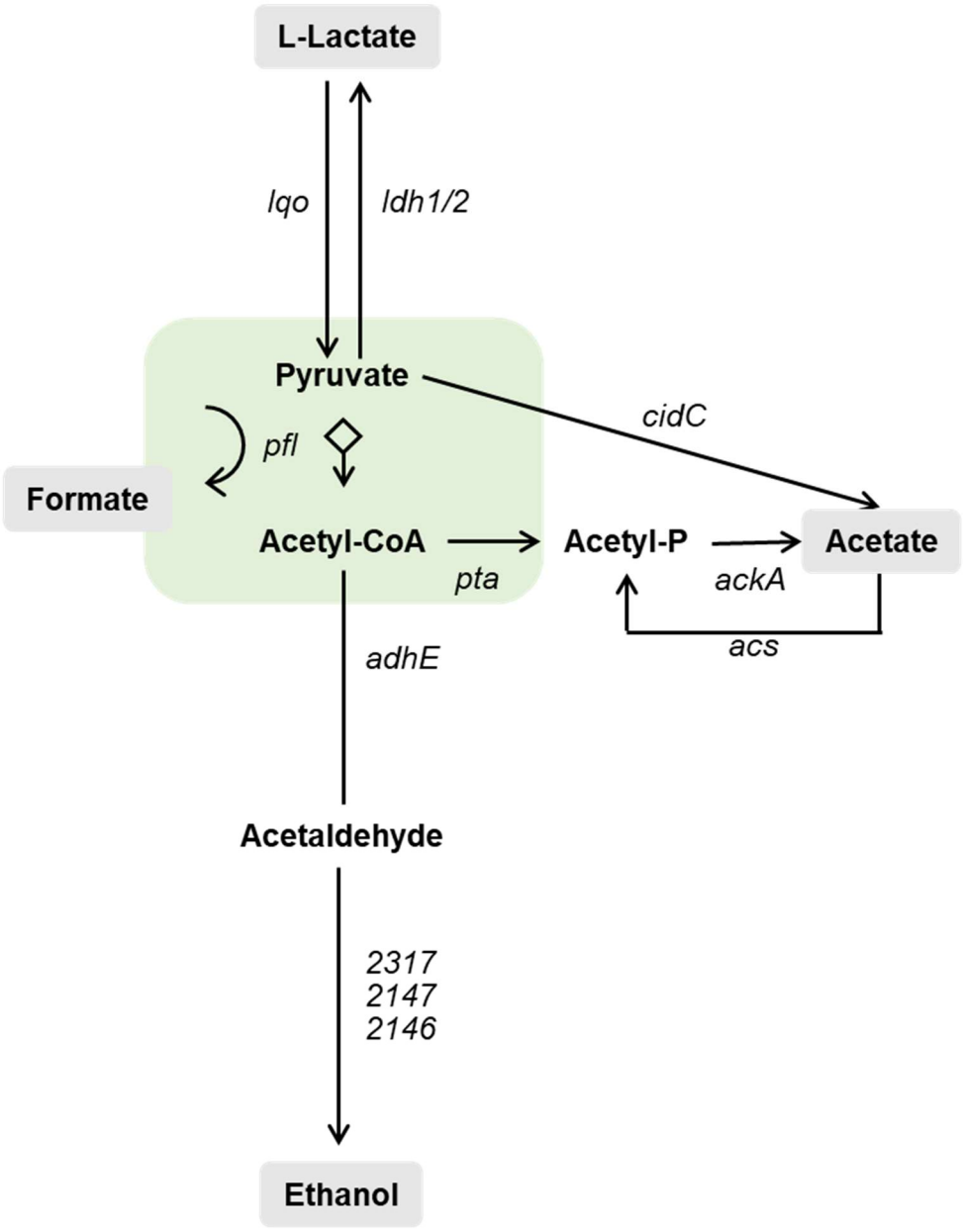

Figure 2. Schematic of the fermentative metabolism. Abbreviations: Acetyl-CoA (Acetyl-coenzyme A); Acetyl-P (Acetyl Phosphate).

Glycolysis, gluconeogenesis, the pentose phosphate pathway, and the TCA cycle. *S. aureus* is capable of utilizing a wide variety of carbon sources including hexoses (i.e. glucose), sorbitol, mannitol, pyruvate, and amino acids (38, 39). *S. aureus* is exquisitely adapted for utilization of carbohydrate carbon sources, and encodes at least 11 carbohydrate transporters, four of which are dedicated to the uptake of glucose (39). Carbohydrates are typically catabolized through glycolysis to produce pyruvate (**Figure 3**). Pyruvate can then be oxidized to acetyl-coenzyme A by pyruvate dehydrogenase during aerobic growth (40). Alternatively, during anaerobic growth, pyruvate is reduced to lactic acid (see section on fermentation, above). The ability to perform glycolysis is essential for *S. aureus* virulence. Glycolysis is required for *S. aureus* survival *in vivo* to resist respiration inhibition by nitric oxide derived from the host during skin and soft tissue infection (38). Conversely, *S. aureus* consumption of glycolytic intermediates also stimulates the immune response and production of IL-1β in keratinocytes, which is required for clearance of *S. aureus* skin infection (41). These studies indicate that staphylococcal carbohydrate utilization is important for pathogenesis and influences antibacterial responses.

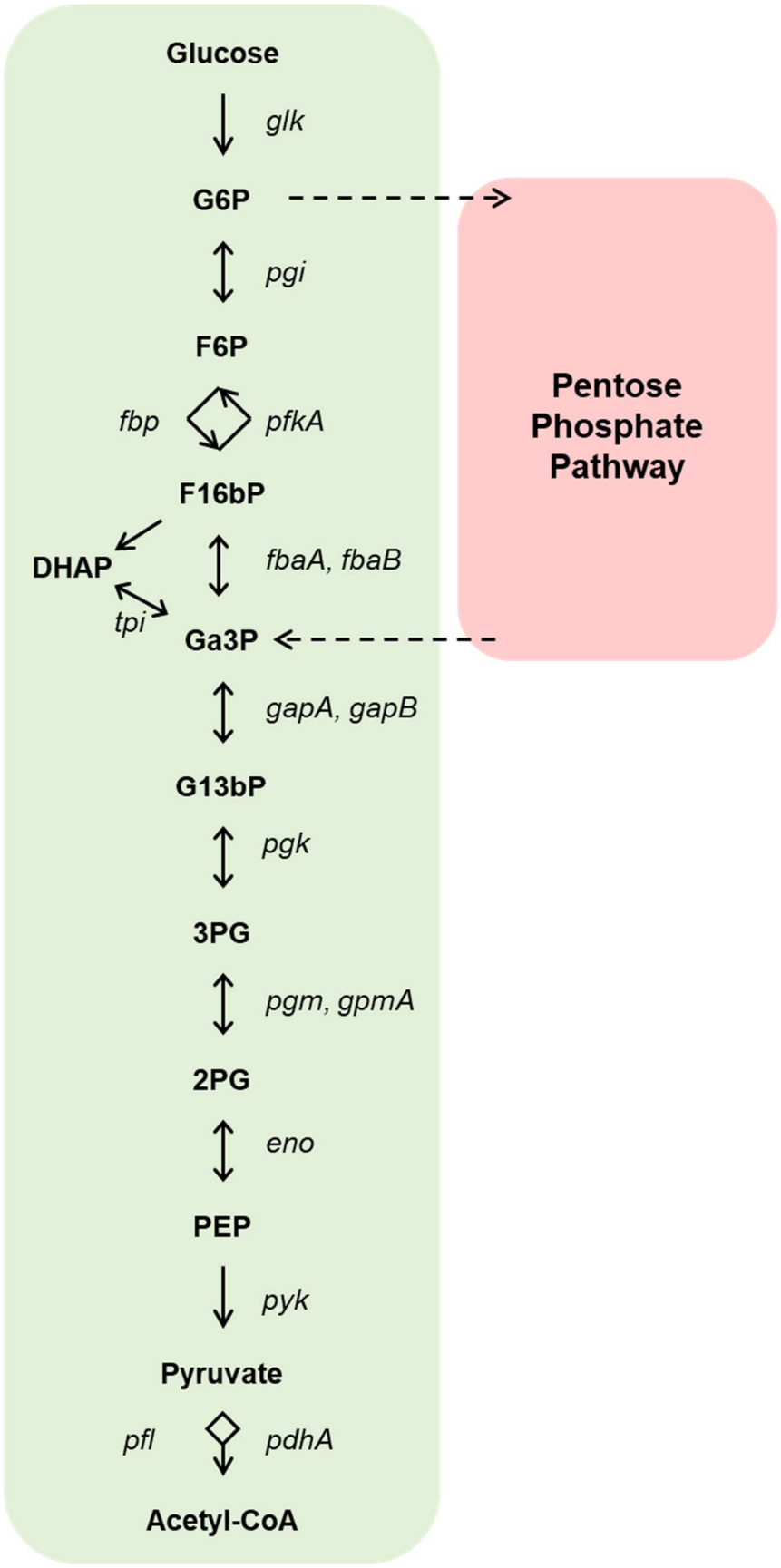
Glucose
glk
G6P
pgi
F6P
fbp
pfkA
F16bP
DHAP
fbaA, fbaB
tpi
Ga3P
gapA, gapB
G13bP
pgk
3PG
pgm, gpmA
2PG
eno
PEP
pyk
Pyruvate
pfl
pdhA
Acetyl-CoA
Pentose Phosphate Pathway

Figure 3. Schematic of glycolysis/gluconeogenesis. Abbreviations: G6P (Glucose-6-Phosphate); F6P (Fructose-6-Phosphate); F16bP (Fructose 1,6-bisphosphate); DHAP (dihydroxyacetone); Ga3P (Glyceraldehyde 3-phosphate); G13bP (1,3- bisphosphoglycerate); G3P (3-phosphoglycerate); G2P (2-phosphoglycerate); PEP (phosphoenolpyruvate); Acetyl-CoA (Acetyl-coenzyme A).

Concomitantly with glycolysis, the pentose phosphate pathway (PPP) generates several essential metabolic precursors (**Figure 4**) (42). The oxidative phase of the PPP synthesizes NADPH from glucose-6-phosphate for the generation of fatty acids and glutamate. The non-oxidative phase produces ribose-5-phosphate (R5P), erythrose-4-phosphate (E4P), and sedoheptulose-7-phosphate (S7P). S7P can be used to generate both R5P and E4P – both of which have important intracellular roles. The first, R5P, is utilized in purine and pyrimidine biosynthesis for generation of DNA and RNA. Purine biosynthesis also generates AMP and GMP which are important nucleic acids involved in energy generation and signaling in prokaryotes. The ability to synthesize purines is essential for bacterial growth *in vivo* in a variety of bacterial pathogens, including *S. aureus*, making R5P an incredibly important metabolic precursor for bacterial survival during infection (43). The remaining precursor E4P is required for the synthesis of the aromatic amino acids, tyrosine, tryptophan, and phenylalanine. Because of its role in essential cellular processes, it is not surprising that the PPP is therefore required for staphylococcal growth and survival *in vitro* and *in vivo* (36, 44, 45).

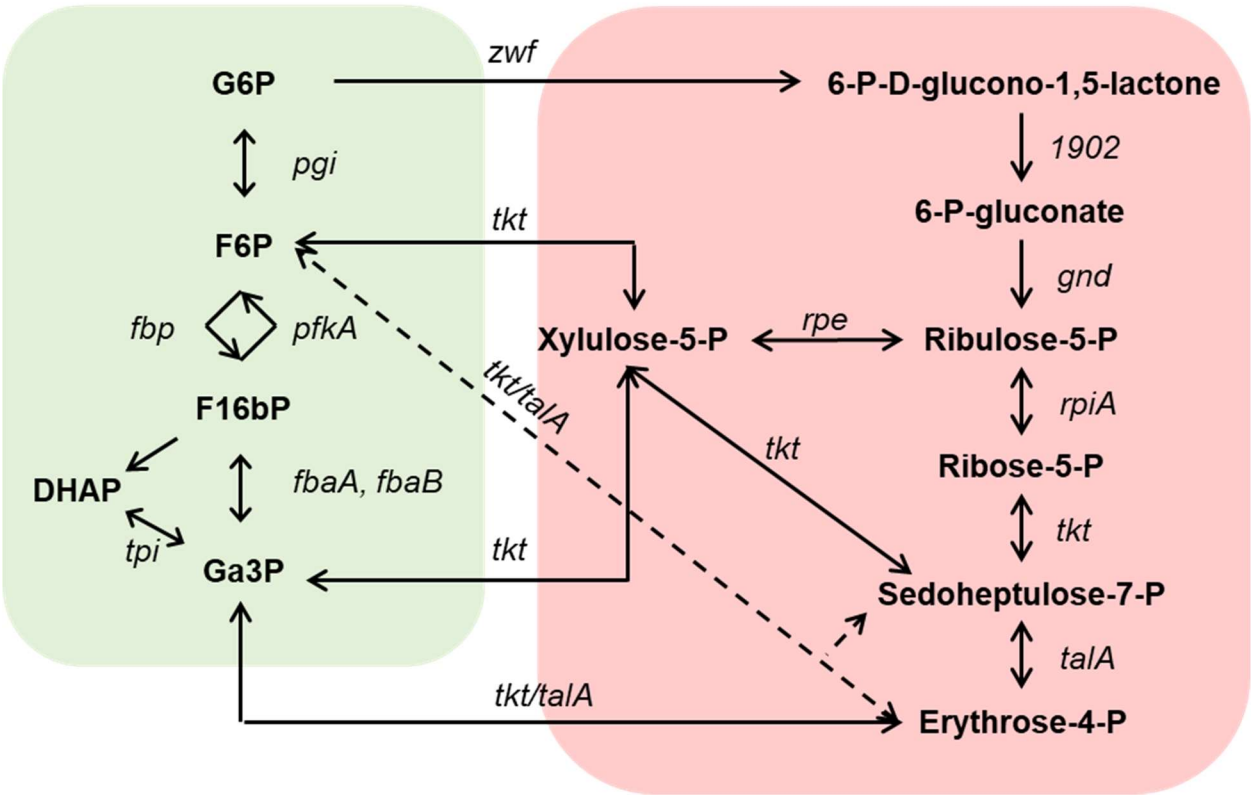

Figure 4. Schematic of the pentose phosphate pathway. Abbreviations: G6P (Glucose-6-Phosphate); F6P (Fructose-6-Phosphate); F16bP (Fructose 1,6-bisphosphate); DHAP (dihydroxyacetone); Ga3P (Glyceraldehyde 3-phosphate).

During growth on nutrient rich substrates in both the presence and absence of oxygen, Acetyl-CoA is utilized for acetogenesis, limiting entry into the TCA cycle (46, 47). Following depletion of preferred carbon sources (i.e. glucose), *S. aureus* can consume acetate, amino acids, and lactate, which requires the TCA cycle and produces ATP and the reducing equivalents NADH and FADH2 (**Figure 5**) (48-50). Gluconeogenesis then restores essential intermediates previously produced by glycolysis, and depletion of essential metabolites by TCA cycle activity is restored by "replenishing reactions" known as anaplerotic reactions. However, carbon source utilization appears to be oxygen/respiration dependent, particularly following consumption of preferred carbon sources. Decreases in oxygen and iron abundance increase glycolytic enzyme production and reduce TCA cycle related gene transcription (51, 52). Several studies have linked the TCA cycle with regulation of *S. aureus* virulence. The TCA cycle is required for the switch to post-exponential growth following depletion of preferred carbon sources and subsequent capsule production, and TCA cycle inhibition alters α-toxin, β-toxin, and δ-toxin production (47, 48, 53). Genes encoding TCA enzymes have also been shown to impact staphylococcal survival in murine models via high-throughput insertional mutagenesis studies, indicating that TCA cycle activation has major impacts on staphylococcal virulence capabilities (45, 54).

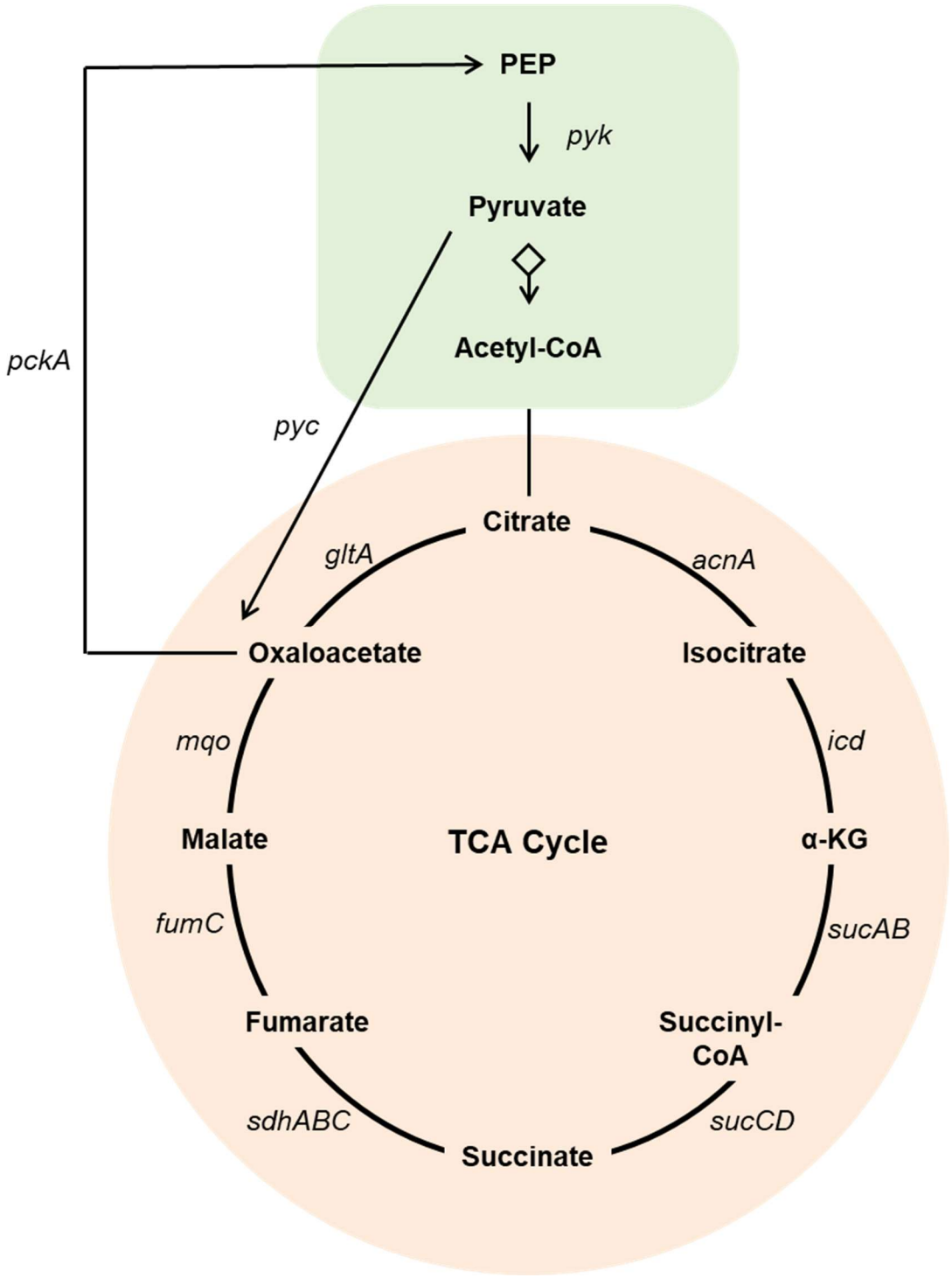

Figure 5. Schematic of the TCA cycle. Abbreviations: PEP (phosphoenolpyruvate); Acetyl-CoA (Acetyl-coenzyme A); α-KG (α-Ketoglutarate).

Intersectionality of virulence and metabolism

S. aureus has an extensive repertoire of virulence factors that mediate survival inside a mammalian host. These virulence factors include secreted and surface associated molecules that mediate a variety of functions including circumvention of host defenses, liberation of essential nutrients for replication, and physical attachment to host substrates. It has become an emerging theme in pathogen biology that bacterial virulence is intimately associated with nutrient sensing, particularly among staphylococcal species. CcpA, SrrAB, and Agr are a select few prominent examples of master regulators in *S. aureus* that sense the nutritional status of the cell and correspondingly regulate virulence (55-65). In order to examine the virulence and metabolic responses of *S. aureus in vivo*, it is therefore essential to have an understanding of how these metabolite-sensing regulators function.

CcpA. Catabolite control protein A (CcpA) is a global regulator of carbon metabolism that is highly conserved among gram-positive bacteria. CcpA is required for glucose mediated regulation, or catabolite repression, of metabolic genes. In *Bacillus subtilis*, CcpA activity is controlled by a corepressor histidine containing protein (HPr) in response to accumulation of the glycolytic intermediates, glucose-6-phosphate and fructose-1,6-bisphosphate, and ATP (66-68). Recent findings suggest that CcpA is also regulated by organic phosphate through serine/threonine protein kinase 1 (Stk1) (69). CcpA repression is then mediated by binding of CcpA to catabolite responsive elements (*cre*) in the promoters of CcpA regulated genes (70). In the presence of preferred carbohydrate sources, CcpA represses genes involved in the TCA cycle, amino acid degradation, and numerous nutrient transporters (49, 71).

In addition to the role of CcpA in metabolic regulation, CcpA also is also a virulence regulator. Glucose decreases transcription, in a CcpA dependent manner, of the immune evasion

protein staphylococcal protein A (*spa*), the immunomodulatory protein immunodominant antigen A (*isaA*), and the adhesive protein autolysin (*atl*) (71). Additionally, CcpA is required for proper biofilm formation (57). The effect of CcpA on biofilm formation is proposed to be mediated through alteration of production of important biofilm components - including upregulation of *cidA*, involved in extracellular DNA production (eDNA), and downregulation of *icaA*, which is required for synthesis of poly *N*-acetyl glucosamine (57). The dramatic impact of *ccpA* mutation on the central metabolic programing of *S. aureus* and biofilm formation and integrity indicates that CcpA is an important regulator of staphylococcal metabolism and virulence.

SrrAB. SrrAB was originally identified as a regulator of oxygen-dependent toxic shock syndrome toxin-1 (TSST-1) expression, and was noted to have homology to the global regulator ResDE in *B. subtilis* (72, 73). ResDE is a two-component system required for anaerobic respiration (74). Subsequent analyses revealed that SrrAB is associated with resistance to oxidative stress and the aerobic/anaerobic shift (59, 60, 72). SrrAB mediates its effects in part through upregulation of a variety of metabolic genes during respiration limitation, including genes involved in fermentation (*pflAB* and *adhE*), anaerobic respiration (*nrdDG*), and cytochrome synthesis (*qoxABCD* and *cydAB*) (59). SrrAB is also required for resistance to nitric oxide – a critical component of the innate immune response – due to upregulation of a nitric oxide dioxygenase (*hmp*) and lactate dehydrogenase (*ldh1*) which manages redox balance in the cell during nitric oxide stress as discussed above (37, 59, 75). The extensive list of metabolic genes present within the SrrAB regulon make this two-component system an important master regulator of metabolism. Further studies revealed that SrrA is capable of downregulating transcription of the *S. aureus* quorum-sensing system, which is also a major virulence regulator in staphylococci (discussed in depth below) (12, 60). SrrAB is also required for appropriate biofilm formation, through repression of

cidABC expression which is required for eDNA production (59, 76, 77). Furthermore, overexpression of SrrAB reduces bacterial burden in a rabbit endocarditis model (60). These findings indicate a link between SrrAB, quorum sensing, and biofilm production and suggest that oxygenation could impact staphylococcal virulence.

Agr. The accessory gene regulator (*agr*) quorum sensing system is a master regulator of virulence and biofilm formation in *S. aureus*, and is a major mediator of bacterial-derived bone destruction during osteomyelitis (12). Mutation of *agr* is a common staphylococcal adaptation to osteomyelitis during chronic infection, which promotes decreased virulence and a biofilm like lifestyle (78-81). The Agr system consists of two divergent promoters, P2 which drives transcription of *agrB*, *agrD*, *agrC*, and *agrA*, and P3 which drives transcription of the effector molecule RNAIII. AgrB is a transmembrane protein involved in the proteolytic processing and export of the Auto Inducing Peptide (AIP) pheromone encoded by *agrD* (82, 83). Accumulation of AIP in the extracellular space is sensed by the AgrC sensor kinase that activates the transcription factor AgrA which auto-regulates transcription through the P2 promoter (84, 85). Upon reaching quorum, AgrA activation mediates several downstream effects on virulence factor production through RNAIII. Alpha-hemolysin (*hla*) and staphylococcal protein A *(spa*) are two major virulence factors directly regulated by RNAIII through base pairing with target gene transcripts (65, 86, 87). However, RNAIII also functions to regulate virulence indirectly through anti-sense binding to the transcriptional regulator, Repressor of Toxins (*rot*), which results in the upregulation of several exoproteins (88). In addition to RNAIII dependent regulation of virulence, AgrA also directly regulates transcription of Phenol Soluble Modulins (PSMs) (89). PSMs are small amphipathic, helical toxins that are non-specifically cytolytic towards mammalian cells and are responsible for cytotoxicity observed towards skeletal cells *in vitro* and *in vivo* (12). PSMs are also

believed to function in biofilm structuring and are required for full biofilm development, making these toxins both a virulence factor and determinant of biofilm lifestyle (90). The Agr system as a whole also has RNAIII dependent and independent effects on the regulation of metabolic genes. In 2008, AgrA was shown to regulate multiple genes involved in nucleotide synthesis, protease production, peptide transport, amino acid metabolism, and carbohydrate utilization (91). Some of this regulation may reflect the incredible metabolic demand on the bacterial cell of producing PSMs and other Agr dependent exoproteins, which make up the most abundant proteins in *S. aureus* culture supernatants. This interplay between metabolic demand and toxin production regulated by a major transcriptional regulator of biofilm formation places Agr in a central role for balancing the intersection of metabolism and virulence in *S. aureus*.

Conclusions

This dissertation describes our contribution to the study of the extensive adaptions *S. aureus* utilizes for survival during invasive infection. In particular, we examined the genetic requirements for staphylococcal virulence – focusing specifically on the metabolic pathways required for staphylococcal survival in bone during osteomyelitis. These pathways are extensively regulated to mitigate appropriate expression within host tissues. This dissertation describes a specific bacterial signaling pathway that modulates both bacterial metabolism and virulence in bone, and a comprehensive analysis of the central metabolic pathways required for *S. aureus* survival during osteomyelitis.

CHAPTER II: BACTERIAL HYPOXIC RESPONSES REVEALED AS CRITICAL DETERMINANTS OF THE HOST-PATHOGEN OUTCOME BY TNSEQ ANALYSIS OF *STAPHYLOCOCCUS AUREUS* INVASIVE INFECTION

Introduction

The mechanisms by which bacterial pathogens adapt to changing host environments are poorly understood, in part due to the technical difficulty in measuring adaptive responses *in vivo*. However, recent advances in high-throughput sequencing have enabled an unprecedented evaluation of the host-pathogen interface. Transposon sequencing (TnSeq) is a sensitive and high-throughput tool combining highly-saturated transposon mutant libraries with massively-parallel sequencing to calculate the fitness of all nonessential bacterial genes under a given selective pressure (92). TnSeq has been successfully used to determine the bacterial genes required for survival in a number of different *in vitro* conditions and infection models (93-97). More recently, a TnSeq library was generated in *S. aureus* and used to determine genes contributing to fitness in abscess and infection-related ecologies (45). These studies illustrate the power of TnSeq analyses to determine the genetic requirements for bacterial adaptation to diverse host environments.

This chapter describes our work that sought to determine the genetic requirements for *S. aureus* survival during invasive infection using TnSeq analysis of acute murine osteomyelitis. TnSeq analysis identified a large number of *S. aureus* genes as essential for growth within bone. Many of the genes identified as essential for growth in bone can be grouped into related pathways – including hypoxic responses. The regulation of interconnected pathways is frequently coordinated by transcriptional regulators. One specialized way *S. aureus* may orchestrate broad transcriptional changes to overarching genetic programs in response to the hostile bone

environment is through the action of two-component systems (TCS). These systems consist of a sensor kinase that changes the phosphorylation state of a conserved aspartate residue on its cognate response regulator in response to an environmental signal (10). The response regulator then differentially binds DNA depending on its phosphorylation state and typically acts as a transcription factor (11). In this way, external stimuli are converted to internal transcriptional changes. The ability of bacteria to sense and respond to oxygen changes using TCSs is well established (12–16). We therefore hypothesized that the ability of *S. aureus* to adapt to changes in available oxygen and shifts in substrate availability in the inflamed bone may rely on a staphylococcal TCS and determine pathogenesis during invasive osteomyelitis. We determined that an oxygen-responsive TCS is responsible for orchestrating several of the changes observed in TnSeq of osteomyelitis. Additionally, intravital oxygen monitoring was utilized to define changes in tissue oxygenation during osteomyelitis. Finally, we evaluated the effects of changing oxygenation on *S. aureus* quorum sensing and virulence factor production. Collectively, the work encompassed in this chapter determines the staphylococcal genes essential for survival during invasive infection of bone, defines shifts in tissue oxygenation during invasive infection, and interrogates the mechanisms by which *S. aureus* can modulate its virulence in response to changes in oxygen availability.

Results

Identification of *S. aureus* genes essential for invasive infection by transposon sequencing analysis of experimental osteomyelitis

In order to characterize the genes required for invasive *S. aureus* infection, TnSeq analysis was performed during experimental osteomyelitis using a recently described *S. aureus* transposon insertion library in strain HG003 (45). To identify potential bottlenecks in bacterial survival during

osteomyelitis, a time course infection was first performed by inoculating murine femurs with strain HG003. An inoculum of $5x10^6$ CFU was chosen based on direct comparison with strain LAC, which has served as the wildtype strain in prior osteomyelitis analyses and is representative of the most common lineage (USA300) of strains causing osteomyelitis in the United States (98). At days 1, 3, 5, 7, and 12 post-infection, infected femurs were harvested and processed for CFU enumeration. After an initial period of replication from day 1 to day 3 post-infection, decreases in bacterial burdens were noted by days 5 and 12 (**Figure 6**). Day 5 was therefore chosen for TnSeq analysis of acute osteomyelitis, as it likely represents the first bottleneck encountered by invading bacteria. For TnSeq analysis of osteomyelitis, mice were infected with the TnSeq library by direct inoculation into the femur. Five days post-infection, femurs from infected mice were processed for genomic DNA extraction. One limitation of TnSeq analysis during invasive infection is the requirement for an outgrowth step after the recovery of bacteria from infected tissues. Although *in vitro* outgrowth could potentially confound fitness calculations, it is necessary to decrease host DNA contamination and allow for efficient sequencing of microbial DNA, and thus has become a standard practice during TnSeq analysis of invasive infection models (45, 95, 99-103). We opted for a short outgrowth in liquid media to minimize any confounding effects on fitness calculation. For an *in vitro* comparator, an equivalent volume of the osteomyelitis inoculum was grown *in vitro* for 24 hours prior to collection and genomic DNA extraction. To determine mutants with compromised *in vivo* fitness, a "dval" was calculated for each gene in each condition (inoculum, *in vitro* comparator, or osteomyelitis).

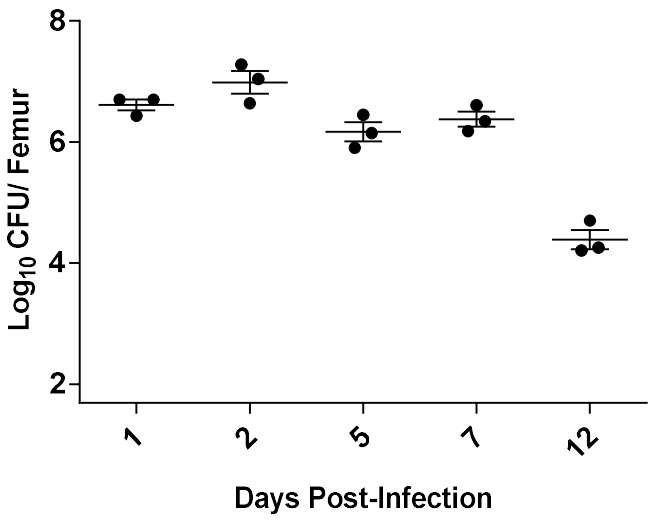

Figure 6. Evaluation of HG003 growth kinetics during experimental osteomyelitis. Groups of mice were subjected to osteomyelitis using strain HG003. Infected femurs were harvested at 1, 3, 5, 7, and 12 days post-infection and processed for CFU enumeration (n=3). Horizontal lines represent the mean. Error bars represent SEM.

A total of 65 genes were found to be essential for survival during osteomyelitis (**Appendix A1**) but not *in vitro* growth, and mutations in an additional 148 genes resulted in significant *in vivo* compromise relative to the *in vitro* comparator (**Appendix A2**). Of the 213 genes identified by TnSeq, 39 essential and 73 compromised genes encode hypothetical proteins, respectively. Of the remaining 101 genes, 12 essential genes and 32 compromised genes have KEGG identifiers. Thirty-two of the 44 genes with KEGG identifiers can broadly be categorized into metabolic pathways, with specific pathways represented including carbon metabolism (9 genes), amino acid biosynthesis (7 genes), and the TCA cycle (5 genes). In the TCA cycle, mutations in genes *sucB* (SAOUHSC_01416), *sucC* (SAOUHSC_01216), and *sucD* (SAOUHSC_01218), which encode enzymes responsible for the conversion of α-ketoglutarate to succinate, each resulted in compromised growth during osteomyelitis. Moreover, genes encoding enzymes in pathways that feed into the TCA cycle were also important for intraosseous growth, including pyruvate carboxylase (SAOUHSC_01064 *pyc*), pyruvate dehydrogenase (SAOUHSC_01040 *pdhA*), and a putative malic enzyme (SAOUHSC_01810). Mutations in 7 *S. aureus* genes encoding amino acid biosynthesis enzymes compromised bacterial growth during osteomyelitis yet did not significantly impair growth *in vitro*. These genes encode enzymes in the biosynthetic pathways for tryptophan (SAOUHSC_01369 *trpC,* SAOUHSC_01367 *trpG*, and SAOUHSC_01377), cysteine (SAOUHSC_00488 *cysK*), lysine (SAOUHSC_01868), leucine (SAOUHSC_02288 *leuD*), and the conversion of serine to glycine (SAOUHSC_02354 *glyA*). Mutations in 6 genes encoding components of purine and pyrimidine metabolic pathways resulted in significant *in vivo* compromise during osteomyelitis. Two of these genes (SAOUHSC_02126 *purB*, SAOUHSC_02360 *tdk*) were essential for staphylococcal survival in bone. A substantial portion of the oxidative phosphorylation pathway was also found to be necessary for staphylococcal

growth during osteomyelitis. Four of the 12 essential genes with KEGG identifiers and 1 of the mutants with compromised growth are involved in oxidative phosphorylation, including components of cytochrome oxidase complexes (SAOUHSC_01000 *qoxC,* SAOUHSC_01032 *cydB*), and 3 subunits of the F-type ATPase (SAOUHSC_02340 *atpC,* SAOUHSC_02343 *atpG,* SAOUHSC_02346 *atpH*). Collectively, the results of TnSeq analysis during experimental osteomyelitis suggest broad adaptations in metabolism and energy production are required for staphylococcal survival during invasive infection of bone.

In contrast to an abundance of genes encoding hypothetical proteins or metabolic pathways, relatively few genes encoding known or putative virulence factors were identified by TnSeq as important for staphylococcal survival in bone. Phosphatidylglycerol lysyltransferase, encoded by *mprF* (SAOUHSC_01359), catalyzes the modification of phosphatidylglycerol with L-lysine and contributes to bacterial defenses against neutrophils, cationic antimicrobial peptides, and certain antibiotics (104). The *mprF* gene was essential for growth during osteomyelitis, suggesting that resistance to antimicrobial peptides and neutrophils are important components of staphylococcal survival in bone. A second virulence-associated gene identified by TnSeq as essential for *S. aureus* osteomyelitis was *isdF* (SAOUHSC_01087), which encodes a component of the iron-regulated surface determinant heme uptake system (105). Interestingly, mutation of the ferric uptake regulator (SAOUHSC_00615 *fur*) gene also resulted in compromised intraosseous growth, illustrating a potential role for iron acquisition in the pathogenesis of staphylococcal osteomyelitis. Mutation in the genes encoding thermonuclease (SAOUHSC_00818 *nuc*), a fibrinogen-binding protein (SAOUHSC_01110), the repressor of toxins (SAOUHSC_01879 *rot*), and two serine proteases (SAOUHSC_01935 *splF,* SAOUHSC_01938 *splD*) also compromised the survival of *S. aureus* during osteomyelitis.

The genes identified by TnSeq as critical for staphylococcal osteomyelitis encode diverse metabolic processes, hypothetical proteins, and select virulence factors. These results suggest that complex bacterial adaptations occur in response to invasive infection of bone. One mechanism by which bacterial pathogens sense and ultimately respond to host-imposed stresses is through TCSs. We therefore hypothesized that staphylococcal TCSs might coordinate the complex adaptations observed during osteomyelitis. Strikingly, TnSeq analysis identified only one *S. aureus* TCS as required for intraosseous survival. The staphylococcal respiratory response (SrrAB) system is involved in coordination of the staphylococcal response to hypoxia and other stresses (59), and has been shown to directly regulate select virulence factors (60). Both the histidine kinase (*srrB*) and the response regulator (*srrA*) components of the SrrAB locus were essential for staphylococcal survival in bone, implying that this TCS might be particularly important for coordination of the metabolic and virulence adaptations to intraosseous growth (**Appendix A1**). In total, these results reveal the power of TnSeq analysis to identify *S. aureus* genes required for invasive infection of bone.

SrrAB differentially regulates *S. aureus* genes under aerobic and hypoxic growth, and is required for survival during osteomyelitis

Among the mutants that exhibited decreased survival in the osteomyelitis model, we identified a single TCS, SrrAB, which coordinates responses to hypoxia and nitrosative stress *in vitro* (59). Moreover, mutations in two additional genes regulated by SrrAB specifically under conditions of nitrosative stress, *cydB* and *qoxC*, also resulted in significantly decreased fitness during osteomyelitis (**Appendix A1 and A2**) (59). Bone and bone marrow are intrinsically hypoxic, leading to the hypothesis that SrrAB contributes to osteomyelitis pathogenesis by sensing and responding to changes in environmental oxygen (106, 107). Because the SrrAB regulon was

previously defined under conditions of nitrosative stress, we sought to further define the oxygen-dependent SrrAB regulon by performing global transcriptional analysis of a clinically relevant strain (LAC) in comparison to a mutant strain lacking *srrAB* expression (*srrA*::Tn) in both aerobic and hypoxic growth conditions. Inactivation of *srrAB* under aerobic conditions resulted in the differential regulation of 64 genes (39 transcripts increased in abundance and 25 decreased in abundance upon inactivation of *srrAB*) (**Appendix B1**). Under hypoxic growth conditions, *srrAB* inactivation led to differential regulation of 78 genes (22 transcripts increased in abundance and 56 decreased in abundance) (**Appendix B2**). Of the genes differentially regulated by SrrAB under aerobic or hypoxic conditions, only 16 were previously identified as members of the SrrAB regulon under nitrosative stress, suggesting that specific stresses might invoke different SrrAB-dependent transcriptional responses (59). Moreover, by defining the SrrAB regulon under aerobic versus hypoxic conditions, we discovered that an additional 7 genes important for survival during osteomyelitis in the TnSeq dataset are also SrrAB-regulated (**Appendix B1 and B2**). The requirement of multiple genes in the SrrAB regulon for survival during osteomyelitis suggests the SrrAB TCS is an important orchestrator of *S. aureus* stress responses in inflamed skeletal tissues.

Previous reports have demonstrated a significant defect in the growth of an *srrAB* mutant under anaerobic conditions but not under hypoxic growth conditions (59, 60, 73). To confirm that SrrAB was not found to be essential in the TnSeq analysis simply because of a defect in growth, the *srrA*::Tn polar transposon mutant and mutations in known genes of the SrrAB regulon (*pflA*, *pflB, qoxA,* and *qoxC*) were analyzed in the LAC strain background. The growth rate of each mutant under aerobic or hypoxic conditions was monitored over time. Under aerobic and hypoxic growth conditions, *srrA*::Tn had an enhanced lag phase compared to Wildtype (WT) but reached equivalent optical densities to WT by 8 hours (**Figure 7**). The *qoxA*::Tn and *qoxC*::Tn mutants

were unable to reach maximal optical densities as previously reported due to disruption of the electron transport chain (59). These results indicate that an *srrAB* mutant is not impaired for growth under hypoxia, further validating our TnSeq methods.

To investigate the role of SrrAB in osteomyelitis in a clinically-relevant background without the potentially confounding influence of competition from other mutants in the TnSeq library, groups of mice were infected with either WT or *srrA*::Tn in the LAC background. At 5 or 14 days post-infection, femurs were either processed to quantify bacterial burdens or subjected to micro-computed tomography (microCT) imaging (day 14) for quantification of cortical bone destruction. Inactivation of SrrAB resulted in a significant reduction in bacterial burdens in infected femurs at both 5 and 14 days post-infection (**Figure 8A**). Moreover, murine femurs infected with *srrA*::Tn sustain significantly less cortical bone destruction than WT-infected femurs (**Figure 8B– D**). These results demonstrate that SrrAB is critical for *S. aureus* survival in infected bone and for induction of pathologic changes in bone remodeling during osteomyelitis. Interestingly, mutants within the SrrAB regulon (*qoxA* and *pflA*) did not exhibit decreased survival in our murine osteomyelitis model (**Figure 7D**). As discussed in Chapter I, staphylococci have two cytochrome oxidases, *qoxA* and *cydA*, however *cydA* also does not have a defect in survival during osteomyelitis. Although it is possible that the alternative cytochrome oxidase compensates for mutation of the other, it has previously been shown that the cytochrome oxidases have distinct roles *in vivo* and are not functionally redundant (30). Our data therefore suggests that *S. aureus* may not require aerobic respiration *in vivo*. Additionally, mutation of *pflB* had no impact of staphylococcal survival at 14 days which likely reflects the fact that PflB is inactivated by NO. These data suggest that staphylococci encounter hypoxic and/or nitrosative stresses during osteomyelitis.

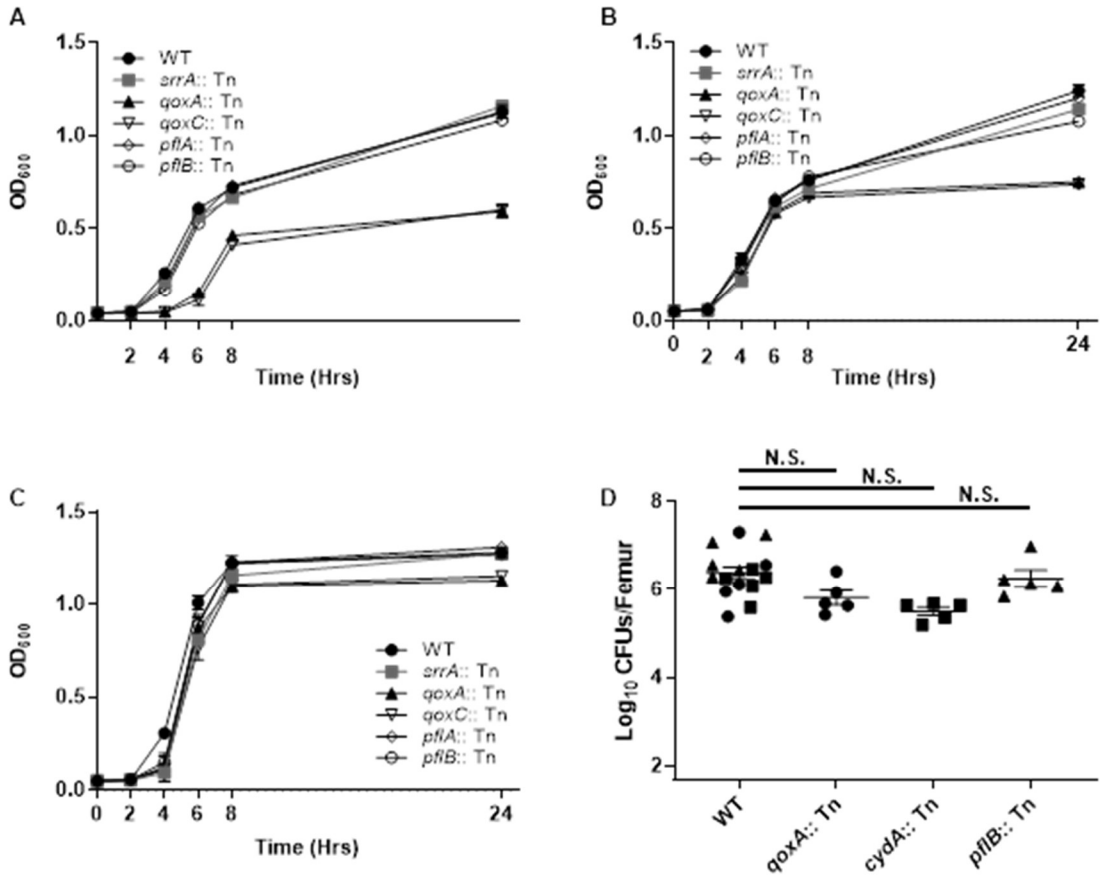

Figure 7. Growth kinetics of *srrA*::Tn and select SrrAB-regulated mutants under aerobic and hypoxic conditions or *in vivo*. Growth of WT, *srrA*::Tn, *pflA*::Tn, *pflB*::Tn, *qoxA*::Tn, and *qoxC*::Tn strains was monitored by OD_{600} with 3 technical replicates at 0, 2, 4, 6, 8, and 24 hours. Data shown is representative of 3 biologically independent experiments. Error bars represent the SEM. (A) Strains grown aerobically in BHI, which served as the *in vitro* comparator media during TnSeq analysis. (B) Strains grown aerobically in TSB. (C) Strains grown hypoxically in TSB by tightly capping Erlenmeyer flasks. (D) Osteomyelitis was induced in groups of mice using WT, *pflB*::Tn, *qoxA*::Tn, and *cydA*::Tn strains. At 14 days post-infection, femurs were processed for colony forming units (CFU) enumeration. N=5 mice per group and horizontal line represents the mean. Different shapes indicate replicates. Error bars represent the SEM. Statistical significance determined by Student's *t* test relative to respective WT comparator.

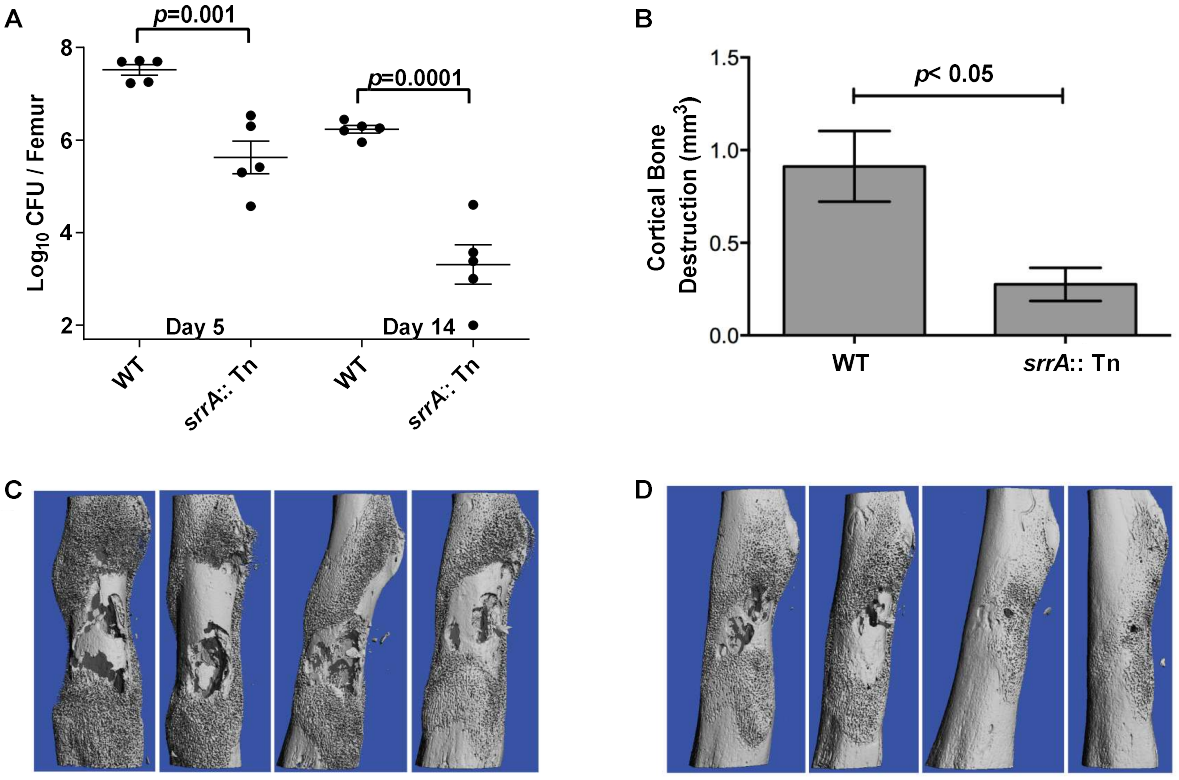

Figure 8. SrrAB is required for intraosseous survival and cortical bone destruction during *S. aureus* osteomyelitis. Osteomyelitis was induced in groups of mice using WT or *srrA*::Tn strains. (A) At 5 and 14 days post-infection, femurs were processed for colony forming units (CFU) enumeration. N=5 mice per group and horizontal line represents the mean. (B) MicroCT imaging analysis of cortical bone destruction (mm^3) 14 days post-inoculation. N=4 mice per group. (C and D) Antero-posterior views of WT (C) or *srrA*::Tn (D) infected femurs at 14 days post-inoculation. Error bars represent the SEM. Statistical significance determined by Student's *t* test.

S. aureus osteomyelitis triggers reduced oxygen availability in skeletal tissues

Normal bone and bone marrow are intrinsically hypoxic, with a physiologic oxygen concentration range of 11.7 to 48.9 mmHg (1.5-6.4% O_2), compared to atmospheric oxygen at approximately 160 mmHg (21% O_2) (106, 107). TnSeq analysis demonstrated that the hypoxia-responsive SrrAB TCS is essential for *S. aureus* survival in bone, suggesting that bacterial invasion and the resulting inflammation associated with osteomyelitis trigger further decreases in skeletal oxygen availability. In order to determine the oxygen concentrations of *S. aureus* infected murine femurs during osteomyelitis, an Oxylite monitor was used to record oxygen tensions at the inoculation site at various times post-infection. In uninfected mice, average pO_2 in the intramedullary canal was 45.2 mmHg, (**Figure 9**) consistent with previously reported bone marrow physoxia (107). As infection progressed, the infectious focus became increasingly hypoxic, with an average oxygen tension of 14.3 mmHg at 10 days post-infection. This decreased oxygen tension was not due to the trauma induced by the inoculation procedure, as mock-infected bone showed an elevated mean pO_2 of 77.5 mmHg by 4 days post-procedure (**Figure 9**). Collectively, these findings demonstrate that skeletal tissues become increasingly hypoxic during *S. aureus* osteomyelitis.

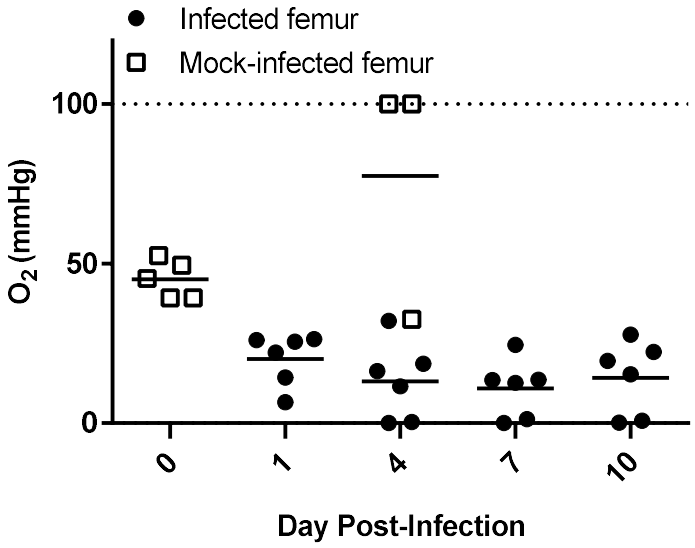

Figure 9. *S. aureus* osteomyelitis triggers reduced oxygen availability in skeletal tissues. Oxygen tension (pO_2) was measured in murine femurs infected with *S. aureus* (black circles) at 1, 4, 7 and 10 days post-infection (n=6 from two independent experiments). Uninfected femurs (open squares) were measured for oxygen tension immediately following (n=5) or 4 days after (n=3) a mock inoculation procedure. Oxygen tension is reported as mmHg. Horizontal lines represent the mean. Dotted line represents the upper limit of detection.

The *srrAB* promoter is active in hypoxic skeletal tissues

Intravital pO_2 monitoring revealed that skeletal tissues become increasingly hypoxic during osteomyelitis, with dramatically reduced oxygen tensions as early as 24 hours after infection. These data and the results of TnSeq analysis suggest that the *srrAB* promoter is active *in vivo*. To test the hypothesis that *srrAB* promoter activity increases with decreasing oxygen availability in infected skeletal tissues, a luminescent reporter construct was created in which expression of the *luxABCDE* operon is driven by the *srrAB* promoter. Mice were infected with WT *S. aureus* containing either this construct or a promoterless vector control, and at 1 hour or 24 hours post-infection infected femurs were explanted and immediately imaged for bioluminescence. No detectable luminescence above background was detected in femurs infected with WT bacteria containing the promoterless control plasmid at 1 hour or 24 hours after infection (**Figure 10**). In contrast, femurs infected with the P*srrAB*-pAmiLux construct showed no detectable luminescence above background at 1 hour post-infection but displayed strong luminescent signal at 24 hours after infection, corresponding to the induction of hypoxia in infected skeletal tissues (**Figure 10**). Collectively, these results demonstrate that the *srrAB* promoter is activated *in vivo* during infection of hypoxic skeletal tissues.

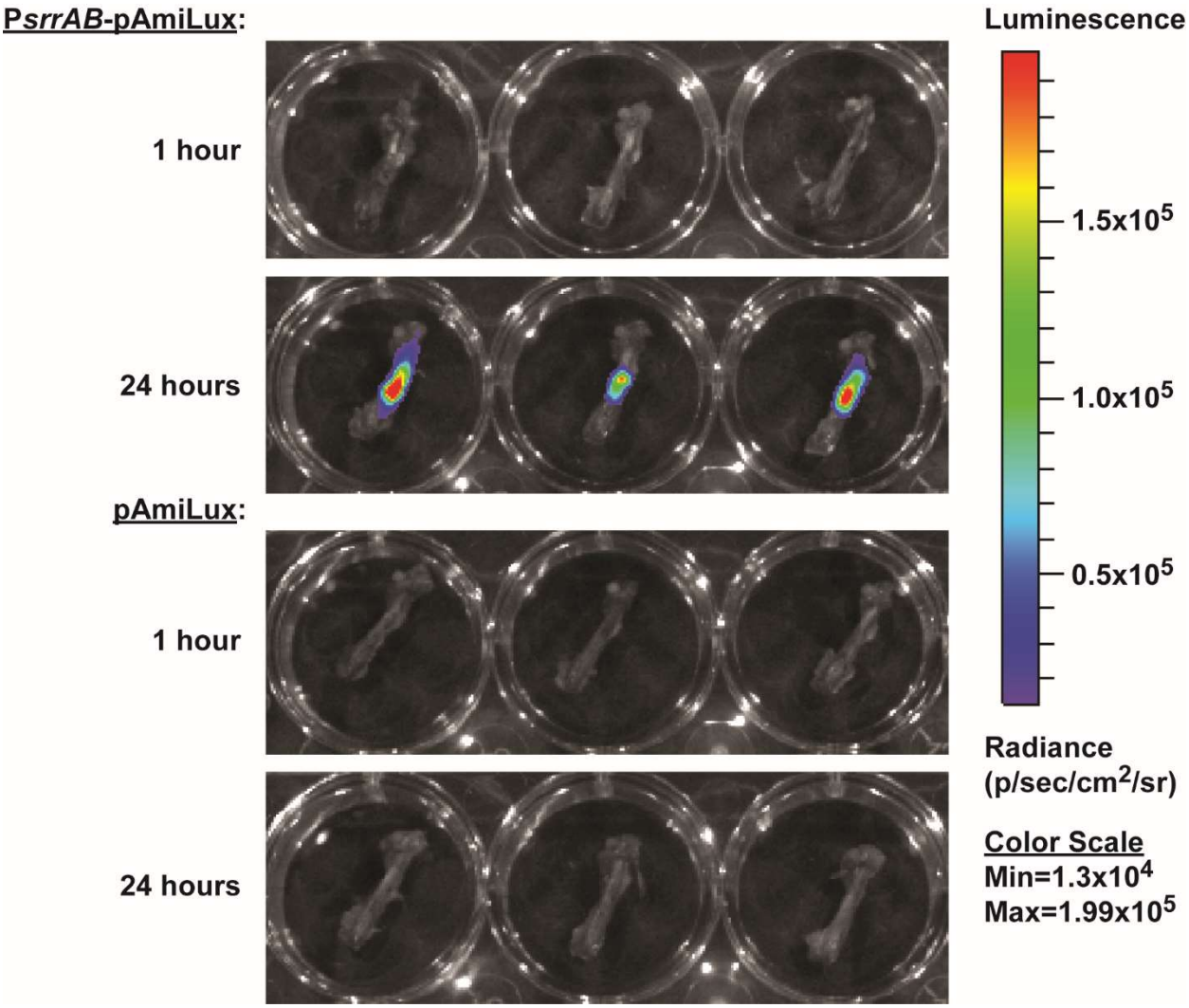

Figure 10. The *srrAB* promoter is active in hypoxic skeletal tissues. Groups of mice (n=3 per group) were subjected to osteomyelitis by infection with WT bacteria containing either P*srrAB*-pAmiLux or pAmiLux (promoterless control). At 1 or 24 hours post-inoculation, infected femurs were explanted and immediately imaged on an IVIS 200 system (5 minute exposure).

Neutrophil depletion rescues the intraosseous growth defect of an *srr* mutant

Intravital oxygen monitoring revealed hypoxia of skeletal tissues upon infection with *S. aureus*, suggesting that inflammation triggers a reduction in skeletal oxygen concentrations. Neutrophils are a significant source of both oxidative and nitrosative stresses *in vivo* and contribute to formation of oxygen-limited abscesses in response to staphylococcal infection (38). To test the hypothesis that SrrAB is necessary to resist hypoxic and/or nitrosative stresses imposed by neutrophils *in vivo*, mice were either rendered neutropenic with serial anti-Ly6G (1A8) monoclonal antibody injections or given an isotype control monoclonal antibody and subsequently infected with WT or *srrA*::Tn (108). At 14 days post-infection, femurs were processed for enumeration of bacterial burdens. In mice treated with control antibody, a significant virulence defect was again observed in mice infected with the *srrA*::Tn mutant (**Figure 11**). However, in mice administered the anti-Ly6G (1A8) antibody, a significant increase in bacterial burdens was observed upon infection with *srrA*::Tn, such that bacterial burdens no longer differed significantly from non-neutropenic mice infected with WT (**Figure 11**). These results suggest that intraosseous survival requires SrrAB to resist hypoxic and/or nitrosative stresses produced by neutrophils in response to *S. aureus* osteomyelitis.

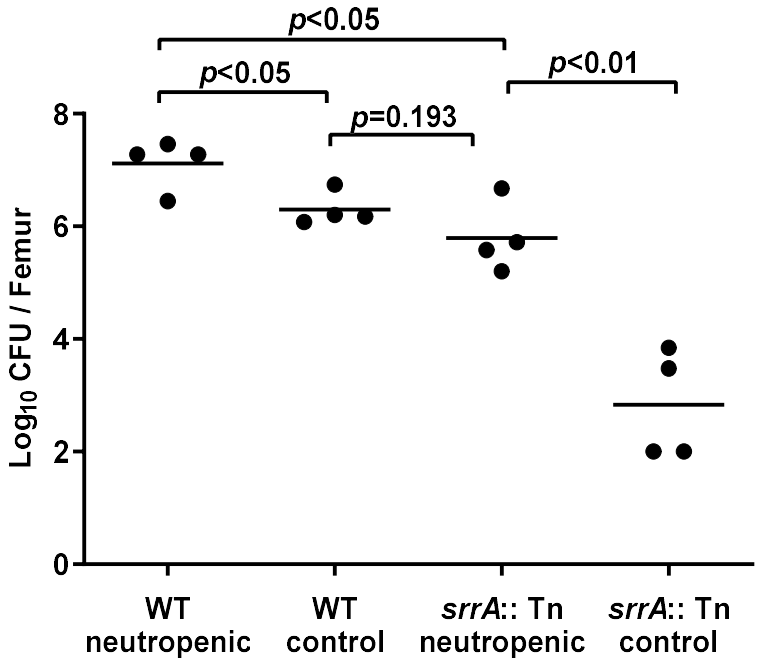

Figure 11. Neutrophil depletion rescues the intraosseous growth defect of an *srrA* mutant. Mice were given serial injections of anti-Ly6G monoclonal antibody. As a control, mice received injections of an isotype control antibody. At 14 days post-infection, femurs were processed for CFU enumeration. N=4 mice per group. Horizontal lines represent the mean. Significance determined by Student's *t* test.

S. aureus modulates quorum sensing and exotoxin production in response to oxygenation

The observation that *S. aureus* infection of murine skeletal tissues leads to dramatically reduced oxygen concentrations prompted further evaluations of how oxygenation impacts the production of staphylococcal virulence factors. We previously demonstrated that secreted toxins regulated by the accessory gene regulator (*agr*) locus are particularly important for the pathogenesis of *S. aureus* osteomyelitis (12, 109). The *agr* locus (*agrABCD*) encodes a quorum sensing system coupled to a TCS, and is responsible for growth phase-dependent regulation of a number of *S. aureus* virulence factors (110). As discussed in Chapter I, the response regulator of the *agr* locus, AgrA, directly regulates the production of alpha-type PSMs, which contribute significantly to the pathology of *S. aureus* osteomyelitis (12, 91). Indeed, alpha-type PSMs were found to be the sole mediators of cytotoxicity in concentrated culture supernatant towards murine and human osteoblasts *in vitro* (12). However, a recent report demonstrated that alpha-type PSM expression is directly linked to alpha toxin (Hla) expression (111). To verify that PSMs are the sole mediators of cytotoxicity toward osteoblastic cells in *S. aureus* concentrated supernatants, strain LAC*Δpsmα1-4* (Δ*psm*) containing the overexpression vector pOS1-*p*lgt driving *hla* expression in trans was tested for cytotoxicity towards osteoblastic cells (**Figure 12**). While WT supernatant displayed maximum cytotoxicity, Δ*psm* and Δ*psm* pOS1-*p*lgt-*hla* did not show significantly different cytotoxicity from control. Deletion of *hla* in an erythromycin-resistant LAC background also failed to attenuate cytotoxicity (**Figure 7**). Moreover, targeted inactivation of RNAIII in LAC did not decrease cytotoxicity, further supporting the AgrA-regulated alpha-type PSMs as the sole secreted mediators of cytotoxicity toward osteoblastic cells (Figure 12).

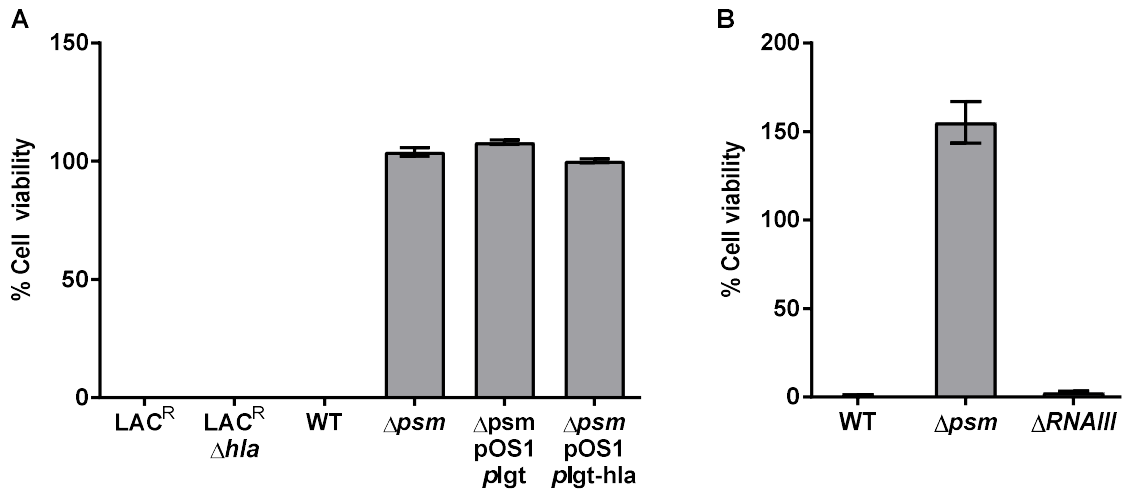

Figure 12. Alpha-hemolysin and inactivation of RNAIII does not impact cytotoxicity of concentrated *S. aureus* supernatants towards osteoblastic cells. (A) Saos-2 or (B) MC3T3 osteoblastic cells were seeded into 96-well plates and cell viability was assessed 24 hours after intoxication with supernatant (30% total media volume) from the indicated strains following hypoxic growth. Results are expressed as percent of RPMI control (n=10). Error bars represent the SEM. LAC^R indicates an erythromycin-resistant derivative of LAC used for construction of the *hla* mutant.

To determine the impact of culture oxygenation on *S. aureus* exotoxin production, concentrated supernatants were prepared from *S. aureus* grown either aerobically or under limited oxygenation. Incubation of several different mammalian cell lines or primary human osteoblasts with varying amounts of concentrated culture supernatant demonstrated dose-dependent cytotoxicity that significantly increased if the bacteria were cultured under lower oxygenation (**Figure 13**). This phenotype was not unique to USA300 strain Lac (**Figure 14**). This enhancement of cytotoxicity was not due to changes in bacterial density (data not shown). These results indicate that *S. aureus* virulence factor production is modulated in response to environmental oxygen levels.

SrrAB regulates select virulence factors under microaerobic conditions in part by directly interacting with the *agr* P2 and P3 promoters (60, 73). This observation, combined with the role of SrrAB in responding to hypoxic stresses, led to the hypothesis that SrrAB may regulate quorum sensing and virulence factor production in response to changes in oxygenation. To investigate the impact of SrrAB on PSM-mediated killing of osteoblasts, osteoblastic cells were incubated with varying amounts of culture supernatant from WT or *srrA*::Tn strains grown either aerobically or under hypoxia. Aerobically grown *srrA*::Tn supernatants demonstrated dose-dependent killing of murine osteoblasts that was significantly increased compared to aerobically grown WT supernatants, mimicking the effect of hypoxia on cytotoxicity (**Figure 15A**). The cytotoxicity of aerobically grown *srrA*::Tn was diminished by expression of the *srrAB* locus in trans (**Figure 16**). These data suggest that SrrAB represses PSM-mediated cytotoxicity under aerobic conditions.

Because SrrAB repressed PSM-mediated cytotoxicity under aerobic conditions, we hypothesized that SrrAB impacts quorum sensing in response to oxygenation. To test this hypothesis, the reporter plasmid pDB59 (*agr*P3 promoter driving YFP expression) was introduced

into WT and *srrA*::Tn (73, 112). Aerobically grown WT cultures demonstrated significantly lower *agr*P3 activation compared to cultures grown under limited oxygenation (**Figure 15B and C**). This decrease was partially SrrAB dependent, as aerobically grown *srrA*::Tn strains demonstrate a 2-fold higher expression of *agr*P3 than aerobic WT cultures (**Figure 15B and C**). To further confirm these results, quantitative RT-PCR was conducted on aerobically and hypoxically grown cultures of WT and *srrA*::Tn. Transcription of *agrA* was increased relative to aerobically grown WT for both *srrA*::Tn and hypoxically grown cultures. Hypoxically grown cultures also demonstrated significantly elevated levels of *psmα* and *RNAIII transcripts* (**Figure 15D**). Inactivation of SrrAB resulted in an over 30-fold increase in *psmα1-4* transcription and a near 20-fold increase in *RNAIII* expression under aerobic conditions. Under hypoxic conditions, inactivation of *srrAB* resulted in a 3000-fold and 160-fold increase in *psmα1-4* and *RNAIII* transcript levels, respectively. Collectively, these data indicate that *S. aureus* quorum sensing and resultant cytotoxicity towards mammalian cells is modulated in an SrrAB-dependent manner in response to changing oxygen availability, and further define SrrAB as an important regulator of metabolic and virulence adaptations during invasive infection

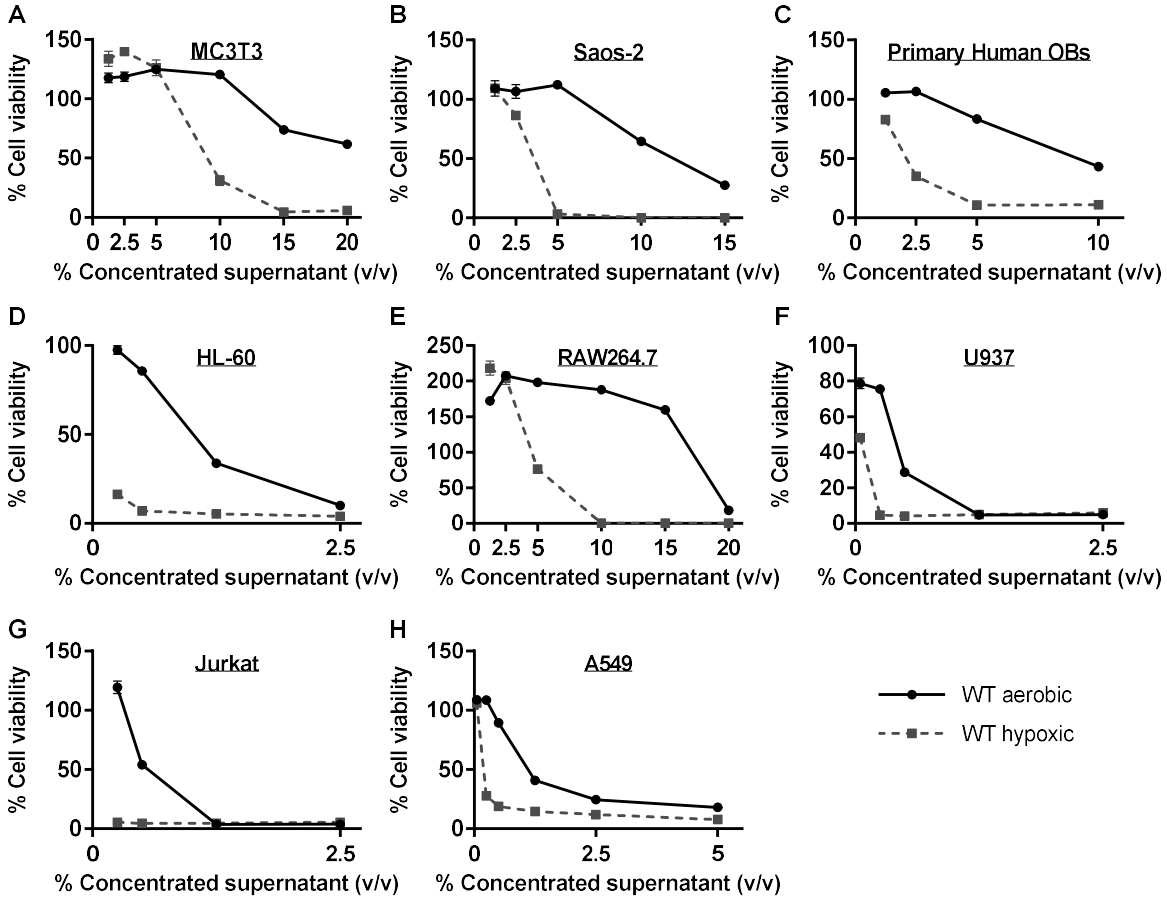

Figure 13. Hypoxically grown bacterial supernatants lead to increased cytotoxicity in human and murine cells. WT supernatants were prepared by inoculating 3 colonies into RPMI and 1% casamino acids and growing for 15 hours either aerobically or hypoxically. MC3T3 murine osteoblastic cells (A), Saos-2 human osteoblastic cells (B), primary human osteoblasts (C), HL-60 premyelocytes (D), RAW264.7 murine macrophages (E), U937 monocytic cells (F), Jurkat T cells (G), or A549 lung epithelial cells (H) were seeded into 96 well plates 24 hours prior to intoxication with concentrated supernatant or RPMI control. Cell viability was assessed 24 hours later. Results are expressed as percent of RPMI control (n=10), and are representative of 2 biologic replicates with the exception of human primary osteoblasts, which represent a single experiment given the limited availability of this resource. Error bars represent the SEM.

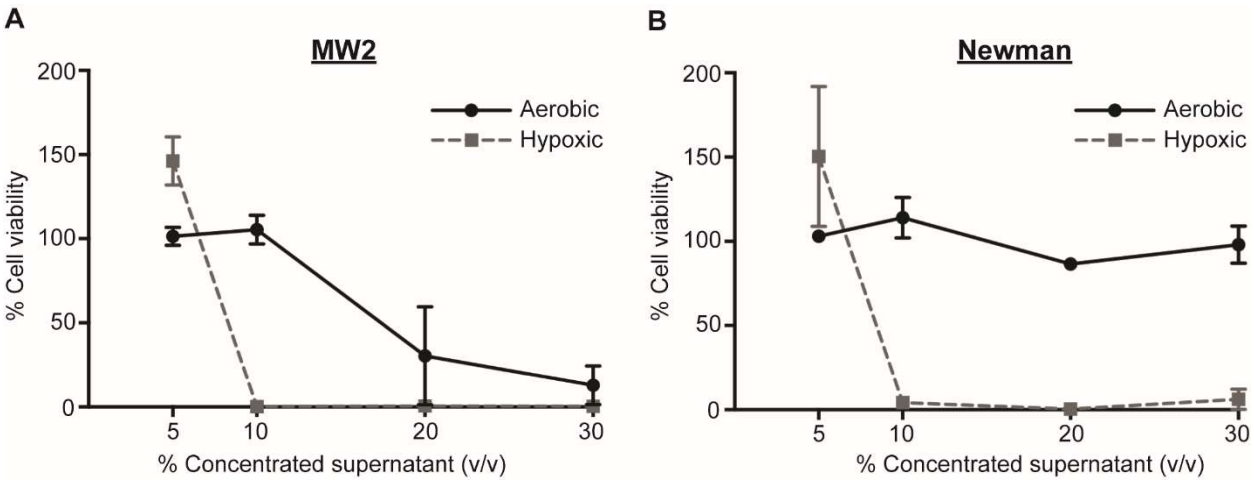

Figure 14. Increased cytotoxicity of hypoxic cultures is not unique to *S. aureus* strain Lac. *S. aureus* strain Newman and MW2 supernatants were prepared as described in Figure 8. Percent viability of MC3T3 cells were assessed as described in Figure 8. Results are expressed as percent of RPMI control (n=10). Data shown is the average of 2 biological replicates. Error bars represent the SEM.

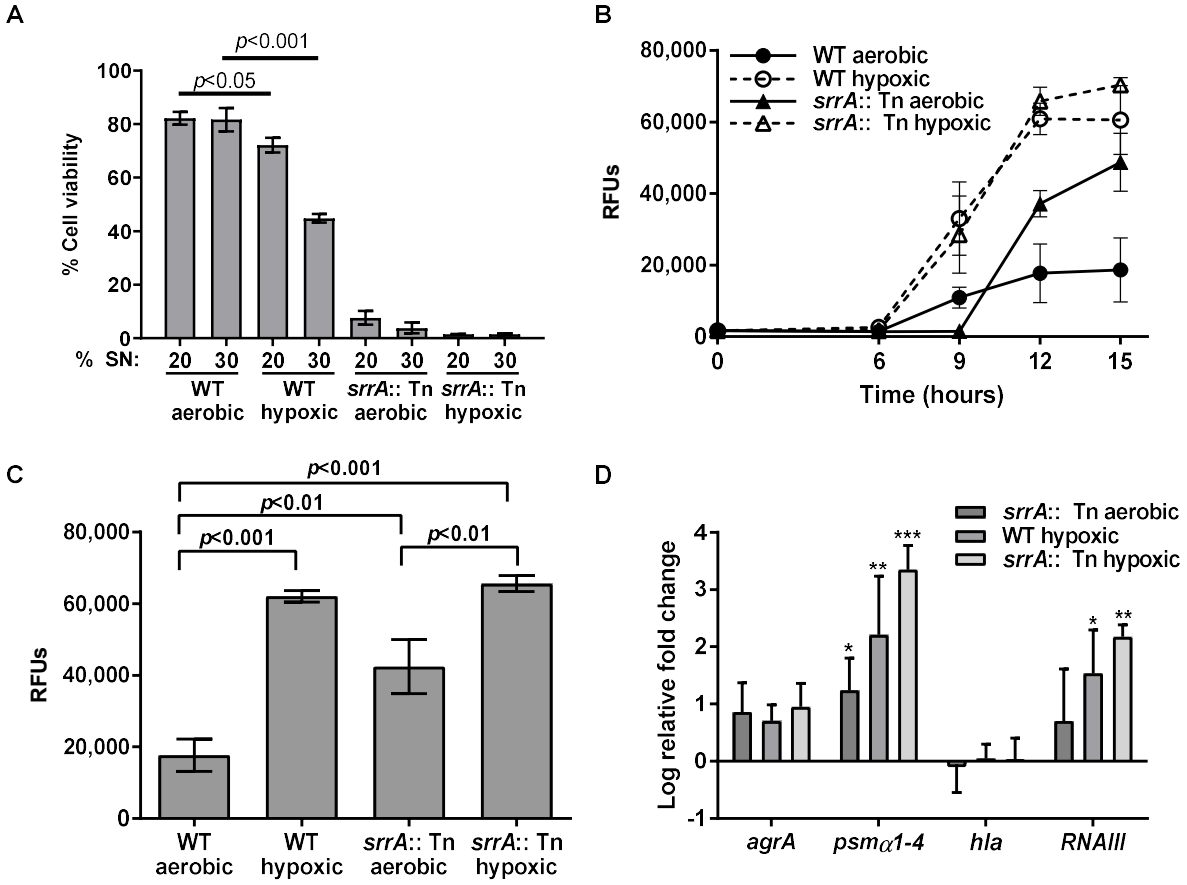
A
p<0.001
p<0.05
% Cell viability
100
80
60
40
20
0
% SN: 20 30 20 30 20 30 20 30
WT aerobic
WT hypoxic
srrA:: Tn aerobic
srrA:: Tn hypoxic
B
WT aerobic
WT hypoxic
srrA:: Tn aerobic
srrA:: Tn hypoxic
RFUs
80,000
60,000
40,000
20,000
0
0 6 9 12 15
Time (hours)
C
p<0.001
p<0.01
p<0.001
p<0.01
RFUs
80,000
60,000
40,000
20,000
0
WT aerobic
WT hypoxic
srrA:: Tn aerobic
srrA:: Tn hypoxic
D
srrA:: Tn aerobic
WT hypoxic
srrA:: Tn hypoxic
Log relative fold change
4
3
2
1
0
-1
*
**
***
*
**
agrA
psmα1-4
hla
RNAIII

Figure 15. *S. aureus* modulates quorum sensing and exotoxin production in response to oxygenation. Supernatants from WT or *srrA*::Tn were prepared by inoculating RPMI and 1% CA with a 1:1000 dilution from overnight cultures and growing for 15 hours either aerobically or hypoxically. Identical culture conditions were used to monitor quorum sensing and transcript levels (see below). (A) MC3T3 cells were seeded into 96 well plates at 5,000 cells per well. After 24 hours, growth media was replaced, and 20% or 30% of the total media volume was replaced with concentrated culture supernatant grown either aerobically or hypoxically, or an equivalent volume of RPMI. Cell viability was assessed 24 hours later, and results are expressed as percent of RPMI control (n=10). Results are representative of at least three independent experiments. Error bars represent the SEM. (B and C) Agr-mediated quorum sensing was monitored using *agr*P3-dependent YFP expression in WT or *srrA*::Tn strains grown aerobically or hypoxically as above. YFP relative fluorescent units (RFUs) were averaged from 3 technical replicates. Error bars represent the SD. Data shown are an average of 3 biologically independent experiments. (B) RFUs monitored at 0, 6, 9, 12, and 15 hours after back-dilution from overnight culture. (C) RFUs measured at 15 hours post back-dilution from overnight culture (n=3). (D) cDNA samples from WT or *srrA*::Tn strains grown aerobically or hypoxically as above were subjected to qRT-PCR. Graph depicts fold change of the indicated transcripts relative to WT aerobic transcript level. Data shown are an average of 3 biologically independent experiments. Significance was determined by two-way ANOVA. * denotes $p<0.05$, ** denotes $p<0.01$, and *** denotes $p<0.001$ relative to WT aerobic. Error bars represent SEM.

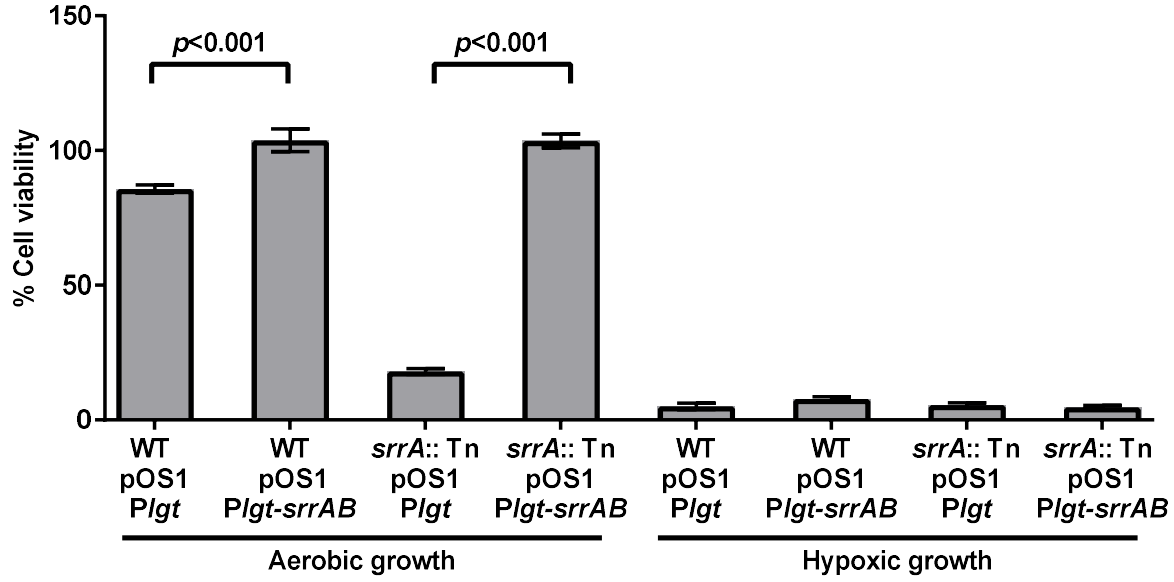

Figure 16. Expression of SrrAB in trans decreases cytotoxicity of aerobic cultures. MC3T3 cells were intoxicated with 30% total media volume of RPMI control or concentrated supernatant from the indicated strains after aerobic or hypoxic growth. Cell viability was determined 24 hours after intoxication. Results are expressed as percent of RPMI control (n=10). Error bars represent the SEM. Significance was determined by Student's *t* test.

Culture pH mediates oxygen responsive virulence production

We hypothesized that decreased oxygen concentrations in hypoxic cultures induce elevated cytotoxicity in an SrrAB dependent manner. To test this, we used a hypoxic chamber and cultured bacterial supernatants under various oxygen concentrations from 21% (atmospheric) to 1% oxygen. Surprisingly, no oxygen concentration tested replicated the cytotoxicity of hypoxic cultures (**Figure 17A**). We next hypothesized that elevated carbon dioxide in capped cultures may mediate the hypertoxicity of hypoxic cultures. To test this, we used a carbon dioxide incubator to culture bacterial supernatants under atmospheric oxygen and a range of carbon dioxide concentrations from 0% (atmospheric) to 5% (physiologic). Interestingly, elevated carbon dioxide also caused elevated cytotoxicity, similar to that found in capped "hypoxic" flasks (**Figure 17B**). This cytotoxicity was still dependent upon PSMs, as supernatants from a Δ*psm* mutant were nontoxic under these conditions (**Figure 17C**). Curiously, the phenol red indicator in RPMI indicated that in all growth conditions exhibiting cytotoxicity towards cultured cells, the supernatants were acidic. *S. aureus* is known to acidify culture media as a result of acetate production during exponential growth, and this acidification is exacerbated during fermentative growth under low oxygen conditions (52, 113, 114). To test the hypothesis that *S. aureus* acidification of growth media causes increased cytotoxicity, we grew WT *S. aureus* in RPMI with increased bicarbonate to improve the buffering capacity of the media. Although standard RPMI contains 0.2% bicarbonate, we found that elevating the bicarbonate concentration to 0.4% decreased the cytotoxicity of hypoxically grown culture supernatants (**Figure 17E**). We hypothesized that the reciprocal would also occur: supernatants from aerobic cultures grown in media with reduced buffering capacity would be more cytotoxic. As expected, *S. aureus* acidified cultures more quickly in media with decreased bicarbonate buffering capacity. Furthermore, even

after returning the pH of supernatants to 7.4 following 15 hours of growth, supernatants from media with decreased bicarbonate buffering capacity had elevated cytotoxicity, which was dependent upon PSMs (**Figure 17G**). The effects of pH on cytotoxicity are not dependent upon bicarbonate buffering, as cultures that are manually maintained at a pH of 7.4 are also non-cytotoxic (**Figure 17H**). The effect of pH on toxin production is not unique to USA300 strain LAC, however pH may drive differing regulation of toxin production, as decreased buffering capacity during growth decreased cytotoxicity of MW2 supernatants (**Figure 18**). These results indicate that the decreased pH of cultures during fermentative growth mediates the oxygen responsive cytotoxicity observed previously.

Because SrrAB controls a variety of metabolic and fermentative genes, we hypothesized that supernatants from an *srrA* mutant may become more acidic during growth than WT, which might induce the elevated cytotoxicity of an *srrA* mutant observed previously (**Figure 15A**). To test this, we measured the pH of an *srrA* mutant throughout growth and found that although these mutants are slightly more acidic than WT cultures, they do not reach the pH required to induce cytotoxicity in WT cultured supernatants (**Figure 17I**). This suggests that the elevated cytotoxicity of an *srrA* mutant is indeed due to SrrAB regulation of cytotoxicity and not due to indirect effects on cytotoxicity through pH.

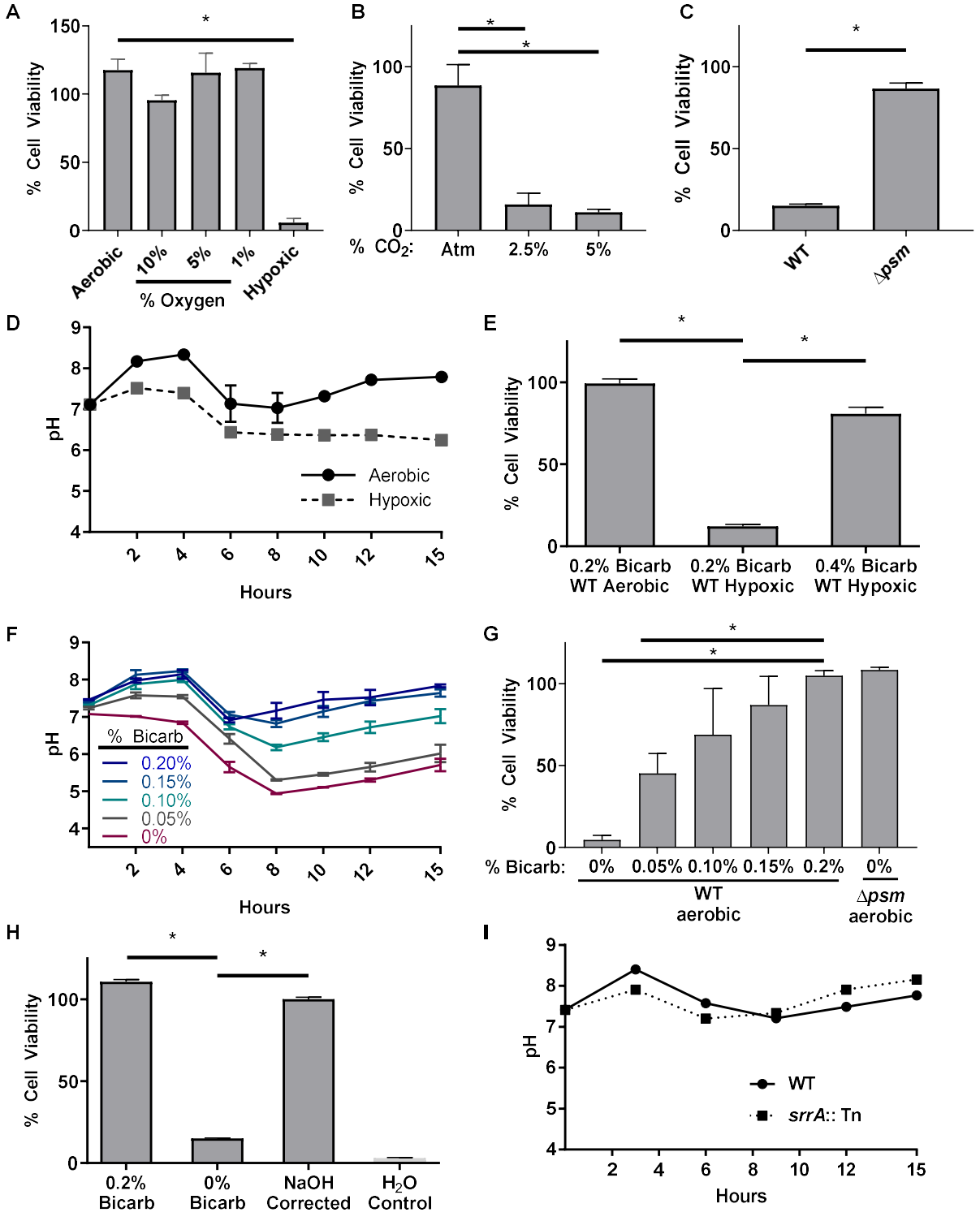
A
% Cell Viability
150
100
50
0
*
Aerobic
10%
5%
1%
Hypoxic
% Oxygen
B
% Cell Viability
100
50
0
*
*
% CO2:
Atm
2.5%
5%
C
% Cell Viability
100
50
0
*
WT
Δpsm
D
pH
9
8
7
6
5
4
Aerobic
Hypoxic
2
4
6
8
10
12
15
Hours
E
% Cell Viability
100
50
0
*
*
0.2% Bicarb
WT Aerobic
0.2% Bicarb
WT Hypoxic
0.4% Bicarb
WT Hypoxic
F
pH
9
8
7
6
5
4
% Bicarb
0.20%
0.15%
0.10%
0.05%
0%
2
4
6
8
10
12
15
Hours
G
% Cell Viability
100
50
0
*
*
% Bicarb:
0%
0.05%
0.10%
0.15%
0.2%
0%
WT
aerobic
Δpsm
aerobic
H
% Cell Viability
100
50
0
*
*
0.2%
Bicarb
0%
Bicarb
NaOH
Corrected
H2O
Control
I
pH
9
8
7
6
5
4
WT
srrA:: Tn
2
4
6
8
10
12
15
Hours

Figure 17. Decreases in culture pH during hypoxic growth mediates *S. aureus* virulence factor production. Cultures of WT *S. aureus* were prepared by inoculating RPMI and 1% Casamino acids with a 1:1000 dilution from overnight cultures and growing for 15 hours. (A) Cultures were grown either aerobically in atmospheric gas levels, hypoxically in a capped flask, or in a hypoxic chamber with controlled oxygen content. (B and C) Cultures were grown in a CO2 incubator with atmospheric oxygen. (E-H) Cultures were grown in RPMI lacking bicarbonate buffer with indicated bicarbonate percentages added and 1% Casamino acids under atmospheric conditions. (H) The pH of each culture was monitored and corrected hourly to a pH of 7.4 with NaOH or treated with a vehicle control. (A-C, E, G, H) MC3T3 cells were seeded into 96 well plates at 5,000 cells per well. After 24 hours, growth media was replaced, and 20% of the total media volume was replaced with concentrated culture supernatant grown as indicated, or an equivalent volume of RPMI unless otherwise indicated. Cell viability was assessed 24 hours later. Results are expressed as percent of RPMI control (n=10). (A, B, G) Results are average of at least three independent experiments. (C, E, H) Results are representative of at least two independent experiments. Error bars represent the SEM. * indicate $p < 0.05$. Significance determined by Student's *t* test. (D, F, I) Culture pH was measured in intervals for 15 hours. Results are the average of two (D), three (F), or one (I) biologic replicates. Error bars represent SEM.

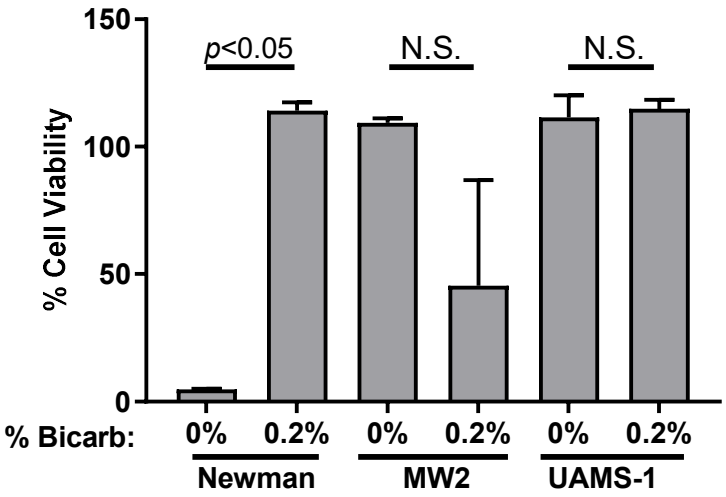

Figure 18. The effect of pH on cytotoxicity may be strain dependent. Cultures of WT *S. aureus* were prepared by inoculating RPMI and 1% Casamino acids with a 1:1000 dilution from overnight cultures and growing for 15 hours either aerobically in atmospheric gas levels. MC3T3 cells were seeded into 96 well plates at 5,000 cells per well. After 24 hours, growth media was replaced, and 20% of the total media volume was replaced with concentrated culture supernatant grown as indicated. Cell viability was assessed 24 hours later, and results are expressed as percent of RPMI control (n=10). Results are the average of two independent experiments. Error bars represent the SEM. Significance determined by Student's *t* test.

An *srrA* and *srrB* mutant have differing virulence responses and survival *in vivo*, indicating atypical TCS regulation

Our results indicate that SrrAB is required for regulation of toxin production during growth *in vitro*. According to prototypical TCS models, phosphorylation of SrrA dictates DNA binding activity. However, SrrA has been shown to be capable of binding the *agr* promoter in the absence of phosphorylation (28). We were curious then if SrrB is required for the elevated cytotoxicity and decreased survival *in vivo* observed previously. To test this, we compared the activation of Agr-mediated quorum sensing using the *agrP3* – YFP reporter plasmid pDB59 in an *srrA*::Tn versus an *srrB*::Tn mutant. Interestingly, an *srrB* mutant had decreased YFP production during aerobic growth at 15 hours compared to an *srrA* mutant, and was not significantly different from WT (**Figure 19A**). These results suggest that SrrA is functional for repression of the *agr* locus under aerobic conditions, despite the absence of phosphorylation by the cognate sensor kinase, SrrB. We then tested if SrrB is required for survival *in vivo* during osteomyelitis. Surprisingly, at 14 days post-infection, the bacterial burdens of an *srrB* mutant do not significantly differ from WT (**Figure 19B**). These studies suggest that SrrA functionality is not dependent upon phosphorylation by SrrB, and may in fact have regulatory activity in both phosphorylated and un-phosphorylated states.

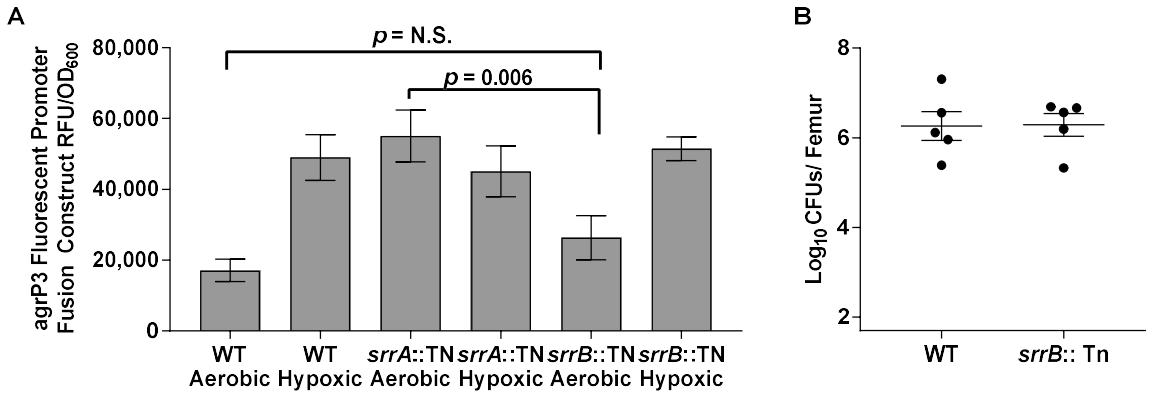

Figure 19. An *srrA* and *srrB* mutant have differing virulence responses and survival *in vivo.* (A) Cultures were prepared by inoculating RPMI and 1% CA with a 1:1000 dilution from overnight cultures and growing for 15 hours either aerobically or hypoxically. Agr-mediated quorum sensing was monitored using *agr*P3-dependent YFP expression in WT, *srrA*::Tn, or *srrB*::Tn strains. YFP relative fluorescent units (RFUs) were averaged from 3 technical replicates. Error bars represent the SD. Data shown are an average of 3 biologically independent experiments. RFUs measured at 15 hours post back-dilution from overnight culture (n=3). (B) Osteomyelitis was induced in groups of mice using WT and *srrB*::Tn strains. At 14 days post-infection, femurs were processed for colony forming units (CFU) enumeration. N=5 mice per group and horizontal line represents the mean. Error bars represent the SEM. Statistical significance determined by Student's *t* test. The data from WT was also utilized to generate the red circles in Figure 2D.

Discussion

TnSeq analysis during experimental osteomyelitis revealed *S. aureus* genes essential for invasive infection. Among the mutants with reduced *in vivo* fitness was one TCS, SrrAB, which was previously characterized as a coordinator of hypoxic and nitrosative stress responses (59). SrrAB is postulated to sense reduced menaquinones, however the exact mechanism by which this system modulates quorum sensing in response to the redox status of the cellular menaquinone pool has yet to be determined (76).

Our data suggest that aerobic growth of *S. aureus* limits quorum sensing and *agr*-dependent virulence factor production in a manner that is partially dependent on SrrAB (**Figure 20**). Conversely, hypoxic growth results in significantly increased cytotoxicity toward mammalian cells. Since equivalent bacterial densities were achieved under conditions of hypoxic and aerobic growth, these results imply that the output of quorum sensing can be functionally uncoupled from bacterial density by changes in culture oxygenation. Such uncoupling could be particularly advantageous for quenching of virulence factor production in environments with higher oxygen availability, such as during colonization of the skin or nares. Since inactivation of SrrAB under aerobic conditions failed to fully restore quorum sensing and cytotoxicity to the levels observed with hypoxic growth, it is likely that this phenomenon is a result of multiple factors. Additional studies are therefore needed to determine the SrrAB-dependent and SrrAB–independent mechanisms by which oxygenation regulates quorum sensing. To this end, it has previously been demonstrated that both the *S. aureus* AIP and AgrA can be functionally inactivated by oxidation (115, 116), suggesting a potential SrrAB-independent mechanism for modulation of quorum sensing by oxygen. Moreover, the *S. aureus* genome is known to encode other redox-sensitive regulators such as Rex, MgrA, SarA, and AirSR (116-120). It is therefore possible that

environmental oxygen is not a direct regulator of quorum sensing, but rather that a change in the redox status of the bacterial cell or oxidative damage triggers changes in virulence factor production. Alternatively, previous literature indicates that pH extremes can modify the lactone ring of quorum sensing molecules, and AIP is commonly inactivated *in vitro* using alkaline hydrolysis (121, 122). Based on the known sensitivity of lactone rings to alkaline mediated hydrolysis, we predict that the acidic pH found in our culture conditions stabilizes AIP and increases signaling though the Agr system. Our data suggest that acidification of the host environment due to bacterial mixed acid fermentation products may link the apparent oxygen responsiveness of quorum sensing under reduced oxygen conditions. Nevertheless, our findings suggest that shifts in available oxygen, as well as the inherent differences in physiologic oxygen concentrations in various host tissues, could have a significant impact on staphylococcal virulence. Additionally, these data highlight the importance of *in vitro* culture conditions on the study of staphylococcal virulence.

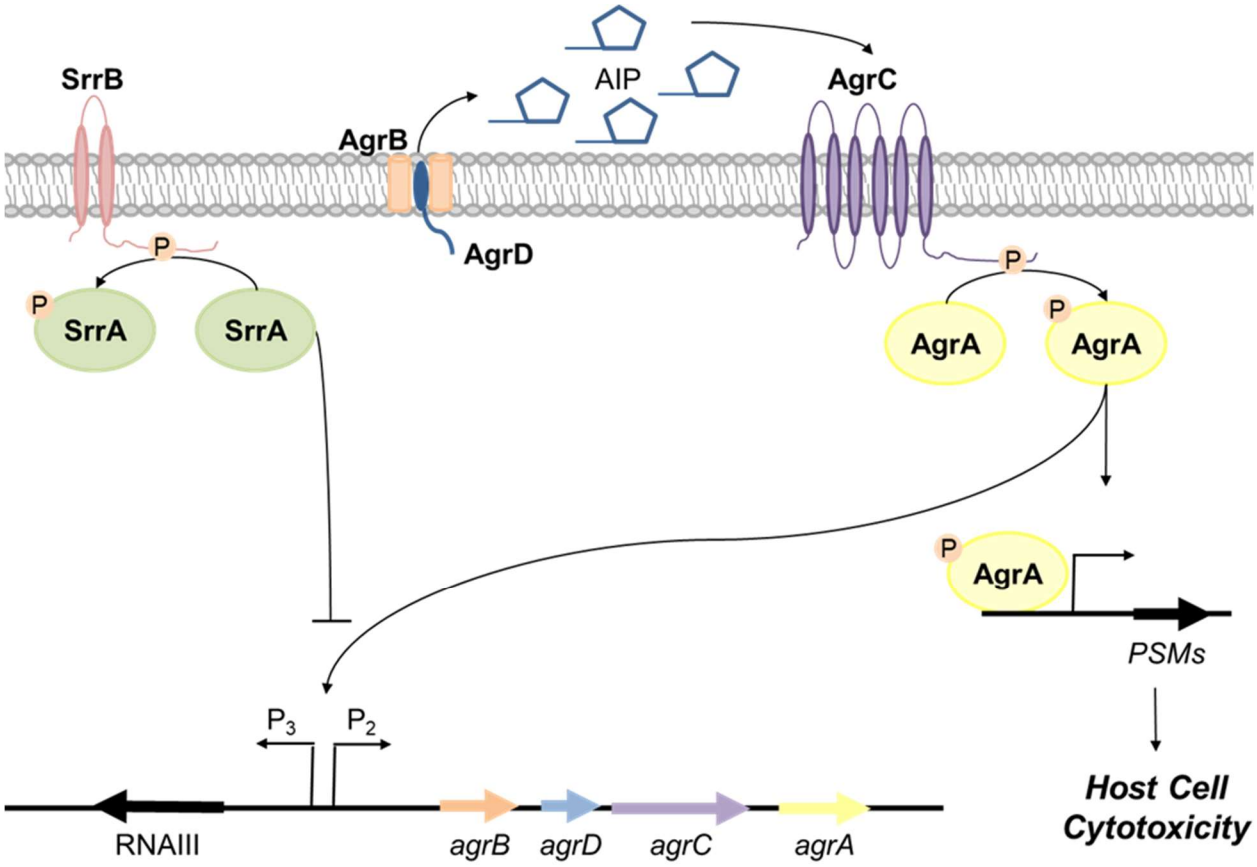

Figure 20. Schematic of *S. aureus agr* regulation.

A quorum sensing reporter revealed that *srrA* and *srrB* mutants exhibit divergent responses *in vitro*. SrrA belongs to the OmpR/PhoB family of response regulators (28). Prototypically, DNA binding and transcriptional regulation of OmpR family response regulators are activated by phosphorylation by the corresponding sensor kinase (35). However, our data indicate that SrrB is not required for functionality of SrrA *in vitro* or *in vivo*. Interestingly, the *B. subtilis* SrrA homolog, ResD, expresses both phosphorylation-dependent and phosphorylation-independent regulation of transcriptional activity (33,34). These studies suggest that SrrA has regulatory activity in both phosphorylated and un-phosphorylated states, and moreover, that phosphorylation status of SrrA may dictate target specificity. Alternatively, these results could also indicate TCS "cross talk" or "cross regulation", in which a non-cognate sensor kinase regulates SrrA in the absence of SrrB. These possibilities will be the topic of further study in our laboratory. Furthermore, these studies highlight the importance of examining TCSs both as a whole, and as individual components.

Global transcriptional analyses defined the SrrAB regulon of *S. aureus* under conditions of aerobic and hypoxic growth. Interestingly, although some overlap was noted with the previously reported SrrAB nitrosative stress regulon, we identified additional SrrAB-regulated genes under conditions of changing oxygenation (59). Although these findings may relate to technical issues or strain-dependent differences in gene regulation, they suggest that SrrAB may integrate multiple environmental signals, or that oxidative and nitrosative stress trigger a common endogenous bacterial pathway that activates SrrAB. In order to begin defining the host components that trigger hypoxic or nitrosative stress responses in *S. aureus*, we examined the role of neutrophils during osteomyelitis. Neutrophils impose nitrosative and oxidative stress to invading pathogens through the respiratory burst, which generates reactive oxygen and nitrogen species. Moreover, neutrophils contribute to tissue hypoxia through abscess formation (38). In support of the role of SrrAB in

resisting such hypoxic and nitrosative stresses, we found that neutrophil depletion rescued the virulence defect of an *srrA* mutant. Additional studies are needed to parse out the effects of neutrophil-derived reactive oxygen and nitrogen species versus abscess-associated tissue hypoxia on the survival of *S. aureus*. Furthermore, it is likely that other innate and adaptive immune responses contribute to changes in tissue oxygenation and thus the redox status of invading pathogens.

In addition to the genes encoding SrrAB and its targets, TnSeq analysis during osteomyelitis revealed a large number of staphylococcal mutants with compromised fitness *in vivo*. Many of the genes identified as essential or compromised during *in vivo* growth can be broadly classified as associated with metabolism. In contrast, very few prototypical virulence factors were identified as essential for osteomyelitis. The lack of traditional secreted virulence factors identified through TnSeq analysis is not surprising due to the nature of the technique. Infection with a pooled transposon library allows for mutants deficient in a particular gene to potentially co-opt bacterial factors from other mutants. Indeed, this phenomenon has been characterized for the exchange of metabolic intermediates in *S. aureus*, and it is conceivable that secreted virulence factors could be "shared" in a similar manner (109). An additional limitation of the technique is the short outgrowth step in BHI following harvest of the transposon library from the infected femur. This outgrowth step may allow recovery of mutants *in vitro* that are unfit during infection. Despite this shortfall, the outgrowth step was necessary to decrease the amount of murine DNA present in the femur homogenate and allow for effective sequencing of bacterial DNA and is a common adjustment in Tnseq (45, 95, 102).

TnSeq analysis of staphylococcal osteomyelitis paralleled a previous TnSeq analysis of staphylococcal growth in soft tissue abscesses (45). In fact, 40 of the 65 genes identified as

essential for growth during osteomyelitis were also essential for growth in murine abscesses. This observation is consistent with our previous data showing that osteomyelitis is characterized by exuberant abscess formation in the bone marrow (12), and suggests common stresses are encountered by staphylococci in neutrophil-rich inflammatory lesions. However, 25 of the 65 genes essential for intraosseous survival were not found to be essential for abscess growth, and may reflect unique adaptations to colonization of skeletal tissues.

Of the genes required for *S. aureus* survival during invasive infection, many encode hypothetical proteins or proteins without a previously characterized role in virulence. This observation highlights the power of TnSeq analysis as an unbiased evaluation of the genetic requirements for bacterial survival in host tissues. In summary, the results of this chapter elucidate bacterial survival strategies during invasive infection, link changes in environmental oxygen to staphylococcal quorum sensing and virulence, and provide a firm foundation to identify new targets for antimicrobial and vaccine design.

Materials and Methods

Bacterial strains and growth conditions

The *S. aureus* TnSeq library in strain HG003 has been previously described (45). All other experiments were conducted in an erythromycin-sensitive, tetracycline-sensitive derivative of the USA300 strain LAC (AH1263), which served as the WT unless otherwise noted (153). Strain LACΔ*psmα1-4* has been previously described (12, 154). Strains *srrA*::Tn, *srrB*::Tn, *qoxA*::Tn, *qoxC*::Tn, *pflA*::Tn, *pflB*::Tn, and *cydA*::Tn in the LAC background were created by bacteriophage phi-85-mediated transduction of *erm*-disrupted alleles from the respective JE2 strain mutants obtained from the NARSA transposon library (155). Strains Δ*psm* pOS1-*p*lgt and Δ*psm* pOS1-*p*lgt-*hla* were provided by Dr. Juliane Bubeck-Wardenburg (111). Construction of strain LAC

Δ*RNAIII* is described below. Plasmid pDB59 (*agr*-P3-YFP) was electroporated into LAC *srrA*::Tn, or *srrB*::Tn for monitoring of *agr*-dependent quorum sensing (112). All strains were grown in glass Erlenmeyer flasks at 37°C with orbital shaking at 180 rpm. All S. *aureus* strains were grown in Tryptic Soy Broth (TSB), Brain-Heart Infusion (BHI), Roswell Park Memorial Institute medium (RPMI) supplemented with 1% casamino acids (CA), or RPMI with 1% CA lacking bicarbonate. *Escherichia coli* was grown in Luria Broth (LB). Erythromycin and chloramphenicol were added to cultures at 10 μg ml^{-1} where indicated. Ampicillin was added to cultures at 100 μg ml^{-1} where indicated. Cadmium chloride was added to cultures at 0.1 mM where indicated. A 5:1 flask to volume ratio was utilized unless otherwise noted. For comparative growth analyses, overnight aerobic cultures were back-diluted 1:1000 into fresh TSB or BHI media and optical density at 600 nm (OD_{600}) was monitored over time. Culture pH monitored by pH meter as indicated.

Construction of LAC Δ*RNAIII*

RNAIII including upstream and downstream flanking regions were amplified using primers 5'-GCATGCGTCGATATCGTAGCTGGGTCAG-3' and 5'-GAATTCGAAGTCACAAGTACTATAAGCTGCG-3', and cloned into the *Hinc*II site of pUC18 (156) to create pGAW1. To delete RNAIII, inverse PCR was performed with primers 5'-TTTGGGCCCTATATTAAAACATGCTAAAAG-3' and 5'-TTTCTCGAGGTAATGAAGAAGGGATGAGTT-3' amplifying RNAIII flanking regions and the remaining plasmid backbone of pGAW1. The vector was religated after treatment with Polynucleotide Kinase (New England Biolabs, MA) and designated pGAW3. To insert an antibiotic resistance cassette, pGAW3 was digested with *Apa*I and *Xho*I, religated with the *Apa*I-*Xho*I fragment from pJC1075 (157) (*cadCA*, conferring resistance to cadmium) and designated

pGAW6. The *Sph*I- *Kpn*I fragment from pGAW6 was cloned into the allelic replacement vector pJC1202 (157) using the same restriction sites and designated pGAW7. Strain RN4220 was electroporated with plasmid pGAW7 and plated on GL agar containing 5 μg chloramphenicol ml^{-1} at 30 °C. Allelic exchange was carried out as previously described (157). Phage 80a was then used to transduce the mutation into LAC to generate LAC *RNAIII::cad*, herein designated LAC Δ*RNAIII*.

Construction of an SrrAB overexpression plasmid

To express *srrAB* in trans, the *srrAB* open reading frame was PCR amplified from genomic DNA of LAC using primers 5'-ATCTCGAGATGTCGAACGAAATACTTATCG-3' and 5'-ATGGATCCTTCAATTTTATTCTGGTTTTGGTAG-3'. The resulting *srrAB* amplicon was then cloned into the shuttle vector pOS1 under control of the *lgt* promoter (158). As a control, wild type and *srrA*::Tn strain LAC were transformed with pOS1-*lgt* lacking an insert.

Construction of a luminescent SrrAB reporter

To examine expression of SrrAB *in vivo the srrAB* promoter was PCR amplified from genomic DNA of LAC using primers 5'-TACCCGGGTGTATTTATCACAAAGTTTGAGAAT-3' and 5'-ATCGTCGACACAGGTCATACCTCCCAC-3'. The resulting amplicon was then cloned into the shuttle vector pAmilux. As a control, wild type stain LAC was transformed with pAmilux lacking an insert.

Murine model of osteomyelitis and micro-computed tomographic analysis

All experiments involving animals were reviewed and approved by the Institutional Animal Care and Use Committee of Vanderbilt University and performed according to NIH guidelines, the Animal Welfare Act, and US Federal law. Osteomyelitis was induced in 7- to 8-week old female C57BL/6J mice as previously reported (12). An inoculum of $1x10^6$ CFU in 2 μl PBS was delivered

into murine femurs. For some experiments, mice were rendered neutropenic by serial intraperitoneal injections of an anti-Ly6G (clone 1A8) monoclonal antibody (BioXcell, West Lebanon, NH) at days -3, 0, 4, 7, and 10 post-infection. As a control, mice received serial injections of an isotype control antibody (rat IgG2a). At various times post-infection, mice were euthanized and the infected femur was removed and either processed for CFU enumeration or imaged by micro-computed tomography (microCT). For CFU enumeration, femurs were homogenized and plated at limiting dilution on Tryptic Soy Agar (TSA). Analysis of cortical bone destruction was determined by microCT imaging as previously described (12). Differences in cortical bone destruction and bacterial burdens were analyzed using Student's *t* test.

Intravital measurements of oxygen concentration

Intravital oxygen concentrations were measured in infected femurs using an Oxylite (Oxford Optronix, United Kingdom) oxygen and temperature monitor in conjunction with a flexible bare-fibre sensor. Mice were anesthetized with isoflurane and the surgical incision was re-opened. Oxygen readings were obtained by insertion of the sensor directly through the intramedullary canal and into the infectious focus. Measurements from the probe were recorded at least 5 minutes after probe placement to allow for temperature equilibration and stabilization of oxygen readings.

Transposon sequencing analysis of experimental acute osteomyelitis

The *S. aureus* TnSeq library in the HG003 background has been previously described (45). In order to identify potential bottlenecks in the murine osteomyelitis model that could confound TnSeq analysis, groups of mice were first infected with strain HG003 using an inoculum of $5x10^6$ CFU and then at various times post-infection the infected femurs were collected and processed for CFU enumeration. Day 5 was chosen as a timepoint for TnSeq analysis of acute osteomyelitis as it likely represents the first bottleneck encountered by invading bacteria. To prepare the TnSeq

library for inoculation into murine femurs, an aliquot of the library containing $5x10^7$ CFU/ml was thawed and inoculated into 100 ml of BHI media in a 500 ml Erlenmeyer flask. This culture was incubated at 37°C for 12 hours and then back-diluted 1:100 into fresh BHI at the same flask to volume ratio and grown an additional 3 hours. Bacterial cells were harvested by centrifugation and resuspended in PBS to a concentration of $7x10^6$ CFU in 2 µl PBS. Genomic DNA was prepared from this inoculum using a Qiagen DNeasy Kit with 40 µg ml^{-1} lysostaphin added to the lysis buffer. The inoculum was used to initiate experimental osteomyelitis in groups of mice as above. Another equivalent aliquot of the inoculum was seeded into a 50 ml BHI culture in a 250 ml Erlenmeyer flask. This culture was grown for 24 hours, after which time the bacterial cells were harvested and genomic DNA was prepared as above. This genomic DNA served as the *in vitro* comparator for TnSeq analysis. At 5 days post-infection, mice inoculated with the TnSeq library were euthanized, and the infected femurs were harvested and homogenized in 1 ml of PBS. 500 µl of this homogenate was archived by freezing at -80°C in 20% glycerol and the remaining 500 µl of the homogenate was seeded into 4ml of BHI media and cultured at 37°C and 180 rpm shaking for 5.5 hours. Bacteria were then collected by centrifugation and subjected to genomic DNA preparation as above. Recovered bacteria from 2 mice were pooled, and 3 biologically independent groups of mice were analyzed separately. Genomic DNA samples were subsequently prepared for sequencing on an Illumina HiSeq 2000 (Tufts University Genomic Core Facility). Sequencing, data analysis, and fitness calculations were performed as previously reported (45). Briefly, a "dval" was calculated for each gene in each condition (inoculum, *in vitro* comparator, or osteomyelitis). The dval represents the observed number of mappable reads of insertions in a gene, divided by the number of mappable reads of insertions predicted for that gene based on its size relative to the genome and the total number of mappable reads obtained for that experiment. Genes with dval of

≤0.01 were considered "essential" in a given condition. Genes with dval of >0.01 but ≤0.1 were considered "compromised" in a given condition, whereas genes with dval >0.1 were considered "fit". A dval ratio was calculated by dividing the dval of a given gene in osteomyelitis by the dval of the same gene during *in vitro* comparator growth.

RNA isolation and Genechip analysis

For genechip analysis, aerobic cultures of WT or *srrA*::Tn were prepared as follows. Three colonies of WT or *srrA*::Tn were inoculated into 10 ml of TSB in a 50 ml Erlenmeyer flask. This culture was grown overnight then back-diluted 1:1000 into 50 ml of TSB in a 250 ml flask. The back-diluted cultures were grown at 37°C and 180 rpm orbital shaking until OD_{600} reached 0.5, at which time an equal volume of ice-cold 1:1 acetone: ethanol was added, and the cultures were stored at -80°C until processed for RNA isolation. For comparison of RNA from aerobic versus hypoxic conditions, TSB cultures of WT or *srrA*::Tn were incubated overnight as above, back-diluted 1:1000 into 100 ml of TSB in a 500 ml flask and grown to an OD_{600} of 0.5. Fifty milliliters of the culture were then placed into a tightly capped 50ml conical (hypoxic condition) and incubated for one hour at 37°C before mixture with acetone: ethanol and storage at -80°C. The remaining 50 ml of culture was moved to a 250 ml Erlenmeyer flask (aerobic condition) and incubated for one hour at 37°C before mixture with acetone: ethanol and storage at -80°C. For RNA isolation, bacterial cells were harvested by centrifugation and resuspended in LETS buffer (0.1 M LiCl, 10 mM EDTA, 10 mM Tris HCl, 1% SDS). The resuspended cells were disrupted in the presence of 0.5 mm RNAase-free zirconium oxide beads in a Bullet Blender (Next Advance, Averill Park, NY, USA). Disrupted cells were heated at 55°C for 5.5 minutes and centrifuged for 10 minutes at 15,000 rpm. The upper phase was collected and transferred to a new tube before adding 1 ml of TRI-Reagent. After mixing, 200 µl of chloroform was added, and the resultant

solution was mixed vigorously for 15 seconds. Samples were centrifuged at 15,000 rpm for 10 min, and the aqueous phase was transferred to a new tube. RNA was precipitated with isopropyl alcohol and subsequently washed with 70% ethanol before drying and resuspension in deionized water. RNA samples were subsequently treated with DNase I and re-purified with a GeneJET RNA Cleanup Kit (Thermo Fisher Scientific, Waltham, MA, USA).

For Genechip analysis, RNA samples were labeled, hybridized to commercially available *S. aureus* Affymetrix Genechips, and processed as per the manufacturer's instructions (Affymetrix, Santa Clara, CA, USA). Briefly, 10 µg of each RNA sample was reverse transcribed, resulting cDNA was purified using QIAquick PCR Purification Kits (Qiagen, Germantown, MD, USA), fragmented with DNase I (Ambion, Carlsbad, CA, USA), and 3' biotinylated using Enzo Bioarray Terminal Labeling Kits (Enzo Life Sciences, Farmingdale, NY, USA). A total of 1.5 µg of a labeled cDNA sample was hybridized to a *S. aureus* GeneChip for 16 hr at 45°C, processed, and scanned in an Affymetrix GeneChip 3000 7G scanner as previously described (159, 160). Signal intensity values for each GeneChip qualifier were normalized to the average signal of the microarray to reduce sample labeling and technical variability and the signal for the biological replicates were averaged using GeneSpring GX software (Agilent Technologies, Redwood City, CA, USA) (160-163). Differentially expressed transcripts were identified as RNA species that generated a two-fold increase or decrease in WT cells in comparison to *srrA*::Tn cells during aerobic and hypoxic conditions (*t*-test, $p = 0.05$). All related GeneChip data files were deposited in the NCBI Gene Expression Omnibus repository in the MIAME-compliant format.

Supernatant preparations

S. aureus strains were used to inoculate RPMI + 1% CA in glass Erlenmeyer flasks. For aerobic growth, the flask opening was covered lightly with aluminum foil. For hypoxic growth, the flask

opening was sealed with a rubber stopper. Cultures were grown for 15 hours. Supernatants were collected after culture centrifugation and were subsequently filtered through a 0.22 μm filter and concentrated with an Amicon Ultra 3 kDa nominal molecular weight limit centrifugal filter unit (Millipore, Billerica, MA, USA) per the manufacturer's instructions. Following concentration, supernatants were filter sterilized again and frozen at -80°C until used.

Mammalian cell culture and cytotoxicity assays

Primary human osteoblasts were obtained from Lonza (Basel, Switzerland) and cultured per manufacturer's recommendations. All cell lines were obtained from the American Type Culture Collection (ATCC) and propagated at 37°C and 5% CO_2 according to ATCC recommendations. Media was replaced every 2-3 days. All cell culture media was prepared with 1X penicillin/streptomycin and filter sterilized using a 0.22 μm filter prior to use. MC3T3 E-1 cells were cultured in α-MEM, supplemented with 10% fetal bovine serum (FBS). The RAW264.7, Saos-2, and A549 cell lines were grown in Dulbecco's MEM (DMEM) with 10% FBS, McCoy's 5A medium with 15% FBS, and F-12K medium with 10% FBS, respectively. The Jurkat, U937, and HL-60 cell lines were propagated using RPMI with 10% FBS. Cytotoxicity assays were performed in 96-well tissue culture grade plates. Cells were seeded one day prior to intoxication with *S. aureus* concentrated supernatants or sterile RPMI diluted in the recommended cell culture medium. The following cell densities were used for cytotoxicity assays: MC3T3 E1 murine pre-osteoblastic cells at 5,000 cells per well, primary human osteoblasts at 3,500 cells per well, Saos-2 human osteoblastic cells at 10,000 cells per well, RAW264.7 murine macrophage cells at 10,000 cells per well, A549 lung epithelial cells at 5,000 cells per well, U937 monocytic cells at 15,000 cells per well, HL-60 premyelocytes at 20,000 cells per well, and Jurkat T cells at 50,000 cells per well. Concentrated supernatants were added as dilutions, by mixing between 0.1 μl to 60 μl in a

total volume of 200 µl per well to give a dilution spectrum of 0.05%-30% concentrated supernatant (volume/volume). Cell lines in suspension were centrifuged at 3000 x g for 5 minutes prior to intoxication. Cell viability was assessed with CellTiter AQueous One (Promega, Madison, WI, USA) per the manufacturer's instructions at 24 hours post-intoxication.

YFP fluorescence measurements

For fluorescence analysis, overnight cultures of WT, *srrA*::Tn, and *srrB*::Tn containing the pDB59 reporter plasmid were back-diluted 1:1000 into 10 ml of RPMI + 1% CA with chloramphenicol in 50ml Erlenmeyer flasks and grown either aerobically or hypoxically as above. YFP was measured using an excitation of 485/20 and emission of 528/20 in a BioTek Synergy HT 96-well plate reader at 0, 6, 9, 12, and 15 hours after back-dilution.

Quantitative RT-PCR

Bacteria were grown for 15 hours as for YFP fluorescence measurements, mixed with 1:1 acetone: ethanol, and stored at -80°C until processed for RNA isolation. RNA isolation was performed as for Genechip analysis. Reverse transcription using 2 µg of RNA and M-MLV reverse transcriptase (Promega, Madison, WI, USA) was performed following the manufacturer's instructions. Quantitative RT-PCR (qRT-PCR) was performed using iQ SYBR Green Supermix (Bio-Rad, Hercules, Ca, USA) and the cDNA generated above for each primer pair, including a no reverse transcriptase negative control for 16S rRNA. PCR was conducted on a CFX96 qPCR cycler (Bio-Rad, Hercules, Ca, USA). The cycling program was carried out as recommended by the manufacturer with an annealing temperature of 56°C. Fold-changes were calculated from Ct values averaged from three technical replicates for at least three biological replicates after normalizing to 16S rRNA. The qRT-PCR primer sequences for *agrA*, *hla*, and *RNAIII* were previously published (164). The qRT-PCR primer sequence for 16S rRNA was also previously published (111).

Coauthor Contributions

Michael Valentino, Michael Gilmore, Eric Skaar, Jim Cassat, and I conceived and designed the experiments, and analyzed the data. Dan Snyder assisted with infections and growth curves. Nicole Putnam assisted with cytotoxicity assays. Neal Hammer and Jim Cassat assisted with infections. Zach Lonergan provided significant intellectual contributions. Scott Hinger isolated RNA. Esar Aysanoa, Michael Valentino, Michael Gilmore, and Jim Cassat contributed to TnSeq analysis. Catlyn Blanchard and Paul Dunman assisted with microarray analysis. Gregory Wasserman, John Chen, Paul Dunman, and Bo Shopsin contributed reagents/materials/analysis tools. I performed all other experiments.

CHAPTER III: SKELETAL NUTRIENT AVAILABILITY DRIVES HOST-PATHOGEN INTERACTIONS DURING *S. AUREUS* OSTEOMYELITIS

Introduction

In Chapter II, we identified metabolic genes as being significant drivers of pathogenesis in skeletal tissues using TnSeq. The importance of metabolism in pathogenesis is not surprising, as bacteria are known to require up to 13 biosynthetic intermediates for life (**Figure 21**) (123). Unfortunately, the competitive nature of TnSeq addressed in the discussion section of Chapter II, prevents a detailed analysis of metabolic pathways from being conducted, due to the ability of pathogens to cross-feed metabolites and complement metabolic defects (109). In order to better understand the metabolic pathways that allow *S. aureus* to survive within the nutritional milieu of bone, we therefore conducted targeted mutagenesis to identify essential pathways within central metabolism for staphylococcal survival in bone. Our data elucidate the central metabolic pathways required for *S. aureus* replication and survival during a model of invasive infection. In the following chapter, we identify the transporter, GltT, as the sole aspartate importer in *S. aureus*. We demonstrate that aspartate generation serves as an essential biosynthetic node for generation of purines, and discover that aspartate biosynthesis is required, despite the presence of a functional aspartate transporter, due to competitive inhibition of aspartate transport through GltT by the structurally similar amino acid glutamate. Furthermore, our data reveal distinct differences in the glutamate concentrations of uninfected and infected bone, suggesting that *S. aureus* relies upon aspartate biosynthesis to overcome aspartate transport inhibition *in vivo*.

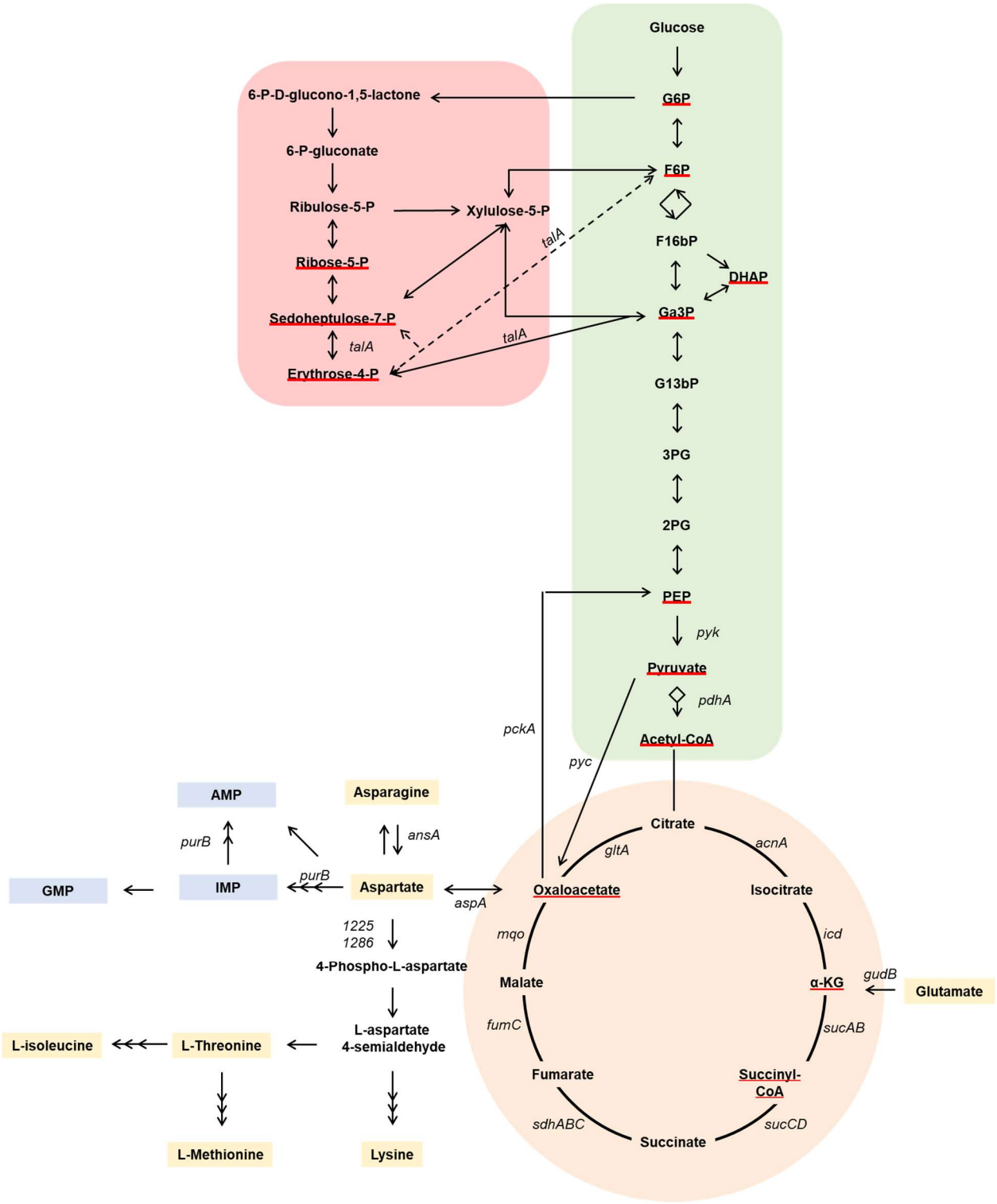
Glucose
G6P
6-P-D-glucono-1,5-lactone
6-P-gluconate
F6P
Ribulose-5-P
Xylulose-5-P
F16bP
Ribose-5-P
DHAP
talA
Sedoheptulose-7-P
Ga3P
talA
talA
Erythrose-4-P
G13bP
3PG
2PG
PEP
pyk
Pyruvate
pdhA
pckA
Acetyl-CoA
pyc
AMP
Asparagine
Citrate
purB
ansA
gltA
acnA
GMP
IMP
purB
Aspartate
Oxaloacetate
Isocitrate
aspA
1225
1286
mqo
icd
4-Phospho-L-aspartate
Malate
α-KG
gudB
Glutamate
L-isoleucine
L-Threonine
L-aspartate
4-semialdehyde
fumC
sucAB
Fumarate
Succinyl-
CoA
sdhABC
sucCD
Succinate
L-Methionine
Lysine

Figure 21. Schematic of *S. aureus* central metabolism. Metabolites are indicated in black standard text. Red underline indicates the 12 essential biosynthetic precursors. Genes of particular interest are notated in italics. Green box indicates glycolysis/gluconeogenesis. Red box indicates pentose phosphate pathway. Peach circle indicates TCA cycle. Yellow indicates amino acids. Blue indicates purine biosynthesis. Abbreviations: G6P (Glucose-6-Phosphate); F6P (Fructose-6-Phosphate); F16bP (Fructose 1,6-bisphosphate); DHAP (dihydroxyacetone); Ga3P (Glyceraldehyde 3-phosphate); G12bP (1,3- bisphosphoglycerate); G3P (3-phosphoglycerate); G2P (2-phosphoglycerate); PEP (phosphoenolpyruvate); Acetyl-CoA (Acetyl-coenzyme A); α-KG (α-ketoglutarate); IMP (Inosine monophosphate) AMP (adenosine monophosphate); GMP (Guanosine monophosphate).

Results

S. aureus does not require gluconeogenesis during osteomyelitis and successfully competes for glycolytic carbon sources during osteomyelitis

During osteomyelitis in humans, damaged tissue is characterized by sequestra of dead bone. These characteristic sequestra are also present within infected femurs within our murine osteomyelitis model (12, 124). Due to the abscesses that form within and around sequestra in infected bone, we hypothesized that bone supplies essential metabolites for *S. aureus* growth. Because osteoblasts and osteoclasts exhibit aerobic glycolysis, we further hypothesized that competition with the host for available glucose during osteomyelitis would necessitate the use of alternative carbon sources, like amino acids, to produce the six biosynthetic precursors generated from glycolysis/gluconeogenesis. Furthermore, collagen within the skeletal matrix is a highly abundant source of amino acids, particularly glycine, proline, and hydroxyproline. We therefore hypothesized that amino acid catabolic pathways would be essential for *S. aureus* survival during osteomyelitis. We tested the essentiality of amino acid catabolic pathways using a mutant in *pyc* (pyruvate into oxaloacetate) which encodes the first enzyme responsible for converting amino acids metabolized through pyruvate into gluconeogenic precursors (**Figure 21**). *Pyc* was also found to be essential/compromised in our TnSeq, indicating that gluconeogenesis may be required for *S. aureus* infection of bone. Using our murine model of osteomyelitis, we found that disruption of *pyc* had a significant effect on the fitness of *S. aureus* at 14 days post-infection (**Figure 22**). The product of Pyc, oxaloacetate, can be used in several additional pathways within central metabolism, therefore, to more directly test the role of gluconeogenesis in *S. aureus* pathogenesis during osteomyelitis, we tested a mutant in *pckA* (oxaloacetate into phosphoenolpyruvate) (**Figure**

22). We discovered that, although, *pyc* was essential for survival*, pckA,* and therefore gluconeogenesis, was not essential for survival during osteomyelitis.

Due to the absence of a survival defect in a gluconeogenic mutant *in vivo*, we revised our hypothesis and postulated that glucose may in fact be abundant *in vivo* to fuel the aerobic glycolysis phenotype of skeletal cells. To test this hypothesis, we examined the fitness of a glycolytic mutant *in vivo*. Using the glycolysis mutant *pyk* (phosphoenolpyruvate into pyruvate), we have found that *S. aureus* requires glycolysis to survive in bone, indicating that glycolysis is required to fuel *S. aureus* growth *in vivo* (**Figure 22**). Together, these results suggest that glycolysis may provide essential biosynthetic intermediates for *S. aureus in vivo* during an osteomyelitis model of invasive infection.

The pentose phosphate pathway is essential *in vitro*

An additional 3 biosynthetic intermediates can be produced using the pentose phosphate pathway. Because only one of the enzymes in this pathway is not essential for growth *in vitro*, we could only test the *talA* (transaldolase) mutant for survival *in vivo*. A *talA* mutant did not have a survival defect during osteomyelitis (**Figure 22**). Because TalA has been found to be redundant or dispensable in several other organisms, we cannot form a conclusion on the pentose phosphate pathway as a whole during osteomyelitis from this experiment. However, we expect that due to the role of the pentose phosphate pathway in essential cellular processes, enzymes within this pathway are likely to be required for growth and survival both *in vitro* and *in vivo*.

The TCA cycle is dispensable during a murine osteomyelitis model of invasive infection

In order to create additional essential biosynthetic precursors, *S. aureus* must utilize either the TCA cycle or anaplerotic reactions. From the TnSeq of osteomyelitis performed in chapter I, we identified several mutants in the TCA cycle as compromised for growth *in vivo*. We therefore

hypothesized that TCA cycle enzymes may provide essential intermediates for growth in bone. To test this hypothesis using our murine osteomyelitis model, we examined the fitness of mutants in each step of the TCA cycle – *pdhA*, *acnA, icd, sucA, sucB, sucC, sdhA, fumC,* and *mqo* (**Figure 22**). Interestingly, none of the TCA cycle mutants tested had a defect for survival *in vivo* with the exception of *pdhA* which demonstrated a bimodal distribution, indicating that overall the TCA cycle is not essential for survival during osteomyelitis.

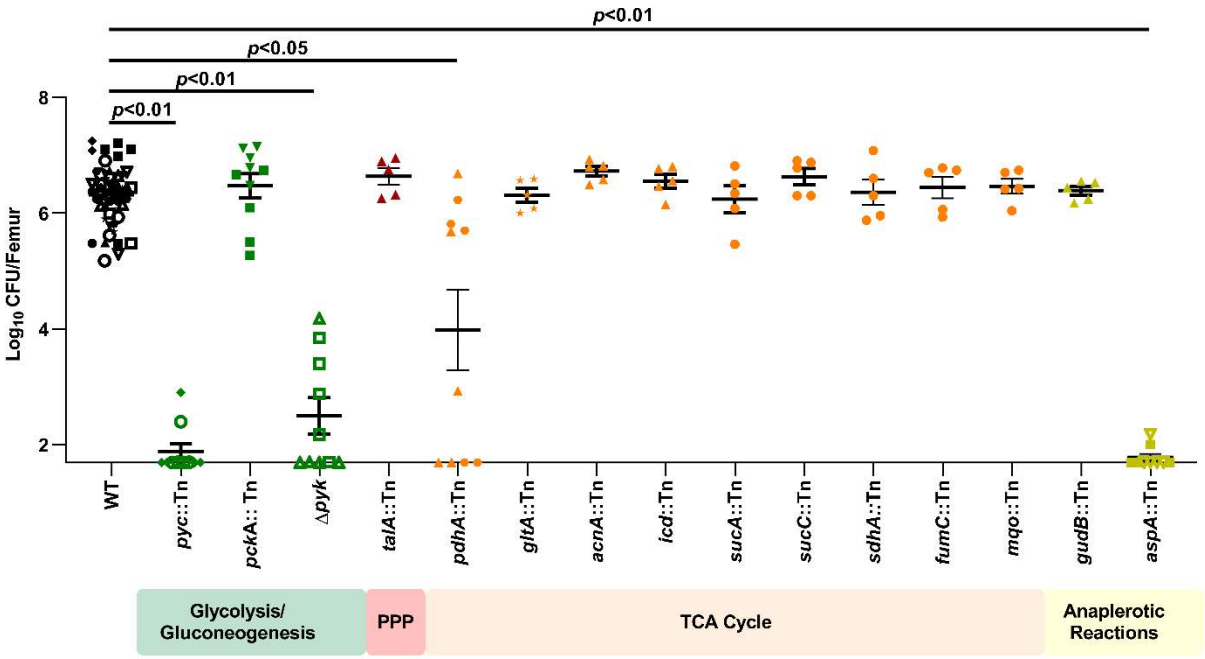

Figure 22. Central metabolic pathways required for *S. aureus* survival *in vivo* during osteomyelitis. Osteomyelitis was induced in groups of mice using WT, *pyc*::Tn, *pckA*::Tn, *Δpyk*, *talA*::Tn, *pdhA*::Tn, *gltA*::Tn, *acnA*::Tn, *icd*::Tn, *sucA*::Tn, *sucC*::Tn, *sdhA*::Tn, *fumC*::Tn, *mqo*::Tn, *gudB*::Tn, or *aspA*::Tn strains. At 14 days post-infection, femurs were processed for CFU enumeration. N> 5 mice per group. Green symbols indicate glycolysis/gluconeogenesis enzymes, red indicates pentose phosphate pathway enzymes, orange indicates TCA cycle enzymes, and yellow indicates anaplerotic reactions. Different shapes indicate replicate experiments. Horizontal line indicates the mean and error bars represent SEM. Statistical significance determined by Student's *t* test compared to corresponding WT comparator. Significance of WT vs. *pdhA*::Tn determined by Mann-Whitney test. Diamond WT data was also used in green circles in Figure 2D.

Specific anaplerotic reactions are essential for the generation of biosynthetic intermediates *in vivo*

Because the TCA cycle is not required *in vivo*, the remaining essential biosynthetic intermediates may be produced through anaplerotic reactions (**Figure 21**). To test this hypothesis, we examined the *in vivo* fitness of a *gudB* mutant (glutamate to alpha-ketoglutarate) (**Figure 22**). Surprisingly, *gudB* had no survival defect *in vivo,* suggesting that neither the TCA cycle nor GudB are the primary producers of alpha-ketoglutarate *in vivo* and it may instead by acquired exogenously. We then examined the fitness of an *aspA* mutant (aspartate to oxaloacetate) *in vivo* and found that it was essential for survival during osteomyelitis (**Figure 22**). Interestingly, the defect of an *aspA* mutant occurs within a single day post infection, and an *aspA* mutant can be cleared by 7 days post-infection (**Figure 23**). The survival defect of an *aspA* mutant can be complemented *in vivo* (**Figure 24**). Both AspA and Pyc reside in a pathway for the synthesis of aspartate, and both mutants demonstrated a defect in survival during osteomyelitis.

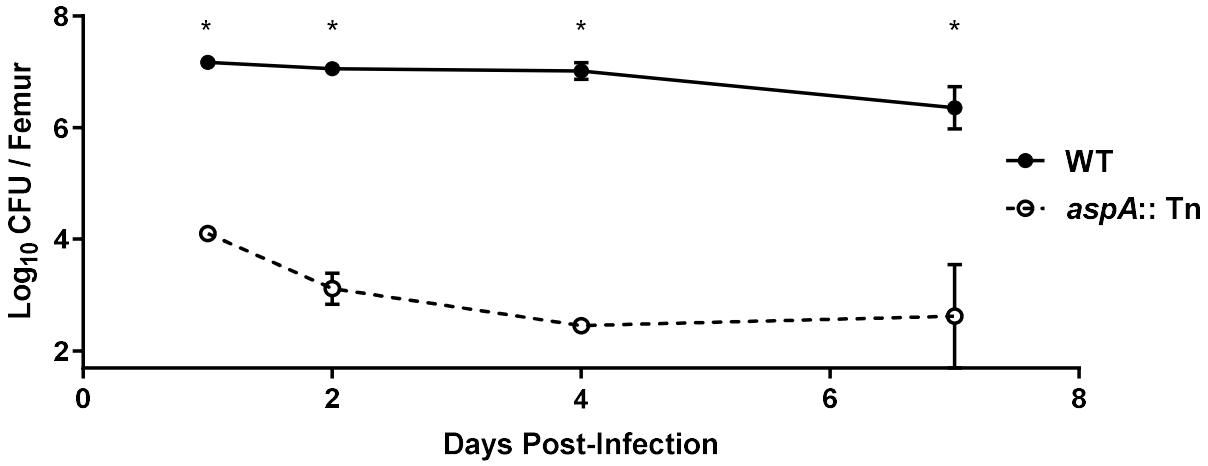

Figure 23. The defect of an *aspA* mutant occurs early in infection Osteomyelitis was induced in groups of mice using WT or *aspA* strains. At 1, 2, 4, or 7 days post-infection, femurs were processed for CFU enumeration. N= 3 mice per strain per timepoint. Horizontal line indicates the mean and error bars represent SEM. Statistical significance determined by multiple *t* test corrected for multiple comparisons by Holm-Sidak method. * indicates adj. $p < 0.05$.

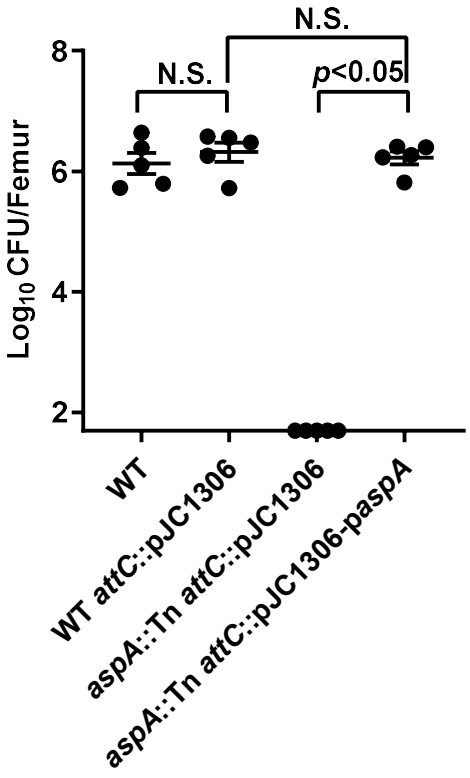

Figure 24. An *aspA* mutant defect can be chromosomally complemented *in vivo*. Osteomyelitis was induced in groups of mice using WT *attC*::pJC1306, *aspA*::Tn *attC*::pJC1306, *aspA*::Tn *attC*::pJC1306-p*aspA* strains. At 14 days post-infection, femurs were processed for CFU enumeration. N= 5 mice per group. Horizontal line indicates the mean and error bars represent SEM. Statistical significance determined by Student's *t* test.

An *ex vivo* approach to analyzing nutritional capacity of homogenized bone

We were curious why an *aspA* mutant was unable to meet aspartate requirements through import of amino acids derived from the nutrient milieu within the host. In order to examine the nutritional capacity of bone, we have developed an *in vitro* culture system in which *S. aureus* is grown in chemically defined media with glucose (CDMG) supplemented with bone homogenate. In this culture system, we can examine the fitness of nutritional mutants for survival in the media depleted of, or replete for, various amino acids. To assess the feasibility of this assay, we examined the ability of homogenized bone to chemically complement *S. aureus* auxotrophies in the absence of a dedicated amino acid source (**Figure 25**). Interestingly, every amino acid component can be removed from CDMG and supplemented by homogenized bone, indicating that bone sufficiently meets the nutritional requirements of WT *S. aureus* (**Figure 25B**).

A

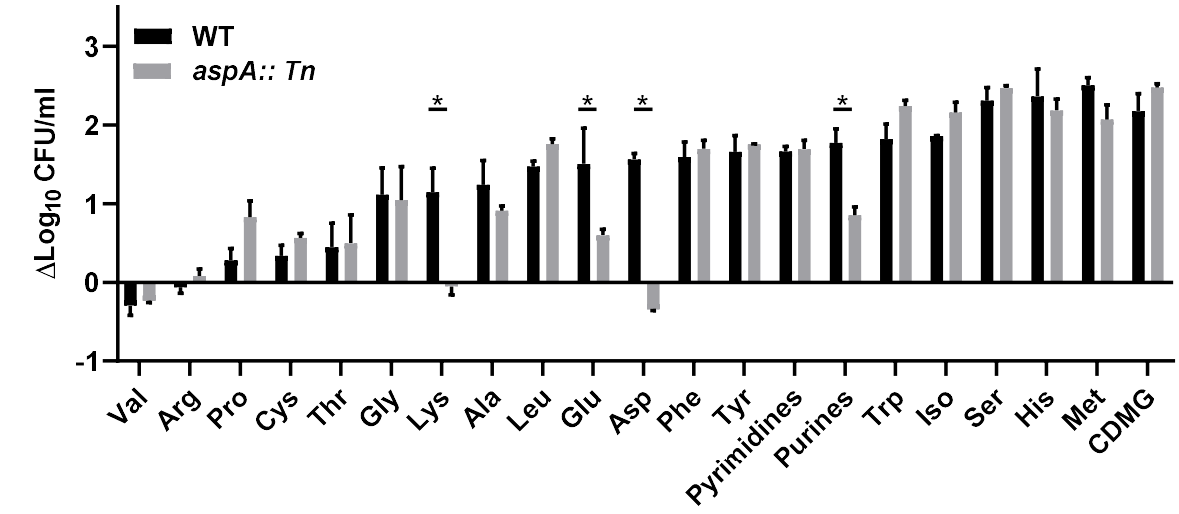
WT
aspA:: Tn
ΔLog10 CFU/ml
3
2
1
0
-1
*
*
*
*
Val
Arg
Pro
Cys
Thr
Gly
Lys
Ala
Leu
Glu
Asp
Phe
Tyr
Pyrimidines
Purines
Trp
Iso
Ser
His
Met
CDMG

B

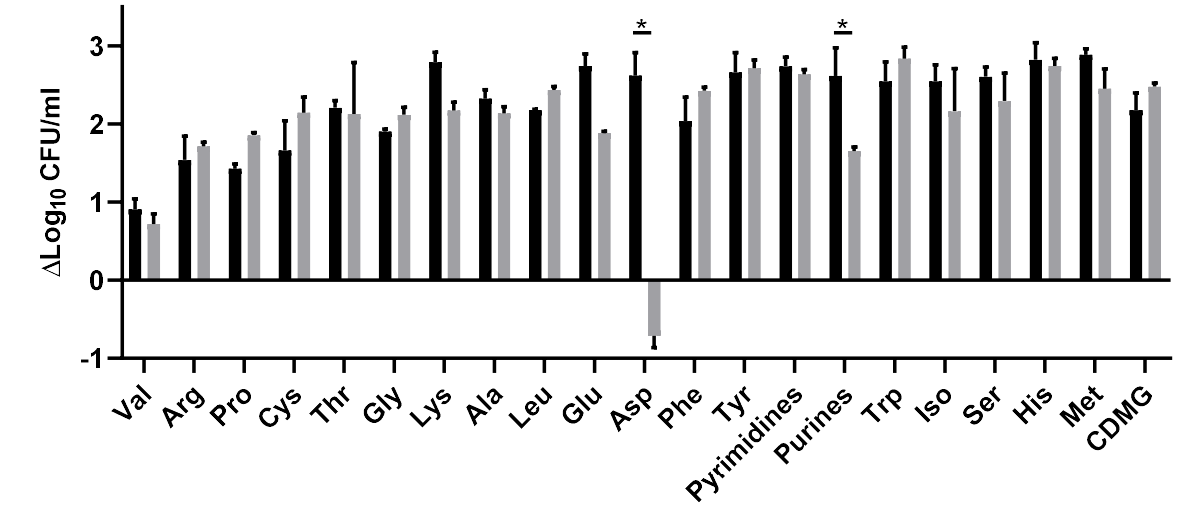
ΔLog10 CFU/ml
3
2
1
0
-1
*
*
Val
Arg
Pro
Cys
Thr
Gly
Lys
Ala
Leu
Glu
Asp
Phe
Tyr
Pyrimidines
Purines
Trp
Iso
Ser
His
Met
CDMG

Figure 25. Bone supplies amino acids required for *S. aureus* growth *in vitro*. (A and B) WT or *aspA*::Tn *S. aureus* was grown for 8 hours in CDMG lacking the indicated amino acid. (B) Eight-week murine femurs were homogenized in CelLytic buffer and added to CDMG lacking the indicated amino acid at 5% V/V. Growth was monitored by CFU enumeration and reported as change in Log CFU at 8 hours compared to inocula at 0 hours. Growth in complete, unsupplemented CDMG at far right. Columns indicate the mean and error bars represent SEM. N = 2 biologic replicates. Significance determined by two-way ANOVA with Holm-Sidak correction for multiple comparisons. * indicates p-value < 0.1.

Considering the abundance of amino acids available within homogenized bone as suggested by our *ex vivo* assays, we expected that in the absence of *de novo* aspartate biosynthesis, *S. aureus* would import exogenous aspartate. We therefore hypothesized that an *aspA* mutant may be unable to survive *in vivo* due to a lack of available exogenous aspartate during infection. Because WT *S. aureus* is prototrophic for aspartate, an *aspA*, aspartate biosynthesis mutant was tested to examine the bioavailability of aspartate in homogenized bone. As expected, an *aspA* mutant demonstrated an induced auxotrophy for aspartate *in vitro* (**Figure 25A**). An *aspA* mutant also demonstrates significantly reduced growth in the absence of lysine, glutamate and purines relative to WT (**Figure 25A**). Homogenized bone can restore growth of an aspA mutant in the absence of lysine and glutamate. Surprisingly however, although bone is an abundant source of many amino acids, homogenized bone does not provide sufficient aspartate or purines to rescue growth of an *aspA* mutant to WT levels (**Figure 25B**).

An *aspA* mutant survival defect *in vivo* is not caused by an inability to synthesize downstream amino acids

In *B. subtilis*, mutants deficient in aspartate biosynthesis are also deficient for synthesis of meso-diaminopimelate (mDAP), a major component of the *B. subtilis* peptidoglycan. Rather than mDAP, *S. aureus* utilizes lysine as a major component of peptidoglycan, and, further, incorporation of lysine into the cell wall is driven by high intracellular concentrations of lysine (125). We therefore hypothesized that aspartate biosynthesis is required for *S. aureus* survival *in vivo* in order provide substrates for synthesis of aspartate derived amino acids – particularly lysine for peptidoglycan biosynthesis (**Figure 21**). To test this hypothesis, we confirmed the growth defect of an *aspA* mutant both in the presence and absence of extracellular lysine (CDMG and CDMG-lys). Again, we observed that although WT *S. aureus* is prototrophic for lysine, we found

that an *aspA* mutant had developed a lysine auxotrophy (**Figure 27A and B**). Interestingly, however, the defect of an *aspA* mutant in the absence of exogenous supplied could be rescued with homogenized bone. This suggested to us that an inability to meet lysine biosynthetic demands may induce a defect in *aspA* mutants *in vitro,* however exogenous lysine in the host tissue milieu may rescue this defect. To test this hypothesis, we examined the growth and survival of mutants in biosynthesis of aspartate derived amino acids. Synthesis of lysine, methionine, threonine, and isoleucine is completed through a branching pathway beginning with the conversion of aspartate to 4-phospho-aspartate by aspartate kinase (**Figure 21 and Figure 26**). *S. aureus* encodes two aspartate kinase isoforms*, usa300_1225* and *usa300_1286* (*lysC*) that are thought to be regulated through feedback inhibition by threonine and lysine respectively (126). We therefore examined the fitness of mutants in both aspartate kinase isoforms. First, we confirmed the phenotype of a *usa300_1225* and *usa300_1286* (*lysC*) mutant in CDMG lacking each of the aspartate derived amino acids (**Figure 27C and D**). We found that a *1225* mutant was defective for growth in media lacking methionine and threonine, and a 1286 mutant is defective for growth in media lacking lysine. These results confirm that in the absence of threonine and methionine, *1286* is not able to compensate for the lack of *1225*. Conversely, in the absence of lysine, 1225 is also not able to compensate for 1286. These results are consistent with the feedback inhibition previously proposed for these enzymes. We next examined fitness of each of these aspartate kinase mutants *in vivo*. Interestingly, neither of the mutants had a defect for survival during osteomyelitis (**Figure 27E**). We hypothesized that the aspartate kinase isoforms may perform redundant functions *in vivo*, therefore, we created a double mutant in *1225/1286*. The aspartate kinase double mutant has a severe defect for growth when grown in the absence of methionine, threonine, and lysine, and also exhibits a defect for growth in CDMG at 24 hours, suggesting that these amino acids may be

rapidly consumed and subsequently depleted from the media, inhibiting growth (**Figure 27C and D**). Despite the inability of an aspartate kinase double mutant to grow in CDMG *in vitro*, we found that the *1225/1286* double mutant was not defective for survival *in vivo*, suggesting that the requirement for exogenous aspartate derived amino acids is indeed sufficiently met by amino acid sources or precursors *in vivo* (**Figure 27E**). These results also indicate that the induced lysine auxotrophy of an *aspA* mutant does not drive the inability of an *aspA* mutant to survive *in vivo*, as there is sufficient lysine and other aspartate derived amino acids to compensate.

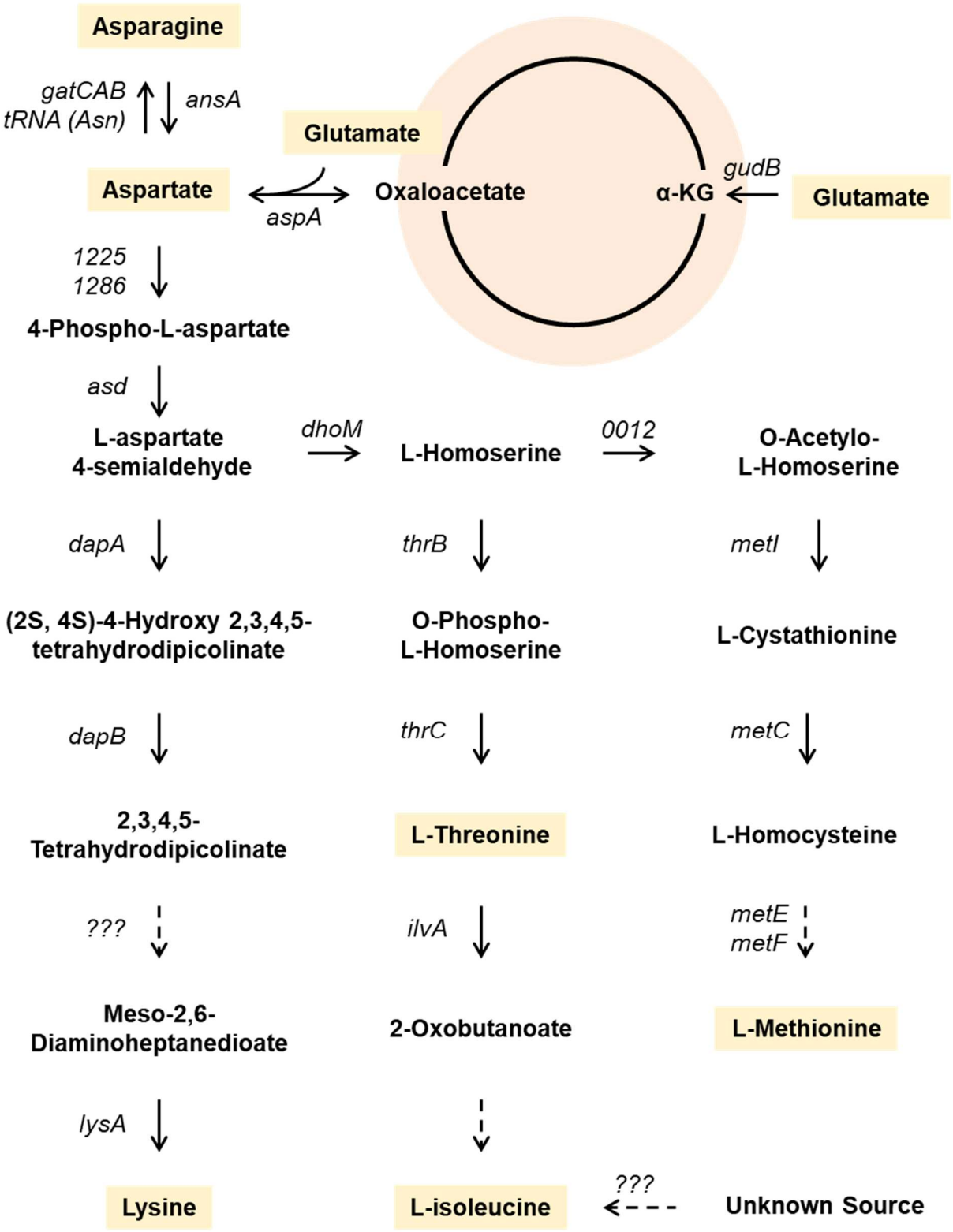

Figure 26. Schematic of aspartate derived amino acid biosynthesis.

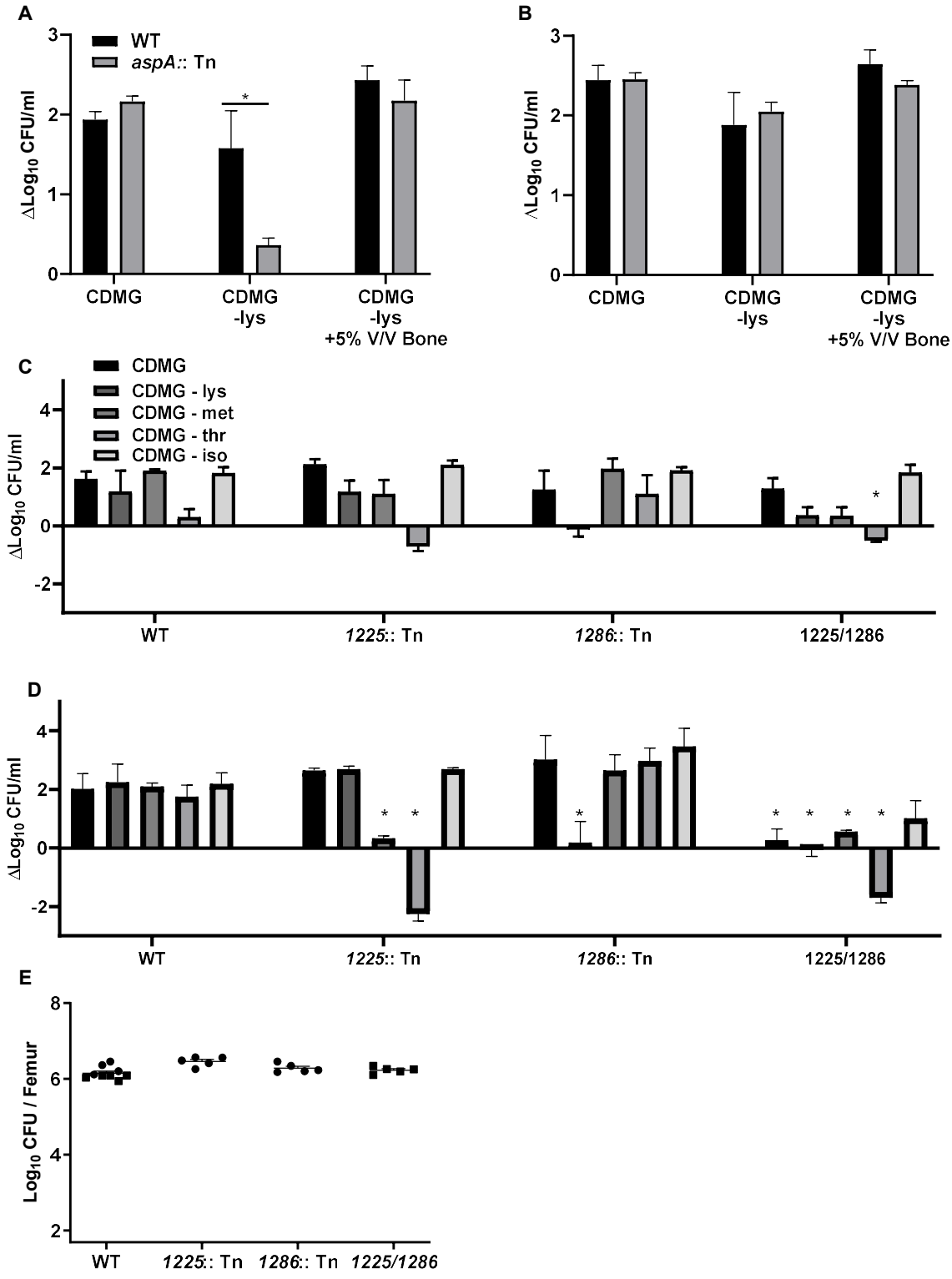
A
WT
aspA:: Tn
ΔLog10 CFU/ml
CDMG
CDMG -lys
CDMG -lys +5% V/V Bone
B
C
CDMG
CDMG - lys
CDMG - met
CDMG - thr
CDMG - iso
WT
1225:: Tn
1286:: Tn
1225/1286
D
E
Log10 CFU / Femur

Figure 27. The lysine auxotrophy of an *aspA* mutant does not drive *in vivo* growth defects. (A and B) WT or *aspA* mutant *S. aureus* were grown for (A) 8 or (B) 24 hours in CDMG, or CDMG lacking lysine. Eight-week murine femurs were homogenized in CelLytic buffer and added to CDMG lacking aspartate at 5% V/V. Growth was monitored by CFU enumeration and reported as change in Log CFU at 8 or 24 hours compared to inocula at 0 hours. Columns indicate the mean and error bars represent SEM. N= 3 biologic replicates. (C and D) WT, *1225*::Tn, *1286*::Tn, or *1225/1286* were grown for (C) 8 or (D) 24 hours in CDMG lacking lysine, methionine, threonine, or isoleucine. Growth was monitored by CFU enumeration and reported as change in Log CFU at 8 or 24 hours compared to inocula at 0 hours. Columns indicate the mean and error bars represent SEM. N= 2 biologic replicates. Significance indicated relative to WT comparator. (A-D) Significance determined by two-way ANOVA with Holm-Sidak correction for multiple comparisons. * indicates p-value < 0.05. (E) Osteomyelitis was induced in groups of mice using WT, *1225*::Tn, *1286*::Tn, or *1225/1286.* At 14 days post-infection, femurs were processed for CFU enumeration. N= 5 mice per group. Different shapes indicate replicates. Horizontal line indicates the mean and error bars represent SEM. Statistical significance determined by Student's *t* test.

Aspartate deficiency results in decreased purine biosynthesis

The survival defect of an *aspA* mutant *in vivo* is not due to an inability to synthesize aspartate-derived amino acids. An *aspA* mutant also exhibited defects for growth in the absence of purines that could not be rescued by homogenized bone (**Figure 25B).** We validated these results and confirmed that an *aspA* mutant does indeed have a growth defect in the absence of purines that cannot be chemically complemented with homogenized bone (**Figure 29A**). Aspartate has several roles in purine biosynthesis, and we noted that several purine biosynthesis mutants were defective for survival in our TnSeq of osteomyelitis in Chapter II (**Figure 21**). We therefore hypothesized that the survival defect of an *aspA* mutant may be due to an inability to synthesize purines *in vivo*. Aspartate functions as a nitrogen donor in the synthesis of adenylosuccinate from inosine monophosphate (IMP) to generate ATP, and in the synthesis of 4-(N-succino)-5-aminoimidazole-4-carboxamide ribonucleotide (SAICAR) from 4-carboxy-5-aminoimidazole ribonucleotide (CAIR) to ultimately generate both GTP and ATP (**Figure 28**). The purine biosynthesis enzyme PurB utilizes these intermediates derived from aspartate, to ultimately generate both ATP and GTP. PurB is a dual functional enzyme that catalyzes the conversion of adenylosuccinate into AMP for generation of ATP and catalyzes the conversion of SAICAR into 5-Aminoimidazole-4-carboxamide ribonucleotide (AICAR) to ultimately generate both GTP and ATP. Using our murine model of osteomyelitis, we confirmed that disruption of *purB* had a significant effect on the fitness of *S. aureus* at 14 days post-infection in mono-infection (**Figure 29C**). The essentially of *purB* indicates that compromise of the GTP and ATP branches of purine biosynthesis critically inhibits the ability of *S. aureus* to survive within skeletal tissue and may drive the survival defect of an *aspA* mutant *in vivo.*

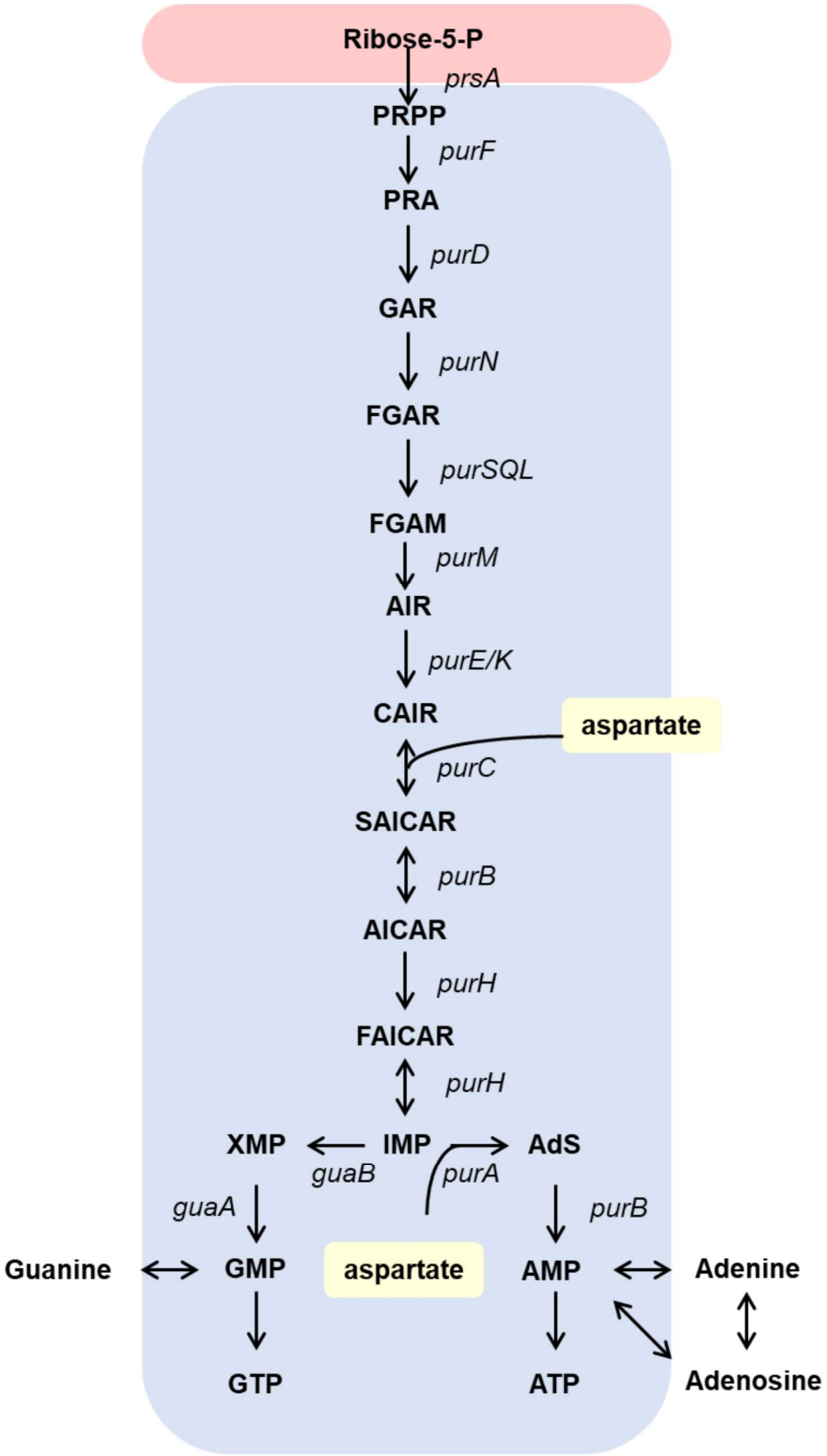

Figure 28. Schematic of purine biosynthesis.

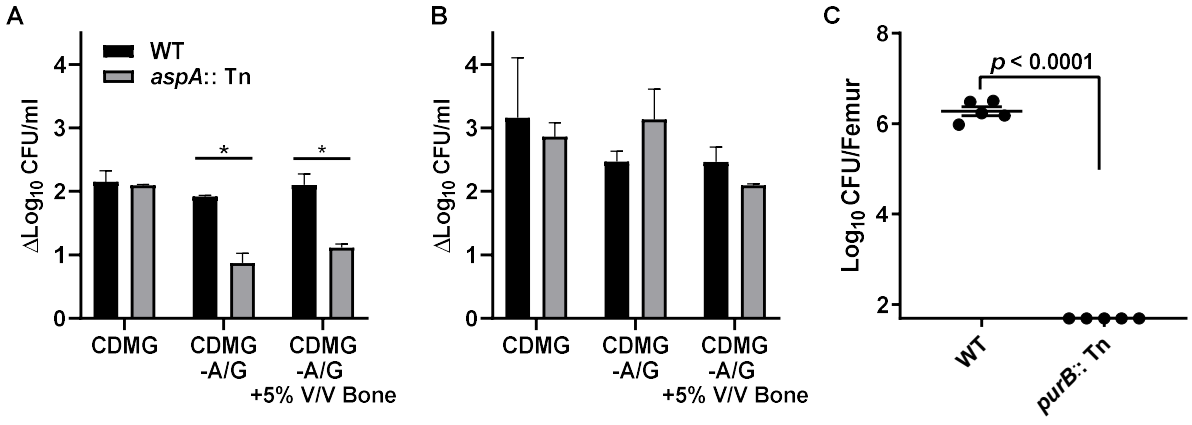

Figure 29. Purine biosynthesis is defective in aspartate deficient mutants and is required for survival *in vivo*. (A and B) WT or *aspA::*Tn *S. aureus* were grown for (A) 8 or (B) 24 hours in CDMG, or CDMG lacking adenine and guanine. Eight-week murine femurs were homogenized in CelLytic buffer and added to CDMG lacking aspartate at 5% V/V. Growth was monitored by CFU enumeration and reported as change in Log CFU at 8 or 24 hours compared to inocula at 0 hours. Columns indicate the mean and error bars represent SEM. N= 3 biologic replicates. Significance determined by two-way ANOVA with Holm-Sidak correction for multiple comparisons. * indicates p-value < 0.05. (C) Osteomyelitis was induced in groups of mice using WT or *purB*::Tn. At 14 days post-infection, femurs were processed for CFU enumeration. Horizontal line indicates the mean and error bars represent SEM. N= 5 mice per group. Statistical significance determined by Student's *t* test.

Excess glutamate competitively inhibits *S. aureus* aspartate transport

An *aspA* mutant can only survive *in vitro* when an exogenous aspartate source is supplied, suggesting that *S. aureus* encodes a functional aspartate transporter (**Figure 25A**). However, we found that an *aspA* mutant is unable to acquire sufficient aspartate from bone for growth *in vitro,* suggesting that aspartate levels within bone may be too low to support growth (**Figure 25B**). We validated the growth of an *aspA* mutant *in vitro* and found that an *aspA* mutant was indeed unable to grow on bone as a sole aspartate source (**Figure 30A and B**). This was surprising, as the concentration of all other amino acids within homogenized bone was sufficient to support the growth of WT *S. aureus.* Interestingly, aspartate biosynthesis is also conditionally essential for growth *in vitro* in *Bacillus subtilis*, despite the ability to acquire aspartate exogenously through the aspartate/glutamate transporter GltT (127). In the presence of a functional GltT, glutamate was found to competitively inhibit aspartate import, despite sufficiently high levels of aspartate in media**.** Furthermore, aspartate transport in *S. aureus* has previously been shown to be competitively inhibited by glutamate *in vitro* (128). We therefore hypothesized that aspartate transport may occur through the *S. aureus* GltT homologue and may be similarly inhibited by glutamate *in vivo*. To test this hypothesis, we first examined the ability of GltT to transport aspartate in *S. aureus*. To confirm that GltT is the only functional transporter of aspartate under our growth conditions, we generated an *aspA/gltT* double mutant. We then tested the ability of *aspA/gltT* to grow in CDMG. We found that although an *aspA* mutant is able to acquire exogenous aspartate from CDMG, the *aspA/gltT* double mutant is incapable of growing in CDMG, indicating that GltT is the only transporter for exogenous aspartate under these conditions (**Figure 30C and D**). Furthermore, the requirement for GltT in an *aspA* mutant can be bypassed by supplying 2mM asparagine which is typically absent from CDMG (**Figure 30C and D**). In *S. aureus,* asparagine

is acquired through alternative transporters from aspartate (128). Asparagine can then subsequently be converted to aspartate using the enzyme AnsA (49). In the absence of AnsA, asparagine can no longer rescue the growth defect of an *aspA* mutant in the absence of aspartate, suggesting that asparagine is serving as an aspartate precursor (**Figure 31A and B**). Catabolism of aspartate generated from asparagine in WT *S. aureus* can generate glutamate and oxaloacetate, however this process requires AspA. Therefore, the ability of asparagine supplementation to bypass the growth defect of an *aspA/gltT* mutant indicates that the defect is not due to an inability to transport glutamate, but rather due to an inability to acquire aspartate.

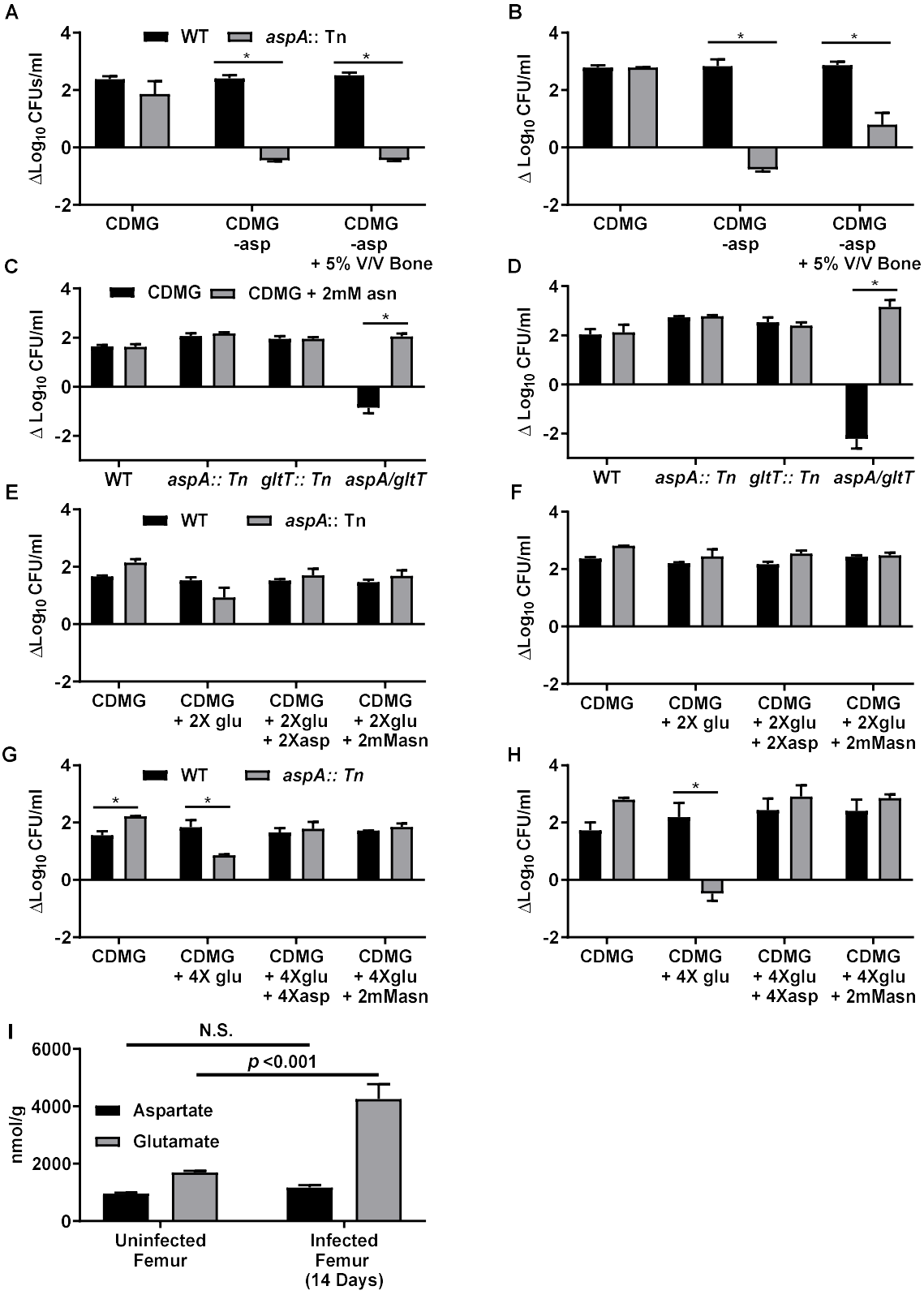
A
WT
aspA:: Tn
ΔLog10 CFUs/ml
CDMG
CDMG -asp
CDMG -asp + 5% V/V Bone
B
Δ Log10 CFU/ml
C
CDMG
CDMG + 2mM asn
WT
aspA:: Tn
gltT:: Tn
aspA/gltT
D
E
CDMG + 2X glu
CDMG + 2Xglu + 2Xasp
CDMG + 2Xglu + 2mMasn
F
G
aspA:: Tn
CDMG + 4X glu
CDMG + 4Xglu + 4Xasp
CDMG + 4Xglu + 2mMasn
H
I
N.S.
p <0.001
nmol/g
Aspartate
Glutamate
Uninfected Femur
Infected Femur (14 Days)

Figure 30. GltT is an aspartate transporter that is inhibited by excess glutamate *in vitro*. (A and B) WT or *aspA* mutant *S. aureus* were grown for (A) 8 or (B) 24 hours in CDMG, or CDMG lacking aspartate. Eight-week murine femurs were homogenized in CelLytic buffer and added to CDMG lacking aspartate at 5% V/V. (C and D) WT, *aspA*::Tn, *gltT*::Tn, or *aspA/gltT S. aureus* was grown for (C) 8 or (D) 24 hours in CDMG or CDMG supplemented with 2mM asparagine. (E-H) WT or *aspA*::Tn *S. aureus* was grown in CDMG supplemented with excess glutamate or aspartate relative to standard CDMG or CDMG supplemented with 2mM asparagine. (A-H) Growth was monitored by CFU enumeration and reported as change in Log CFU at 8 or 24 hours compared to inocula at 0 hours. Columns indicate the mean and error bars represent SEM. (A-D) N= 3 biologic replicates. (E-H) N = 2 biologic replicates. Significance determined by two-way ANOVA with Holm-Sidak correction for multiple comparisons. * indicates p-value < 0.05.

Because transport of aspartate is thought to be competitively inhibited by glutamate in *S. aureus*, we hypothesized that the ratio of glutamate to aspartate in bone may be increased, preventing acquisition of exogenous aspartate *in vivo* and in our *ex vivo* assay (128). To test the hypothesis that glutamate is elevated relative to aspartate in bone, we measured aspartate and glutamate levels in homogenized femurs. We found that glutamate is ~2 fold higher than aspartate in uninfected tissues, and furthermore, that glutamate drastically increases in infected tissues to ~4-5 fold higher than aspartate concentrations (**Figure 30I**). We hypothesized that this ratio of glutamate to aspartate may inhibit acquisition of aspartate by an *aspA* mutant. To test this hypothesis, we grew an *aspA* mutant in CDMG containing physiologic ratios of glutamate and aspartate and examined if glutamate competitively inhibits utilization of aspartate in *S. aureus* in these conditions. We found that in CDMG containing only normal skeletal ratios of aspartate and glutamate (1:2) or in CDMG containing ratios of aspartate and glutamate found in infected bone (1:4), growth of an *aspA* mutant was inhibited compared to WT *S. aureus* (**Figure 30E-H**). Furthermore, this inhibition can be overcome by equalizing the aspartate/glutamate ratio in the media or by supplementation of asparagine. We hypothesized that the competitive inhibition of aspartate transport could be overcome by increasing expression of *gltT*, effectively decreasing saturation of the GltT transporter. To test this hypothesis, we generated a *gltT* overexpression construct driven by the constitutively active *lgt* promoter. Expression of this *gltT* overexpression construct *in trans* on the multicopy plasmid pOS1 in an *aspA* mutant rescues the growth defect of an *aspA* mutant *in vitro* in CDMG with excess glutamate (**Figure 32A and B**). Furthermore, constitutive expression of *gltT* expressed *in trans* provides a significant growth advantage to an *aspA* mutant *in vivo* (**Figure 26**). Together, these data suggest that although *S. aureus* is able to acquire exogenous aspartate through the GltT transporter, excess glutamate in tissues, particularly

during infection, competitively inhibits aspartate transport and necessitates aspartate biosynthesis *in vivo.* As a whole, this study suggests that the survival defect of an *aspA* mutant *in vivo* during osteomyelitis is driven by an inability to synthesize purines *de novo* during infection because of inhibition of aspartate uptake through the aspartate transporter, GltT.

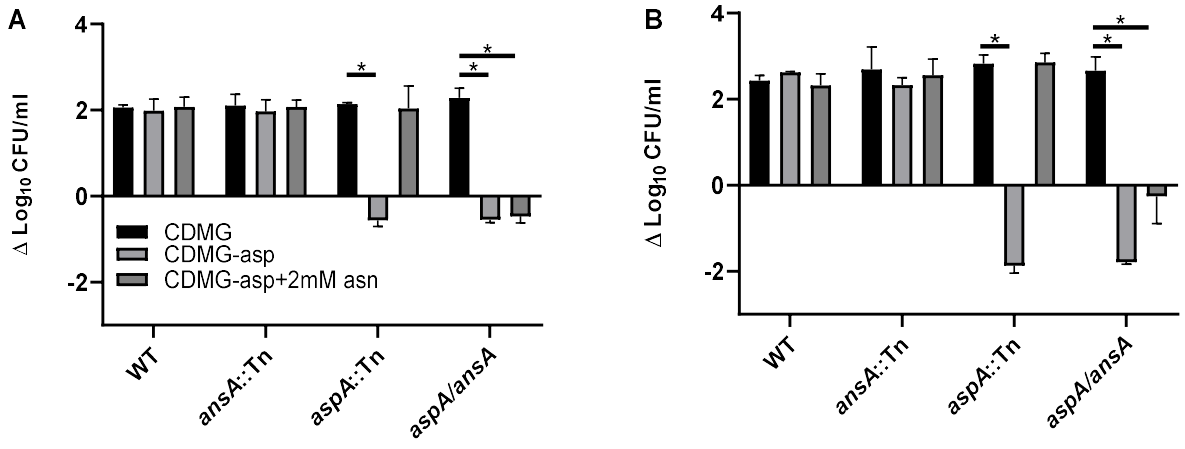

Figure 31. Asparagine can rescue the defect of an *aspA* mutant in the absence of exogenous aspartate. (A) WT, *ansA*::Tn*, aspA*::Tn*,* or *aspA/ansA S. aureus* were grown for (A) 8 hours or (B) 24 hours in CDMG, CDMG lacking aspartate, CDMG lacking aspartate supplemented with 2mM asparagine. Growth was monitored by CFU enumeration and reported as change in Log CFU at (A) 8 hours or (B) 24 hours compared to inocula at 0 hours. Columns indicate the mean and error bars represent SEM. N= 3 biologic replicates. Significance determined by two-way ANOVA with Holm-Sidak correction for multiple comparisons. * indicates adj. $p < 0.05$.

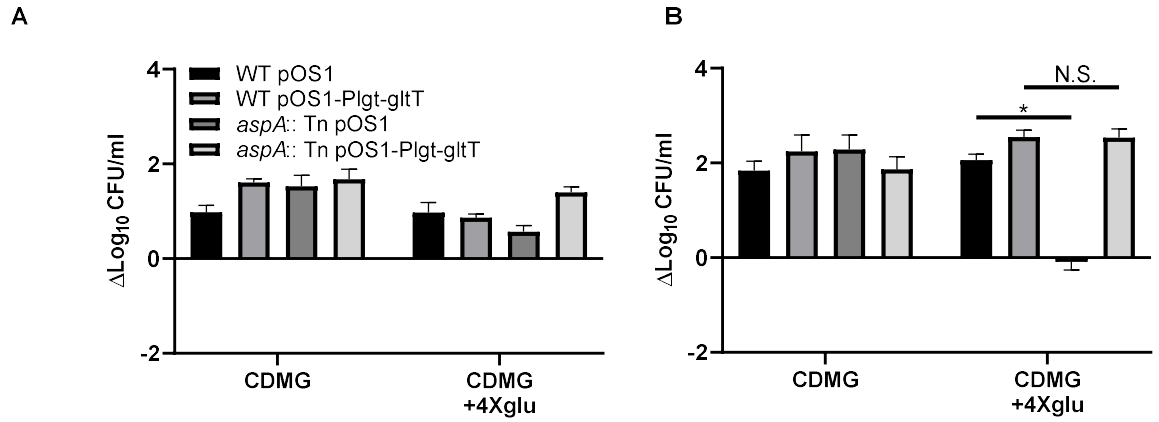

Figure 32. Increased expression of *gltT* rescues growth defects of an *aspA* mutant. (A and B) WT or *aspA* mutant constitutively expressing single copy of chromosomally integrated *gltT* or empty vector control were grown for (A) 8 or (B) 24 hour in CDMG supplemented with excess glutamate relative to standard CDMG. Growth was monitored by CFU enumeration and reported as change in Log CFU at 8 or 24 hours compared to innocula at 0 hours. Columns indicate the mean and error bars represent SEM. N= 2 biologic replicates. Significance determined by two-way ANOVA with Holm-Sidak correction for multiple comparisons. * indicates adj. $p < 0.05$.

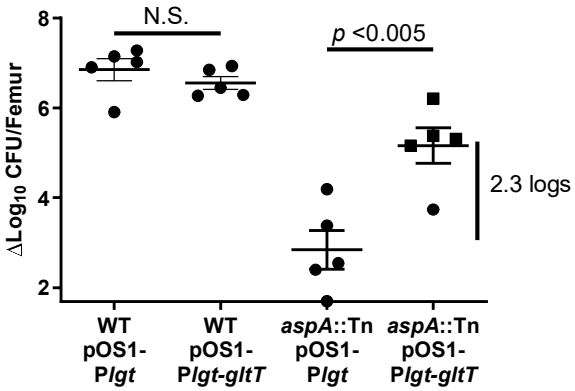

Figure 33. Overexpression of *gltT* restores the *in vivo* survival defect of an *aspA* mutant. Osteomyelitis was induced in groups of mice using WT pOS1-p*lgt*, WT pOS1-P*lgt-gltT, aspA*::Tn pOS1-p*lgt*, *aspA*::Tn pOS1-P*lgt-gltT* strains. At 4 days post-infection, femurs were processed for CFU enumeration. N= 5 mice per group. Horizontal line indicates the mean and error bars represent SEM. Statistical significance determined by Student's *t* test.

Discussion

Because *S. aureus* can infect a variety of host tissue types, it must have the metabolic flexibility to acquire or produce nutrients in these different environments. Interestingly, previous studies have focused on the metabolic capabilities of *S. aureus* in the absence of glucose, as the centers of abscesses are predicted to be glucose limited (49). Transcripts and protein levels of gluconeogenic enzymes in *S. aureus* have also been found to be highly increased during invasive infection, and in osteomyelitis specifically (129, 130). Our studies, however, suggest that *S. aureus* requires glycolysis and glycolytic carbon sources to survive *in vivo*. *S. aureus* is known to have a remarkable ability to scavenge glucose from its environment due to its arsenal of at least four high affinity glucose transporters (39). This preference for glycolytic metabolism reflects the adaptation of *S. aureus* to non-respiratory conditions within inflamed host tissues (38). The conflicting increase of gluconeogenic enzymes observed in the literature with the requirement for glycolysis observed here may reflect temporal changes in glucose availability during infection.

Interestingly, several cell types unique to bone, namely osteoclasts and osteoblasts, rely on the catabolism of glucose to fuel aerobic glycolysis. During infection, we have observed profound dysregulation of skeletal homeostasis (13). This is due, in part to intoxication of skeletal and immune cells by *S. aureus*, which may eliminate competition for available glucose at the site of infection (12, 89). However, we have also recently found that *S. aureus* stimulates the differentiation of osteoclasts to resorb damaged bone (13). As osteoclasts are highly glycolytic, this stimulation of osteoclast differentiation as well as the influx of glycolytic immune cells may alter glucose homeostasis at the site of infection. The temporal changes in nutrient availability to *S. aureus* due to stimulation and death of skeletal and immune cells is therefore the subject of future studies in our lab.

As discussed in Chapter I, the TCA cycle has been generally discussed in staphylococcal literature as being important for staphylococcal virulence – however, the evidence supporting this assumption is fairly limited. Few TCA cycle enzymes have been implicated as being required for virulence in *S. aureus*, with only moderate attenuation phenotypes that are frequently tissue specific (54, 131-133). When we tested mutants from each of the pathways involved in the TCA cycle comprehensively, none of the TCA cycle enzymes were required for survival during osteomyelitis, except PdhA. PdhA is not a true TCA enzyme, but rather provides a link between glycolysis and the TCA cycle. The product of PdhA, Acetyl-CoA, is also used for fatty acid biosynthesis, and therefore may explain the requirement for PdhA *in vivo*. The lack of a virulence defect in TCA cycle mutants in our model is not surprising, as several factors present in bone during infection are known to inhibit TCA cycle activity. Three TCA enzyme complexes (SdhA, FumC/CitG, and AcnA/CitB) rely on iron-sulfur clusters and production of many TCA cycle enzymes is decreased *in vivo* due to iron limitation as a host nutritional immunity strategy (51, 134). Furthermore, many of these enzymes can be inactivated by ROS/RNS which are abundant during infection (37). Additionally, it is well known that the TCA cycle is repressed in the presence of glucose through CcpA (57, 71). Our observation that *S. aureus* requires glycolysis *in vivo* suggests that levels of glycolytic carbon sources are likely sufficient to induce catabolite repression through CcpA. Together, these results demonstrate the TCA cycle is non-essential in bone, likely as a consequence of adaptation to enzyme inactivation and transcriptional repression *in vivo*.

Our data indicate that *S. aureus* requires biosynthesis of aspartate for survival during osteomyelitis. This finding appears to be characteristic of invasive infection, as several other groups have identified *aspA* as essential for survival in unbiased screens *in vivo* (36, 44, 45). Our data indicate that *S. aureus* depends upon endogenous aspartate biosynthesis despite the presence

of exogenous aspartate in tissues. Our studies indicate that this is due, in part, to competitive inhibition of aspartate transport by excess glutamate in tissues. Although we demonstrated that the aspartate : glutamate ratio of infected bone is increased compared to uninfected bone, we suspect that these levels are underestimated, as the spatial distribution of analytes is destroyed by traditional metabolite analysis. Local tissue glutamate levels have been found to increase more than 30-fold within staphylococcal brain abscesses (135). Glutamate levels may therefore be significantly higher than predicted within bone surrounding the infection site. The mechanism of glutamate increase during infection is unknown and may reflect release of cytoplasmic contents following tissue destruction. Alternatively, the stimulation of osteoclast differentiation that occurs during infection, may also increase overall tissue glutamate levels, as mature osteoclasts, but not pre-osteoclasts, are known to release glutamate (136). Likely, a combination of host metabolic changes and tissue destruction drive glutamate elevation during infection, and this mechanism is a topic of further investigation in the lab.

The dependence of *S. aureus* on endogenous aspartate synthesis may reflect the inability of pathogens in general to import exogenous aspartate through the GltT transporter. GltT transporters are highly conserved across kingdom – having homology not only across prokaryotes but also in archaea and eukaryotes as well (137, 138). A majority of these GltT homologs have similar affinities for glutamate and aspartate (137, 139, 140). It is therefore likely that the competitive inhibition of aspartate transport by glutamate through GltT is present in a wide variety of prokaryotes that rely on aspartate/glutamate transporters. However, the observation has been unappreciated, as the ratio of aspartate to glutamate *in vivo* has not previously been reported in the context of aspartate biosynthesis mutants. Rather, the inability of an *aspA* mutant to survive in host tissues has been attributed to the “low” level of aspartate found in sera (141). Our observations

suggest that the capacity of *S. aureus* to utilize exogenous AAs are dependent, not only on total amino acid levels, but also on the context of the nutrient milieu. Furthermore, our results suggest that pathogens may have adapted to rely on aspartate biosynthesis to overcome aspartate transport limitations through this conserved transporter.

Previous studies suggested that the requirement for aspartate biosynthesis *in vivo* arises from the demand for aspartate derived amino acids, particularly lysine, in *S. aureus* (126). High lysine concentrations are particularly important for peptidoglycan biosynthesis in *S. aureus*, as elevated lysine concentrations drive appropriate incorporation into the cell wall (125). The enzymes involved in synthesis of aspartate derived amino acids have thus long been considered for development of therapeutics, as mammalian hosts lack the enzymatic machinery for synthesis of aspartate family amino acids (lysine, methionine, threonine, isoleucine) which minimizes the potential for off target effects (142). Although we did observe an increased reliance on exogenous lysine in an aspartate biosynthesis mutant, lysine is sufficiently abundant within host tissues to meet import needs of *S. aureus*. Our data indicate that *S. aureus* is capable of obtaining aspartate derived amino acids from host tissue and inactivation of aspartate family amino acid biosynthesis may not be as attractive of a target for therapeutic development against staphylococci in this setting.

In addition to synthesis of the aspartate family amino acids, *S. aureus* also can utilize aspartate to indirectly synthesize asparagine through transamidation of aspartyl-tRNA by Aspartyl/glutamyl-tRNA$^{Asn/Gln}$ amidotransferase (GatCAB) (143). This mechanism directly links asparagine synthesis with its use in protein production, suggesting that overall synthesis of asparagine is relatively low. Alternatively, Staphylococci can directly load free asparagine onto tRNA through asparaginyl-tRNA synthetase (*asnC*) (143, 144). In the TnSeq conducted in Chapter

II, we observed that *asnC* was compromised for survival *in vivo* during osteomyelitis, suggesting that *S. aureus* utilizes free asparagine within the host (~62 μM in human plasma) rather than relying on indirect synthesis from aspartate through GatCAB (145). Furthermore, in CDMG lacking aspartate, asparagine supplementation is not able to rescue the defect of an *aspA/ansA* mutant, suggesting that the defect of an *aspA* mutant is not driven by the lack of downstream asparagine production. Together these results indicate that the defect of an *aspA* mutant is not derived from an inability to synthesize downstream amino acids, as these are sufficiently provided exogenously from the host.

The phenotype of an *aspA* mutant appears to be largely driven by an inability to synthesize purines in the absence of aspartate. Aspartate contributes directly to synthesis of the purine intermediates SAICAR and adenylosuccinate. These intermediates are required for the endogenous synthesis of purine nucleotides adenine and guanine, and the high energy nucleoside triphosphates ATP and GTP. Inhibition of the purine biosynthesis pathway is well known for causing defects in pathogenesis of a variety of bacterial pathogens, and several high throughput screens have identified purine biosynthesis genes in *S. aureus* (43, 45, 146-148). Furthermore, in several high-profile studies, defects in aspartate availability have been linked to insufficient purine biosynthesis in humans as well (149, 150). The inhibition of purine biosynthesis at two metabolic intermediates appears to cripple the ability of cells to proliferate, as purines are required for replication of DNA and transcription of RNA for protein expansion.

Interestingly, the defect of mutants affecting purine biosynthesis may be two-fold. The ability *of S. aureus* to survive *in vivo* is dependent on the ability to suppress immune clearance through the synthesis of adenosine from AMP (151, 152). Adenosine has been found to poison the purine salvage pathway of immune cells, resulting in activation of caspase-3-induced cell death

(151). Because adenosine biosynthesis requires the substrate AMP, we predict that mutants deficient in purine biosynthesis are also unable to synthesize adenosine. We therefore attribute the severe inability of an aspartate biosynthesis mutant to survive *in vivo* to both nutritional and virulence defects stemming from defects in purine biosynthesis that impact both replication and bacterial clearance. Our results therefore provide an explanation for the well-established survival defect of *S. aureus* aspartate biosynthesis mutants *in vivo*. Overall, our studies define the nutritional capabilities of a unique infection site, bone, to support the growth of invasive pathogens *in vivo* - emphasizing the importance of characterizing the nutritional milieu within the host tissue environment for future development of metabolically based therapeutics.

Materials and Methods

Bacterial strains and culture conditions

As was done for Chapter II, all experiments were conducted in an erythromycin-sensitive, tetracycline-sensitive derivative of the USA300 strain LAC (AH1263), which served as the WT unless otherwise noted (153). Strains *pyc*::Tn, *pckA*::Tn, *aspA*::Tn, *talA*::Tn, *gudB*::Tn, *pdhA*::Tn, *gltA*::Tn, *acnA*::Tn, *icd*::Tn, *sucA*::Tn, *sucB*::Tn, *sucC*::Tn, *sdhA*::Tn, *fumC*::Tn, *mqo*::Tn, *1225::Tn, 1286::Tn, ansA::Tn,* and *purB*::Tn in the LAC background were created by bacteriophage phi-85-mediated transduction of *erm*-disrupted alleles from the respective JE2 strain mutants obtained from the NARSA transposon library(155). To facilitate the generation of double mutants, strains *aspA*::Tn^{TetR} and *1225*::Tn^{TetR} were created by allelic exchange of the erythromycin resistance cassette in LAC transposon mutants for a tetracycline cassette as previously described(165). *aspA*::Tn^{TetR} in *gltT*::Tn^{ErmR} or *ansA*::Tn^{ErmR} background and *1225*::Tn^{TetR} in *1286*::Tn^{ErmR} background were created by bacteriophage phi-85-mediated transduction of *tet*-disrupted alleles from the allelic exchange LAC mutants. Strain Δ*pyk* in the

LAC background was created by bacteriophage phi-85-mediated transduction of Δ*pyk* in the Newman background described elsewhere(38). Strain Δ*pyk* and WT comparators were grown in TSB without dextrose supplemented with 1% pyruvate. Construction of pJC1306-*aspA* and pOS1-P*lgt-gltT* is described below. Plasmid pJC1306 or pJC1306-*aspA* was introduced into WT LAC or Lac *aspA*::Tn as described elsewhere to create strains WT *attC::pJC1306, aspA*::Tn *attC::pJC1306, aspA*::Tn *attC::pJC1306-aspA*. (166). Plasmid pOS1-P*lgt* or pOS1-P*lgt-gltT* was introduced into LAC WT and Lac *aspA*::Tn to generate WT pOS1, WT pOS1-P*lgt-gltT, aspA*::Tn pOS1, and *aspA*::Tn pOS1-P*lgt-gltT.* All *S. aureus* strains were grown at 37°C in TSB unless otherwise noted. *Escherichia coli* was grown in LB. Erythromycin and chloramphenicol were added to cultures at 10 μg ml^{-1} where indicated. Ampicillin was added to cultures at 100 μg ml^{-1} where indicated. Tetracycline was added to cultures at 2 μg ml^{-1} where indicated.

Construction of *aspA* chromosomal complementation construct

aspA including the upstream flanking region was amplified using primers 5'-GCGGATCCTTACATATTATTCGTTAATTCACC-3' and 5'-ATGGTACCTTATCTTAAGTCATCAATCGC-3',

and cloned into pJC1306 digested with BamHI and KpnI to create pJC1306_*aspA*(166). Strain RN4220 was electroporated with plasmid pJC1306_*aspA* or pJC1306 as described. Phage 80α was then used to transduce the mutation into LAC WT or Lac *aspA*::Tn, to generate LAC *attC::pJC1306,* LAC *aspA*::Tn *attC::pJC1306, and* LAC *aspA*::Tn *attC::pJC1306-aspA.*

Construction of *gltT* overexpression plasmid

To express *gltT in trans*, the *gltT* open reading frame was PCR amplified from genomic DNA of LAC using primers 5'-AGAGCTCGAGATGGCTCTATTCAAGAG-3' and 5'-AGATGGATCCTTAAATTGATTTTAAATATTCTTGAC-3'. The resulting *gltT* amplicon was

then cloned into the shuttle vector pOS1 under control of the *lgt* promoter and transformed into WT, *aspA*::Tn, and *gltT*::Tn strain LAC (167). As a control, wild type and *gltT*::Tn strain LAC were transformed with pOS1-P*lgt* lacking an insert.

Murine model of osteomyelitis

Osteomyelitis was induced in 7- to 8-week old female C57BL/6J mice as previously reported in methods section for Chapter II.

Comparative growth analysis and chemically defined media composition

Chemically defined media (CDM), in which primary carbon source and amino acid composition could be modified, was made as previously described (168, 169). Glucose was added at 1% to create CDMG. For comparative growth analysis, overnight cultures of WT and mutant cultures washed in PBS and were back-diluted 1:1000 into CDM and grown in 96 well plates at 37°C with orbital shaking at 180 rpm. Viable CFUs were measured by plating at limiting dilution in TSA at the timepoints indicated. To make CDMG with bone, femurs from 8- to 11-week old female C57BL/6J mice were harvested and frozen at -80 prior to use. Immediately prior to inoculating media with bacteria, femurs were homogenized in 500 µl of CelLytic MT Cell Lysis Reagent (Sigma) and added at 5% V/V. As an internal control, equivalent volumes of vehicle were added to CDMG as needed.

Enzymatic determination of metabolite levels

Tissues were harvested from 8-week-old female C57BL/6J mice and frozen immediately on dry ice to limit changes in metabolites. Tissues were stored at -80º before being homogenized in 500 µl PBS. Aspartate concentrations were measured by Aspartate Colorimetric Assay Kit (BioVision, San Francisco, CA, USA) according to manufacturer instructions. Glutamate concentrations were measured by EnzyChrom Glutamate Assay Kit (BioAssay Systems, Hayward, CA, USA)

according to manufacturer instructions. For aspartate measures, tissue supernatants were treated with serum cleanup solution and deproteinated using an Amicon Ultra 10KDa centrifugal filter before analysis of aspartate levels as recommended by manufacturer instructions. Absorbances were measured by BioTek Synergy HT 96-well plate reader. Metabolite concentrations were normalized to wet tissue weight.

Coauthor Contributions

Jim Cassat and I conceived and designed the experiments and analyzed results. Jacob Curry assisted with strain generation and infections. Caleb Ford and Jim Cassat assisted with infections. Casey Butrico and Srivarun Tummakarota contributed to strain generation. I performed all other experiments.

CHAPTER IV: FUTURE DIRECTIONS

Introduction

This dissertation describes our investigations into the metabolic and virulence pathways that impact *S. aureus* survival during osteomyelitis, a debilitating manifestation of invasive staphylococcal infection. In Chapter II, we identified major genes required for *S. aureus* survival *in vivo* and discuss the role of the master virulence regulator, SrrAB, in modulating toxin production and facilitating responses to hypoxia during infection. In Chapter III, we investigated *S. aureus* central metabolism to identify essential metabolic pathways and nutritional interactions between host and pathogen. Although these studies represent a cursory look into the requirements of staphylococci for growth and survival in bone, extensive investigation into the mechanisms of SrrAB as a regulator of hypoxic responses and the temporal and spatial regulation of *S. aureus* metabolism *in vivo* is required to gain a comprehensive understanding of the host-pathogen interaction.

SrrAB as a regulator of hypoxic responses

In Chapter II, we demonstrated that *S. aureus* increases transcription of the quorum-responsive toxins PSMs, which kill a variety of mammalian cells including bone-depositing osteoblasts, in response to hypoxia *in vitro*. Moreover, we found that *S. aureus* can suppress quorum-dependent PSM production in aerobic environments, despite high population densities that should activate quorum responses. This is accomplished by repression of the Agr quorum-sensing system in aerobic conditions by the SrrAB TCS, effectively decoupling quorum-responsive gene expression from bacterial concentration during oxygenated conditions. SrrAB is also a critical regulator of anaerobic metabolism, emphasizing its importance in the hypoxic bone environment. These findings implicate SrrAB as essential for sensing and responding to the

hypoxic host environment during osteomyelitis and dictating the virulence and metabolic processes of *S. aureus.* In Chapter II, we also demonstrated that an s*rrB* mutant had differing phenotypes from an *srrA* mutant, further suggesting that SrrA may have phosphorylation-independent regulatory activity. These studies therefore warrant further investigation to determine how phosphorylation impacts SrrAB-mediated gene regulation. Future work should include investigations into (1) the direct regulon of SrrA, (2) phosphorylation-dependent and -independent binding of SrrA to genes within the SrrAB regulon, (3) contribution of the SrrAB regulon to survival *in vivo*.

The direct regulon of SrrA. Because of the intersection of SrrA with other major regulatory proteins, including Agr, the current established regulon of SrrAB includes both direct and indirectly regulated transcripts. The lack of an established direct regulon stems largely from the fact that current investigations, including our own, rely on evaluating broad transcriptional and proteomic changes following SrrAB mutagenesis, which can have far reaching effects on the *S. aureus* transcriptome (59, 73). Further confounding these results, a consensus sequence for SrrA binding has not been established (60, 170). A major next step in understanding the impact of SrrAB on staphylococcal metabolism and virulence is therefore to establish a direct regulon and consensus sequence. One way in which this can be done is through Chromatin Immunoprecipitation – Sequences (ChIP-Seq).

ChIP-Seq utilizes an antibody specific to the protein of interest to immunoprecipitate DNA fragments that have been crosslinked to the protein. These DNA fragments can then be eluted and subjected to sequencing to map the recovered DNA fragments back to the genome (171, 172). The DNA fragments recovered are considered to be sites of protein binding. The indirect SrrA regulon identified by our microarray can be utilized as internal controls for this project. Following ChIP-

Seq, Hidden Markov Modeling can be used to align the newly identified SrrA DNA binding sites and identify a consensus sequence by analyzing for regions of homology between target genes. The SrrA consensus sequence will help inform how affinity of SrrA for a given promoter, determined by fidelity to the consensus sequence, determines SrrA regulation of these genes. Furthermore, the location of the binding sequences relative to the transcription start site of the gene can be compared to examine the effect of SrrA binding location on DNA regulation.

Phosphorylation-dependent and -independent binding of SrrA to genes within the SrrAB regulon. Prototypical TCSs consist of a response regulator that is differentially phosphorylated by a corresponding sensor kinase to activate DNA binding activity. Although SrrAB is positioned to function as a prototypical TCS, the requirement of the sensor kinase, SrrB, to dictate activity of the response regulator, SrrA, is not established. Furthermore, although we have determined that SrrAB regulates the *S. aureus* quorum-sensing system differently in aerobic and hypoxic conditions, the impact of SrrA phosphorylation state on this regulation is unknown. Moreover, SrrA is capable of binding the *agr* promoter without *in vitro* phosphorylation, suggesting phospho-independent regulatory activity (60). Interestingly, the *B. subtilis* SrrA homolog, ResD, expresses both phosphorylation-dependent and phosphorylation-independent regulation of transcriptional activity (173, 174). These studies suggest that SrrA has regulatory activity in both phosphorylated and un-phosphorylated states, and moreover, that phosphorylation status of SrrA may dictate target specificity.

Investigations into phosphorylation dependence of TCSs typically rely on the generation of phospho-derivatives of the response regulator that mimic the phosphorylated and non-phosphorylated states of the protein by site directed mutagenesis (175, 176)**.** The phospho-mimetic construct is created by mutating the conserved aspartate codon to encode glutamic acid, mimicking

the negative charge of the phosphorylated RR. Homology with the related RR in *B. subtilis*, ResD, indicates that residue D53 is the conserved aspartate in SrrA (72, 173). Similarly, this aspartate can be substituted for an alanine, a non-phosphorylatable residue, creating a "phospho-locked off" construct. Using these phospho-derivative constructs, the phosphorylation-dependence of SrrAB can then be investigated through the functional assays established in Chapter II and through electrophoretic mobility shift assays.

Contribution of the SrrAB regulon to survival *in vivo*. As discussed in Chapter I, mutagenesis of selected genes from within the SrrAB regulon are known to impact *S. aureus* survival *in vivo*. However, we discovered in Chapter II that other genes within the SrrAB regulon, *qoxA* and *pflB* are not required for fitness during osteomyelitis. Furthermore, recent studies indicated that constitutive activation of SrrB can lead to increased growth of small colony variants (SCVs) (177). SCVs represent an adaptation to host and antibiotic stressors, in which inactivation of the respiratory chain decreases membrane potential and prevents the influx of aminoglycoside antibiotics (178). Due to respiration inhibition, SCVs are characterized by a slow growth phenotype *in vitro*, however, constitutive activation of SrrB results in increased growth of these SCVs, without inhibiting antibiotic resistance (177). Although in Chapter II we attributed the defect of an SrrAB mutant to the inability to respond to hypoxic and nitrosative stress, the increased growth of SCVs with overactivation of SrrAB can be attributed to the enhanced ability to utilize amino acid fermentation (177). These results are not surprising in the context of the indirect regulon of SrrAB we established in Chapter II, as several genes involved in catabolism of amino acids into pyruvate and α-ketoglutarate were represented. These results do, however, indicate that the metabolic pathways regulated by SrrAB are more far reaching than previously hypothesized. Although the investigations into the metabolic requirements of staphylococci

conducted in Chapter III indicate that glycolysis is required for *S. aureus* survival *in vivo*, the activation of amino acid catabolism by SrrAB suggests that the metabolism of *S. aureus* is likely more complicated *in vivo* than our results have captured. A more thorough understanding of the metabolic and virulence pathways SrrAB regulates, informed by characterization of the direct regulon of SrrAB, is therefore required if appropriate therapeutics targeting SrrAB are to be developed.

Analyzing metabolism of bacterial pathogens *in vivo*

In Chapter II, we conducted a TnSeq analysis of genes required for staphylococcal survival during osteomyelitis. A majority of the pathways required for staphylococcal survival were metabolic genes, which is a common finding of TnSeq for most bacterial species. Interestingly, many of the metabolic pathways required for *S. aureus* survival during osteomyelitis overlap with genes required for survival in other tissue sites (36, 44, 45). Despite the power of these high-throughput techniques, however, several discrepancies in the metabolic pathways required for staphylococcal survival *in vivo* have arisen when compared to traditional mono-infections. For example, we determined by TnSeq that cytochrome oxidases and several TCA cycle enzymes are required for full fitness of *S. aureus in vivo*, however these results did not replicate in mono infections. Conversely, pathways required for full bacterial burdens in mono-infection i.e. glycolysis were not identified by TnSeq. These results stem in part from nature of TnSeq infections, in which minor defects in survival are amplified by competition with neighboring mutants or diminished by cross-complementation of extracellular proteins and metabolites. Additionally, the *in vitro* inocula preparation and outgrowth steps characteristic of TnSeq results in selection against mutants that are required for growth *in vitro*. The selection is especially apparent for mutants in glycolysis, which have a distinct disadvantage for growth in the rich media

used for preparation of the TnSeq library. Some of these disadvantages can be mitigated through selective curation of a TnSeq library as in Grosser *et al*., or through encapsulation of individual transposon mutants to prevent metabolite-cross feeding *in vitro* as in Thibault *et al*.(36, 179). Unfortunately, these methods are subject to their own limitations for widespread use either through labor intensiveness or technical limitations to use *in vivo*. Alternative methods for analyzing metabolism of bacterial pathogens during invasive infection is therefore needed. Future work in this direction will require the integration of multiple techniques including (1) curated libraries of barcoded mutants, (2) fluorescent reporters for analysis of spatial and temporal gene activation *in vivo*, and (3) improved biochemical methods for examining the nutrient milieu *in vivo*.

Curated libraries of barcoded mutants. In order to circumvent media specific disadvantages associated with for generation of TnSeq libraries and outgrowth steps, our lab is currently developing small curated pools of metabolic mutants that can be mixed in equal ratios. This technique allows for the defects associated with specific metabolic mutants – like the inability of the glycolysis mutant *pyk* to grow in the presence of glucose – to be chemically complemented *in vitro* prior to pooling these metabolic mutants for inoculation into animal models. One advantage of this technique is that the number of infections required to test each individual mutant in mono- infection, which in this study represented over 200 mice, can be dramatically reduced. Further, this reduction in infection number can allow for an increase in the number of timepoints that can be evaluated, allowing for a detailed investigation into the kinetics of metabolic requirements during infection. Additional investigations into the impact of host phenotype on bacterial metabolic requirements can be facilitated by utilization of these barcoded mutants as well. Our studies into the metabolic requirements for infection in C57Bl/6 mice revealed that glycolysis is a major requirement for staphylococcal survival *in vivo*. This naturally raises questions about

the survival of staphylococci within hosts with altered glucose metabolism, like diabetics – which demonstrate increased prevalence of invasive *S. aureus* infection and have particularly high incidence of osteomyelitis (180-184). The ability to investigate survival of bacterial mutants within major metabolic nodes within a single mouse opens the possibility to investigate the impact of host metabolism and immunity on staphylococcal metabolism *in vivo* and investigate the mechanisms behind vulnerability to staphylococcal infection in susceptible populations.

Fluorescent reporters. The data we have generated from mono-infections *in vivo*, suggest that *S. aureus* requires glycolysis, and that gluconeogenesis and the TCA cycle are dispensable for survival during osteomyelitis; however, transcriptional and proteomic based methods suggest that *S. aureus* upregulates transcription and synthesis of gluconeogenic and TCA enzymes (129, 130). Furthermore, our TnSeq data also suggests that TCA enzymes are required for full fitness during osteomyelitis. These contradictory results suggest that the metabolism of *S. aureus* may be more complicated than can be captured with mono-infections at a single timepoint. TnSeq, RNA-Seq, and proteomic based techniques by nature destroy the spatial architecture of bacterial abscesses, which may significantly influence the metabolic requirements of *S. aureus in vivo*. The distribution of nutrients within tissues is heterogenous, and collaborative studies involving our lab have observed further alterations in nutrient distribution during infection (185). Bacteria are also known to exhibit heterogenous responses within abscesses *in vivo* (186). Techniques that can capture the spatial heterogeneity of *S. aureus* infections are therefore required to gain a complete picture of staphylococcal metabolism *in vivo*. In Davis *et al*., fluorescent transcriptional reporters for genes of interest were utilized *in vivo* to examine spatial regulation of bacterial virulence expression. The same technique can be utilized in staphylococci to examine regulation of metabolic genes *in vivo*. Examination of metabolic gene expression in a spatial and temporal manner will inform how the

nutritional requirements of *S. aureus* change *in vivo* over time and assist in the development of effective therapeutics by defining the impact of tissue niche on metabolic targets.

Biochemical methods for examining the host nutrient milieu. The virulence responses of bacterial pathogens do not occur in a vacuum. It is therefore essential to understand the environmental context bacteria experience during invasive infection. In Chapter III discusses the impact of the host nutrient milieu on aspartate import in *S. aureus*. Although we broadly observed changes in tissue glutamate levels which impedes import of aspartate through the transporter, GltT, we anticipate that local changes in glutamate are drastically increased relative to whole tissue. The ability to spatially examine changes in nutrient concentration *in vivo* would significantly enhance the ability to analyze bacterial metabolism during infection. Technological advances to this end are currently under development. The standard for metabolomics *in vitro*, LC-MS, also suffers from a lack of spatial resolution due to tissue homogenization during sample processing (187). Exciting advancements in imaging mass spectrometry have enhanced the ability of the scientific community to spatially resolve host and bacterial analytes, particularly of proteins, pioneering a new field in molecular histology (130, 185). Adaptation of these imagining modalities to the metabolites impacting staphylococcal growth *in vivo* discussed in Chapter III like glycolytic carbohydrates, aspartate, glutamate, and purines was only recently developed (188, 189). Future work investigating the nutritional milieu of infectious foci and bacterial metabolic responses to host tissue will likely rely heavily on these innovative imaging technologies.

Concluding remarks

In the work described in this dissertation, we investigated the genetic programs and metabolic pathways of *S. aureus* required for survival *in vivo*. The resulting datasets have revealed key regulatory proteins involved in modulating hypoxic responses and generated a comprehensive

picture of central metabolism in *S. aureus in vivo* during osteomyelitis. This research contributes a deeper understanding of the nature of *S. aureus* metabolic adaptations *in vivo* and highlights the emerging recognition of the intersection of metabolism and virulence.

APPENDIX A. Transposon Sequencing Results

A1. Genes identified as essential for osteomyelitis by TnSeq analysis

8325 Locus	8325 Uniprot ID	8325 annotation	USA300 Locus	USA300 annotation	Product	Length	In vitro dval	osteo dval	Osteo stdev	dval_ratio	Compromised in vitro?	Essential in Abscess Infection
SAOUHSC_00358	Q2G103	hypothetical protein	SAUSA300_0374	hypothetical protein	YP_498947.1	251	0.058	0.001	0.001	0.014	X	X
SAOUHSC_00460	Q2G190	hypothetical protein	N/A	N/A	YP_499039.1	155	0.102	0.001	0.001	0.010		
SAOUHSC_00473	Q2G051	hypothetical protein	N/A	N/A	YP_499052.1	110	0.048	0.007	0.009	0.135	X	
SAOUHSC_00541	Q2G0I9	tadA; tRNA-specific adenosine deaminase	SAUSA300_0543	tRNA-specific adenosine deaminase	YP_499113.1	470	0.011	0.000	0.000	0.000	X	X
SAOUHSC_00580	Q2G0I5	hypothetical protein	SAUSA300_0575	hypothetical protein	YP_499147.1	341	0.064	0.000	0.001	0.005	X	X
SAOUHSC_00650	Q2G2E3	hypothetical protein	N/A	N/A	YP_499209.1	92	0.133	0.001	0.001	0.005		
SAOUHSC_00680	Q2G0C5	hypothetical protein	N/A	N/A	YP_499239.1	95	0.571	0.001	0.002	0.002		
SAOUHSC_00841	Q2FZZ3	hypothetical protein	SAUSA300_0795	putative thioredoxin	YP_499395.1	296	0.044	0.000	0.000	0.000	X	X
SAOUHSC_00873	Q2FZW2	hypothetical protein	SAUSA300_0839	hypothetical protein	YP_499426.1	242	0.214	0.001	0.001	0.004		
SAOUHSC_00880	Q2FZV5	hypothetical protein	SAUSA300_0846	Na+/H+ antiporter family protein	YP_499433.1	1316	0.039	0.007	0.010	0.183	X	X
SAOUHSC_00919	Q2FZS1	hypothetical protein	SAUSA300_0884	hypothetical protein	YP_499472.1	185	0.069	0.000	0.001	0.004	X	
SAOUHSC_00964	Q2FZN6	hypothetical protein	SAUSA300_0931	hypothetical protein	YP_499517.1	176	0.015	0.010	0.018	0.701	X	X
SAOUHSC_01000	Q2FZK1	qoxC; cytochrome c oxidase subunit III	SAUSA300_0961	quinol oxidase, subunit III	YP_499552.1	605	0.029	0.008	0.008	0.269	X	
SAOUHSC_01034	Q2FZH1	trkA; potassium uptake protein	SAUSA300_0988	trkA; potassium uptake protein	YP_499582.1	662	0.140	0.000	0.000	0.001		X
SAOUHSC_01087	Q2FZE4	iron compound ABC transporter permease	N/A	N/A	YP_499632.1	293	0.058	0.000	0.000	0.003	X	
SAOUHSC_01099	Q2FZD3	Endonuclease MutS2	SAUSA300_1043	MutS2 protein	YP_499643.1	2348	0.056	0.004	0.006	0.070	X	X
SAOUHSC_01193	Q2FZ58	hypothetical protein	SAUSA300_1119	hypothetical protein	YP_499732.1	1646	0.046	0.008	0.008	0.176	X	X
SAOUHSC_01206	Q2FZ47	hypothetical protein	SAUSA300_1129	UPF0122 protein	YP_499743.1	332	0.016	0.010	0.017	0.605	X	X
SAOUHSC_01256	Q2FZ15	hypothetical protein	SAUSA300_1172	Peptidase, M16 family;	YP_499789.1	1286	0.024	0.010	0.009	0.417	X	
SAOUHSC_01289	Q2FZY4	hypothetical protein	N/A	N/A	YP_499820.1	224	0.010	0.000	0.000	0.000	X	
SAOUHSC_01304	Q2FZW9	hypothetical protein	SAUSA300_1211	hypothetical protein	YP_499835.1	194	0.030	0.000	0.000	0.000	X	
SAOUHSC_01325	Q2FZU9	hypothetical protein	N/A	N/A	YP_499855.1	104	0.010	0.000	0.000	0.000	X	X
SAOUHSC_01344	Q2FZT1	hypothetical protein	N/A	N/A	YP_499873.1	488	0.013	0.001	0.001	0.089	X	X
SAOUHSC_01359	Q2G2W2	mprF; Phosphatidylglycerol lysyltransferase	SAUSA300_1255	oxacillin resistance-related FmtC protein	YP_499886.1	2522	0.040	0.009	0.010	0.227	X	X
SAOUHSC_01367	Q2FYR8	anthranilate synthase component II	SAUSA300_1263	Anthranilate synthase, glutamine amidotransferase, component II; ; trpG	YP_499894.1	566	0.401	0.003	0.005	0.008		
SAOUHSC_01439	Q2FYK1	hypothetical protein	N/A	N/A	YP_499964.1	221	0.034	0.000	0.000	0.007	X	X
SAOUHSC_01500	Q2FYF2	hypothetical protein	N/A	N/A	YP_500018.1	116	0.483	0.001	0.002	0.002		
SAOUHSC_01549	Q2FYB5	transcriptional activator rinB-like protein	SAUSA300_1412	PhiSLT ORF 50-like protein	YP_500065.1	167	0.053	0.009	0.014	0.167	X	X
SAOUHSC_01555	Q2FYA9	Conserved hypothetical phage protein	N/A	N/A	YP_500071.1	347	0.070	0.000	0.000	0.002	X	
SAOUHSC_01586	Q2FY79	Transcriptional regulatory protein SrrA	SAUSA300_1442	Staphylococcal respiratory response protein, SrrA	YP_500101.1	725	0.482	0.001	0.000	0.003		X
SAOUHSC_01595	Q2FY70	hypothetical protein	N/A	N/A	YP_500110.1	248	0.043	0.000	0.000	0.000	X	X
SAOUHSC_01621	Q2FY45	nusB; N utilization substance protein B homolog	SAUSA300_1473	N utilization substance protein B homolog; nusB	YP_500135.1	389	0.041	0.010	0.016	0.244	X	X
SAOUHSC_01645	Q2FY28	hypothetical protein	SAUSA300_1506	hypothetical protein	YP_500157.1	329	0.062	0.002	0.003	0.030	X	
SAOUHSC_01671	Q2FY03	Diacylglycerol kinase, putative	SAUSA300_1529	Diacylglycerol kinase; ; dgkA	YP_500182.1	344	0.172	0.004	0.008	0.026		X
SAOUHSC_01759	Q2FX66	cell shape-determining protein MreC	SAUSA300_1605	Rod shape-determining protein MreC	YP_500264.1	842	0.021	0.005	0.008	0.233	X	
SAOUHSC_01770	Q2FXR5	hypothetical protein	N/A	N/A	YP_500275.1	101	0.065	0.000	0.000	0.000	X	
SAOUHSC_01804	Q2FXN1	Transposase, putative	N/A	N/A	YP_500309.1	806	0.065	0.009	0.014	0.140	X	
SAOUHSC_01812	Q2FXM3	hypothetical protein	SAUSA300_1650	hypothetical protein	YP_500317.1	941	0.116	0.000	0.000	0.004		
SAOUHSC_01853	Q2G246	hypothetical protein	N/A	N/A	YP_500357.1	104	0.658	0.002	0.001	0.003		
SAOUHSC_01902	Q2FXE7	hypothetical protein	N/A	N/A	YP_500403.1	302	0.026	0.001	0.001	0.028	X	X
SAOUHSC_01906	Q2FXE3	Truncated transposase, putative	N/A	N/A	YP_500407.1	608	0.021	0.003	0.005	0.137	X	
SAOUHSC_01930	Q2FXD3	hypothetical protein	SAUSA300_1749	hypothetical protein	YP_500431.1	359	0.080	0.001	0.000	0.011	X	X
SAOUHSC_01953	Q2FXB2	Gallidermin superfamily epiA, putative	SAUSA300_1767	Lantibiotic epidermin biosynthesis protein EpiA	YP_500452.1	143	0.635	0.004	0.001	0.006		
SAOUHSC_01967	Q2G2F1	ABC transporter, ATP-binding protein, putative	SAUSA300_1786	ABC transporter, ATP-binding protein EcsA	YP_500465.1	740	0.017	0.000	0.000	0.004	X	X
SAOUHSC_01977	Q2FXA0	UPF0342 protein	SAUSA300_1795	hypothetical protein	YP_500474.1	344	0.070	0.005	0.008	0.070	X	
SAOUHSC_01986	Q2FX91	hypothetical protein	SAUSA300_1803	hypothetical protein	YP_500483.1	152	0.129	0.001	0.001	0.006		X
SAOUHSC_02015	Q2FX81	hypothetical protein	N/A	N/A	YP_500512.1	101	0.217	0.000	0.000	0.000		
SAOUHSC_02059	Q2FX41	pin PVL orf 52-like protein	N/A	N/A	YP_500552.1	245	0.112	0.006	0.010	0.057		X
SAOUHSC_02126	Q2G2S0	purB; adenylosuccinate lyase	SAUSA300_1889	Adenylosuccinate lyase; purB	YP_500617.1	1295	0.948	0.003	0.001	0.003		X
SAOUHSC_02153	Q2FWW8	hypothetical protein	SAUSA300_1912	putative membrane protein	YP_500643.1	680	0.019	0.008	0.005	0.430	X	X
SAOUHSC_02222	Q2FWQ8	Conserved hypothetical phage protein	N/A	N/A	YP_500707.1	221	0.190	0.001	0.001	0.008		
SAOUHSC_02290	Q2FWJ8	hypothetical protein	N/A	N/A	YP_500772.1	155	0.032	0.000	0.000	0.000	X	
SAOUHSC_02333	Q2FWF8	Probable transglycosylase SceD	SAUSA300_2051	Probable transglycosylase sceD	YP_500812.1	695	0.055	0.000	0.000	0.002	X	
SAOUHSC_02340	Q2FWF1	atpC; ATP synthase epsilon chain	SAUSA300_2057	ATP synthase epsilon chain; atpC	YP_500819.1	404	0.029	0.000	0.000	0.005	X	X
SAOUHSC_02343	Q2FWE9	atpG; ATP synthase gamma chain	SAUSA300_2059	ATP synthase gamma chain; atpG	YP_500821.2	866	0.015	0.000	0.000	0.004	X	X
SAOUHSC_02346	Q2FWE7	atpH; ATP synthase subunit delta	SAUSA300_2061	ATP synthase subunit delta; atpH	YP_500823.1	539	0.041	0.000	0.001	0.008	X	X
SAOUHSC_02360	Q2FWD9	tdk; thymidine kinase	SAUSA300_2073	Thymidine kinase; tdk	YP_500836.1	599	0.027	0.002	0.003	0.069	X	X
SAOUHSC_02364	Q2FWD5	hypothetical protein	SAUSA300_2077	hypothetical protein	YP_500840.1	335	0.139	0.004	0.002	0.025		X
SAOUHSC_02378	Q2FWC0	hypothetical protein	N/A	N/A	YP_500855.1	128	0.068	0.000	0.001	0.006	X	
SAOUHSC_02602	Q2FVU0	hypothetical protein	N/A	N/A	YP_501063.1	359	0.575	0.002	0.001	0.003		
SAOUHSC_02707	Q2FVK4	hypothetical protein	N/A	N/A	YP_501169.1	182	0.159	0.000	0.001	0.002		X
SAOUHSC_02845	Q2FV89	hypothetical protein	SAUSA300_2474	hypothetical protein	YP_501303.1	344	0.040	0.000	0.000	0.004	X	X
SAOUHSC_A02811	Q2FUK6	hypothetical protein	N/A	N/A	YP_501420.1	167	0.130	0.001	0.001	0.005		
SAOUHSC_01585	Q2FY80	respiratory response protein SrrB	SAUSA300_1441	srrB; respiratory response protein	YP_500100.1	1751	1.195	0.010	0.005	0.008		X
SAOUHSC_02053	Q2FX47	Transcriptional activator rinb-related protein	SAUSA300_1412	similar to transcriptional activator rinB	YP_500546.1	188	0.239	0.010	0.013	0.040		X

A2. Transposon mutants with compromised fitness during osteomyelitis, but not *in vitro* growth, identified by TnSeq analysis.

8325 Locus	8325 Uniprot ID	8325 annotation	USA300 locus	USA300 annotation	Accession number	Length	In vitro dval	Osteo avg_dval	Osteo stdev	dval ratio
SAOUHSC_00087	Q2G1M0	hypothetical protein	SAUSA300_RS00675	hypothetical protein	YP_498688.1	122	0.192	0.044	0.069	0.228
SAOUHSC_00179	Q2G1E6	hypothetical protein	SAUSA300_0212	Gfo/Idh/MocA family oxidoreductase	YP_498776.1	1076	0.264	0.085	0.031	0.324
SAOUHSC_00208	Q2G216	hypothetical protein	SAUSA300_RS01255	hypothetical protein	YP_498804.1	143	0.279	0.028	0.046	0.099
SAOUHSC_00331	Q2G1V7	hypothetical protein	SAUSA300_0350	Cro/CI family transcriptional regulator-like protein	YP_498920.1	203	0.382	0.043	0.073	0.113
SAOUHSC_00346	Q2G115	GTP-dependent nucleic acid-binding protein EngD	SAUSA300_0364	GTP-binding protein YchF	YP_498935.1	1097	0.139	0.028	0.025	0.200
SAOUHSC_00347	Q2G114	hypothetical protein	SAUSA300_0365	hypothetical protein	YP_498936.1	191	0.337	0.028	0.015	0.084
SAOUHSC_00350	Q2G111	30S ribosomal protein S18	SAUSA300_0368	rpsR; 30S ribosomal protein S18	YP_498939.1	242	0.459	0.042	0.033	0.092
SAOUHSC_00372	Q2G0Y9	xanthine phosphoribosyltransferase	SAUSA300_0386	xpt; xanthine phosphoribosyltransferase	YP_498961.1	578	0.507	0.047	0.076	0.093
SAOUHSC_00380	Q2G0Y2	hypothetical protein	N/A	N/A	YP_498968.1	260	0.109	0.077	0.133	0.706
SAOUHSC_00397	Q2G0X6	type I restriction-modification system, M subunit	SAUSA300_0405	hsdM; type I restriction-modification system, M subunit	YP_498984.1	1472	0.214	0.078	0.049	0.365
SAOUHSC_00414	Q2G0W0	hypothetical protein	SAUSA300_0427	hypothetical protein	YP_499000.1	362	0.100	0.047	0.050	0.476
SAOUHSC_00420	Q2G0V5	Transporter	SAUSA300_0432	hypothetical protein	YP_499005.1	1337	0.127	0.080	0.044	0.633
SAOUHSC_00463	Q2G0T1	rnmV; Ribonuclease M5	SAUSA300_0469	hypothetical protein	YP_499042.1	536	0.214	0.090	0.130	0.422
SAOUHSC_00464	Q2G0T0	rsmA; Ribosomal RNA small subunit methyltransferase A	SAUSA300_0470	ksgA; dimethyladenosine transferase	YP_499043.1	893	0.574	0.084	0.033	0.147
SAOUHSC_00483	Q2G0R3	S1 RNA binding domain protein	SAUSA300_0486	hypothetical protein	YP_499060.1	401	0.119	0.046	0.056	0.389
SAOUHSC_00488	Q2G0Q8	Cysteine synthase	SAUSA300_0491	cysK; cysteine synthase A	YP_499065.1	932	0.176	0.073	0.084	0.416
SAOUHSC_00656	Q2G0E9	hypothetical protein	SAUSA300_0637	dihydroxyacetone kinase subunit DhaL	YP_499215.1	584	0.528	0.077	0.057	0.145
SAOUHSC_00670	Q2G0D5	hypothetical protein	SAUSA300_0650	phosphate transporter family protein	YP_499229.1	1007	1.413	0.033	0.019	0.023
SAOUHSC_00685	Q2G0C0	hypothetical protein	SAUSA300_0663	hypothetical protein	YP_499244.1	395	0.378	0.090	0.058	0.238
SAOUHSC_00705	Q2G0A0	Cys-tRNA(Pro)/Cys-tRNA(Cys) deacylase	SAUSA300_0682	ybaK; ybaK/ebsC protein	YP_499264.1	482	0.302	0.034	0.031	0.112
SAOUHSC_00719	Q2G1X7	queE; 7-carboxy-7-deazaguanine synthase	SAUSA300_0695	radical activating enzyme family protein	YP_499278.1	713	0.149	0.038	0.082	0.389
SAOUHSC_00802	Q2G0Z5	est; carboxylesterase	SAUSA300_0763	lest	YP_499358.1	740	0.276	0.060	0.041	0.217
SAOUHSC_00809	Q2G018	hypothetical protein	N/A	N/A	YP_499365.1	155	0.892	0.093	0.094	0.104
SAOUHSC_00818	Q2G010	nuc; thermonuclease	SAUSA300_0776	nuc; thermonuclease	YP_499373.1	686	0.266	0.037	0.019	0.137
SAOUHSC_00826	Q2G1T2	hypothetical protein	SAUSA300_0781	hypothetical protein	YP_499381.1	236	0.199	0.013	0.022	0.064
SAOUHSC_00843	Q2FZZ1	hypothetical protein	SAUSA300_0797	ABC transporter permease	YP_499397.1	695	0.197	0.028	0.024	0.130
SAOUHSC_00951	Q2FZP9	Putative phosphoesterase	SAUSA300_0916	hypothetical protein	YP_499504.1	509	0.660	0.083	0.121	0.126
SAOUHSC_00979	Q2FZM1	hypothetical protein	SAUSA300_0943	acetyltransferase	YP_499532.1	551	0.135	0.089	0.091	0.663
SAOUHSC_01008	Q2FZJ5	purE; N5-carboxyaminoimidazole ribonucleotide mutase	SAUSA300_0966	purE; phosphoribosylaminoimidazole carboxylase, catalytic subunit	YP_499558.1	419	0.141	0.069	0.118	0.489
SAOUHSC_01030	Q2FZH4	hypothetical protein	SAUSA300_0985	hypothetical protein	YP_499579.1	233	0.318	0.022	0.036	0.069
SAOUHSC_01032	Q2FZH2	Cytochrome c ubiquinol oxidase, subunit II, putative	SAUSA300_0987	cytochrome D ubiquinol oxidase, subunit II	YP_499581.1	1019	0.314	0.078	0.051	0.248
SAOUHSC_01037	Q2FZG7	hypothetical protein	SAUSA300_RS05335	hypothetical protein	YP_499586.1	122	0.101	0.022	0.037	0.218
SAOUHSC_01040	Q2FZG4	Pyruvate dehydrogenase complex, E1 component, alpha subunit, putative	SAUSA300_0993	pdhA; pyruvate dehydrogenase E1 component, alpha subunit	YP_499589.1	1112	0.770	0.074	0.038	0.096
SAOUHSC_01044	Q2G2A2	UPF0223 protein	SAUSA300_0997	hypothetical protein	YP_499593.1	275	0.132	0.018	0.023	0.138
SAOUHSC_01049	Q2G2A8	Spermidine/putrescine ABC transporter, spermidine/putrescine-binding protein, putative	SAUSA300_1002	potD; spermidine/putrescine ABC transporter spermidine/putrescine-binding protein	YP_499598.1	1073	0.183	0.047	0.030	0.256
SAOUHSC_01054	Q2G2G7	UPF0637 protein	SAUSA300_1006	hypothetical protein	YP_499602.1	614	0.148	0.028	0.026	0.190
SAOUHSC_01064	Q2G2C1	pyruvate carboxylase	SAUSA300_1014	pyruvate carboxylase	YP_499610.1	3452	0.620	0.078	0.047	0.125
SAOUHSC_01098	Q2FZD4	DNA-dependent DNA polymerase beta chain, putative	SAUSA300_1042	hypothetical protein	YP_499642.1	1712	0.177	0.040	0.027	0.224
SAOUHSC_01110	Q2FZC2	fibrinogen-binding protein-like protein	SAUSA300_1052	fibrinogen-binding protein	YP_499654.1	329	0.170	0.097	0.165	0.573
SAOUHSC_01111	Q2FZC1	hypothetical protein	SAUSA300_RS05675	hypothetical protein	YP_499655.1	92	0.155	0.025	0.044	0.164
SAOUHSC_01122	Q2G1X4	hypothetical protein	SAUSA300_RS05725	membrane protein	YP_499666.1	146	0.276	0.038	0.059	0.129
SAOUHSC_01215	Q2FZ38	rnhB; ribonuclease HII	SAUSA300_1137	rnhB; ribonuclease HII	YP_499752.1	767	0.192	0.070	0.048	0.364
SAOUHSC_01216	Q2FZ37	sucC; succinyl-CoA synthetase subunit beta	SAUSA300_1138	Succinyl-CoA synthetase subunit beta; SucC	YP_499753.1	1166	0.102	0.035	0.043	0.346
SAOUHSC_01218	Q2FZ36	sucD; succinyl-CoA synthetase subunit alpha	SAUSA300_1139	Succinyl-CoA ligase [ADP-forming] subunit alpha; sucD	YP_499754.1	908	0.100	0.037	0.058	0.365
SAOUHSC_01284	Q2FYY8	hypothetical protein	SAUSA300_1199	hypothetical protein	YP_499816.1	1238	0.103	0.039	0.012	0.378
SAOUHSC_01292	Q2FYY1	hypothetical protein	SAUSA300_1204	hypothetical protein	YP_499823.1	185	0.487	0.064	0.047	0.132
SAOUHSC_01296	Q2FYX7	hypothetical protein	SAUSA300_1207	hypothetical protein	YP_499827.1	584	0.102	0.028	0.029	0.257
SAOUHSC_01302	Q2FYX1	hypothetical protein	SAUSA300_1209	hypothetical protein	YP_499833.1	134	0.249	0.021	0.023	0.084
SAOUHSC_01326	Q2FYU8	gamma-aminobutyrate permease	SAUSA300_1231	gamma-aminobutyrate permease	YP_499856.1	1454	1.059	0.076	0.037	0.071
SAOUHSC_01336	Q2FYT9	UPF0291 protein	SAUSA300_1238	DUF896 Superfamily, conserved in B. Subtilis (SOS response)	YP_499865.1	239	0.221	0.082	0.101	0.372
SAOUHSC_01343	Q2FYT2	hypothetical protein	SAUSA300_1243	sbcC; exonuclease	YP_499872.1	107	0.541	0.072	0.079	0.133
SAOUHSC_01356	Q2GZN4	glcT	SAUSA300_1253	glcT; transcription antiterminator	YP_499883.1	851	0.670	0.086	0.068	0.128
SAOUHSC_01369	Q2FYR6	trpC; indole-3-glycerol-phosphate synthase	SAUSA300_1265	trpC; indole-3-glycerol-phosphate synthase	YP_499896.1	782	0.178	0.015	0.012	0.082
SAOUHSC_01377	Q2FYQ8	Putative oligopeptide transport ATP-binding protein oppF2	SAUSA300_1273	opp-2F oligopeptide permease, ATP-binding protein	YP_499904.1	701	0.174	0.033	0.041	0.193
SAOUHSC_01388	Q2FYP7	hypothetical protein	N/A	N/A	YP_499915.1	107	0.505	0.022	0.038	0.044
SAOUHSC_01404	Q2FYN1	hypothetical protein	SAUSA300_RS07040	hypothetical protein	YP_499931.1	188	0.461	0.039	0.028	0.086
SAOUHSC_01413	Q2GJI8	hypothetical protein	SAUSA300_1302	ATPase family protein	YP_499940.1	791	0.271	0.070	0.035	0.258
SAOUHSC_01414	Q2GJ27	hypothetical protein	SAUSA300_1303	hypothetical protein	YP_499941.1	335	0.322	0.065	0.056	0.201
SAOUHSC_01416	Q2FYM2	odhB; Dihydrolipoyllysine-residue succinyltransferase component of 2-oxoglutarate dehydrogenase complex	SAUSA300_1305	sucB; dihydrolipoamide succinyltransferase	YP_499943.1	1268	0.166	0.097	0.086	0.587
SAOUHSC_01433	Q2FYK7	hypothetical protein	SAUSA300_1318	hypothetical protein	YP_499958.1	839	0.155	0.058	0.027	0.370
SAOUHSC_01443	Q2FYJ7	hypothetical protein	SAUSA300_1326	putative cell wall enzyme EbsB	YP_499968.1	401	0.394	0.072	0.013	0.182
SAOUHSC_01448	Q2FYJ5	Quinolone resistance protein NorB	SAUSA300_1328	putative drug transporter	YP_499970.1	1391	0.255	0.073	0.013	0.286
SAOUHSC_01459	Q2FYI7	hypothetical protein	SAUSA300_1335	hypothetical protein	YP_499978.1	332	0.183	0.021	0.034	0.114
SAOUHSC_01468	Q2FYH9	hypothetical protein	SAUSA300_1342	hypothetical protein	YP_499986.1	341	0.306	0.043	0.051	0.142
SAOUHSC_01471	Q2FYH6	asnS; Asparagine--tRNA ligase	SAUSA300_1345	asnC; asparaginyl-tRNA synthetase	YP_499989.1	1292	0.379	0.071	0.046	0.186
SAOUHSC_01484	Q2FYG8	hypothetical protein	SAUSA300_RS07400	membrane protein	YP_500002.1	200	0.215	0.014	0.020	0.065
SAOUHSC_01527	Q2G2K3	hypothetical protein	SAUSA300_1395	phiSLT ORF116b-like protein	YP_500044.1	350	0.296	0.090	0.084	0.304
SAOUHSC_01528	Q2G2K2	bacteriophage L54a1g-like domain-containing protein	SAUSA300_1396	phiSLT ORF151-like protein, major tail protein	YP_500045.1	455	0.199	0.050	0.023	0.250
SAOUHSC_01531	Q2G2S5	SLT orf 123-like protein	SAUSA300_1398	phiSLT ORF123-like protein	YP_500048.1	401	0.353	0.072	0.063	0.205
SAOUHSC_01539	Q2FYC5	terminase-small subunit	SAUSA300_1405	phiSLT ORF 101-like protein, terminase, small subunit	YP_500055.1	305	0.177	0.013	0.021	0.075
SAOUHSC_01558	Q2FYA6	PVL orf 51-like protein	SAUSA300_1953	phiPVL ORF051-like protein	YP_500074.1	242	0.246	0.026	0.107	0.393
SAOUHSC_01560	Q2FYA4	Conserved hypothetical phage protein	SAUSA300_1420	Conserved hypothetical phage protein	YP_500076.1	257	0.121	0.017	0.029	0.137
SAOUHSC_01567	Q2FY98	Conserved hypothetical phage protein	SAUSA300_1426	hypothetical protein	YP_500082.1	362	0.164	0.077	0.075	0.469
SAOUHSC_01584	Q2FY81	hypothetical protein	SAUSA300_1440	hypothetical protein	YP_500099.1	869	0.281	0.034	0.029	0.122
SAOUHSC_01603	Q2FY62	hypothetical protein	N/A	N/A	YP_500118.1	254	0.204	0.058	0.100	0.285
SAOUHSC_01610	Q2FY55	UPF0403 protein	SAUSA300_1463	hypothetical protein	YP_500125.1	437	0.220	0.077	0.096	0.351
SAOUHSC_01612	Q2FY53	2-oxoisovalerate dehydrogenase, E1 component, beta subunit, putative	SAUSA300_1465	2-oxoisovalerate dehydrogenase, E1 component, beta subunit	YP_500127.1	983	0.404	0.080	0.041	0.197
SAOUHSC_01655	Q2FY19	fur; ferric uptake regulation protein	SAUSA300_1514	fur; ferric uptake regulation protein	YP_500166.1	410	0.128	0.097	0.104	0.752
SAOUHSC_01673	Q2FY01	hypothetical protein	SAUSA300_1531	phoH; PhoH family phosphate starvation-induced protein	YP_500184.1	947	0.320	0.047	0.060	0.147
SAOUHSC_01676	Q2FXZ9	UPF0365 protein	SAUSA300_1533	hypothetical protein	YP_500186.1	989	0.171	0.082	0.055	0.479
SAOUHSC_01689	Q2FXY6	rpsT; 30S ribosomal protein S20	SAUSA300_1545	rpsT	YP_500199.1	251	0.123	0.013	0.015	0.090
SAOUHSC_01703	Q2FXX7	hypothetical protein	N/A	N/A	YP_500213.1	161	0.545	0.051	0.085	0.094
SAOUHSC_01723	Q2FXV8	recD2; ATP-dependent RecD-like DNA helicase	SAUSA300_1576	RecD/TraA family helicase	YP_500232.1	2477	0.121	0.079	0.058	0.649
SAOUHSC_01729	Q2FXV2	hypothetical protein	SAUSA300_1581	hypothetical protein	YP_500238.1	146	0.357	0.099	0.087	0.278
SAOUHSC_01732	Q2FXV0	hypothetical protein	SAUSA300_1583	hypothetical protein	YP_500240.1	350	0.147	0.013	0.018	0.091
SAOUHSC_01761	Q2FXS4	hypothetical protein	SAUSA300_1606	hypothetical protein	YP_500266.1	473	0.548	0.012	0.009	0.022
SAOUHSC_01768	Q2FXR7	hypothetical protein	SAUSA300_1612	tag; DNA-3-methyladenine glycosidase	YP_500273.1	560	0.438	0.092	0.100	0.210
SAOUHSC_01779	Q2FXQ6	tig; trigger factor	SAUSA300_1622	tig	YP_500284.1	1301	0.469	0.065	0.059	0.128
SAOUHSC_01810	Q2FXM5	NADP-dependent malic enzyme, putative	SAUSA300_1648	putative NADP-dependent malic enzyme	YP_500315.1	1229	0.140	0.089	0.105	0.638
SAOUHSC_01824	Q2FXL1	thiI; Probable tRNA sulfurtransferase	SAUSA300_1661	thiamine biosynthesis protein ThiI	YP_500329.1	1223	0.114	0.058	0.017	0.518
SAOUHSC_01834	Q2FXK0	hypothetical protein	SAUSA300_RS09120	hypothetical protein	YP_500340.1	95	0.123	0.023	0.040	0.187
SAOUHSC_01866	Q2FXI1	hypothetical protein	SAUSA300_1695	hypothetical protein	YP_500369.1	725	0.315	0.037	0.027	0.117
SAOUHSC_01868	Q2FXH9	Putative dipeptidase	SAUSA300_1697	dipeptidase PepV	YP_500371.1	1409	0.152	0.072	0.017	0.475
SAOUHSC_01869	Q2FXH8	hypothetical protein	SAUSA300_1698	hypothetical protein	YP_500372.1	422	0.206	0.014	0.022	0.066
SAOUHSC_01879	Q9RFJ6	HTH-type transcriptional regulator rot	SAUSA300_1708	accessory regulator Rot	YP_500382.1	401	0.131	0.065	0.020	0.498
SAOUHSC_01881	Q2FXG6	hypothetical protein	SAUSA300_0267	transposase	YP_500384.1	491	0.161	0.097	0.052	0.604
SAOUHSC_01935	Q2FXC8	serine protease SplF	SAUSA300_1753	serine protease SplF	YP_500436.1	719	0.176	0.058	0.038	0.332
SAOUHSC_01938	Q2FXC5	serine protease SplD	SAUSA300_1755	serine protease SplD	YP_500439.1	719	0.343	0.087	0.111	0.254
SAOUHSC_01969	Q2GZT0	hypothetical protein	SAUSA300_1788	hypothetical protein	YP_500467.1	365	0.277	0.052	0.024	0.186
SAOUHSC_01971	Q2GZ59	hypothetical protein	SAUSA300_1789	hypothetical protein	YP_500468.1	557	0.323	0.076	0.077	0.236
SAOUHSC_01972	Q2GZ56	Foldase protein PrsA	SAUSA300_1790	foldase protein PrsA	YP_500469.1	962	0.256	0.099	0.125	0.388
SAOUHSC_01974	Q2GZ58	hypothetical protein	SAUSA300_1792	hypothetical protein	YP_500471.1	2936	0.834	0.072	0.046	0.077
SAOUHSC_02007	Q2GZV8	hypothetical protein	SAUSA300_RS10110	hypothetical protein	YP_500504.1	230	0.610	0.083	0.142	0.136
SAOUHSC_02011	Q2G2G9	Regulatory protein RecX	SAUSA300_1854	recombination regulator RecX	YP_500508.1	818	0.212	0.045	0.062	0.215
SAOUHSC_02012	Q93Q23	Monofunctional glycosyltransferase	SAUSA300_1855	sgtB; glycosyltransferase	YP_500509.1	809	2.062	0.023	0.013	0.010
SAOUHSC_02013	P0A0K3	hypothetical protein	SAUSA300_1856	hypothetical protein	YP_500510.1	515	0.431	0.088	0.062	0.205
SAOUHSC_02020	Q2FX76	helin	N/A	N/A	YP_500517.1	437	0.177	0.093	0.023	0.526
SAOUHSC_02052	Q2FX48	Hypothetical phage protein	N/A	N/A	YP_500545.1	146	0.542	0.023	0.034	0.042
SAOUHSC_02076	Q2FXZ9	Phi PVL orf 38-like protein-related protein	SAUSA300_1429	phiSLT ORF53-like protein	YP_500569.1	161	0.208	0.091	0.071	0.440
SAOUHSC_02096	Q2FXI1	hypothetical protein	SAUSA300_1863	hypothetical protein	YP_500587.1	275	0.185	0.012	0.010	0.062
SAOUHSC_02155	Q2FWW6	hypothetical protein	SAUSA300_1914	GntR family regulatory protein	YP_500645.1	380	0.201	0.078	0.106	0.389
SAOUHSC_02158	Q2FWW3	hypothetical protein	SAUSA300_1916	hypothetical protein	YP_500648.1	1286	0.508	0.049	0.033	0.096
SAOUHSC_02170	Q2FWV4	peptidoglycan hydrolase	SAUSA300_1921	truncated amidase	YP_500657.1	296	0.957	0.079	0.122	0.082
SAOUHSC_02174	Q2FWV1	Holin, phage phi LC3 family	SAUSA300_1924	Holin	YP_500660.1	254	0.296	0.046	0.042	0.155
SAOUHSC_02188	Q2FWT7	phage head-tail adaptor	SAUSA300_1936	hypothetical protein	YP_500674.1	335	0.366	0.098	0.096	0.268
SAOUHSC_02207	Q2FWS3	Phi PVL/orf 52-like protein	SAUSA300_1418	phiSLT ORF 82-like protein	YP_500692.1	254	0.254	0.013	0.019	0.050
SAOUHSC_02220	Q2FWR0	Phi ETA orf 18-like protein	N/A	N/A	YP_500705.1	551	0.245	0.076	0.044	0.311
SAOUHSC_02221	Q2FWQ9	Conserved hypothetical phage protein	N/A	N/A	YP_500706.1	779	0.130	0.044	0.054	0.340
SAOUHSC_02227	Q2FWQ3	Conserved hypothetical phage protein	N/A	N/A	YP_500712.1	140	0.278	0.023	0.035	0.074
SAOUHSC_02228	Q2FWQ2	Conserved hypothetical phage protein	N/A	N/A	YP_500713.1	197	0.328	0.039	0.065	0.119
SAOUHSC_02233	Q2FWP8	phi PVL orf 32-like protein	N/A	N/A	YP_500717.1	260	0.273	0.022	0.016	0.082
SAOUHSC_02268	Q2FWM1	Sucrose-6-phosphate dehydrogenase, putative	SAUSA300_1994	scrB; sucrose-6-phosphate hydrolase	YP_500749.1	1484	0.265	0.088	0.052	0.333
SAOUHSC_02275	Q2FWL4	hypothetical protein	N/A	N/A	YP_500756.1	128	0.114	0.023	0.040	0.203
SAOUHSC_02288	Q2FWK0	leuD; 3-isopropylmalate dehydratase small subunit	SAUSA300_2013	leuD; isopropylmalate isomerase small subunit	YP_500770.1	572	0.236	0.085	0.078	0.358
SAOUHSC_02352	Q2GZF5	UDP-N-acetylglucosamine 2-epimerase	SAUSA300_2065	UDP-GlcNAc 2-epimerase	YP_500828.1	1127	0.329	0.063	0.097	0.192
SAOUHSC_02353	Q2FWE6	upp; uracil phosphoribosyltransferase	SAUSA300_2066	upp	YP_500829.1	629	0.457	0.050	0.037	0.110
SAOUHSC_02354	Q2FWE5	glyA; serine hydroxymethyltransferase	SAUSA300_2067	glyA; serine hydroxymethyltransferase	YP_500830.1	1238	0.373	0.048	0.047	0.129
SAOUHSC_02355	Q2FWE4	UPF0340 protein	SAUSA300_2068	hypothetical protein	YP_500831.1	524	0.446	0.082	0.070	0.185
SAOUHSC_02358	Q2FWE1	prmC; Release factor glutamine methyltransferase	SAUSA300_2071	HemK family modification methylase	YP_500834.1	752	0.793	0.026	0.028	0.033
SAOUHSC_02394	Q2FWA4	hypothetical protein	SAUSA300_RS11585	hypothetical protein	YP_500871.1	92	0.336	0.092	0.160	0.275
SAOUHSC_02462	Q2FW55	hypothetical protein	N/A	N/A	YP_500930.1	167	0.122	0.014	0.024	0.112
SAOUHSC_02473	Q2FW44	hypothetical protein	N/A	N/A	YP_500941.1	92	0.571	0.037	0.063	0.065
SAOUHSC_02521	Q2FVZ9	hypothetical protein	SAUSA300_RS12190	hypothetical protein	YP_500986.1	131	0.178	0.019	0.032	0.107
SAOUHSC_02540	Q2FVY2	Molybdopterin converting factor moa, putative	SAUSA300_2222	molybdopterin converting factor, subunit 2	YP_501003.1	446	0.254	0.028	0.027	0.115
SAOUHSC_02543	Q2FVX9	moaC; Cyclic pyranopterin monophosphate synthase accessory protein	SAUSA300_2225	molybdenum cofactor biosynthesis protein MoaC	YP_501006.1	494	0.106	0.077	0.125	0.723
SAOUHSC_02559	Q2G2K6	ureB; urease subunit beta	SAUSA300_2239	ureB; urease subunit beta	YP_501021.1	410	0.150	0.055	0.020	0.364
SAOUHSC_02703	Q2FVK8	gpmA; 2,3-bisphosphoglycerate-dependent phosphoglycerate mutase	SAUSA300_2362	gpmA; phosphoglyceromutase	YP_501165.1	686	0.528	0.098	0.060	0.186
SAOUHSC_02805	Q2GJ07	hypothetical protein	N/A	N/A	YP_501264.1	302	0.270	0.040	0.045	0.149
SAOUHSC_02824	Q2FVA9	hypothetical protein	SAUSA300_2457	phospholipase/carboxylesterase family protein	YP_501283.1	593	0.105	0.080	0.036	0.765
SAOUHSC_02838	Q2FV96	hypothetical protein	SAUSA300_RS13695	hypothetical protein	YP_501296.1	98	0.346	0.029	0.050	0.084
SAOUHSC_02861	Q2FV75	Methylated-DNA--protein-cysteine methyltransferase, putative	SAUSA300_2485	methylated DNA-protein cysteine methyltransferase	YP_501317.1	521	0.224	0.036	0.029	0.159
SAOUHSC_A00332	Q2G125	hypothetical protein	SAUSA300_RS01880	hypothetical protein	YP_498525.1	158	0.292	0.072	0.063	0.247
SAOUHSC_A01079	Q2FZB5	hypothetical protein	SAUSA300_RS05700	hypothetical protein	YP_499661.1	155	1.143	0.077	0.112	0.063
SAOUHSC_A02013	Q2FXD4	hypothetical protein	N/A	N/A	YP_500594.1	188	0.269	0.043	0.043	0.160
SAOUHSC_A02169	Q2FWK8	hypothetical protein	SAUSA300_RS11030	hypothetical protein	YP_500762.1	155	0.285	0.028	0.023	0.097
SAOUHSC_A02331	Q2FW60	hypothetical protein	SAUSA300_RS11885	hypothetical protein	YP_500925.1	161	0.367	0.051	0.084	0.138
SAOUHSC_A02503	Q2GJ24	hypothetical protein	SAUSA300_RS12725	hypothetical protein	YP_501097.1	269	0.610	0.092	0.157	0.150
SAOUHSC_T00046	tRNA-OTHER	tRNA				74	1.113	0.037	0.032	0.033

APPENDIX B. Microarray Results of *srrAB* Mutant in Aerobic and Hypoxic Conditions

B1. Transcripts differentially regulated by SrrAB during aerobic growth

COL Locus	Annotation[1]	Fold Increase[2]	p-value	Regulated under nitrosative stress[3]	TnSeq Analysis[4]
SA0008	hutH; histidine ammonia-lyase {N315}	-2.3	0.04		
SA0138	cap5C; capsular polysaccharide biosynthesis protein Cap5C (cap5C) {Staphylococcus aureus COL}	-2.1	0.00		
SA0204	pflB; formate acetyltransferase (pflB) {Staphylococcus aureus COL}	3.8	0.02	X	
SA0205	pflA; pyruvate formate-lyase-activating enzyme (pflA) {Staphylococcus aureus COL}	4.2	0.04	X	
SA0211	acetyl-CoA acetyltransferase {Staphylococcus aureus COL}	-6.7	0.01		
SA0212	3-hydroxyacyl-CoA dehydrogenase protein {Staphylococcus aureus COL}	-8.6	0.03		
SA0213	acyl-CoA dehydrogenase family protein {Staphylococcus aureus COL}	-8.0	0.02		
SA0214	long-chain-fatty-acid--CoA ligase, putative {Staphylococcus aureus COL}	-8.0	0.02		
SA0215	propionate CoA-transferase, putative {Staphylococcus aureus COL}	-4.8	0.02		
SA0218	conserved hypothetical protein {Staphylococcus aureus COL}	3.0	0.01	X	
SA0219	hypothetical protein {Staphylococcus aureus COL}	2.8	0.00	X	
SA0220	flavohemoprotein, putative {Staphylococcus aureus COL}	2.6	0.00	X	
SA0244	scdA; ScdA protein (scdA) {Staphylococcus aureus COL}	9.7	0.00	X	
SA0265	hypothetical protein {Staphylococcus aureus COL}	-2.1	0.02		
SA0267	hypothetical protein {Staphylococcus aureus COL}	-2.8	0.04		
SA0278	hypothetical protein {Staphylococcus aureus COL}	-2.3	0.04		
SA0299	hypothetical protein {Staphylococcus aureus COL}	-2.3	0.03		
SA0300	hypothetical protein {Staphylococcus aureus COL}	-2.2	0.01		
SA0311	sodium:solute symporter family protein {Staphylococcus aureus COL}	-2.5	0.04		
SA0312	nanA; N-acetylneuraminate lyase (nanA) {Staphylococcus aureus COL}	-2.3	0.00		
SA0585	rplJ; ribosomal protein L10 (rplJ) {Staphylococcus aureus COL}	-2.3	0.04		
SA0599	conserved hypothetical protein {Staphylococcus aureus COL}	-2.6	0.01		
SA0872	OsmC/Ohr family protein {Staphylococcus aureus COL}	2.5	0.01		
SA0910	conserved hypothetical protein, similar to quinol oxidase polypeptide IV QoxD	2.4	0.01		
SA0959	NADH-dependent flavin oxidoreductase, Oye family {Staphylococcus aureus COL}	3.1	0.02		
SA0965	ctaB;conserved cytochrome caa3 oxidase (assembly factor) homolog {N315}	2.0	0.00		
SA1062	atl; bifunctional autolysin (atl) {Staphylococcus aureus COL}	-2.1	0.03		
SA1094	cydA;cytochrome d ubiquinol oxidase, subunit I (cydA) {Staphylococcus aureus COL}	2.1	0.01	X	
SA1124	ctaA; cytochrome oxidase assembly protein (ctaA) {Staphylococcus aureus COL}	4.2	0.00		
SA1126	conserved hypothetical protein {Staphylococcus aureus COL}	2.1	0.01	X	
SA1225	hypothetical protein {Staphylococcus aureus COL}	-2.5	0.05		
SA1360	aspartate kinase {Staphylococcus aureus COL}	6.8	0.01		
SA1362	hom; homoserine dehydrogenase (hom) {Staphylococcus aureus COL}	3.1	0.02		
SA1363	thrC; threonine synthase (thrC) {Staphylococcus aureus COL}	3.1	0.03		
SA1593	glycine cleavage system P protein, subunit 2 {Staphylococcus aureus COL}	-3.4	0.00		
SA1594	glycine cleavage system P protein, subunit 1 {Staphylococcus aureus COL}	-3.3	0.00		
SA1595	gcvT; glycine cleavage system T protein (gcvT) {Staphylococcus aureus COL}	-3.6	0.00		
SA1622	glyS; glycyl-tRNA synthetase (glyS) {Staphylococcus aureus COL}	2.3	0.02		
SA1659	conserved hypothetical protein {Staphylococcus aureus COL}	-2.4	0.05		
SA1660	LamB/YcsF family protein {Staphylococcus aureus COL}	-2.0	0.03		
SA1661	acetyl-CoA carboxylase, biotin carboxylase, putative {Staphylococcus aureus COL}	-2.0	0.01		
SA1662	acetyl-CoA carboxylase, biotin carboxyl carrier protein, putative {Staphylococcus aureus COL}	-2.2	0.03		
SA1663	urea amidolyase-related protein {Staphylococcus aureus COL}	-2.2	0.04		
SA1705	hypothetical protein {Staphylococcus aureus COL}	2.0	0.01		C
SA1741	icd; isocitrate dehydrogenase, NADP-dependent (icd) {Staphylococcus aureus COL}	-2.0	0.00		
SA1742	gltA; citrate synthase (gltA) {Staphylococcus aureus COL}	-2.3	0.01		
SA1758	Ald; alanine dehydrogenase (ald) {Staphylococcus aureus COL}	-2.1	0.01		
SA1996	ABC transporter, ATP-binding protein {Staphylococcus aureus COL}	-2.6	0.04		
SA1997	transcriptional regulator, GntR family {Staphylococcus aureus COL}	-2.3	0.03		C
SA2192	conserved hypothetical protein {MRSA252, Mu50, MW2, MSSA476, N315}	2.4	0.02		
SA2198	aldC; alpha-acetolactate decarboxylase (aldC) {Staphylococcus aureus COL}	-2.6	0.03		
SA2199	budB; acetolactate synthase, catabolic (budB) {Staphylococcus aureus COL}	-2.5	0.02		
SA2323	hutI; imidazolonepropionase (hutI) {Staphylococcus aureus COL}	-3.4	0.04		
SA2324	hutU; urocanate hydratase (hutU) {Staphylococcus aureus COL}	-3.8	0.03		
SA2338	hypothetical protein {Staphylococcus aureus COL}	-2.1	0.04		
SA2462	icaC; intercellular adhesion protein C {MRSA252, MSSA476, MW2, N315}	-2.7	0.01		
SA2521	transporter, putative {Staphylococcus aureus COL}	-2.0	0.02		
SA2563	ATP-dependent Clp protease, putative {Staphylococcus aureus COL}	3.4	0.02	X	
SA2571	conserved hypothetical protein {Staphylococcus aureus COL}	2.9	0.00		
SA2626	conserved hypothetical protein {Staphylococcus aureus COL}	2.3	0.04		
SA2634	nrdG; anaerobic ribonucleoside-triphosphate reductase activating protein (nrdG) {Staphylococcus aureus COL}	6.2	0.02	X	
SA2635	nrdD; anaerobic ribonucleoside-triphosphate reductase (nrdD) {Staphylococcus aureus COL}	5.5	0.01	X	
SA2636	citrate transporter, permease protein {Staphylococcus aureus COL}	-2.3	0.01		
SAV1941	putative membrane protein {MRSA252, MSSA476, MW2, Mu50}	2.1	0.01		

[1] Annotation obtain from the COL genome unless otherwise noted.

[2] Fold increase is the ratio of transcript abundance in WT relative to the *srrA* mutant; Grey shading indicates that fold increase is estimated because the transcript was below threshold in the comparator condition.

[3] See Kinkel et al, PMID: 24222487

[4] "C" denotes compromised during TnSeq analysis of osteomyelitis

B2. Transcripts differentially regulated by SrrAB during hypoxic growth.

COL Locus	Annotation[1]	Fold Increase[2]	p-value	Regulated under nitrosative stress[3]	TnSeq Analysis[4]
SA0078	plc; 1-phosphatidylinositol phosphodiesterase (plc) {Staphylococcus aureus COL}	9.9	0.00		
SA0089	antigen, 67 kDa {Staphylococcus aureus COL}	11.3	0.01	X	
SA0135	alcohol dehydrogenase, iron-containing {Staphylococcus aureus COL}	2.9	0.00		
SA0162	conserved NAD-dependent formate dehydrogenase {all strains, COL}	-3.7	0.04		
SA0176	conserved hypothetical protein {Staphylococcus aureus COL}	3.4	0.01		
SA0177	glucokinase regulator-related protein {Staphylococcus aureus COL}	3.5	0.02		
SA0178	PTS system, IIBC components {Staphylococcus aureus COL}	3.0	0.02		
SA0202	sensor histidine kinase family protein {Staphylococcus aureus COL}	3.3	0.03		
SA0203	iron compound ABC transporter, iron compound-binding protein, putative {Staphylococcus aureus COL}	3.6	0.02		
SA0204	pflB; formate acetyltransferase (pflB) {Staphylococcus aureus COL}	7.4	0.02	X	
SA0205	pflA; pyruvate formate-lyase-activating enzyme (pflA) {Staphylococcus aureus COL}	8.2	0.00	X	
SA0207	conserved domain protein {Staphylococcus aureus COL}	3.3	0.00		
SA0211	acetyl-CoA acetyltransferase {Staphylococcus aureus COL}	-4.1	0.01		
SA0212	3-hydroxyacyl-CoA dehydrogenase protein {Staphylococcus aureus COL}	-3.8	0.05		
SA0213	acyl-CoA dehydrogenase family protein {Staphylococcus aureus COL}	-5.6	0.01		
SA0214	long-chain-fatty-acid--CoA ligase, putative {Staphylococcus aureus COL}	-7.9	0.02		
SA0215	propionate CoA-transferase, putative {Staphylococcus aureus COL}	-7.1	0.01		
SA0217	ABC transporter, substrate-binding protein {Staphylococcus aureus COL}	7.5	0.02	X	
SA0218	conserved hypothetical protein {Staphylococcus aureus COL}	8.5	0.00	X	
SA0219	hypothetical protein {Staphylococcus aureus COL}	5.2	0.04	X	
SA0220	flavohemoprotein, putative {Staphylococcus aureus COL}	3.9	0.03	X	
SA0244	scdA; ScdA protein (scdA) {Staphylococcus aureus COL}	37.4	0.00	X	
SA0245	lytS; sensor histidine kinase LytS (lytS) {Staphylococcus aureus COL}	2.4	0.03		
SA0277	hypothetical protein {Staphylococcus aureus COL}	-2.3	0.02		
SA0486	staphylococcus tandem lipoprotein {Staphylococcus aureus COL}	-2.1	0.03		
SA0517	alpha-amylase family protein {Staphylococcus aureus COL}	6.3	0.02		
SA0518	transcriptional regulator, GntR family {Staphylococcus aureus COL}	6.3	0.01		
SA0599	conserved hypothetical protein {Staphylococcus aureus COL}	-2.5	0.01		
SA0600	ilvE; branched-chain amino acid aminotransferase (ilvE) {Staphylococcus aureus COL}	2.1	0.04		
SA0602	hydrolase, haloacid dehalogenase-like family {Staphylococcus aureus COL}	2.8	0.05		
SA0648	conserved hypothetical protein {N315}	-2.1	0.04		
SA0660	alcohol dehydrogenase, zinc-containing {Staphylococcus aureus COL}	3.9	0.01	X	
SA0748	oxidoreductase, aldo/keto reductase family {Staphylococcus aureus COL}	2.1	0.03		
SA0860	nuc; thermonuclease precursor (nuc) {Staphylococcus aureus COL}	2.1	0.04		C
SA0871	acetyltransferase, putative {Staphylococcus aureus COL}	2.9	0.00		
SA0910	conserved hypothetical protein, similar to quinol oxidase polypeptide IV QoxD	3.8	0.01		
SA0962	glycerophosphoryl diester phosphodiesterase GlpQ, putative {Staphylococcus aureus COL}	5.0	0.05		
SA0965	ctaB; conserved cytochrome caa3 oxidase (assembly factor) homolog {N315}	4.2	0.01		
SA1093	conserved hypothetical protein {Staphylococcus aureus COL}	-2.8	0.00		C
SA1124	ctaA; cytochrome oxidase assembly protein (ctaA) {Staphylococcus aureus COL}	7.3	0.03		
SA1126	conserved hypothetical protein {Staphylococcus aureus COL}	4.1	0.01	X	
SA1181	arcB; ornithine carbamoyltransferase (arcB) {Staphylococcus aureus COL}	21.5	0.02		
SA1182	arc; carbamate kinase (arcC) {Staphylococcus aureus COL}	12.1	0.03		
SA1189	acetyltransferase (GNAT) family protein {COL}	-2.4	0.01		
SA1308	pyruvate ferredoxin oxidoreductase, alpha subunit {Staphylococcus aureus COL}	2.4	0.04		
SA1350	conserved hypothetical protein {Staphylococcus aureus COL}	-2.8	0.01		
SA1358	conserved hypothetical protein {Staphylococcus aureus COL}	2.0	0.03		
SA1362	hom; homoserine dehydrogenase (hom) {Staphylococcus aureus COL}	3.9	0.02		
SA1364	thrB; homoserine kinase (thrB) {Staphylococcus aureus COL}	5.5	0.03		
SA1475	drug transporter, putative {Staphylococcus aureus COL}	4.1	0.02		C
SA1476	amino acid permease {Staphylococcus aureus COL}	5.8	0.01		
SA1477	ilvA; threonine dehydratase, catabolic (ilvA) {Staphylococcus aureus COL}	3.5	0.01		
SA1478	Ald; alanine dehydrogenase (ald) {Staphylococcus aureus COL}	4.7	0.00		
SA1532	hypothetical protein {Staphylococcus aureus COL}	-2.6	0.01		
SA1533	hypothetical protein {Staphylococcus aureus COL}	-2.5	0.02		C
SA1719	hemA; glutamyl-tRNA reductase (hemA) {Staphylococcus aureus COL}	2.1	0.03	X	
SA1742	gltA; citrate synthase (gltA) {Staphylococcus aureus COL}	-2.3	0.05		
SA1866	serine protease SplD, putative {Staphylococcus aureus COL}	2.4	0.03		C
SA1868	splB; serine protease SplB (splB) {Staphylococcus aureus COL}	3.0	0.03		
SA1976	nitric-oxide synthase, oxygenase subunit {Staphylococcus aureus COL}	6.8	0.01		
SA1977	pheA; prephenate dehydratase (pheA) {Staphylococcus aureus COL}	6.2	0.01		
SA2192	conserved hypothetical protein {MRSA252, Mu50, MW2, MSSA476, N315}	11.9	0.03		
SA2338	hypothetical protein {Staphylococcus aureus COL}	-2.2	0.01		
SA2348	drug transporter, putative {Staphylococcus aureus COL}	-2.6	0.04		
SA2401	formate/nitrite transporter family protein {Staphylococcus aureus COL}	3.1	0.02		
SA2496	conserved hypothetical protein {N315}	7.9	0.02		
SA2521	transporter, putative {Staphylococcus aureus COL}	-2.9	0.00		
SA2554.1	cidA; LrgA family protein {Staphylococcus aureus COL}	-7.7	0.04	X	
SA2563	ATP-dependent Clp protease, putative {Staphylococcus aureus COL}	7.2	0.00	X	
SA2609	conserved hypothetical protein {Staphylococcus aureus COL}	-2.2	0.02		
SA2618	idh; L-lactate dehydrogenase (ldh) {Staphylococcus aureus COL}	5.0	0.02		
SA2626	conserved hypothetical protein {Staphylococcus aureus COL}	2.3	0.03		
SA2634	nrdG; anaerobic ribonucleoside-triphosphate reductase activating protein (nrdG) {Staphylococcus aureus COL}	53.6	0.00	X	
SA2635	nrdD; anaerobic ribonucleoside-triphosphate reductase (nrdD) {Staphylococcus aureus COL}	35.9	0.00	X	
SA2662	transcriptional antiterminator, BglG family {Staphylococcus aureus COL}	4.8	0.02		
SA2717	hypothetical protein {Staphylococcus aureus COL}	-3.0	0.01		
SA2732	transcriptional regulator, putative {Staphylococcus aureus COL}	6.3	0.01		
SA2734	conserved hypothetical protein {Staphylococcus aureus COL}	9.8	0.00		

[1] **Annotation obtained from the COL genome unless otherwise noted.**

[2] **Fold increase is the ratio of transcript abundance in WT relative to the *srrA* mutant; Grey shading indicates that fold increase is estimated because the transcript was below threshold in the comparator condition.**

[3] **See Kinkel et al, PMID: 24222487**

[4] **"C" denotes compromised during TnSeq analysis of osteomyelitis**

APPENDIX C. Bacterial Hypoxic Responses Revealed as Critical Determinants of the Host-Pathogen Outcome by TnSeq Analysis of *Staphylococcus aureus* Invasive Infection

PLOS | PATHOGENS

RESEARCH ARTICLE

Bacterial Hypoxic Responses Revealed as Critical Determinants of the Host-Pathogen Outcome by TnSeq Analysis of *Staphylococcus aureus* Invasive Infection

Aimee D. Wilde[1], Daniel J. Snyder[1], Nicole E. Putnam[1], Michael D. Valentino[2¤a], Neal D. Hammer[1], Zachery R. Lonergan[1], Scott A. Hinger[3], Esar E. Aysanoa[1], Catlyn Blanchard[4], Paul M. Dunman[4], Gregory A. Wasserman[5¤b], John Chen[6¤c], Bo Shopsin[5], Michael S. Gilmore[2], Eric P. Skaar[1,7], James E. Cassat[1,8]*

1 Department of Pathology, Microbiology, and Immunology, Vanderbilt University Medical Center, Nashville, Tennessee, United States of America, **2** Departments of Ophthalmology and Microbiology and Immunology, Harvard Medical School, Boston, Massachusetts, United States of America, **3** Department of Biological Sciences, Vanderbilt University, Nashville, Tennessee, United States of America, **4** Department of Microbiology and Immunology, University of Rochester Medical Center, Rochester, New York, United States of America, **5** Departments of Medicine and Microbiology, New York University School of Medicine, New York, New York, United States of America, **6** Skirball Institute Program in Molecular Pathogenesis, Departments of Microbiology and Medicine, New York University Medical Center, New York, New York, United States of America, **7** Veterans Affairs Tennessee Valley Healthcare Services, Nashville, Tennessee, United States of America, **8** Department of Pediatrics, Division of Pediatric Infectious Diseases, Vanderbilt University Medical Center, Nashville, Tennessee, United States of America

¤a Current address: Exosome Diagnostics, Inc. Riverside Technology Center, Cambridge, Massachusetts, United States of America
¤b Current address: Department of Microbiology, Boston University School of Medicine, Boston, Massachusetts, United States of America
¤c Current address: Department of Microbiology and Immunology, Yong Loo Lin School of Medicine, National University of Singapore, Singapore
* jim.cassat@vanderbilt.edu

OPEN ACCESS

Citation: Wilde AD, Snyder DJ, Putnam NE, Valentino MD, Hammer ND, Lonergan ZR, et al. (2015) Bacterial Hypoxic Responses Revealed as Critical Determinants of the Host-Pathogen Outcome by TnSeq Analysis of *Staphylococcus aureus* Invasive Infection. PLoS Pathog 11(12): e1005341. doi:10.1371/journal.ppat.1005341

Editor: Michael Otto, National Institutes of Health, UNITED STATES

Received: September 30, 2015

Accepted: November 23, 2015

Published: December 18, 2015

Data Availability Statement: All relevant data are within the paper and its Supporting Information files. All related GeneChip data files were deposited in the NCBI Gene Expression Omnibus repository in the MIAME-compliant format under accession number GSE75516.

Funding: JEC is supported by National Institute of Allergy and Infectious Diseases (http://www.niaid.nih.gov) grant 1K08AI113107 and by a Burroughs Wellcome Fund (www.bwfund.org) Career Award for Medical Scientists. MSG is supported by National

Abstract

Staphylococcus aureus is capable of infecting nearly every organ in the human body. In order to infiltrate and thrive in such diverse host tissues, staphylococci must possess remarkable flexibility in both metabolic and virulence programs. To investigate the genetic requirements for bacterial survival during invasive infection, we performed a transposon sequencing (TnSeq) analysis of *S. aureus* during experimental osteomyelitis. TnSeq identified 65 genes essential for staphylococcal survival in infected bone and an additional 148 mutants with compromised fitness *in vivo*. Among the loci essential for *in vivo* survival was SrrAB, a staphylococcal two-component system previously reported to coordinate hypoxic and nitrosative stress responses *in vitro*. Healthy bone is intrinsically hypoxic, and intravital oxygen monitoring revealed further decreases in skeletal oxygen concentrations upon *S. aureus* infection. The fitness of an *srrAB* mutant during osteomyelitis was significantly increased by depletion of neutrophils, suggesting that neutrophils impose hypoxic and/or nitrosative stresses on invading bacteria. To more globally evaluate staphylococcal responses to changing oxygenation, we examined quorum sensing and virulence factor

Institute of Allergy and Infectious Diseases (http://www.niaid.nih.gov) grants R21AI107248 and P01AI08321. EPS is supported by National Institute of Allergy and Infectious Diseases (http://www.niaid.nih.gov) grants R01AI069233 and AI073843. BS is supported by National Institute of Allergy and Infectious Diseases (http://www.niaid.nih.gov) grant R01-AI103268. ADW is supported by National Institute of Allergy and Infectious Diseases (http://www.niaid.nih.gov) training grant T32AI112541. ZRL is supported by National Institute of Environmental Health Sciences (http://www.niehs.nih.gov) training grant 5T32ES007028-41. NDH is a Cystic Fibrosis Foundation (https://www.cff.org/) Ann Weinberg Memorial Research Fellow. The funders had no role in study design, data collection and analysis, decision to publish, or preparation of the manuscript.

Competing Interests: The authors have declared that no competing interests exist.

production in staphylococci grown under aerobic or hypoxic conditions. Hypoxic growth resulted in a profound increase in quorum sensing-dependent toxin production, and a concomitant increase in cytotoxicity toward mammalian cells. Moreover, aerobic growth limited quorum sensing and cytotoxicity in an SrrAB-dependent manner, suggesting a mechanism by which *S. aureus* modulates quorum sensing and toxin production in response to environmental oxygenation. Collectively, our results demonstrate that bacterial hypoxic responses are key determinants of the staphylococcal-host interaction.

Author Summary

Staphylococcus aureus is a leading cause of infectious death, yet is also capable of harmlessly colonizing healthy individuals. These disparate observations imply that *S. aureus* can modulate its growth and virulence in response to different host environments. To characterize the staphylococcal genetic programs required to sustain invasive infection, we applied a technique known as TnSeq to experimental osteomyelitis. Osteomyelitis is one of the most common invasive manifestations of staphylococcal infection, and a better understanding of the bacterial factors required to colonize and destroy bone will aid in vaccine and antimicrobial development. TnSeq identified more than 200 genes important for invasive staphylococcal infection of bone. Two of these genes encode a bacterial two-component system, SrrAB, which is known to help *S. aureus* survive in low oxygen. Consistent with this finding, we discovered that oxygen levels in bone decrease during osteomyelitis. Furthermore, we discovered that staphylococcal virulence is augmented by environmental oxygen levels, suggesting one strategy by which *S. aureus* can respond to different host environments. Collectively, our results define the genetic and metabolic programs required for *S. aureus* to sustain invasive infection.

Introduction

Staphylococcus aureus is a major human pathogen, capable of causing a variety of life-threatening, invasive diseases and infecting nearly every organ in the human body. Yet *S. aureus* also innocuously colonizes the skin and nares of one-third to one-half of the population [1]. These facts suggest a remarkable flexibility in terms of metabolic and virulence programs, allowing staphylococci to adapt to diverse and changing host environments during invasive infection, while also enabling a commensal lifestyle characterized by low virulence and immunotolerance. The mechanisms by which bacterial pathogens adapt to changing host environments are poorly understood, in part due to the technical difficulty in measuring adaptive responses *in vivo*. However, recent advances in high-throughput sequencing have enabled an unprecedented evaluation of the host-pathogen interface. Transposon sequencing (TnSeq) is a sensitive and high-throughput tool combining highly-saturated transposon mutant libraries with massively-parallel sequencing to calculate the fitness of all nonessential bacterial genes under a given selective pressure [2]. TnSeq has been successfully used to determine the bacterial genes required for survival in a number of different *in vitro* conditions and infection models [3–7]. More recently, a TnSeq library was generated in *S. aureus* and used to determine genes contributing to fitness in abscess and infection-related ecologies [8]. These studies illustrate the power of TnSeq analyses to determine the genetic requirements for bacterial adaptation to diverse host environments.

One of the most common invasive disease manifestations of staphylococcal infection is osteomyelitis, and *S. aureus* is by far the most common pathogen causing musculoskeletal infection. Osteomyelitis causes enormous morbidity, including functional disabilities, the requirement for invasive procedures, and the propensity to evolve into chronic infection even with appropriate management [9,10]. Two factors contribute to the therapeutic recalcitrance of osteomyelitis. First, skeletal tissues are intrinsically hypoxic, and bacterial infection further disrupts the vascular architecture of bone [11–13]. Second, the human skeleton is constantly being remodeled through the opposing actions of osteoblasts and osteoclasts. The kinetics of bone remodeling are affected dramatically by bacterial infection through osteo-immunologic crosstalk [14–16]. Thus, pathogens invading the bone must adapt to hypoxia as well as constant shifts in the available host substrates for adhesion and nutrient acquisition. While these factors would seemingly create an inhospitable environment for bacterial proliferation, bone is one of the most common locations of metastatic infection following *S. aureus* bacteremia [17]. One mechanism by which bacterial pathogens adapt to potentially hostile host environments is through the actions of one or more two-component systems (TCSs). Bacterial TCSs consist of a membrane bound histidine kinase sensor, which upon binding of its cognate ligand phosphorylates a response regulator. Response regulators most often function as transcriptional factors, and differentially coordinate changes in gene expression in response to a given stress. We therefore hypothesized that the ability of *S. aureus* to adapt to changes in available oxygen and shifts in substrate availability in inflamed skeletal tissues may rely on one or more TCSs, and that these responses would be key determinants of pathogenesis during osteomyelitis.

In this study, we employed TnSeq analysis during acute murine osteomyelitis to determine the genetic requirements for *S. aureus* survival during invasive infection. A large number of *S. aureus* genes were identified as essential for growth within bone, some of which have previously been implicated in hypoxic responses. Intravital oxygen monitoring was utilized to define changes in tissue oxygenation during osteomyelitis. Finally, we evaluated the effects of changing oxygenation on *S. aureus* quorum sensing and virulence factor production. Collectively, these studies determine the staphylococcal genes essential for survival during invasive infection of bone, define shifts in tissue oxygenation during invasive infection, and interrogate the mechanisms by which *S. aureus* can modulate its virulence in response to changes in oxygen availability.

Results

Identification of *S. aureus* genes essential for invasive infection by transposon sequencing (TnSeq) analysis of experimental osteomyelitis

In order to characterize the genes required for invasive *S. aureus* infection, TnSeq analysis was performed during experimental osteomyelitis using a recently described *S. aureus* transposon insertion library in strain HG003 [8]. To identify potential bottlenecks in bacterial survival during osteomyelitis, a timecourse infection was first performed by inoculating murine femurs with strain HG003. An inoculum of $5x10^6$ CFU was chosen based on direct comparison with strain LAC, which has served as the wildtype strain in prior osteomyelitis analyses and is representative of the most common lineage (USA300) of strains causing osteomyelitis in the United States [18]. At days 1, 3, 5, 7, and 12 post-infection, infected femurs were harvested and processed for CFU enumeration. After an initial period of replication from day 1 to day 3 post-infection, decreases in bacterial burdens were noted by days 5 and 12 (S1 Fig). Day 5 was therefore chosen for TnSeq analysis of acute osteomyelitis, as it likely represents the first bottleneck encountered by invading bacteria. For TnSeq analysis of osteomyelitis, mice were infected with the TnSeq library by direct inoculation into the femur. Five days post-infection, femurs from

infected mice were processed for genomic DNA extraction. One limitation of TnSeq analysis during invasive infection is the requirement for an outgrowth step after the recovery of bacteria from infected tissues. Although *in vitro* outgrowth could potentially confound fitness calculations, it is necessary to decrease host DNA contamination and allow for efficient sequencing of microbial DNA, and thus has become a standard practice during TnSeq analysis of invasive infection models [5,8,19–23]. We opted for a short outgrowth in liquid media to minimize any confounding effects on fitness calculation. For an *in vitro* comparator, an equivalent volume of the osteomyelitis inoculum was grown *in vitro* for 24 hours prior to collection and genomic DNA extraction. To determine mutants with compromised *in vivo* fitness, a "dval" was calculated for each gene in each condition (inoculum, *in vitro* comparator, or osteomyelitis).

A total of 65 genes were found to be essential for survival during osteomyelitis (S1 Table) but not *in vitro* growth, and mutations in an additional 148 genes resulted in significant *in vivo* compromise relative to the *in vitro* comparator (S2 Table). Of the 213 genes identified by TnSeq, 39 essential and 73 compromised genes encode hypothetical proteins, respectively. Of the remaining 101 genes, 12 essential genes and 32 compromised genes have Kyoto Encyclopedia of Genes and Genomes (KEGG) identifiers. Thirty-two of the 44 genes with KEGG identifiers can broadly be categorized into metabolic pathways, with specific pathways represented including carbon metabolism (9 genes), amino acid biosynthesis (7 genes), and the TCA cycle (5 genes). In the TCA cycle, mutations in genes *sucB* (SAOUHSC_01416), *sucC* (SAOUHSC_01216), and *sucD* (SAOUHSC_01218), which encode enzymes responsible for the conversion of α-ketoglutarate to succinate, each resulted in compromised growth during osteomyelitis. Moreover, genes encoding enzymes in pathways that feed into the TCA cycle were also important for intraosseous growth, including pyruvate carboxylase (SAOUHSC_01064 *pyc*), pyruvate dehydrogenase (SAOUHSC_01040 *pdhA*), and a putative malic enzyme (SAOUHSC_01810). Mutations in 7 *S. aureus* genes encoding amino acid biosynthesis enzymes compromised bacterial growth during osteomyelitis, yet did not significantly impair growth *in vitro*. These genes encode enzymes in the biosynthetic pathways for tryptophan (SAOUHSC_01369 *trpC*, SAOUHSC_01367 *trpG*, and SAOUHSC_01377), cysteine (SAOUHSC_00488 *cysK*), lysine (SAOUHSC_01868), leucine (SAOUHSC_02288 *leuD*), and the conversion of serine to glycine (SAOUHSC_02354 *glyA*). Mutations in 6 genes encoding components of purine and pyrimidine metabolic pathways resulted in significant *in vivo* compromise during osteomyelitis. Two of these genes (SAOUHSC_02126 *purB*, SAOUHSC_02360 *tdk*) were essential for staphylococcal survival in bone. A substantial portion of the oxidative phosphorylation pathway was also found to be necessary for staphylococcal growth during osteomyelitis. Four of the 12 essential genes with KEGG identifiers and 1 of the mutants with compromised growth are involved in oxidative phosphorylation, including components of quinol oxidase complexes (SAOUHSC_01000 *qoxC*, SAOUHSC_01032 *cydB*), and 3 subunits of the F-type ATPase (SAOUHSC_02340 *atpC*, SAOUHSC_02343 *atpG*, SAOUHSC_02346 *atpH*). Collectively, the results of TnSeq analysis during experimental osteomyelitis suggest broad adaptations in metabolism and energy production are required for staphylococcal survival during invasive infection of bone.

In contrast to an abundance of genes encoding hypothetical proteins or metabolic pathways, relatively few genes encoding known or putative virulence factors were identified by TnSeq as important for staphylococcal survival in bone. Phosphatidylglycerol lysyltransferase, encoded by *mprF* (SAOUHSC_01359), catalyzes the modification of phosphatidylglycerol with L-lysine and contributes to bacterial defenses against neutrophils, cationic antimicrobial peptides, and certain antibiotics [24]. The *mprF* gene was essential for growth during osteomyelitis, suggesting that resistance to antimicrobial peptides and neutrophils are important components of staphylococcal survival in bone. A second virulence-associated gene identified by TnSeq as

essential for *S. aureus* osteomyelitis was *isdF* (SAOUHSC_01087), which encodes a component of the iron-regulated surface determinant heme uptake system [25]. Interestingly, mutation of the ferric uptake regulator (SAOUHSC_00615 *fur*) gene also resulted in compromised intraosseous growth, illustrating a potential role for iron acquisition in the pathogenesis of staphylococcal osteomyelitis. Mutation in the genes encoding thermonuclease (SAOUHSC_00818 *nuc*), a fibrinogen-binding protein (SAOUHSC_01110), the repressor of toxins (SAOUHSC_01879 *rot*), and two serine proteases (SAOUHSC_01935 *splF*, SAOUHSC_01938 *splD*) also compromised the survival of *S. aureus* during osteomyelitis.

The genes identified by TnSeq as critical for staphylococcal osteomyelitis encode diverse metabolic processes, hypothetical proteins, and select virulence factors. These results suggest that complex bacterial adaptations occur in response to invasive infection of bone. One mechanism by which bacterial pathogens sense and ultimately respond to host-imposed stresses is through TCSs. We therefore hypothesized that staphylococcal TCSs might coordinate the complex adaptations observed during osteomyelitis. Strikingly, TnSeq analysis identified only one *S. aureus* TCS as required for intraosseous survival. The staphylococcal respiratory response (SrrAB) system is involved in coordination of the staphylococcal response to hypoxia and other stresses [26], and has been shown to directly regulate select virulence factors [27]. Both the histidine kinase (*srrB*) and the response regulator (*srrA*) components of the SrrAB locus were essential for staphylococcal survival in bone, implying that this TCS might be particularly important for coordination of the metabolic and virulence adaptations to intraosseous growth (S1 Table). In total, these results reveal the power of TnSeq analysis to identify *S. aureus* genes required for invasive infection of bone.

SrrAB differentially regulates *S. aureus* genes under aerobic and hypoxic growth, and is required for survival during osteomyelitis

Among the mutants that exhibited decreased survival in the osteomyelitis model, we identified a single TCS, SrrAB, which coordinates responses to hypoxia and nitrosative stress *in vitro* [26]. Moreover, mutations in two additional genes regulated by SrrAB specifically under conditions of nitrosative stress, *cydB* and *qoxC*, also resulted in significantly decreased fitness during osteomyelitis (**S1 and S2 Tables**) [26]. Bone and bone marrow are intrinsically hypoxic, leading to the hypothesis that SrrAB contributes to osteomyelitis pathogenesis by sensing and responding to changes in environmental oxygen [11,28]. Because the SrrAB regulon was previously defined under conditions of nitrosative stress, we sought to further define the oxygen-dependent SrrAB regulon by performing global transcriptional analysis of a clinically relevant strain (LAC) in comparison to a mutant strain lacking *srrAB* expression (Δ*srrA*) in both aerobic and hypoxic growth conditions. Inactivation of *srrAB* under aerobic conditions resulted in the differential regulation of 64 genes (39 transcripts increased in abundance and 25 decreased in abundance upon inactivation of *srrAB*) (S3 Table). Under hypoxic growth conditions, *srrAB* inactivation led to differential regulation of 78 genes (22 transcripts increased in abundance and 56 decreased in abundance) (S4 Table). Of the genes differentially regulated by SrrAB under aerobic or hypoxic conditions, only 16 were previously identified as members of the SrrAB regulon under nitrosative stress, suggesting that specific stresses might invoke different SrrAB-dependent transcriptional responses [26]. Moreover, by defining the SrrAB regulon under aerobic versus hypoxic conditions, we discovered that an additional 7 genes important for survival during osteomyelitis in the TnSeq dataset are also SrrAB-regulated (**S3 and S4 Tables**). The requirement of multiple genes in the SrrAB regulon for survival during osteomyelitis suggests that the SrrAB TCS is an important orchestrator of *S. aureus* stress responses in inflamed skeletal tissues.

Previous reports have demonstrated a significant defect in the growth of an *srrAB* mutant under anaerobic conditions but not under hypoxic growth conditions [26,27,29]. To confirm that SrrAB was not found to be essential in the TnSeq analysis simply because of a defect in growth, the Δ*srrA* polar transposon mutant and mutations in known genes of the SrrAB regulon (*pflA*, *pflB*, *qoxA*, and *qoxC*) were analyzed in the LAC strain background. The growth rate of each mutant under aerobic or hypoxic conditions was monitored over time. Under aerobic and hypoxic growth conditions, Δ*srrA* had an enhanced lag phase compared to WT but reached equivalent optical densities to WT by 8 hours (S2 Fig). The Δ*qoxA* and Δ*qoxC* mutants were unable to reach maximal optical densities as previously reported due to disruption of the electron transport chain [26]. These results indicate that an *srrAB* mutant is not impaired for growth under hypoxia, further validating our TnSeq methods.

To investigate the role of SrrAB in osteomyelitis in a clinically-relevant background without the potentially confounding influence of competition from other mutants in the TnSeq library, groups of mice were infected with either WT or Δ*srrA* in the LAC background. At 5 or 14 days post-infection, femurs were either processed to quantify bacterial burdens or subjected to micro-computed tomography (microCT) imaging (day 14) for quantification of cortical bone destruction. Inactivation of SrrAB resulted in a significant reduction in bacterial burdens in infected femurs at both 5 and 14 days post-infection (Fig 1A). Moreover, murine femurs infected with Δ*srrA* sustain significantly less cortical bone destruction than WT-infected femurs (Fig 1B–1D). These results demonstrate that SrrAB is critical for *S. aureus* survival in infected bone and for induction of pathologic changes in bone remodeling during osteomyelitis. Furthermore, the data suggest that staphylococci encounter hypoxic and/or nitrosative stresses during osteomyelitis.

S. aureus osteomyelitis triggers reduced oxygen availability in skeletal tissues

Normal bone and bone marrow are intrinsically hypoxic, with a physiologic oxygen concentration range of 11.7 to 48.9 mmHg (1.5–6.4% O_2), compared to atmospheric oxygen at approximately 160 mmHg (21% O_2) [11,28]. TnSeq analysis demonstrated that the hypoxia-responsive SrrAB TCS is essential for *S. aureus* survival in bone, suggesting that bacterial invasion and the resulting inflammation associated with osteomyelitis trigger further decreases in skeletal oxygen availability. In order to determine the oxygen concentrations of *S. aureus* infected murine femurs during osteomyelitis, an Oxylite monitor was used to record oxygen tensions at the inoculation site at various times post-infection. In uninfected mice, average pO_2 in the intramedullary canal was 45.2 mmHg, (Fig 2) consistent with previously reported bone marrow physoxia [28]. As infection progressed, the infectious focus became increasingly hypoxic, with an average oxygen tension of 14.3 mmHg at 10 days post-infection. This decreased oxygen tension was not due to the trauma induced by the inoculation procedure, as mock-infected bone showed an elevated mean pO_2 of 77.5 mmHg by 4 days post-procedure (Fig 2). Collectively, these findings demonstrate that skeletal tissues become increasingly hypoxic during *S. aureus* osteomyelitis.

The *srrAB* promoter is active in hypoxic skeletal tissues

Intravital pO_2 monitoring revealed that skeletal tissues become increasingly hypoxic during osteomyelitis, with dramatically reduced oxygen tensions as early as 24 hours after infection. These data and the results of TnSeq analysis suggest that the *srrAB* promoter is active *in vivo*. To test the hypothesis that *srrAB* promoter activity increases with decreasing oxygen availability in infected skeletal tissues, a luminescent reporter construct was created in which expression

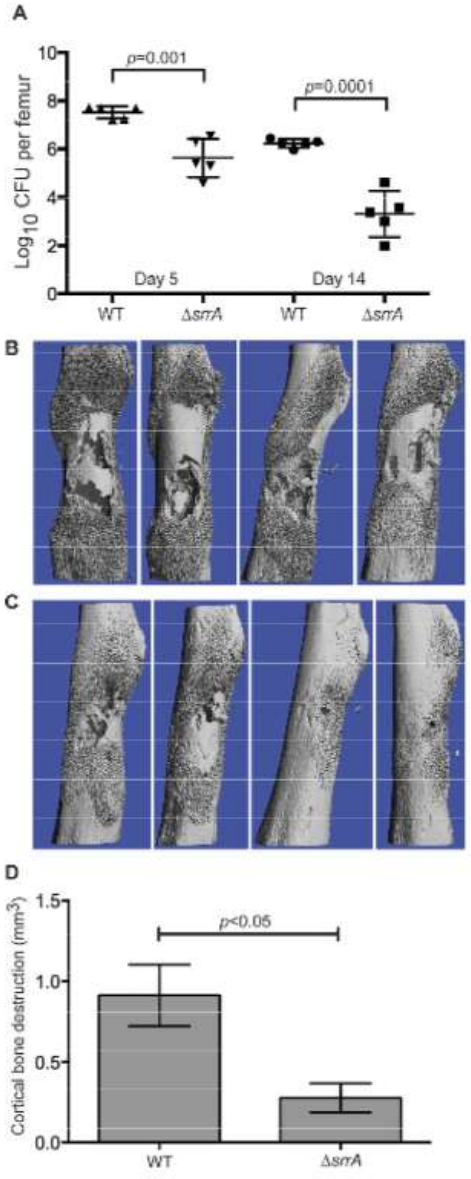
A
p=0.001
p=0.0001
Log10 CFU per femur
10
8
6
4
2
0
Day 5
Day 14
WT
ΔsrtA
WT
ΔsrtA
B
C
D
p<0.05
Cortical bone destruction (mm3)
1.5
1.0
0.5
0.0
WT
ΔsrtA

Fig 1. SrrAB is required for intraosseous survival and cortical bone destruction during *S. aureus* osteomyelitis. Osteomyelitis was induced in groups of mice using WT or Δ*srrA* strains. (A) At 5 and 14 days post-infection, femurs were processed for colony forming units (CFU) enumeration. N = 5 mice per group. Horizontal line represents the mean and error bars represent SD. (B and C) Antero-posterior views of WT (B) or Δ*srrA* (C) infected femurs at 14 days post-inoculation. (D) MicroCT imaging analysis of cortical bone destruction (mm^3) 14 days post-inoculation. N = 4 mice per group. Error bars represent the SEM. Statistical significance determined by Students *t* test.

doi:10.1371/journal.ppat.1005341.g001

of the *luxABCDE* operon is driven by the *srrAB* promoter. Mice were infected with WT *S. aureus* containing either this construct or a promoterless vector control, and at 1 hour or 24 hours post-infection infected femurs were explanted and immediately imaged for bioluminescence. No detectable luminescence above background was detected in femurs infected with WT bacteria containing the promoterless control plasmid at 1 hour or 24 hours after infection (Fig 3). In contrast, femurs infected with the P*srrAB*-pAmiLux construct showed no detectable luminescence above background at 1 hour post-infection, but displayed strong luminescent signal at 24 hours after infection, corresponding to the induction of hypoxia in infected skeletal tissues (Fig 3). Collectively, these results demonstrate that the *srrAB* promoter is activated *in vivo* during infection of hypoxic skeletal tissues.

Neutrophil depletion rescues the intraosseous growth defect of an *srr* mutant

Intravital oxygen monitoring revealed hypoxia of skeletal tissues upon infection with *S. aureus*, suggesting that inflammation triggers a reduction in skeletal oxygen concentrations. Neutrophils are a significant source of both oxidative and nitrosative stresses *in vivo* and contribute to formation of oxygen-limited abscesses in response to staphylococcal infection [30]. To test the hypothesis that SrrAB is necessary to resist hypoxic and/or nitrosative stresses imposed by

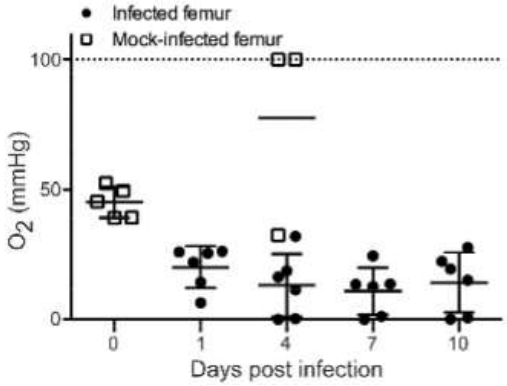

Fig 2. *S. aureus* osteomyelitis triggers reduced oxygen availability in skeletal tissues. Oxygen tension (pO_2) was measured in murine femurs infected with *S. aureus* (black circles) at 1, 4, 7 and 10 days post-infection (n = 6 from two independent experiments). Uninfected femurs (open squares) were measured for oxygen tension immediately following (n = 5) or 4 days after (n = 3) a mock inoculation procedure. Oxygen tension is reported as mmHg. Horizontal lines represent the mean. Error bars represent the SD. Dotted line represents the upper limit of detection.

doi:10.1371/journal.ppat.1005341.g002

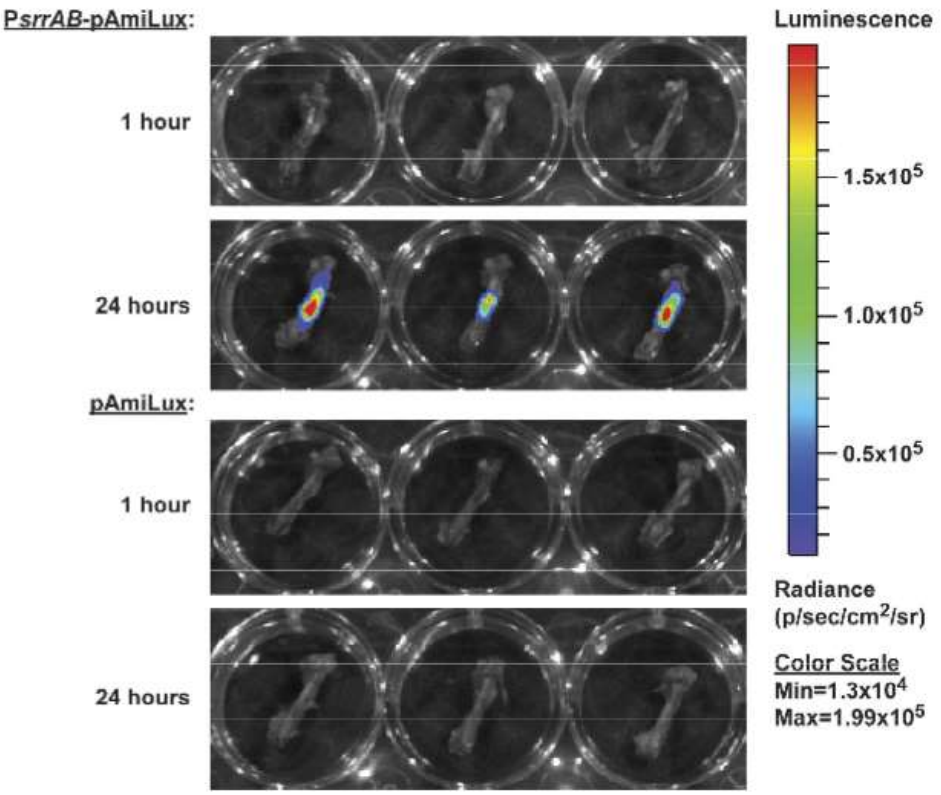

Fig 3. The *srrAB* promoter is active in hypoxic skeletal tissues. Groups of mice (n = 3 per group) were subjected to osteomyelitis by infection with WT bacteria containing either P*srrAB*-pAmiLux or pAmiLux (promoterless control). At 1 or 24 hours post-inoculation, infected femurs were explanted and immediately imaged on an IVIS 200 system (5 minute exposure).

doi:10.1371/journal.ppat.1005341.g003

neutrophils *in vivo*, mice were either rendered neutropenic with serial anti-Ly6G (1A8) monoclonal antibody injections or given an isotype control monoclonal antibody and subsequently infected with WT or Δ*srrA* [31]. At 14 days post-infection, femurs were processed for enumeration of bacterial burdens. In mice treated with control antibody, a significant virulence defect was again observed in mice infected with the Δ*srrA* mutant (Fig 4). However, in mice administered the anti-Ly6G (1A8) antibody, a significant increase in bacterial burdens was observed upon infection with Δ*srrA*, such that bacterial burdens no longer differed significantly from non-neutropenic mice infected with WT (Fig 4). These results suggest that intraosseous survival requires SrrAB to resist hypoxic and/or nitrosative stresses produced by neutrophils in response to *S. aureus* osteomyelitis.

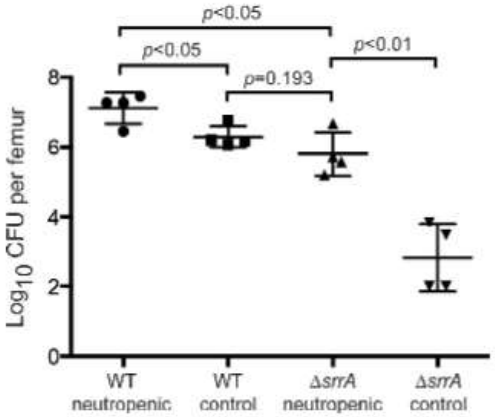

Fig 4. Neutrophil depletion rescues the intraosseous growth defect of an *srrA* mutant. Mice were given serial injections of anti-Ly6G monoclonal antibody. As a control, mice received injections of an isotype control antibody. At 14 days post-infection, femurs were processed for CFU enumeration. N = 4 mice per group. Horizontal lines represent the mean. Error bars represent SD. Significance determined by Students *t* test.

doi:10.1371/journal.ppat.1005341.g004

S. aureus modulates quorum sensing and exotoxin production in response to oxygenation

The observation that *S. aureus* infection of murine skeletal tissues leads to dramatically reduced oxygen concentrations prompted further evaluations of how oxygenation impacts the production of staphylococcal virulence factors. We previously demonstrated that secreted toxins regulated by the accessory gene regulator (*agr*) locus are particularly important for the pathogenesis of *S. aureus* osteomyelitis [32,33]. The *agr* locus (*agrABCD*) encodes a quorum sensing system coupled to a TCS, and is responsible for growth phase-dependent regulation of a number of *S. aureus* virulence factors [34]. The response regulator of the *agr* locus, AgrA, directly regulates the production of alpha-type phenol soluble modulins (PSMs), which contribute significantly to the pathology of *S. aureus* osteomyelitis [32,35]. Indeed, alpha-type PSMs were found to be the sole mediators of cytotoxicity in concentrated culture supernatant towards murine and human osteoblasts *in vitro* [32]. However, a recent report demonstrated that alpha-type PSM expression is directly linked to alpha toxin (Hla) expression [36]. To verify that PSMs are the sole mediators of cytotoxicity toward osteoblastic cells in *S. aureus* concentrated supernatants, strain LAC*Δpsmα1–4* (*Δpsm*) containing the overexpression vector pOS1-*p*lgt driving *hla* expression in trans was tested for cytotoxicity towards osteoblastic cells (S3 Fig). While WT supernatant displayed maximum cytotoxicity, *Δpsm* and *Δpsm* pOS1-*p*lgt-*hla* did not show significantly different cytotoxicity from control. Deletion of *hla* in an erythromycin-resistant LAC background also failed to attenuate cytotoxicity (S3 Fig). Moreover, targeted inactivation of RNAIII in LAC did not decrease cytotoxicity, further supporting the AgrA-regulated alpha-type PSMs as the sole secreted mediators of cytotoxicity toward osteoblastic cells (S4 Fig).

To determine the impact of culture oxygenation on *S. aureus* exotoxin production, concentrated supernatants were prepared from *S. aureus* grown either aerobically or under limited oxygenation. Incubation of several different mammalian cell lines or primary human osteoblasts with varying amounts of concentrated culture supernatant demonstrated dose-

dependent cytotoxicity that significantly increased if the bacteria were cultured under lower oxygenation (Fig 5). This phenomenon was not strain dependent, as hypoxic growth also increased the cytotoxicity of strains MW2 and Newman towards osteoblastic cells (S5 Fig). These results indicate that *S. aureus* virulence factor production is modulated in response to environmental oxygen levels.

SrrAB regulates select virulence factors under microaerobic conditions in part by directly interacting with the *agr* P2 and P3 promoters [27,29]. This observation, combined with the role of SrrAB in responding to hypoxic stresses led to the hypothesis that SrrAB may regulate quorum sensing and virulence factor production in response to changes in oxygenation. To investigate the impact of SrrAB on PSM-mediated killing of osteoblasts, osteoblastic cells were incubated with varying amounts of culture supernatant from WT or Δ*srrA* strains grown either aerobically or under hypoxia. Aerobically grown Δ*srrA* supernatants demonstrated dose-dependent killing of murine osteoblasts that was significantly increased compared to aerobically grown WT supernatants, mimicking the effect of hypoxia on cytotoxicity (Fig 6A). The cytotoxicity of aerobically grown Δ*srrA* was diminished by expression of the *srrAB* locus in trans (S6 Fig). These data suggest that SrrAB represses PSM-mediated cytotoxicity under aerobic conditions.

Because SrrAB repressed PSM-mediated cytotoxicity under aerobic conditions, we hypothesized that SrrAB impacts quorum sensing in response to oxygenation. To test this hypothesis, the reporter plasmid pDB59 (*agr*P3 promoter driving YFP expression) was introduced into WT and Δ*srrA* [37]. Aerobically grown WT cultures demonstrated significantly lower *agr*P3 activation compared to cultures grown under limited oxygenation (Fig 6B). This decrease was partially SrrAB dependent, as aerobically grown Δ*srrA* strains demonstrate a 2-fold higher expression of *agr*P3 than aerobic WT cultures (Fig 6B). To further confirm these results, quantitative RT-PCR was conducted on aerobically and hypoxically grown cultures of WT and Δ*srrA*. Transcription of *agrA* was increased relative to aerobically grown WT for both Δ*srrAB* and hypoxically grown cultures. Hypoxically grown cultures also demonstrated significantly elevated levels of *psmα* and *RNAIII transcripts* (Fig 6C). Inactivation of SrrAB resulted in an over 30-fold increase in *psmα1–4* transcription and a near 20-fold increase in *RNAIII* expression under aerobic conditions. Under hypoxic conditions, inactivation of *srrAB* resulted in a 3000-fold and 160-fold increase in *psmα1–4* and *RNAIII* transcript levels, respectively. Collectively, these data indicate that *S. aureus* quorum sensing and resultant cytotoxicity towards mammalian cells is modulated in an SrrAB-dependent manner in response to changing oxygen availability, and further define SrrAB as an important regulator of metabolic and virulence adaptations during invasive infection.

Discussion

TnSeq analysis during experimental osteomyelitis revealed *S. aureus* genes essential for invasive infection. Among the mutants with reduced *in vivo* fitness was one TCS, SrrAB, which was previously characterized as a coordinator of hypoxic and nitrosative stress responses [26]. SrrAB was originally identified as a regulator of oxygen-dependent toxic shock syndrome toxin-1 (TSST-1) expression, and was noted to have homology to the global respiratory regulator ResDE in *Bacillus subtilis* [29,38]. Subsequent analyses revealed that SrrA is capable of binding to the *agr* P2 and P3 promoter regions, and that overexpression of SrrAB reduces virulence in a rabbit endocarditis model [27]. These findings indicate a link between SrrAB and quorum sensing and suggest that oxygenation could impact staphylococcal virulence. Yet the specific signal(s) that activate SrrAB, and the mechanism by which this system modulates quorum sensing have yet to be determined.

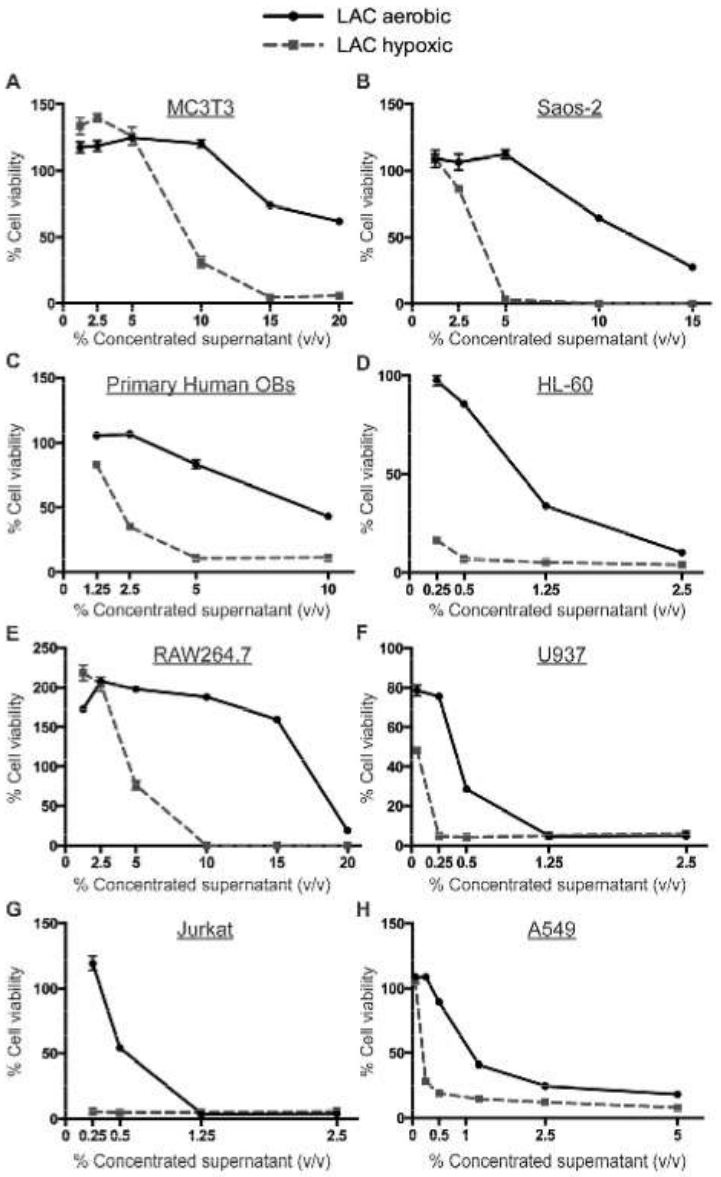
LAC aerobic
LAC hypoxic
A
MC3T3
B
Saos-2
C
Primary Human OBs
D
HL-60
E
RAW264.7
F
U937
G
Jurkat
H
A549
% Cell viability
% Concentrated supernatant (v/v)

Fig 5. Hypoxically grown bacterial supernatants lead to increased cytotoxicity in human and murine cells. WT supernatants were prepared by inoculating 3 colonies into RPMI and 1% casamino acids (CA) and growing for 15 hours either aerobically or hypoxically. MC3T3 murine osteoblastic cells (A), Saos-2 human osteoblastic cells (B), primary human osteoblasts (C), HL-60 premyelocytes (D), RAW264.7 murine macrophages (E), U937 monocytic cells (F), Jurkat T cells (G), or A549 lung epithelial cells (H) were seeded into 96 well plates 24 hours prior to intoxication with concentrated supernatant or RPMI control. Cell viability was assessed 24 hours later. Results are expressed as percent of RPMI control (n = 10), and are representative of 2 biologic replicates with the exception of human primary osteoblasts, which represent a single experiment given the limited availability of this resource. Error bars represent the SEM.

doi:10.1371/journal.ppat.1005341.g005

Our data suggest that aerobic growth of *S. aureus* limits quorum sensing and *agr*-dependent virulence factor production in a manner that is partially dependent on SrrAB. Conversely, hypoxic growth results in significantly increased cytotoxicity toward mammalian cells. Since equivalent bacterial densities were achieved under conditions of hypoxic and aerobic growth, these results imply that the output of quorum sensing can be functionally uncoupled from bacterial density by changes in culture oxygenation. Such uncoupling could be particularly advantageous for quenching of virulence factor production in environments with higher oxygen availability, such as during colonization of the skin or nares. Since inactivation of SrrAB under aerobic conditions failed to fully restore quorum sensing and cytotoxicity to the levels observed with hypoxic growth, it is likely that this phenomenon is a result of multiple factors. Additional studies are therefore needed to determine the SrrAB-dependent and SrrAB–independent mechanisms by which oxygenation regulates quorum sensing. To this end, it has previously been demonstrated that both the *S. aureus* autoinducing peptide (AIP) and AgrA can be functionally inactivated by oxidation [39,40], suggesting a potential SrrAB-independent mechanism for modulation of quorum sensing by oxygen. Moreover, the *S. aureus* genome is known to encode other redox-sensitive regulators such as Rex, MgrA, SarA, and AirSR [41–45]. It is therefore possible that environmental oxygen is not a direct regulator of quorum sensing, but rather that a change in the redox status of the bacterial cell or oxidative damage triggers changes in virulence factor production. Nevertheless, our findings suggest that shifts in available oxygen, as well as the inherent differences in physiologic oxygen concentrations in various host tissues, could have a significant impact on staphylococcal virulence. Additionally, these data highlight the importance of *in vitro* culture conditions on the study of staphylococcal virulence.

Global transcriptional analyses defined the SrrAB regulon of *S. aureus* under conditions of aerobic and hypoxic growth. Interestingly, although some overlap was noted with the previously reported SrrAB nitrosative stress regulon, we identified additional SrrAB-regulated genes under conditions of changing oxygenation [26]. Although these findings may relate to technical issues or strain-dependent differences in gene regulation, they suggest that SrrAB may integrate multiple environmental signals, or that oxidative and nitrosative stress trigger a common endogenous bacterial pathway that activates SrrAB. In order to begin defining the host components that trigger hypoxic or nitrosative stress responses in *S. aureus*, we examined the role of neutrophils during osteomyelitis. Neutrophils impose nitrosative and oxidative stress to invading pathogens through the respiratory burst, which generates reactive oxygen and nitrogen species. Moreover, neutrophils contribute to tissue hypoxia through abscess formation [30]. In support of the role of SrrAB in resisting such hypoxic and nitrosative stresses, we found that neutrophil depletion partially rescued the virulence defect of an *srrA* mutant. Additional studies are needed to parse out the effects of neutrophil-derived reactive oxygen and nitrogen species versus abscess-associated tissue hypoxia on the survival of *S. aureus*. Furthermore, it is likely that other innate and adaptive immune responses contribute to changes in tissue oxygenation and thus the redox status of invading pathogens.

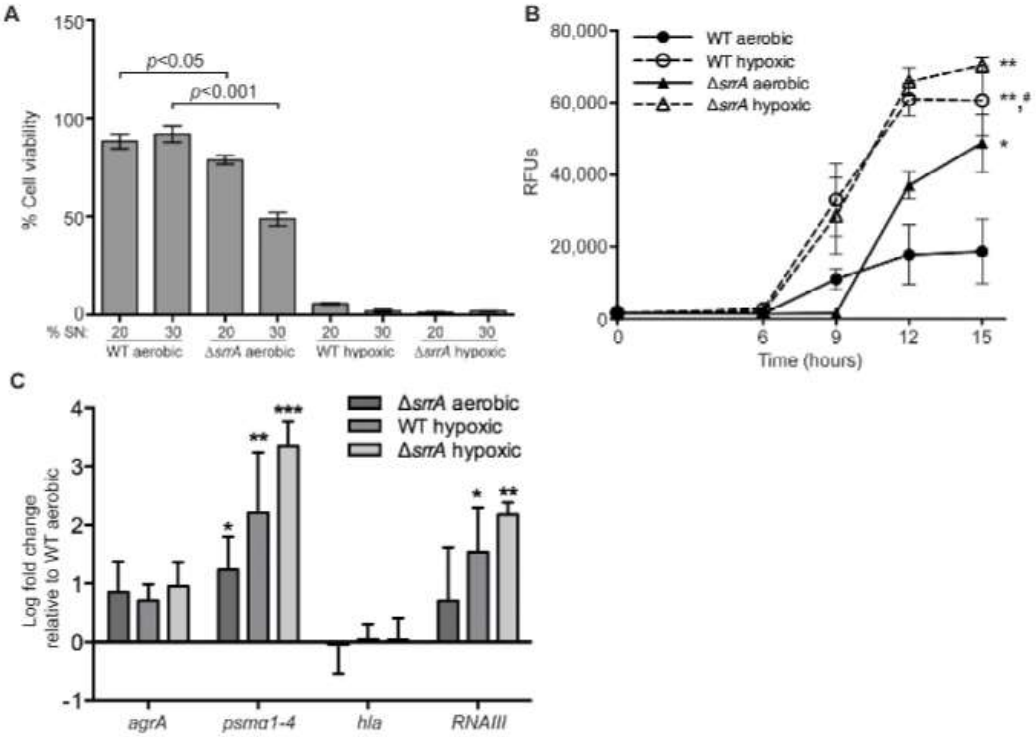

Fig 6. *S. aureus* modulates quorum sensing and exotoxin production in response to oxygenation. Supernatants from WT or Δ*srrA* were prepared by inoculating RPMI and 1% CA with a 1:1000 dilution from overnight cultures and growing for 15 hours either aerobically or hypoxically. Identical culture conditions were used to monitor quorum sensing and transcript levels (see below). (A) MC3T3 cells were seeded into 96 well plates at 5,000 cells per well. After 24 hours, growth media was replaced, and 20% or 30% of the total media volume was replaced with concentrated culture supernatant grown either aerobically or hypoxically, or an equivalent volume of RPMI. Cell viability was assessed 24 hours later, and results are expressed as percent of RPMI control (n = 10). Results are representative of at least three independent experiments. Error bars represent the SEM. (B) Agr-mediated quorum sensing was monitored using *agr*P3-dependent YFP expression in WT or Δ*srrA* strains grown aerobically or hypoxically as above. YFP relative fluorescent units (RFUs) were averaged from 3 technical replicates. Error bars represent the SD. Data shown are an average of 3 biologically independent experiments. RFUs monitored at 0, 6, 9, 12, and 15 hours after back-dilution from overnight culture. * and ** represent $p<0.05$ and 0.01, respectively relative to WT aerobic at 15 hours as determined by Student's *t* test. # represents $p<0.05$ relative to Δ*srrA* aerobic. (C) cDNA samples from WT or Δ*srrA* strains grown aerobically or hypoxically as above for 15 hours were subjected to qRT-PCR. Graph depicts fold change of the indicated transcripts relative to WT aerobic transcript level. Data shown are an average of 3 biologically independent experiments. Error bars represent the SEM. Significance was determined by two way ANOVA. * denotes $p<0.05$, ** denotes $p<0.01$, and *** denotes $p<0.001$ relative to WT aerobic.

doi:10.1371/journal.ppat.1005341.g006

In addition to the genes encoding SrrAB and its targets, TnSeq analysis during osteomyelitis revealed a large number of staphylococcal mutants with compromised fitness *in vivo*. Many of the genes identified as essential or compromised during *in vivo* growth can be broadly classified as associated with metabolism. In contrast, very few prototypical virulence factors were identified as essential for osteomyelitis. The lack of traditional secreted virulence factors identified through TnSeq analysis is not surprising due to the nature of the technique. Infection with a pooled transposon library allows for mutants deficient in a particular gene to potentially co-

opt bacterial factors from other mutants. Indeed, this phenomenon has been characterized for the exchange of metabolic intermediates in *S. aureus*, and it is conceivable that secreted virulence factors could be "shared" in a similar manner [33]. An additional limitation of TnSeq analysis is the requirement for a short outgrowth step in liquid media following harvest of the transposon library from infected bone. This outgrowth step could potentially confound our results by altering the fitness of mutants recovered from infected tissues. However, a brief outgrowth step is necessary to decrease the amount of murine DNA present in the femur homogenate and allow for effective sequencing of bacterial DNA, and is a common adjustment in TnSeq analyses of infected tissues [5, 8, 22].

TnSeq analysis of staphylococcal osteomyelitis paralleled a previous TnSeq analysis of staphylococcal growth in soft tissue abscesses [8]. In fact, 40 of the 65 genes identified as essential for growth during osteomyelitis were also essential for growth in murine abscesses. This observation is consistent with our previous data showing that osteomyelitis is characterized by exuberant abscess formation in the bone marrow [32], and suggests common stresses are encountered by staphylococci in neutrophil-rich inflammatory lesions. However, 25 of the 65 genes essential for intraosseous survival were not found to be essential for abscess growth, and may reflect unique adaptations to colonization of skeletal tissues.

Of the genes required for *S. aureus* survival during invasive infection, many encode hypothetical proteins or proteins without a previously characterized role in virulence. This observation highlights the power of TnSeq analysis as an unbiased evaluation of the genetic requirements for bacterial survival in host tissues. In summary, the results of this study elucidate bacterial survival strategies during invasive infection, link changes in environmental oxygen to staphylococcal quorum sensing and virulence, and provide a firm foundation to identify new targets for antimicrobial and vaccine design.

Materials and Methods

Ethics statement

All experiments involving animals were reviewed and approved by the Institutional Animal Care and Use Committee of Vanderbilt University and performed according to NIH guidelines, the Animal Welfare Act, and US Federal law.

Bacterial strains and growth conditions

The *S. aureus* TnSeq library in strain HG003 has been previously described [8]. All other experiments were conducted in an erythromycin-sensitive, tetracycline-sensitive derivative of the USA300 strain LAC (AH1263), which served as the wildtype (WT) unless otherwise noted [46]. Strain LAC*Δpsmα1–4* has been previously described [32,47]. Strains Δ*srrA*, Δ*qoxA*, Δ*qoxC*, Δ*pflA*, and Δ*pflB* in the LAC background were created by bacteriophage phi-85-mediated transduction of *erm*-disrupted alleles from the respective JE2 strain mutants obtained from the NARSA transposon library [48]. Strains Δ*psm* pOS1-*p*lgt and Δ*psm* pOS1-*p*lgt-*hla* were provided by Dr. Juliane Bubeck-Wardenburg [36]. Construction of strain LAC Δ*RNAIII* is described below. Plasmid pDB59 (*agr*-P3-YFP) was electroporated into LAC or Δ*srrA* for monitoring of *agr*-dependent quorum sensing [37]. All strains were grown in glass Erlenmeyer flasks at 37°C with orbital shaking at 180 rpm. All S. *aureus* strains were grown in Tryptic Soy Broth (TSB), Brain-Heart Infusion (BHI), or Roswell Park Memorial Institute medium (RPMI) supplemented with 1% casamino acids (CA). *Escherichia coli* was grown in Luria Broth (LB). Erythromycin and chloramphenicol were added to cultures at 10 μg ml^{-1} where indicated. Ampicillin was added to cultures at 100 μg ml^{-1} where indicated. Cadmium chloride was added to cultures at 0.1 mM where indicated. A 5:1 flask to volume ratio was utilized unless otherwise

noted. For comparative growth analyses, overnight aerobic cultures were back-diluted 1:1000 into fresh TSB or BHI media and optical density at 600 nm (OD_{600}) was monitored over time.

Construction of LAC Δ*RNAIII*

RNAIII including upstream and downstream flanking regions were amplified using primers 5'-GCATGCGTCGATATCGTAGCTGGGTCAG-3' and 5'-GAATTCGAAGTCACAAGTAC TATAAGCTGCG-3', and cloned into the *Hinc*II site of pUC18 [49] to create pGAW1. To delete RNAIII, inverse PCR was performed with primers 5'-TTTGGGCCCTATATTAAAAC ATGCTAAAAG-3' and 5'-TTTCTCGAGGTAATGAAGAAGGGATGAGTT-3' amplifying RNAIII flanking regions and the remaining plasmid backbone of pGAW1. The vector was religated after treatment with Polynucleotide Kinase (New England Biolabs, MA) and designated pGAW3. To insert an antibiotic resistance cassette, pGAW3 was digested with *Apa*I and *Xho*I, religated with the *Apa*I-*Xho*I fragment from pJC1075 [50] (*cadCA*, conferring resistance to cadmium) and designated pGAW6. The *Sph*I- *Kpn*I fragment from pGAW6 was cloned into the allelic replacement vector pJC1202 [50] using the same restriction sites and designated pGAW7. Strain RN4220 was electroporated with plasmid pGAW7 and plated on GL agar containing 5 μg chloramphenicol ml^{-1} at 30°C. Allelic exchange was carried out as previously described [50]. Phage 80a was then used to transduce the mutation into LAC to generate LAC *RNAIII::cad*, herein designated LAC Δ*RNAIII*.

Construction of an SrrAB overexpression plasmid

To express *srrAB* in trans, the *srrAB* open reading frame was PCR amplified from genomic DNA of LAC using primers 5'-ATCTCGAGATGTCGAACGAAATACTTATCG-3' and 5'- ATGGATCCTTCAATTTTATTCTGGTTTTGGTAG-3'. The resulting *srrAB* amplicon was then cloned into the shuttle vector pOS1 under control of the *lgt* promoter [51]. As a control, wild type and Δ*srrA* strain LAC were transformed with pOS1-*lgt* lacking an insert.

Construction of an *srrAB* bioluminescent reporter

To examine expression of *srrAB in vivo* the *srrAB* promoter was PCR amplified from genomic DNA of LAC using primers 5'-TACCCGGGTGTATTTATCACAAAGTTTGAGAAT-3' and 5'-ATCGTCGACACAGGTCATACCTCCCAC-3'. The resulting amplicon was then cloned into the shuttle vector pAmiLux, kindly provided by Dr. Julian Davies [52]. As a control, wild type stain LAC was transformed with pAmilux lacking an insert.

Murine model of osteomyelitis and micro-computed tomographic analysis

Osteomyelitis was induced in 7- to 8-week old female C57BL/6J mice as previously reported [32]. An inoculum of $1x10^6$ colony-forming units (CFU) in 2 μl PBS was delivered into murine femurs. For some experiments, mice were rendered neutropenic by serial intraperitoneal injections of an anti-Ly6G (clone 1A8) monoclonal antibody (BioXcell, West Lebanon, NH) at days -3, 0, 4, 7, and 10 post-infection. As a control, mice received serial injections of an isotype control antibody (rat IgG2a). At various times post-infection, mice were euthanized and the infected femur was removed and either processed for CFU enumeration or imaged by micro-computed tomography (microCT). For CFU enumeration, femurs were homogenized and plated at limiting dilution on Tryptic Soy Agar (TSA). Analysis of cortical bone destruction was determined by microCT imaging as previously described [32]. Differences in cortical bone destruction and bacterial burdens were analyzed using Student's *t* test.

Bioluminescent imaging

Bioluminescent imaging was performed on infected femurs explanted into sterile multiwell plates at either 1 or 24 hours after infection with WT bacteria containing P*srrAB*-pAmiLux or pAmiLux. Luminescence was measured in an IVIS 200 Imaging System (Perkin Elmer, Akron, OH) with an exposure time of 5 minutes, f-stop of 1, and binning of 4. All images were manually scaled to the same minimum and maximum values to exclude background and include the peak luminescent value.

Intravital measurements of oxygen concentration

Intravital oxygen concentrations were measured in infected femurs using an Oxylite (Oxford Optronix, United Kingdom) oxygen and temperature monitor in conjunction with a flexible bare-fibre sensor. Mice were anesthetized with isoflurane and the surgical incision was re-opened. Oxygen readings were obtained by insertion of the sensor directly through the intramedullary canal and into the infectious focus. Measurements from the probe were recorded at least 5 minutes after probe placement to allow for temperature equilibration and stabilization of oxygen readings.

Transposon sequencing analysis of experimental acute osteomyelitis

The *S. aureus* TnSeq library in the HG003 background has been previously described [8]. In order to identify potential bottlenecks in the murine osteomyelitis model that could confound TnSeq analysis, groups of mice were first infected with strain HG003 using an inoculum of $5x10^6$ CFU and then at various times post-infection the infected femurs were collected and processed for CFU enumeration. Day 5 was chosen as a timepoint for TnSeq analysis of acute osteomyelitis as it likely represents the first bottleneck encountered by invading bacteria. To prepare the TnSeq library for inoculation into murine femurs, an aliquot of the library containing $5x10^7$ CFU/ml was thawed and inoculated into 100 ml of BHI media in a 500 ml Erlenmeyer flask. This culture was incubated at 37°C for 12 hours and then back-diluted 1:100 into fresh BHI at the same flask to volume ratio and grown an additional 3 hours. Bacterial cells were harvested by centrifugation and resuspended in PBS to a concentration of $7x10^6$ CFU in 2 μl PBS. This inoculum dose failed to cause mortality or severe morbidity requiring euthanasia when administered to five wildtype mice by retro-orbital injection (mice were monitored for a total of 4 days). Genomic DNA was prepared from the inoculum using a Qiagen DNeasy Kit with 40 μg ml^{-1} lysostaphin added to the lysis buffer. The inoculum was used to initiate experimental osteomyelitis in groups of mice as above. Another equivalent aliquot of the inoculum was seeded into a 50 ml BHI culture in a 250 ml Erlenmeyer flask. This culture was grown for 24 hours, after which time the bacterial cells were harvested and genomic DNA was prepared as above. This genomic DNA served as the *in vitro* comparator for TnSeq analysis. At 5 days post-infection, mice inoculated with the TnSeq library were euthanized, and the infected femurs were harvested and homogenized in 1 ml of PBS. 500 μl of this homogenate was archived by freezing at -80°C in 20% glycerol and the remaining 500 μl of the homogenate was seeded into 4ml of BHI media and cultured at 37°C and 180 rpm shaking for 5.5 hours. Bacteria were then collected by centrifugation and subjected to genomic DNA preparation as above. Recovered bacteria from 2 mice were pooled, and 3 biologically independent groups of mice were analyzed separately. Genomic DNA samples were subsequently prepared for sequencing on an Illumina HiSeq 2000 (Tufts University Genomic Core Facility). Sequencing, data analysis, and fitness calculations were performed as previously reported [8]. Briefly, a "dval" was calculated for each gene in each condition (inoculum, *in vitro* comparator, or osteomyelitis). The dval represents the observed number of mappable reads of insertions in a gene, divided by the

number of mappable reads of insertions predicted for that gene based on its size relative to the genome and the total number of mappable reads obtained for that experiment. Genes with dval of ≤ 0.01 were considered "essential" in a given condition. Genes with dval of >0.01 but ≤ 0.1 were considered "compromised" in a given condition, whereas genes with dval >0.1 were considered "fit". A dval ratio was calculated by dividing the dval of a given gene in osteomyelitis by the dval of the same gene during *in vitro* comparator growth.

RNA isolation and Genechip analysis

For genechip analysis, aerobic cultures of WT or Δ*srrA* were prepared as follows. Three colonies of WT or Δ*srrA* were inoculated into 10 ml of TSB in a 50 ml Erlenmeyer flask. This culture was grown overnight then back-diluted 1:1000 into 50 ml of TSB in a 250 ml flask. The back-diluted cultures were grown at 37°C and 180 rpm orbital shaking until OD_{600} reached 0.5, at which time an equal volume of ice-cold 1:1 acetone:ethanol was added and the cultures were stored at -80°C until processed for RNA isolation. For comparison of RNA from aerobic versus hypoxic conditions, TSB cultures of WT or Δ*srrA* were incubated overnight as above, back-diluted 1:1000 into 100 ml of TSB in a 500 ml flask and grown to an OD_{600} of 0.5. Fifty milliliters of the culture was then placed into a tightly capped 50ml conical (hypoxic condition) and incubated for one hour at 37°C before mixture with acetone:ethanol and storage at -80°C. The remaining 50 ml of culture was moved to a 250 ml Erlenmeyer flask (aerobic condition) and incubated for one hour at 37°C before mixture with acetone:ethanol and storage at -80°C. For RNA isolation, bacterial cells were harvested by centrifugation and resuspended in LETS buffer (0.1 M LiCl, 10 mM EDTA, 10 mM Tris HCl, 1% SDS). The resuspended cells were disrupted in the presence of 0.5 mm RNAase-free zirconium oxide beads in a Bullet Blender (Next Advance, Averill Park, NY, USA). Disrupted cells were heated at 55°C for 5.5 minutes and centrifuged for 10 minutes at 15,000 rpm. The upper phase was collected and transferred to a new tube before adding 1 ml of TRI-Reagent. After mixing, 200 μl of chloroform was added, and the resultant solution was mixed vigorously for 15 seconds. Samples were centrifuged at 15,000 rpm for 10 min, and the aqueous phase was transferred to a new tube. RNA was precipitated with isopropyl alcohol and subsequently washed with 70% ethanol before drying and resuspension in deionized water. RNA samples were subsequently treated with DNase I and re-purified with a GeneJET RNA Cleanup Kit (Thermo Fisher Scientific, Waltham, MA, USA).

For Genechip analysis, RNA samples were labeled, hybridized to commercially available *S. aureus* Affymetrix Genechips, and processed as per the manufacturer's instructions (Affymetrix, Santa Clara, CA, USA). Briefly, 10 μg of each RNA sample was reverse transcribed, resulting cDNA was purified using QIAquick PCR Purification Kits (Qiagen, Germantown, MD, USA), fragmented with DNase I (Ambion, Carlsbad, CA, USA), and 3' biotinylated using Enzo Bioarray Terminal Labeling Kits (Enzo Life Sciences, Farmingdale, NY, USA). A total of 1.5 μg of a labeled cDNA sample was hybridized to a *S. aureus* GeneChip for 16 hr at 45°C, processed, and scanned in an Affymetrix GeneChip 3000 7G scanner as previously described [53,54]. Signal intensity values for each GeneChip qualifier were normalized to the average signal of the microarray to reduce sample labeling and technical variability and the signal for the biological replicates were averaged using GeneSpring GX software (Agilent Technologies, Redwood City, CA, USA) [54–57]. Differentially expressed transcripts were identified as RNA species that generated a two-fold increase or decrease in WT cells in comparison to Δ*srrA* cells during aerobic and hypoxic conditions (*t*-test, $p = 0.05$). All related GeneChip data files were deposited in the NCBI Gene Expression Omnibus repository in the MIAME-compliant format.

Supernatant preparations

S. aureus strains were used to inoculate RPMI + 1% CA in glass Erlenmeyer flasks. For aerobic growth, the flask opening was covered lightly with aluminum foil. For hypoxic growth, the flask opening was sealed with a rubber stopper. Cultures were grown for 15 hours. Supernatants were collected after culture centrifugation, and were subsequently filtered through a 0.22 μm filter and concentrated with an Amicon Ultra 3 kDa nominal molecular weight limit centrifugal filter unit (Millipore, Billerica, MA, USA) per the manufacturer's instructions. Following concentration, supernatants were filter sterilized again and frozen at -80°C until used.

Mammalian cell culture and cytotoxicity assays

Primary human osteoblasts were obtained from Lonza (Basel, Switzerland) and cultured per manufacturer's recommendations. All cell lines were obtained from the American Type Culture Collection (ATCC) and propagated at 37°C and 5% CO_2 according to ATCC recommendations. Media was replaced every 2–3 days. All cell culture media was prepared with 1X penicillin/streptomycin and filter sterilized using a 0.22 μm filter prior to use. MC3T3 E-1 cells were cultured in α-MEM, supplemented with 10% fetal bovine serum (FBS). The RAW264.7, Saos-2, and A549 cell lines were grown in Dulbecco's MEM (DMEM) with 10% FBS, McCoy's 5A medium with 15% FBS, and F-12K medium with 10% FBS, respectively. The Jurkat, U937, and HL-60 cell lines were propagated using RPMI with 10% FBS. Cytotoxicity assays were performed in 96-well tissue culture grade plates. Cells were seeded one day prior to intoxication with *S. aureus* concentrated supernatants or sterile RPMI diluted in the recommended cell culture medium. The following cell densities were used for cytotoxicity assays: MC3T3 E1 murine pre-osteoblastic cells at 5,000 cells per well, primary human osteoblasts at 3,500 cells per well, Saos-2 human osteoblastic cells at 10,000 cells per well, RAW264.7 murine macrophage cells at 10,000 cells per well, A549 lung epithelial cells at 5,000 cells per well, U937 monocytic cells at 15,000 cells per well, HL-60 premyelocytes at 20,000 cells per well, and Jurkat T cells at 50,000 cells per well. Concentrated supernatants were added as dilutions, by mixing between 0.1 μl to 60 μl in a total volume of 200 μl per well to give a dilution spectrum of 0.05%-30% concentrated supernatant (volume/volume). Cell lines in suspension were centrifuged at 3000 x g for 5 minutes prior to intoxication. Cell viability was assessed with CellTiter AQueous One (Promega, Madison, WI, USA) per the manufacturer's instructions at 24 hours post-intoxication.

YFP fluorescence measurements

For fluorescence analysis, overnight cultures of WT and Δ*srrA* containing the pDB59 reporter plasmid were back-diluted 1:1000 into 10 ml of RPMI + 1% CA with chloramphenicol in 50ml Erlenmeyer flasks and grown either aerobically or hypoxically as above. YFP was measured using an excitation of 485/20 and emission of 528/20 in a BioTek Synergy HT 96-well plate reader at 0, 6, 9, 12, and 15 hours after back-dilution.

Quantitative RT-PCR

Bacteria were grown for 15 hours as for YFP fluorescence measurements, mixed with 1:1 acetone:ethanol, and stored at -80°C until processed for RNA isolation. RNA isolation was performed as for Genechip analysis. Reverse transcription using 2 μg of RNA and M-MLV reverse transcriptase (Promega, Madison, WI, USA) was performed following the manufacturer's instructions. Quantitative RT-PCR (qRT-PCR) was performed using iQ SYBR Green Supermix (Bio-Rad, Hercules, Ca, USA) and the cDNA generated above for each primer pair, including a no reverse transcriptase negative control for 16S rRNA. PCR was conducted on a CFX96 qPCR

cycler (Bio-Rad, Hercules, Ca, USA). The cycling program was carried out as recommended by the manufacturer with an annealing temperature of 56°C. Fold-changes were calculated from Ct values averaged from three technical replicates for at least three biological replicates after normalizing to 16S rRNA. The qRT-PCR primer sequences for *agrA*, *hla*, and *RNAIII* were previously published [58]. The qRT-PCR primer sequence for 16S rRNA was also previously published [36].

Supporting Information

S1 Table. Genes identified as essential for osteomyelitis by TnSeq analysis.
(PDF)

S2 Table. Transposon mutants with compromised fitness during osteomyelitis, but not *in vitro* growth, as identified by TnSeq analysis.
(PDF)

S3 Table. Transcripts differentially regulated by SrrAB during aerobic growth.
(PDF)

S4 Table. Transcripts differentially regulated by SrrAB during hypoxic growth.
(PDF)

S1 Fig. Evaluation of HG003 growth kinetics during experimental osteomyelitis. Groups of mice were subjected to osteomyelitis using strain HG003. Infected femurs were harvested at 1, 3, 5, 7, and 12 days post-infection and processed for CFU enumeration (n = 3). Horizontal lines represent the mean. Error bars represent the SD. Significance was determined by Students *t* test.
(TIF)

S2 Fig. Growth kinetics of *ΔsrrA* and select SrrAB-regulated mutants under aerobic or hypoxic conditions. Growth of WT, *ΔsrrA*, *ΔpflA*, *ΔpflB*, *ΔqoxA*, and *ΔqoxC* strains was monitored by OD_{600} with 3 technical replicates at 0, 2, 4, 6, 8, and 24 hours. Data shown is representative of 3 biologically independent experiments. Error bars represent the SEM. (A) Strains grown aerobically in BHI, which served as the *in vitro* comparator media during TnSeq analysis. (B) Strains grown aerobically in TSB. (C) Strains grown hypoxically in TSB by tightly capping Erlenmeyer flasks.
(TIF)

S3 Fig. Alpha-hemolysin does not impact cytotoxicity of concentrated *S. aureus* supernatants towards osteoblastic cells. Saos-2 osteoblastic cells were seeded into 96-well plates and cell viability was assessed 24 hours after intoxication with supernatant (30% total media volume) from the indicated strains following hypoxic growth. Results are expressed as percent of RPMI control (n = 10). Error bars represent the SEM. LAC^R indicates an erythromycin-resistant derivative of LAC used for construction of the *hla* mutant.
(TIF)

S4 Fig. Inactivation of RNAIII does not impact cytotoxicity of concentrated *S. aureus* supernatants towards osteoblastic cells. MC3T3 osteoblastic cells were seeded into 96-well plates and cell viability was assessed 24 hours after intoxication with supernatant (30% total media volume) from the indicated strains following hypoxic growth. Results are expressed as percent of RPMI control (n = 10). Error bars represent the SEM.
(TIF)

S5 Fig. Hypoxic growth enhances the cytotoxicity of strains MW2 and Newman. WT supernatants were prepared from strains MW2 (A) and Newman (B) by inoculating 3 colonies into RPMI and 1% casamino acids (CA) and growing for 15 hours either aerobically or hypoxically. MC3T3 murine osteoblastic cells were seeded into 96 well plates 24 hours prior to intoxication with concentrated supernatant or RPMI control. Cell viability was assessed 24 hours later. Results are expressed as percent of RPMI control (n = 10), and are the average of 2 biologic replicates. Error bars represent the SEM.
(TIF)

S6 Fig. Expression of SrrAB in trans decreases cytotoxicity of aerobic cultures. MC3T3 cells were intoxicated with 30% total media volume of RPMI control or concentrated supernatant from the indicated strains after aerobic or hypoxic growth. Cell viability was determined 24 hours after intoxication. Results are expressed as percent of RPMI control (n = 10). Error bars represent the SEM. Significance was determined by Students *t* test.
(TIF)

Acknowledgments

We thank Alex Horswill for plasmid pDB59. We thank Dr. Juliane Bubeck-Wardenburg for strains Δ*psm* pOS1-*plgt* and Δ*psm* pOS1-*plgt-hla*. Several mutants used in this study were provided by the Network on Antimicrobial Resistance in *Staphylococcus aureus* (NARSA) for distribution by BEI Resources, NIAID.

Author Contributions

Conceived and designed the experiments: ADW MDV BS MSG EPS JEC. Performed the experiments: ADW DJS NEP MDV NDH ZRL SAH EEA CB PMD GAW JC JEC. Analyzed the data: ADW MDV BS MSG EPS JEC. Contributed reagents/materials/analysis tools: GAW JC PMD BS. Wrote the paper: ADW MDV MSG EPS JEC.

References

1. Kuehnert MJ, Kruszon-Moran D, Hill HA, McQuillan G, McAllister SK, et al. (2006) Prevalence of *Staphylococcus aureus* nasal colonization in the United States, 2001–2002. J Infect Dis 193: 172–179. PMID: 16362880
2. van Opijnen T, Bodi KL, Camilli A (2009) Tn-seq: high-throughput parallel sequencing for fitness and genetic interaction studies in microorganisms. Nat Methods 6: 767–772. doi: 10.1038/nmeth.1377 PMID: 19767758
3. Barquist L, Boinett CJ, Cain AK (2013) Approaches to querying bacterial genomes with transposon-insertion sequencing. RNA Biol 10: 1161–1169. doi: 10.4161/rna.24765 PMID: 23635712
4. Roux D, Danilchanka O, Guillard T, Cattoir V, Aschard H, et al. (2015) Fitness cost of antibiotic susceptibility during bacterial infection. Sci Transl Med 7: 297ra114. doi: 10.1126/scitranslmed.aab1621 PMID: 26203082
5. Bachman MA, Breen P, Deornellas V, Mu Q, Zhao L, et al. (2015) Genome-Wide Identification of *Klebsiella pneumoniae* Fitness Genes during Lung Infection. MBio 6.
6. Shan Y, Lazinski D, Rowe S, Camilli A, Lewis K (2015) Genetic basis of persister tolerance to aminoglycosides in *Escherichia coli*. MBio 6.
7. Turner KH, Wessel AK, Palmer GC, Murray JL, Whiteley M (2015) Essential genome of *Pseudomonas aeruginosa* in cystic fibrosis sputum. Proc Natl Acad Sci U S A 112: 4110–4115. doi: 10.1073/pnas.1419677112 PMID: 25775563
8. Valentino MD, Foulston L, Sadaka A, Kos VN, Villet RA, et al. (2014) Genes contributing to *Staphylococcus aureus* fitness in abscess- and infection-related ecologies. MBio 5: e01729–01714. doi: 10.1128/mBio.01729-14 PMID: 25182329
9. Lew DP, Waldvogel FA (2004) Osteomyelitis. Lancet 364: 369–379. PMID: 15276398

10. Rubin RJ, Harrington CA, Poon A, Dietrich K, Greene JA, et al. (1999) The economic impact of *Staphylococcus aureus* infection in New York City hospitals. Emerg Infect Dis 5: 9–17. PMID: 10081667

11. Spencer JA, Ferraro F, Roussakis E, Klein A, Wu J, et al. (2014) Direct measurement of local oxygen concentration in the bone marrow of live animals. Nature 508: 269–273. doi: 10.1038/nature13034 PMID: 24590072

12. Harrison JS, Rameshwar P, Chang V, Bandari P (2002) Oxygen saturation in the bone marrow of healthy volunteers. Blood 99: 394. PMID: 11783438

13. Lu C, Saless N, Wang X, Sinha A, Decker S, et al. (2013) The role of oxygen during fracture healing. Bone 52: 220–229. doi: 10.1016/j.bone.2012.09.037 PMID: 23063782

14. Bar-Shavit Z (2008) Taking a toll on the bones: regulation of bone metabolism by innate immune regulators. Autoimmunity 41: 195–203. doi: 10.1080/08916930701694469 PMID: 18365832

15. Wright JA, Nair SP (2010) Interaction of staphylococci with bone. Int J Med Microbiol 300: 193–204. doi: 10.1016/j.ijmm.2009.10.003 PMID: 19889575

16. Takayanagi H (2009) Osteoimmunology and the effects of the immune system on bone. Nat Rev Rheumatol 5: 667–676. doi: 10.1038/nrrheum.2009.217 PMID: 19884898

17. Gerber JS, Coffin SE, Smathers SA, Zaoutis TE (2009) Trends in the incidence of methicillin-resistant *Staphylococcus aureus* infection in children's hospitals in the United States. Clin Infect Dis 49: 65–71. doi: 10.1086/599348 PMID: 19463065

18. Carrillo-Marquez MA, Hulten KG, Hammerman W, Mason EO, Kaplan SL (2009) USA300 is the predominant genotype causing *Staphylococcus aureus* septic arthritis in children. Pediatr Infect Dis J 28: 1076–1080. doi: 10.1097/INF.0b013e3181adbcfe PMID: 19820424

19. Subashchandrabose S, Smith SN, Spurbeck RR, Kole MM, Mobley HL (2013) Genome-wide detection of fitness genes in uropathogenic *Escherichia coli* during systemic infection. PLoS Pathog 9: e1003788. doi: 10.1371/journal.ppat.1003788 PMID: 24339777

20. Kamp HD, Patimalla-Dipali B, Lazinski DW, Wallace-Gadsden F, Camilli A (2013) Gene fitness landscapes of *Vibrio cholerae* at important stages of its life cycle. PLoS Pathog 9: e1003800. doi: 10.1371/journal.ppat.1003800 PMID: 24385900

21. Wong SM, Bernui M, Shen H, Akerley BJ (2013) Genome-wide fitness profiling reveals adaptations required by *Haemophilus* in coinfection with influenza A virus in the murine lung. Proc Natl Acad Sci U S A 110: 15413–15418. doi: 10.1073/pnas.1311217110 PMID: 24003154

22. Palace SG, Proulx MK, Lu S, Baker RE, Goguen JD (2014) Genome-wide mutant fitness profiling identifies nutritional requirements for optimal growth of *Yersinia pestis* in deep tissue. MBio 5.

23. Skurnik D, Roux D, Aschard H, Cattoir V, Yoder-Himes D, et al. (2013) A comprehensive analysis of *in vitro* and *in vivo* genetic fitness of *Pseudomonas aeruginosa* using high-throughput sequencing of transposon libraries. PLoS Pathog 9: e1003582. doi: 10.1371/journal.ppat.1003582 PMID: 24039572

24. Peschel A, Jack RW, Otto M, Collins LV, Staubitz P, et al. (2001) *Staphylococcus aureus* resistance to human defensins and evasion of neutrophil killing via the novel virulence factor MprF is based on modification of membrane lipids with l-lysine. J Exp Med 193: 1067–1076. PMID: 11342591

25. Mazmanian SK, Skaar EP, Gaspar AH, Humayun M, Gornicki P, et al. (2003) Passage of heme-iron across the envelope of *Staphylococcus aureus*. Science 299: 906–909. PMID: 12574635

26. Kinkel TL, Roux CM, Dunman PM, Fang FC (2013) The *Staphylococcus aureus* SrrAB two-component system promotes resistance to nitrosative stress and hypoxia. MBio 4: e00696–00613. doi: 10.1128/mBio.00696-13 PMID: 24222487

27. Pragman AA, Yarwood JM, Tripp TJ, Schlievert PM (2004) Characterization of virulence factor regulation by SrrAB, a two-component system in *Staphylococcus aureus*. J Bacteriol 186: 2430–2438. PMID: 15060046

28. Carreau A, El Hafny-Rahbi B, Matejuk A, Grillon C, Kieda C (2011) Why is the partial oxygen pressure of human tissues a crucial parameter? Small molecules and hypoxia. J Cell Mol Med 15: 1239–1253. doi: 10.1111/j.1582-4934.2011.01258.x PMID: 21251211

29. Throup JP, Zappacosta F, Lunsford RD, Annan RS, Carr SA, et al. (2001) The srhSR gene pair from *Staphylococcus aureus*: genomic and proteomic approaches to the identification and characterization of gene function. Biochemistry 40: 10392–10401. PMID: 11513618

30. Vitko NP, Spahich NA, Richardson AR (2015) Glycolytic dependency of high-level nitric oxide resistance and virulence in *Staphylococcus aureus*. MBio 6.

31. Daley JM, Thomay AA, Connolly MD, Reichner JS, Albina JE (2008) Use of Ly6G-specific monoclonal antibody to deplete neutrophils in mice. J Leukoc Biol 83: 64–70. PMID: 17884993

32. Cassat JE, Hammer ND, Campbell JP, Benson MA, Perrien DS, et al. (2013) A secreted bacterial protease tailors the *Staphylococcus aureus* virulence repertoire to modulate bone remodeling during osteomyelitis. Cell Host Microbe 13: 759–772. doi: 10.1016/j.chom.2013.05.003 PMID: 23768499

33. Hammer ND, Cassat JE, Noto MJ, Lojek LJ, Chadha AD, et al. (2014) Inter- and intraspecies metabolite exchange promotes virulence of antibiotic-resistant *Staphylococcus aureus*. Cell Host Microbe 16: 531–537. doi: 10.1016/j.chom.2014.09.002 PMID: 25299336

34. Geisinger E, Muir TW, Novick RP (2009) agr receptor mutants reveal distinct modes of inhibition by staphylococcal autoinducing peptides. Proc Natl Acad Sci U S A 106: 1216–1221. doi: 10.1073/pnas.0807760106 PMID: 19147840

35. Queck SY, Jameson-Lee M, Villaruz AE, Bach TH, Khan BA, et al. (2008) RNAIII-independent target gene control by the *agr* quorum-sensing system: insight into the evolution of virulence regulation in *Staphylococcus aureus*. Mol Cell 32: 150–158. doi: 10.1016/j.molcel.2008.08.005 PMID: 18851841

36. Berube BJ, Sampedro GR, Otto M, Bubeck Wardenburg J (2014) The *psmalpha* locus regulates production of *Staphylococcus aureus* alpha-toxin during infection. Infect Immun 82: 3350–3358. doi: 10.1128/IAI.00089-14 PMID: 24866799

37. Yarwood JM, Bartels DJ, Volper EM, Greenberg EP (2004) Quorum sensing in *Staphylococcus aureus* biofilms. J Bacteriol 186: 1838–1850. PMID: 14996815

38. Yarwood JM, McCormick JK, Schlievert PM (2001) Identification of a novel two-component regulatory system that acts in global regulation of virulence factors of *Staphylococcus aureus*. J Bacteriol 183: 1113–1123. PMID: 11157922

39. Rothfork JM, Timmins GS, Harris MN, Chen X, Lusis AJ, et al. (2004) Inactivation of a bacterial virulence pheromone by phagocyte-derived oxidants: new role for the NADPH oxidase in host defense. Proc Natl Acad Sci U S A 101: 13867–13872. PMID: 15353593

40. Sun F, Liang H, Kong X, Xie S, Cho H, et al. (2012) Quorum-sensing *agr* mediates bacterial oxidation response via an intramolecular disulfide redox switch in the response regulator AgrA. Proc Natl Acad Sci U S A 109: 9095–9100. doi: 10.1073/pnas.1200603109 PMID: 22586129

41. Ingavale SS, Van Wamel W, Cheung AL (2003) Characterization of RAT, an autolysis regulator in *Staphylococcus aureus*. Mol Microbiol 48: 1451–1466. PMID: 12791130

42. Pagels M, Fuchs S, Pane-Farre J, Kohler C, Menschner L, et al. (2010) Redox sensing by a Rex-family repressor is involved in the regulation of anaerobic gene expression in *Staphylococcus aureus*. Mol Microbiol 76: 1142–1161. doi: 10.1111/j.1365-2958.2010.07105.x PMID: 20374494

43. Chen PR, Bae T, Williams WA, Duguid EM, Rice PA, et al. (2006) An oxidation-sensing mechanism is used by the global regulator MgrA in *Staphylococcus aureus*. Nat Chem Biol 2: 591–595. PMID: 16980961

44. Fujimoto DF, Higginbotham RH, Sterba KM, Maleki SJ, Segall AM, et al. (2009) *Staphylococcus aureus* SarA is a regulatory protein responsive to redox and pH that can support bacteriophage lambda integrase-mediated excision/recombination. Mol Microbiol 74: 1445–1458. doi: 10.1111/j.1365-2958.2009.06942.x PMID: 19919677

45. Sun F, Ji Q, Jones MB, Deng X, Liang H, et al. (2012) AirSR, a [2Fe-2S] cluster-containing two-component system, mediates global oxygen sensing and redox signaling in *Staphylococcus aureus*. J Am Chem Soc 134: 305–314. doi: 10.1021/ja2071835 PMID: 22122613

46. Boles BR, Thoendel M, Roth AJ, Horswill AR (2010) Identification of genes involved in polysaccharide-independent *Staphylococcus aureus* biofilm formation. PLoS One 5: e10146. doi: 10.1371/journal.pone.0010146 PMID: 20418950

47. Kaito C, Saito Y, Nagano G, Ikuo M, Omae Y, et al. (2011) Transcription and translation products of the cytolysin gene *psm-mec* on the mobile genetic element SCCmec regulate *Staphylococcus aureus* virulence. PLoS Pathog 7: e1001267. doi: 10.1371/journal.ppat.1001267 PMID: 21304931

48. Fey PD, Endres JL, Yajjala VK, Widhelm TJ, Boissy RJ, et al. (2013) A genetic resource for rapid and comprehensive phenotype screening of nonessential *Staphylococcus aureus* genes. MBio 4: e00537–00512.

49. Yanisch-Perron C, Vieira J, Messing J (1985) Improved M13 phage cloning vectors and host strains: nucleotide sequences of the M13mp18 and pUC19 vectors. Gene 33: 103–119. PMID: 2985470

50. Chen J, Novick RP (2007) *svrA*, a multi-drug exporter, does not control *agr*. Microbiology 153: 1604–1608. PMID: 17464075

51. Bubeck Wardenburg J, Williams WA, Missiakas D (2006) Host defenses against *Staphylococcus aureus* infection require recognition of bacterial lipoproteins. Proc Natl Acad Sci U S A 103: 13831–13836. PMID: 16954184

52. Mesak LR, Yim G, Davies J (2009) Improved *lux* reporters for use in *Staphylococcus aureus*. Plasmid 61: 182–187. doi: 10.1016/j.plasmid.2009.01.003 PMID: 19399993

53. Dunman PM, Murphy E, Haney S, Palacios D, Tucker-Kellogg G, et al. (2001) Transcription profiling-based identification of *Staphylococcus aureus* genes regulated by the *agr* and/or *sarA* loci. J Bacteriol 183: 7341–7353. PMID: 11717293

54. Beenken KE, Dunman PM, McAleese F, Macapagal D, Murphy E, et al. (2004) Global gene expression in *Staphylococcus aureus* biofilms. J Bacteriol 186: 4665–4684. PMID: 15231800

55. Bischoff M, Dunman P, Kormanec J, Macapagal D, Murphy E, et al. (2004) Microarray-based analysis of the *Staphylococcus aureus sigmaB* regulon. J Bacteriol 186: 4085–4099. PMID: 15205410

56. Anderson KL, Roberts C, Disz T, Vonstein V, Hwang K, et al. (2006) Characterization of the *Staphylococcus aureus* heat shock, cold shock, stringent, and SOS responses and their effects on log-phase mRNA turnover. J Bacteriol 188: 6739–6756. PMID: 16980476

57. Roberts C, Anderson KL, Murphy E, Projan SJ, Mounts W, et al. (2006) Characterizing the effect of the *Staphylococcus aureus* virulence factor regulator, SarA, on log-phase mRNA half-lives. J Bacteriol 188: 2593–2603. PMID: 16547047

58. Khodaverdian V, Pesho M, Truitt B, Bollinger L, Patel P, et al. (2013) Discovery of antivirulence agents against methicillin-resistant *Staphylococcus aureus*. Antimicrob Agents Chemother 57: 3645–3652. doi: 10.1128/AAC.00269-13 PMID: 23689713

REFERENCES

1. Kuehnert MJ, Kruszon-Moran D, Hill HA, McQuillan G, McAllister SK, Fosheim G, McDougal LK, Chaitram J, Jensen B, Fridkin SK, Killgore G, Tenover FC. Prevalence of Staphylococcus aureus nasal colonization in the United States, 2001-2002. J Infect Dis. 2006;193(2):172-9. Epub 2005/12/20. doi: 10.1086/499632. PubMed PMID: 16362880.

2. Huang H, Flynn NM, King JH, Monchaud C, Morita M, Cohen SH. Comparisons of community-associated methicillin-resistant Staphylococcus aureus (MRSA) and hospital-associated MSRA infections in Sacramento, California. J Clin Microbiol. 2006;44(7):2423-7. Epub 2006/07/11. doi: 10.1128/jcm.00254-06. PubMed PMID: 16825359; PMCID: PMC1489486.

3. Lew DP, Waldvogel FA. Osteomyelitis. Lancet. 2004;364(9431):369-79. Epub 2004/07/28. doi: 10.1016/s0140-6736(04)16727-5. PubMed PMID: 15276398.

4. Gerber JS, Coffin SE, Smathers SA, Zaoutis TE. Trends in the incidence of methicillin-resistant Staphylococcus aureus infection in children's hospitals in the United States. Clin Infect Dis. 2009;49(1):65-71. Epub 2009/05/26. doi: 10.1086/599348. PubMed PMID: 19463065; PMCID: PMC2897056.

5. Kremers HM, Nwojo ME, Ransom JE, Wood-Wentz CM, Melton LJ, Huddleston PM. Trends in the Epidemiology of Osteomyelitis: A Population-Based Study, 1969 to 2009. J Bone Joint Surg Am2015. p. 837-45.

6. Saavedra-Lozano J, Mejias A, Ahmad N, Peromingo E, Ardura MI, Guillen S, Syed A, Cavuoti D, Ramilo O. Changing trends in acute osteomyelitis in children: impact of methicillin-resistant Staphylococcus aureus infections. J Pediatr Orthop. 2008;28(5):569-75. Epub 2008/06/27. doi: 10.1097/BPO.0b013e31817bb816. PubMed PMID: 18580375.

7. Sarkissian EJ, Gans I, Gunderson MA, Myers SH, Spiegel DA, Flynn JM. Community-acquired Methicillin-resistant Staphylococcus aureus Musculoskeletal Infections: Emerging Trends Over the Past Decade. J Pediatr Orthop. 2016;36(3):323-7. Epub 2015/03/19. doi: 10.1097/bpo.0000000000000439. PubMed PMID: 25785593.

8. Belthur MV, Birchansky SB, Verdugo AA, Mason EO, Jr., Hulten KG, Kaplan SL, Smith EO, Phillips WA, Weinberg J. Pathologic fractures in children with acute Staphylococcus aureus osteomyelitis. J Bone Joint Surg Am. 2012;94(1):34-42. Epub 2012/01/06. doi: 10.2106/jbjs.j.01915. PubMed PMID: 22218380.

9. Liu T, Zhang X, Li Z, Peng D. Management of combined bone defect and limb-length discrepancy after tibial chronic osteomyelitis. Orthopedics. 2011;34(8):e363-7. Epub 2011/08/06. doi: 10.3928/01477447-20110627-12. PubMed PMID: 21815577.

10. Masters EA, P TR, de Mesy Bentley KL, Boyce BF, Gill AL, Gill SR, Nishitani K, Ishikawa M, Morita Y, Ito H, Bello-Irizarry SN, Ninomiya M, Brodell JD, Lee CC, Hao SP, Oh

I, Xie C, Awad HA, Daiss JL, Owen JR, Kates SL, Schwarz EM, Muthukrishnan G. Evolving concepts in bone infection: redefining “biofilm”, “acute vs. chronic osteomyelitis”, “the immune proteome” and “local antibiotic therapy”. Bone Research. 2019;7(1):20. doi: doi:10.1038/s41413-019-0061-z.

11. Siddiqui JA, Partridge NC. Physiological Bone Remodeling: Systemic Regulation and Growth Factor Involvement. Physiology (Bethesda). 2016;31(3):233-45. Epub 2016/04/08. doi: 10.1152/physiol.00061.2014. PubMed PMID: 27053737.

12. Cassat JE, Hammer ND, Campbell JP, Benson MA, Perrien DS, Mrak LN, Smeltzer MS, Torres VJ, Skaar EP. A secreted bacterial protease tailors the Staphylococcus aureus virulence repertoire to modulate bone remodeling during osteomyelitis. Cell Host Microbe. 2013;13(6):759-72. Epub 2013/06/19. doi: 10.1016/j.chom.2013.05.003. PubMed PMID: 23768499; PMCID: PMC3721972.

13. Putnam NE, Fulbright LE, Curry JM, Ford CA, Petronglo JR, Hendrix AS, Cassat JE. MyD88 and IL-1R signaling drive antibacterial immunity and osteoclast-driven bone loss during Staphylococcus aureus osteomyelitis. PLoS Pathog. 2019;15(4):e1007744. Epub 2019/04/13. doi: 10.1371/journal.ppat.1007744. PubMed PMID: 30978245.

14. Bar-Shavit Z. Taking a Toll on the bones: Regulation of bone metabolism by innate immune regulators. Autoimmunity. 2008;41(3):195--203. doi: 10.1080/08916930701694469. PubMed PMID: Bar-Shavit2008.

15. Wright JA, Nair SP. Interaction of staphylococci with bone. Int J Med Microbiol. 2010;300(2-3):193-204. Epub 2009/11/06. doi: 10.1016/j.ijmm.2009.10.003. PubMed PMID: 19889575; PMCID: PMC2814006.

16. Takayanagi H. Osteoimmunology and the effects of the immune system on bone. Nature Reviews Rheumatology. 2009;5(12):667--76. doi: 10.1038/nrrheum.2009.217. PubMed PMID: Takayanagi2009.

17. Esen E, Long F. Aerobic glycolysis in osteoblasts. Curr Osteoporos Rep. 2014;12(4):433-8. Epub 2014/09/10. doi: 10.1007/s11914-014-0235-y. PubMed PMID: 25200872; PMCID: PMC4216598.

18. Kim JM, Jeong D, Kang HK, Jung SY, Kang SS, Min BM. Osteoclast precursors display dynamic metabolic shifts toward accelerated glucose metabolism at an early stage of RANKL-stimulated osteoclast differentiation. Cell Physiol Biochem. 2007;20(6):935-46. Epub 2007/11/06. doi: 10.1159/000110454. PubMed PMID: 17982276.

19. Peck WA, J. BS, A. FS. Bone Cells: Biochemical and Biological Studies after Enzymatic Isolation. Science (New York, NY). 1964;146(3650):1476--7. PubMed PMID: PECK1964.

20. Cohn DV, K. FB. Aerobic metabolism of glucose by bone. The Journal of biological chemistry. 1962;237:615--8. PubMed PMID: COHN1962.

21. Borle AB, Nichols N, Nichols G, Jr. Metabolic studies of bone in vitro. I. Normal bone. J Biol Chem. 1960;235:1206-10. Epub 1960/04/01. PubMed PMID: 13802861.

22. Heinemann M, Kummel A, Ruinatscha R, Panke S. In silico genome-scale reconstruction and validation of the Staphylococcus aureus metabolic network. Biotechnol Bioeng. 2005;92(7):850-64. Epub 2005/09/13. doi: 10.1002/bit.20663. PubMed PMID: 16155945.

23. Neidhardt FC, Ingraham JL, Schaechter M. Physiology of the bacterial cell. A molecular approach. Sunderland, MA: Sinauer associates; 1990.

24. Becker SA, Palsson BO. Genome-scale reconstruction of the metabolic network in Staphylococcus aureus N315: an initial draft to the two-dimensional annotation. BMC Microbiol. 2005;5:8. Epub 2005/03/09. doi: 10.1186/1471-2180-5-8. PubMed PMID: 15752426; PMCID: PMC1079855.

25. Mayer S, Steffen W, Steuber J, Gotz F. The Staphylococcus aureus NuoL-like protein MpsA contributes to the generation of membrane potential. J Bacteriol. 2015;197(5):794-806. Epub 2014/12/03. doi: 10.1128/jb.02127-14. PubMed PMID: 25448817; PMCID: PMC4325100.

26. Zhang X, Bayles KW, Luca S. Staphylococcus aureus CidC Is a Pyruvate:Menaquinone Oxidoreductase. Biochemistry. 2017;56(36):4819-29. doi: 10.1021/acs.biochem.7b00570. PubMed PMID: 28809546; PMCID: 5853648.

27. Fuller JR, Vitko NP, Perkowski EF, Scott E, Khatri D, Spontak JS, Thurlow LR, Richardson AR. Identification of a Lactate-Quinone Oxidoreductase in Staphylococcus aureus that is Essential for Virulence. Front Cell Infect Microbiol. 2011;1. doi: 10.3389/fcimb.2011.00019. PubMed PMID: 22919585; PMCID: 3417369.

28. Schwan WR, Polanowski R, Dunman PM, Medina-Bielski S, Lane M, Rott M, Lipker L, Wescott A, Monte A, Cook JM, Baumann DD, Tiruveedhula V, Witzigmann CM, Mikel C, Rahman MT. Identification of Staphylococcus aureus Cellular Pathways Affected by the Stilbenoid Lead Drug SK-03-92 Using a Microarray. Antibiotics (Basel). 2017;6(3). Epub 2017/09/12. doi: 10.3390/antibiotics6030017. PubMed PMID: 28892020; PMCID: PMC5617981.

29. Gaupp R, Schlag S, Liebeke M, Lalk M, Gotz F. Advantage of upregulation of succinate dehydrogenase in Staphylococcus aureus biofilms. J Bacteriol. 2010;192(9):2385-94. Epub 2010/03/09. doi: 10.1128/jb.01472-09. PubMed PMID: 20207757; PMCID: PMC2863491.

30. Hammer ND, Reniere ML, Cassat JE, Zhang Y, Hirsch AO, Indriati Hood M, Skaar EP. Two heme-dependent terminal oxidases power Staphylococcus aureus organ-specific colonization of the vertebrate host. MBio. 2013;4(4). Epub 2013/08/01. doi: 10.1128/mBio.00241-13. PubMed PMID: 23900169; PMCID: PMC3735196.

31. Taber HW, Morrison M. Electron transport in staphylococci. Properties of a particle preparation from exponential phase *Staphylococcus aureus*. Arch Biochem Biophys. 1964;105:367-79. Epub 1964/05/01. PubMed PMID: 14186744.

32. Tynecka Z, Szczesniak Z, Malm A, Los R. Energy conservation in aerobically grown Staphylococcus aureus. Res Microbiol. 1999;150(8):555-66. Epub 1999/11/30. PubMed PMID: 10577488.

33. Voggu L, Schlag S, Biswas R, Rosenstein R, Rausch C, Gotz F. Microevolution of cytochrome bd oxidase in Staphylococci and its implication in resistance to respiratory toxins released by Pseudomonas. J Bacteriol. 2006;188(23):8079-86. Epub 2006/11/17. doi: 10.1128/jb.00858-06. PubMed PMID: 17108291; PMCID: PMC1698191.

34. Clements MO, Watson SP, Poole RK, Foster SJ. CtaA of Staphylococcus aureus is required for starvation survival, recovery, and cytochrome biosynthesis. J Bacteriol. 1999;181(2):501-7. Epub 1999/01/12. PubMed PMID: 9882664; PMCID: PMC93404.

35. Sasarman A, Purvis P, Portelance V. Role of Menaquinone in Nitrate Respiration in Staphylococcus aureus. J Bacteriol. 1974;117(2):911-3. PubMed PMID: 4811551; PMCID: 285591.

36. Grosser MR, Paluscio E, Thurlow LR, Dillon MM, Cooper VS, Kawula TH, Richardson AR. Genetic requirements for Staphylococcus aureus nitric oxide resistance and virulence. PLoS Pathog. 2018;14(3):e1006907. Epub 2018/03/20. doi: 10.1371/journal.ppat.1006907. PubMed PMID: 29554137; PMCID: PMC5884563.

37. Richardson AR, Libby SJ, Fang FC. A nitric oxide-inducible lactate dehydrogenase enables Staphylococcus aureus to resist innate immunity. Science. 2008;319(5870):1672-6. Epub 2008/03/22. doi: 10.1126/science.1155207. PubMed PMID: 18356528.

38. Vitko NP, Spahich NA, Richardson AR. Glycolytic dependency of high-level nitric oxide resistance and virulence in Staphylococcus aureus. MBio. 2015;6(2). Epub 2015/04/09. doi: 10.1128/mBio.00045-15. PubMed PMID: 25852157; PMCID: PMC4453550.

39. Vitko NP, Grosser MR, Khatri D, Lance TR, Richardson AR. Expanded Glucose Import Capability Affords Staphylococcus aureus Optimized Glycolytic Flux during Infection. MBio. 2016;7(3). Epub 2016/06/23. doi: 10.1128/mBio.00296-16. PubMed PMID: 27329749; PMCID: PMC4916373.

40. Gardner JF, Lascelles J. The requirement for acetate of a streptomycin-resistant strain of Staphylococcus aureus. J Gen Microbiol. 1962;29:157-64. Epub 1962/09/01. doi: 10.1099/00221287-29-1-157. PubMed PMID: 13896903.

41. Wickersham M, Wachtel S, Wong Fok Lung T, Soong G, Jacquet R, Richardson A, Parker D, Prince A. Metabolic Stress Drives Keratinocyte Defenses against Staphylococcus aureus Infection. Cell Rep. 2017;18(11):2742-51. Epub 2017/03/16. doi: 10.1016/j.celrep.2017.02.055. PubMed PMID: 28297676.

42. Slonczewski J, Foster JW. Microbiology : an evolving science. 2nd ed. New York: W.W. Norton; 2011. xxxiv, 1097, 153 p. p.

43. Samant S, Lee H, Ghassemi M, Chen J, Cook JL, Mankin AS, Neyfakh AA. Nucleotide Biosynthesis Is Critical for Growth of Bacteria in Human Blood. PLoS Pathog2008.

44. Ibberson CB, Stacy A, Fleming D, Dees JL, Rumbaugh K, Gilmore MS, Whiteley M. Co-infecting microorganisms dramatically alter pathogen gene essentiality during polymicrobial infection. Nat Microbiol. 2017;2:17079. Epub 2017/05/31. doi: 10.1038/nmicrobiol.2017.79. PubMed PMID: 28555625; PMCID: PMC5774221.

45. Valentino MD, Foulston L, Sadaka A, Kos VN, Villet RA, Santa Maria J, Jr., Lazinski DW, Camilli A, Walker S, Hooper DC, Gilmore MS. Genes contributing to Staphylococcus aureus fitness in abscess- and infection-related ecologies. mBio. 2014;5(5):e01729-14. doi: 10.1128/mBio.01729-14. PubMed PMID: 25182329; PMCID: 4173792.

46. Strasters KC, Winkler KC. Carbohydrate metabolism of *Staphylococcus aureus*. J Gen Microbiol. 1963;33:213-29. Epub 1963/11/01. doi: 10.1099/00221287-33-2-213. PubMed PMID: 14121198.

47. Somerville GA, Cockayne A, Dürr M, Peschel A, Otto M, Musser JM. Synthesis and Deformylation of Staphylococcus aureus δ-Toxin Are Linked to Tricarboxylic Acid Cycle Activity2003. doi: 10.1128/JB.185.22.6686-6694.2003.

48. Somerville GA, Chaussee MS, Morgan CI, Fitzgerald JR, Dorward DW, Reitzer LJ, Musser JM. Staphylococcus aureus Aconitase Inactivation Unexpectedly Inhibits Post-Exponential-Phase Growth and Enhances Stationary-Phase Survival2002. doi: 10.1128/IAI.70.11.6373-6382.2002.

49. Halsey CR, Lei S, Wax JK, Lehman MK, Nuxoll AS, Steinke L, Sadykov M, Powers R, Fey PD. Amino Acid Catabolism in Staphylococcus aureus and the Function of Carbon Catabolite Repression. mBio2017.

50. Spahich NA, Vitko NP, Thurlow LR, Temple B, Richardson AR. Staphylococcus aureus Lactate- and Malate-quinone Oxidoreductases Contribute to Nitric Oxide Resistance and Virulence. Mol Microbiol. 2016;100(5):759-73. doi: 10.1111/mmi.13347. PubMed PMID: 26851155; PMCID: 4894658.

51. Friedman DB, Stauff DL, Pishchany G, Whitwell CW, Torres VJ, Skaar EP. Staphylococcus aureus Redirects Central Metabolism to Increase Iron Availability. PLoS Pathog2006.

52. Fuchs S, Pane-Farre J, Kohler C, Hecker M, Engelmann S. Anaerobic gene expression in Staphylococcus aureus. J Bacteriol. 2007;189(11):4275-89. Epub 2007/03/27. doi: 10.1128/jb.00081-07. PubMed PMID: 17384184; PMCID: PMC1913399.

53. Dassy B, Fournier JM. Respiratory activity is essential for post-exponential-phase production of type 5 capsular polysaccharide by Staphylococcus aureus. Infect Immun. 1996;64(7):2408-14. Epub 1996/07/01. PubMed PMID: 8698459; PMCID: PMC174090.

54. Mei JM, Nourbakhsh F, Ford CW, Holden DW. Identification of Staphylococcus aureus virulence genes in a murine model of bacteraemia using signature-tagged mutagenesis. Mol Microbiol. 1997;26(2):399-407. Epub 1998/02/12. PubMed PMID: 9383163.

55. Pohl K, Francois P, Stenz L, Schlink F, Geiger T, Herbert S, Goerke C, Schrenzel J, Wolz C. CodY in Staphylococcus aureus: a Regulatory Link between Metabolism and Virulence Gene Expression2009. doi: 10.1128/JB.01492-08.

56. Seidl K, Stucki M, Ruegg M, Goerke C, Wolz C, Harris L, Berger-Bachi B, Bischoff M. Staphylococcus aureus CcpA affects virulence determinant production and antibiotic resistance. Antimicrob Agents Chemother. 2006;50(4):1183-94. Epub 2006/03/30. doi: 10.1128/aac.50.4.1183-1194.2006. PubMed PMID: 16569828; PMCID: PMC1426959.

57. Seidl K, Goerke C, Wolz C, Mack D, Berger-Bachi B, Bischoff M. Staphylococcus aureus CcpA affects biofilm formation. Infect Immun. 2008;76(5):2044-50. Epub 2008/03/19. doi: 10.1128/iai.00035-08. PubMed PMID: 18347047; PMCID: PMC2346702.

58. Wilde AD, Snyder DJ, Putnam NE, Valentino MD, Hammer ND, Lonergan ZR, Hinger SA, Aysanoa EE, Blanchard C, Dunman PM, Wasserman GA, Chen J, Shopsin B, Gilmore MS, Skaar EP, Cassat JE. Bacterial Hypoxic Responses Revealed as Critical Determinants of the Host-Pathogen Outcome by TnSeq Analysis of Staphylococcus aureus Invasive Infection. PLoS Pathog. 2015;11(12):e1005341. Epub 2015/12/20. doi: 10.1371/journal.ppat.1005341. PubMed PMID: 26684646; PMCID: PMC4684308.

59. Kinkel TL, Roux CM, Dunman PM, Fang FC. The Staphylococcus aureus SrrAB two-component system promotes resistance to nitrosative stress and hypoxia. MBio. 2013;4(6):e00696-13. Epub 2013/11/14. doi: 10.1128/mBio.00696-13. PubMed PMID: 24222487; PMCID: PMC3892780.

60. Pragman AA, Yarwood JM, Tripp TJ, Schlievert PM. Characterization of virulence factor regulation by SrrAB, a two-component system in Staphylococcus aureus. Journal of bacteriology. 2004;186(8):2430-8. PubMed PMID: 15060046; PMCID: 412142.

61. Horsburgh MJ, Ingham E, Foster SJ. In Staphylococcus aureus, Fur Is an Interactive Regulator with PerR, Contributes to Virulence, and Is Necessary for Oxidative Stress Resistance through Positive Regulation of Catalase and Iron Homeostasis. J Bacteriol2001. p. 468-75.

62. Torres VJ, Attia AS, Mason WJ, Hood MI, Corbin BD, Beasley FC, Anderson KL, Stauff DL, McDonald WH, Zimmerman LJ, Friedman DB, Heinrichs DE, Dunman PM, Skaar EP. Staphylococcus aureus fur regulates the expression of virulence factors that contribute to the pathogenesis of pneumonia. Infect Immun. 2010;78(4):1618-28. Epub 2010/01/27. doi: 10.1128/iai.01423-09. PubMed PMID: 20100857; PMCID: PMC2849423.

63. Zhu Y, Nandakumar R, Sadykov MR, Madayiputhiya N, Luong TT, Gaupp R, Lee CY, Somerville GA. RpiR Homologues May Link Staphylococcus aureus RNAIII Synthesis and Pentose Phosphate Pathway Regulation2011. doi: 10.1128/JB.05930-11.

64. Balasubramanian D, Ohneck EA, Chapman J, Weiss A, Kim MK, Reyes-Robles T, Zhong J, Shaw LN, Lun DS, Ueberheide B, Shopsin B, Torres VJ, Projan SJ. Staphylococcus aureus Coordinates Leukocidin Expression and Pathogenesis by Sensing Metabolic Fluxes via RpiRc2016. doi: 10.1128/mBio.00818-16.

65. Novick RP, Ross HF, Projan SJ, Kornblum J, Kreiswirth B, Moghazeh S. Synthesis of staphylococcal virulence factors is controlled by a regulatory RNA molecule. Embo j. 1993;12(10):3967-75. Epub 1993/10/01. PubMed PMID: 7691599; PMCID: PMC413679.

66. Deutscher J, Kuster E, Bergstedt U, Charrier V, Hillen W. Protein kinase-dependent HPr/CcpA interaction links glycolytic activity to carbon catabolite repression in gram-positive bacteria. Mol Microbiol. 1995;15(6):1049-53. Epub 1995/03/01. PubMed PMID: 7623661.

67. Hanson KG, Steinhauer K, Reizer J, Hillen W, Stulke J. HPr kinase/phosphatase of Bacillus subtilis: expression of the gene and effects of mutations on enzyme activity, growth and carbon catabolite repression. Microbiology. 2002;148(Pt 6):1805-11. Epub 2002/06/11. doi: 10.1099/00221287-148-6-1805. PubMed PMID: 12055300.

68. Monedero V, Poncet S, Mijakovic I, Fieulaine S, Dossonnet V, Martin-Verstraete I, Nessler S, Deutscher J. Mutations lowering the phosphatase activity of HPr kinase/phosphatase switch off carbon metabolism. Embo j. 2001;20(15):3928-37. Epub 2001/08/03. doi: 10.1093/emboj/20.15.3928. PubMed PMID: 11483496; PMCID: PMC149165.

69. Leiba J, Hartmann T, Cluzel ME, Cohen-Gonsaud M, Delolme F, Bischoff M, Molle V. A novel mode of regulation of the Staphylococcus aureus catabolite control protein A (CcpA) mediated by Stk1 protein phosphorylation. J Biol Chem. 2012;287(52):43607-19. Epub 2012/11/08. doi: 10.1074/jbc.M112.418913. PubMed PMID: 23132867; PMCID: PMC3527947.

70. Nicholson WL, Park YK, Henkin TM, Won M, Weickert MJ, Gaskell JA, Chambliss GH. Catabolite repression-resistant mutations of the Bacillus subtilis alpha-amylase promoter affect transcription levels and are in an operator-like sequence. J Mol Biol. 1987;198(4):609-18. Epub 1987/12/20. PubMed PMID: 3123701.

71. Seidl K, Müller S, François P, Kriebitzsch C, Schrenzel J, Engelmann S, Bischoff M, Berger-Bächi B. Effect of a glucose impulse on the CcpA regulon in Staphylococcus aureus. BMC Microbiol. 2009;9:95. doi: 10.1186/1471-2180-9-95. PubMed PMID: 19450265.

72. Yarwood JM, McCormick JK, Schlievert PM. Identification of a novel two-component regulatory system that acts in global regulation of virulence factors of Staphylococcus aureus. Journal of bacteriology. 2001;183(4):1113-23. doi: 10.1128/JB.183.4.1113-1123.2001. PubMed PMID: 11157922; PMCID: 94983.

73. Throup JP, Zappacosta F, Lunsford RD, Annan RS, Carr SA, Lonsdale JT, Bryant AP, McDevitt D, Rosenberg M, Burnham MK. The srhSR gene pair from Staphylococcus aureus: genomic and proteomic approaches to the identification and characterization of gene function. Biochemistry. 2001;40(34):10392-401. Epub 2001/08/22. doi: 10.1021/bi0102959. PubMed PMID: 11513618.

74. Nakano MM, Zuber P, Glaser P, Danchin A, Hulett FM. Two-component regulatory proteins ResD-ResE are required for transcriptional activation of fnr upon oxygen limitation in Bacillus subtilis. J Bacteriol. 1996;178(13):3796-802. Epub 1996/07/01. doi: 10.1128/jb.178.13.3796-3802.1996. PubMed PMID: 8682783; PMCID: PMC232639.

75. James KL, Mogen AB, Brandwein JN, Orsini SS, Ridder MJ, Markiewicz MA, Bose JL, Rice KC. Interplay of Nitric Oxide Synthase (NOS) and SrrAB in Modulation of Staphylococcus aureus Metabolism and Virulence. Infect Immun. 2019;87(2). Epub 2018/11/14. doi: 10.1128/iai.00570-18. PubMed PMID: 30420450; PMCID: PMC6346124.

76. Mashruwala AA, van de Guchte A, Boyd JM. Impaired respiration elicits SrrAB-dependent programmed cell lysis and biofilm formation in Staphylococcus aureus. eLife. 2017;6. doi: 10.7554/eLife.23845. PubMed PMID: 28221135.

77. Windham IH, Chaudhari SS, Bose JL, Thomas VC, Bayles KW. SrrAB Modulates Staphylococcus aureus Cell Death through Regulation of cidABC Transcription. J Bacteriol2016. p. 1114-22.

78. Suligoy CM, Lattar SM, Noto Llana M, González CD, Alvarez LP, Robinson DA, Gómez MI, Buzzola FR, Sordelli DO. Mutation of Agr Is Associated with the Adaptation of Staphylococcus aureus to the Host during Chronic Osteomyelitis. Front Cell Infect Microbiol. 2018;8. doi: 10.3389/fcimb.2018.00018. PubMed PMID: 29456969; PMCID: 5801681.

79. Gillaspy AF, Hickmon SG, Skinner RA, Thomas JR, Nelson CL, Smeltzer MS. Role of the accessory gene regulator (agr) in pathogenesis of staphylococcal osteomyelitis. Infect Immun. 1995;63(9):3373-80. PubMed PMID: 7642265; PMCID: 173464.

80. Vuong C, Saenz HL, Gotz F, Otto M. Impact of the agr quorum-sensing system on adherence to polystyrene in Staphylococcus aureus. J Infect Dis. 2000;182(6):1688-93. Epub 2000/11/09. doi: 10.1086/317606. PubMed PMID: 11069241.

81. Vuong C, Gerke C, Somerville GA, Fischer ER, Otto M. Quorum-sensing control of biofilm factors in Staphylococcus epidermidis. J Infect Dis. 2003;188(5):706-18. Epub 2003/08/23. doi: 10.1086/377239. PubMed PMID: 12934187.

82. Zhang L, Gray L, Novick RP, Ji G. Transmembrane topology of AgrB, the protein involved in the post-translational modification of AgrD in Staphylococcus aureus. J Biol Chem. 2002;277(38):34736-42. Epub 2002/07/18. doi: 10.1074/jbc.M205367200. PubMed PMID: 12122003.

83. Ji G, Beavis RC, Novick RP. Cell density control of staphylococcal virulence mediated by an octapeptide pheromone. Proc Natl Acad Sci U S A. 1995;92(26):12055-9. Epub 1995/12/19. doi: 10.1073/pnas.92.26.12055. PubMed PMID: 8618843; PMCID: PMC40295.

84. Novick RP, Projan SJ, Kornblum J, Ross HF, Ji G, Kreiswirth B, Vandenesch F, Moghazeh S. The agr P2 operon: an autocatalytic sensory transduction system in Staphylococcus aureus. Mol Gen Genet. 1995;248(4):446-58. Epub 1995/08/30. PubMed PMID: 7565609.

85. Novick RP. Autoinduction and signal transduction in the regulation of staphylococcal virulence - Novick - 2003 - Molecular Microbiology - Wiley Online Library. Molecular Microbiology. 2019. doi: 10.1046/j.1365-2958.2003.03526.x.

86. Benito Y, Kolb FA, Romby P, Lina G, Etienne J, Vandenesch F. Probing the structure of RNAIII, the Staphylococcus aureus agr regulatory RNA, and identification of the RNA domain involved in repression of protein A expression. Rna. 2000;6(5):668-79. Epub 2000/06/03. PubMed PMID: 10836788; PMCID: PMC1369947.

87. Morfeldt E, Taylor D, von Gabain A, Arvidson S. Activation of alpha-toxin translation in Staphylococcus aureus by the trans-encoded antisense RNA, RNAIII. Embo j. 1995;14(18):4569-77. Epub 1995/09/15. PubMed PMID: 7556100; PMCID: PMC394549.

88. Boisset S, Geissmann T, Huntzinger E, Fechter P, Bendridi N, Possedko M, Chevalier C, Helfer AC, Benito Y, Jacquier A, Gaspin C, Vandenesch F, Romby P. Staphylococcus aureus RNAIII coordinately represses the synthesis of virulence factors and the transcription regulator Rot by an antisense mechanism. Genes Dev. 2007;21(11):1353-66. Epub 2007/06/05. doi: 10.1101/gad.423507. PubMed PMID: 17545468; PMCID: PMC1877748.

89. Wang R, Braughton KR, Kretschmer D, Bach TH, Queck SY, Li M, Kennedy AD, Dorward DW, Klebanoff SJ, Peschel A, DeLeo FR, Otto M. Identification of novel cytolytic peptides as key virulence determinants for community-associated MRSA. Nat Med. 2007;13(12):1510-4. Epub 2007/11/13. doi: 10.1038/nm1656. PubMed PMID: 17994102.

90. Periasamy S, Joo HS, Duong AC, Bach TH, Tan VY, Chatterjee SS, Cheung GY, Otto M. How Staphylococcus aureus biofilms develop their characteristic structure. Proc Natl Acad Sci U S A. 2012;109(4):1281-6. Epub 2012/01/11. doi: 10.1073/pnas.1115006109. PubMed PMID: 22232686; PMCID: PMC3268330.

91. Queck SY, Jameson-Lee M, Villaruz AE, Bach TH, Khan BA, Sturdevant DE, Ricklefs SM, Li M, Otto M. RNAIII-independent target gene control by the agr quorum-sensing system: insight into the evolution of virulence regulation in Staphylococcus aureus. Mol Cell. 2008;32(1):150-8. Epub 2008/10/15. doi: 10.1016/j.molcel.2008.08.005. PubMed PMID: 18851841; PMCID: PMC2575650.

92. van Opijnen T, Bodi KL, Camilli A. Tn-seq: high-throughput parallel sequencing for fitness and genetic interaction studies in microorganisms. Nat Methods. 2009;6(10):767-72. Epub 2009/09/22. doi: 10.1038/nmeth.1377. PubMed PMID: 19767758; PMCID: PMC2957483.

93. Barquist L, Boinett CJ, Cain AK. Approaches to querying bacterial genomes with transposon-insertion sequencing. RNA biology. 2013;10(7):1161-9. doi: 10.4161/rna.24765. PubMed PMID: 23635712; PMCID: 3849164.

94. Roux D, Danilchanka O, Guillard T, Cattoir V, Aschard H, Fu Y, Angoulvant F, Messika J, Ricard JD, Mekalanos JJ, Lory S, Pier GB, Skurnik D. Fitness cost of antibiotic susceptibility during bacterial infection. Science translational medicine. 2015;7(297):297ra114. doi: 10.1126/scitranslmed.aab1621. PubMed PMID: 26203082.

95. Bachman MA, Breen P, Deornellas V, Mu Q, Zhao L, Wu W, Cavalcoli JD, Mobley HL. Genome-Wide Identification of Klebsiella pneumoniae Fitness Genes during Lung Infection. mBio. 2015;6(3). doi: 10.1128/mBio.00775-15. PubMed PMID: 26060277; PMCID: 4462621.

96. Shan Y, Lazinski D, Rowe S, Camilli A, Lewis K. Genetic basis of persister tolerance to aminoglycosides in Escherichia coli. mBio. 2015;6(2). doi: 10.1128/mBio.00078-15. PubMed PMID: 25852159; PMCID: 4453570.

97. Turner KH, Wessel AK, Palmer GC, Murray JL, Whiteley M. Essential genome of Pseudomonas aeruginosa in cystic fibrosis sputum. Proceedings of the National Academy of Sciences of the United States of America. 2015;112(13):4110-5. doi: 10.1073/pnas.1419677112. PubMed PMID: 25775563; PMCID: 4386324.

98. Carrillo-Marquez MA, Hulten KG, Hammerman W, Mason EO, Kaplan SL. USA300 is the predominant genotype causing Staphylococcus aureus septic arthritis in children. The Pediatric infectious disease journal. 2009;28(12):1076-80. doi: 10.1097/INF.0b013e3181adbcfe. PubMed PMID: 19820424.

99. Subashchandrabose S, Smith SN, Spurbeck RR, Kole MM, Mobley HL. Genome-wide detection of fitness genes in uropathogenic Escherichia coli during systemic infection. PLoS pathogens. 2013;9(12):e1003788. doi: 10.1371/journal.ppat.1003788. PubMed PMID: 24339777; PMCID: 3855560.

100. Kamp HD, Patimalla-Dipali B, Lazinski DW, Wallace-Gadsden F, Camilli A. Gene fitness landscapes of Vibrio cholerae at important stages of its life cycle. PLoS pathogens. 2013;9(12):e1003800. doi: 10.1371/journal.ppat.1003800. PubMed PMID: 24385900; PMCID: 3873450.

101. Wong SM, Bernui M, Shen H, Akerley BJ. Genome-wide fitness profiling reveals adaptations required by Haemophilus in coinfection with influenza A virus in the murine lung. Proceedings of the National Academy of Sciences of the United States of America. 2013;110(38):15413-8. doi: 10.1073/pnas.1311217110. PubMed PMID: 24003154; PMCID: 3780910.

102. Palace SG, Proulx MK, Lu S, Baker RE, Goguen JD. Genome-wide mutant fitness profiling identifies nutritional requirements for optimal growth of Yersinia pestis in deep tissue. mBio. 2014;5(4). doi: 10.1128/mBio.01385-14. PubMed PMID: 25139902; PMCID: 4147864.

103. Skurnik D, Roux D, Aschard H, Cattoir V, Yoder-Himes D, Lory S, Pier GB. A comprehensive analysis of in vitro and in vivo genetic fitness of Pseudomonas aeruginosa using high-throughput sequencing of transposon libraries. PLoS pathogens. 2013;9(9):e1003582. doi: 10.1371/journal.ppat.1003582. PubMed PMID: 24039572; PMCID: 3764216.

104. Peschel A, Jack RW, Otto M, Collins LV, Staubitz P, Nicholson G, Kalbacher H, Nieuwenhuizen WF, Jung G, Tarkowski A, van Kessel KP, van Strijp JA. Staphylococcus aureus resistance to human defensins and evasion of neutrophil killing via the novel virulence factor MprF is based on modification of membrane lipids with l-lysine. The Journal of experimental medicine. 2001;193(9):1067-76. PubMed PMID: 11342591; PMCID: 2193429.

105. Mazmanian SK, Skaar EP, Gaspar AH, Humayun M, Gornicki P, Jelenska J, Joachmiak A, Missiakas DM, Schneewind O. Passage of heme-iron across the envelope of Staphylococcus aureus. Science. 2003;299(5608):906-9. doi: 10.1126/science.1081147. PubMed PMID: 12574635.

106. Spencer JA, Ferraro F, Roussakis E, Klein A, Wu J, Runnels JM, Zaher W, Mortensen LJ, Alt C, Turcotte R, Yusuf R, Cote D, Vinogradov SA, Scadden DT, Lin CP. Direct measurement of local oxygen concentration in the bone marrow of live animals. Nature. 2014;508(7495):269-73. Epub 2014/03/05. doi: 10.1038/nature13034. PubMed PMID: 24590072; PMCID: PMC3984353.

107. Carreau A, El Hafny-Rahbi B, Matejuk A, Grillon C, Kieda C. Why is the partial oxygen pressure of human tissues a crucial parameter? Small molecules and hypoxia. J Cell Mol Med. 2011;15(6):1239-53. Epub 2011/01/22. doi: 10.1111/j.1582-4934.2011.01258.x. PubMed PMID: 21251211; PMCID: PMC4373326.

108. Daley JM, Thomay AA, Connolly MD, Reichner JS, Albina JE. Use of Ly6G-specific monoclonal antibody to deplete neutrophils in mice. J Leukoc Biol. 2008;83(1):64-70. Epub 2007/09/22. doi: 10.1189/jlb.0407247. PubMed PMID: 17884993.

109. Hammer ND, Cassat JE, Noto MJ, Lojek LJ, Chadha AD, Schmitz JE, Creech CB, Skaar EP. Inter- and intraspecies metabolite exchange promotes virulence of antibiotic-resistant Staphylococcus aureus. Cell Host Microbe. 2014;16(4):531-7. Epub 2014/10/10. doi: 10.1016/j.chom.2014.09.002. PubMed PMID: 25299336; PMCID: PMC4197139.

110. Geisinger E, Muir TW, Novick RP. agr receptor mutants reveal distinct modes of inhibition by staphylococcal autoinducing peptides. Proceedings of the National Academy of Sciences of the United States of America. 2009;106(4):1216-21. doi: 10.1073/pnas.0807760106. PubMed PMID: 19147840; PMCID: 2633565.

111. Berube BJ, Sampedro GR, Otto M, Bubeck Wardenburg J. The psmalpha locus regulates production of Staphylococcus aureus alpha-toxin during infection. Infect Immun. 2014;82(8):3350-8. Epub 2014/05/29. doi: 10.1128/iai.00089-14. PubMed PMID: 24866799; PMCID: PMC4136214.

112. Yarwood JM, Bartels DJ, Volper EM, Greenberg EP. Quorum sensing in Staphylococcus aureus biofilms. Journal of bacteriology. 2004;186(6):1838-50. PubMed PMID: 14996815; PMCID: 355980.

113. Ferreira MT, Manso AS, Gaspar P, Pinho MG, Neves AR. Effect of oxygen on glucose metabolism: utilization of lactate in Staphylococcus aureus as revealed by in vivo NMR studies. PLoS One. 2013;8(3):e58277. Epub 2013/03/09. doi: 10.1371/journal.pone.0058277. PubMed PMID: 23472168; PMCID: PMC3589339.

114. Somerville GA, Saïd-Salim B, Wickman JM, Raffel SJ, Kreiswirth BN, Musser JM. Correlation of Acetate Catabolism and Growth Yield in Staphylococcus aureus: Implications for Host-Pathogen Interactions. Infect Immun2003. p. 4724-32.

115. Rothfork JM, Timmins GS, Harris MN, Chen X, Lusis AJ, Otto M, Cheung AL, Gresham HD. Inactivation of a bacterial virulence pheromone by phagocyte-derived oxidants: new role for the NADPH oxidase in host defense. Proceedings of the National Academy of Sciences of the United States of America. 2004;101(38):13867-72. doi: 10.1073/pnas.0402996101. PubMed PMID: 15353593; PMCID: 518845.

116. Sun F, Ji Q, Jones MB, Deng X, Liang H, Frank B, Telser J, Peterson SN, Bae T, He C. AirSR, a [2Fe-2S] cluster-containing two-component system, mediates global oxygen sensing and redox signaling in Staphylococcus aureus. Journal of the American Chemical Society. 2012;134(1):305-14. doi: 10.1021/ja2071835. PubMed PMID: 22122613; PMCID: 3257388.

117. Ingavale SS, Van Wamel W, Cheung AL. Characterization of RAT, an autolysis regulator in Staphylococcus aureus. Molecular microbiology. 2003;48(6):1451-66. PubMed PMID: 12791130.

118. Pagels M, Fuchs S, Pane-Farre J, Kohler C, Menschner L, Hecker M, McNamarra PJ, Bauer MC, von Wachenfeldt C, Liebeke M, Lalk M, Sander G, von Eiff C, Proctor RA, Engelmann S. Redox sensing by a Rex-family repressor is involved in the regulation of anaerobic gene expression in Staphylococcus aureus. Molecular microbiology. 2010;76(5):1142-61. doi: 10.1111/j.1365-2958.2010.07105.x. PubMed PMID: 20374494; PMCID: 2883068.

119. Chen PR, Bae T, Williams WA, Duguid EM, Rice PA, Schneewind O, He C. An oxidation-sensing mechanism is used by the global regulator MgrA in Staphylococcus aureus. Nature chemical biology. 2006;2(11):591-5. doi: 10.1038/nchembio820. PubMed PMID: 16980961.

120. Fujimoto DF, Higginbotham RH, Sterba KM, Maleki SJ, Segall AM, Smeltzer MS, Hurlburt BK. Staphylococcus aureus SarA is a regulatory protein responsive to redox and pH that can support bacteriophage lambda integrase-mediated excision/recombination. Molecular microbiology. 2009;74(6):1445-58. doi: 10.1111/j.1365-2958.2009.06942.x. PubMed PMID: 19919677; PMCID: 2879156.

121. Malone CL, Boles BR, Horswill AR. Biosynthesis of Staphylococcus aureus Autoinducing Peptides by Using the Synechocystis DnaB Mini-Intein ▿ . Appl Environ Microbiol. 2007;73(19):6036-44. doi: 10.1128/aem.00912-07. PubMed PMID: 17693565.

122. Yates EA, Philipp B, Buckley C, Atkinson S, Chhabra SR, Sockett RE, Goldner M, Dessaux Y, Camara M, Smith H, Williams P. N-acylhomoserine lactones undergo lactonolysis in a pH-, temperature-, and acyl chain length-dependent manner during growth of Yersinia pseudotuberculosis and Pseudomonas aeruginosa. Infect Immun. 2002;70(10):5635-46. Epub 2002/09/14. doi: 10.1128/iai.70.10.5635-5646.2002. PubMed PMID: 12228292; PMCID: PMC128322.

123. Richardson AR, Somerville GA, Sonenshein AL. Regulating the Intersection of Metabolism and Pathogenesis in Gram-positive Bacteria. Microbiol Spectr. 2015;3(3). doi: 10.1128/microbiolspec.MBP-0004-2014. PubMed PMID: 26185086; PMCID: 4540601.

124. Brandt SL, Putnam NE, Cassat JE, Serezani CH. Innate Immunity to Staphylococcus aureus: Evolving Paradigms in Soft Tissue and Invasive Infections. J Immunol. 2018;200(12):3871-80. Epub 2018/06/06. doi: 10.4049/jimmunol.1701574. PubMed PMID: 29866769; PMCID: PMC6028009.

125. Ruane KM, Lloyd AJ, Fulop V, Dowson CG, Barreteau H, Boniface A, Dementin S, Blanot D, Mengin-Lecreulx D, Gobec S, Dessen A, Roper DI. Specificity determinants for lysine incorporation in Staphylococcus aureus peptidoglycan as revealed by the structure of a MurE enzyme ternary complex. J Biol Chem. 2013;288(46):33439-48. Epub 2013/09/26. doi: 10.1074/jbc.M113.508135. PubMed PMID: 24064214; PMCID: PMC3829189.

126. Oogai Y, Yamaguchi M, Kawada-Matsuo M, Sumitomo T, Kawabata S, Komatsuzawa H, Müller V. Lysine and Threonine Biosynthesis from Aspartate Contributes to Staphylococcus aureus Growth in Calf Serum2016. doi: 10.1128/AEM.01399-16.

127. Zhao H, Roistacher DM, Helmann JD. Aspartate deficiency limits peptidoglycan synthesis and sensitizes cells to antibiotics targeting cell wall synthesis in Bacillus subtilis. Mol Microbiol. 2018;109(6):826-44. Epub 2018/07/12. doi: 10.1111/mmi.14078. PubMed PMID: 29995990; PMCID: PMC6185803.

128. Short SA, White DC, Kaback HR. Mechanisms of active transport in isolated bacterial membrane vesicles. IX. The kinetics and specificity of amino acid transport in Staphylococcus aureus membrane vesicles. J Biol Chem. 1972;247(23):7452-8. Epub 1972/12/10. PubMed PMID: 4636316.

129. Szafranska AK, Oxley APA, Chaves-Moreno D, Horst SA, Roßlenbroich S, Peters G, Goldmann O, Rohde M, Sinha B, Pieper DH, Löffler B, Jauregui R, Wos-Oxley ML, Medina E, Horswill AR, McDaniel LS. High-Resolution Transcriptomic Analysis of the Adaptive Response of Staphylococcus aureus during Acute and Chronic Phases of Osteomyelitis2014. doi: 10.1128/mBio.01775-14.

130. Ryan DJ, Patterson NH, Putnam NE, Wilde AD, Weiss A, Perry WJ, Cassat JE, Skaar EP, Caprioli RM, Spraggins JM. MicroLESA: Integrating Autofluorescence Microscopy, In Situ Micro-Digestions, and Liquid Extraction Surface Analysis for High Spatial Resolution Targeted Proteomic Studies. Anal Chem. 2019. Epub 2019/06/01. doi: 10.1021/acs.analchem.8b05889. PubMed PMID: 31149808.

131. Sheldon JR, Marolda CL, Heinrichs DE. TCA cycle activity in Staphylococcus aureus is essential for iron-regulated synthesis of staphyloferrin A, but not staphyloferrin B: the benefit of a second citrate synthase. Mol Microbiol. 2014;92(4):824-39. Epub 2014/03/29. doi: 10.1111/mmi.12593. PubMed PMID: 24666349.

132. Zhu Y, Xiong YQ, Sadykov MR, Fey PD, Lei MG, Lee CY, Bayer AS, Somerville GA. Tricarboxylic acid cycle-dependent attenuation of Staphylococcus aureus in vivo virulence by selective inhibition of amino acid transport. Infect Immun. 2009;77(10):4256-64. Epub 2009/08/12. doi: 10.1128/iai.00195-09. PubMed PMID: 19667045; PMCID: PMC2747957.

133. Coulter SN, Schwan WR, Ng EY, Langhorne MH, Ritchie HD, Westbrock-Wadman S, Hufnagle WO, Folger KR, Bayer AS, Stover CK. Staphylococcus aureus genetic loci impacting growth and survival in multiple infection environments. Mol Microbiol. 1998;30(2):393-404. Epub 1998/10/29. PubMed PMID: 9791183.

134. Schaible UE, Kaufmann SH. Iron and microbial infection. Nat Rev Microbiol. 2004;2(12):946-53. Epub 2004/11/20. doi: 10.1038/nrmicro1046. PubMed PMID: 15550940.

135. Hassel B, Dahlberg D, Mariussen E, Goverud IL, Antal EA, Tonjum T, Maehlen J. Brain infection with Staphylococcus aureus leads to high extracellular levels of glutamate, aspartate, gamma-aminobutyric acid, and zinc. J Neurosci Res. 2014;92(12):1792-800. Epub 2014/07/22. doi: 10.1002/jnr.23444. PubMed PMID: 25043715.

136. Morimoto R, Uehara S, Yatsushiro S, Juge N, Hua Z, Senoh S, Echigo N, Hayashi M, Mizoguchi T, Ninomiya T, Udagawa N, Omote H, Yamamoto A, Edwards RH, Moriyama Y. Secretion of L-glutamate from osteoclasts through transcytosis. EMBO J. 2006;25(18):4175-86. doi: 10.1038/sj.emboj.7601317. PubMed PMID: 16957773.

137. Zaprasis A, Bleisteiner M, Kerres A, Hoffmann T, Bremer E, Spormann AM. Uptake of Amino Acids and Their Metabolic Conversion into the Compatible Solute Proline Confers Osmoprotection to Bacillus subtilis2015. doi: 10.1128/AEM.02797-14.

138. Slotboom DJ, Konings WN, Lolkema JS. Structural Features of the Glutamate Transporter Family. Microbiol Mol Biol Rev1999. p. 293-307.

139. Arriza JL, Fairman WA, Wadiche JI, Murdoch GH, Kavanaugh MP, Amara SG. Functional comparisons of three glutamate transporter subtypes cloned from human motor cortex. J Neurosci. 1994;14(9):5559-69. Epub 1994/09/01. PubMed PMID: 7521911.

140. Groeneveld M. On the mechanism of prokaryotic glutamate transporter homologues: Groningen: s.n.; 2010.

141. Benton BM, Zhang JP, Bond S, Pope C, Christian T, Lee L, Winterberg KM, Schmid MB, Buysse JM. Large-scale identification of genes required for full virulence of Staphylococcus aureus. J Bacteriol. 2004;186(24):8478-89. Epub 2004/12/04. doi: 10.1128/jb.186.24.8478-8489.2004. PubMed PMID: 15576798; PMCID: PMC532413.

142. Viola RE. The central enzymes of the aspartate family of amino acid biosynthesis. Acc Chem Res. 2001;34(5):339-49. Epub 2001/05/16. PubMed PMID: 11352712.

143. Mladenova SR, Stein KR, Bartlett L, Sheppard K. Relaxed tRNA specificity of the Staphylococcus aureus aspartyl-tRNA synthetase enables RNA-dependent asparagine biosynthesis. FEBS Lett. 2014;588(9):1808-12. Epub 2014/04/02. doi: 10.1016/j.febslet.2014.03.042. PubMed PMID: 24685427.

144. Sheppard K, Akochy PM, Salazar JC, Soll D. The Helicobacter pylori amidotransferase GatCAB is equally efficient in glutamine-dependent transamidation of Asp-tRNAAsn and Glu-

tRNAGln. J Biol Chem. 2007;282(16):11866-73. Epub 2007/03/03. doi: 10.1074/jbc.M700398200. PubMed PMID: 17329242.

145. Gitlitz PH, Sunderman FW, Jr., Hohnadel DC. Ion-exchange chromatography of amino acids in sweat collected from healthy subjects during sauna bathing. Clin Chem. 1974;20(10):1305-12. Epub 1974/10/01. PubMed PMID: 4413985.

146. Connolly J, Boldock E, Prince LR, Renshaw SA, Whyte MK, Foster SJ. Identification of Staphylococcus aureus Factors Required for Pathogenicity and Growth in Human Blood. Infect Immun2017.

147. Kofoed EM, Yan D, Katakam AK, Reichelt M, Lin B, Kim J, Park S, Date SV, Monk IR, Xu M, Austin CD, Maurer T, Tan MW. De Novo Guanine Biosynthesis but Not the Riboswitch-Regulated Purine Salvage Pathway Is Required for Staphylococcus aureus Infection In Vivo. J Bacteriol. 2016;198(14):2001-15. Epub 2016/05/11. doi: 10.1128/jb.00051-16. PubMed PMID: 27161118; PMCID: PMC4936099.

148. Li L, Abdelhady W, Donegan NP, Seidl K, Cheung A, Zhou YF, Yeaman MR, Bayer AS, Xiong YQ. Role of Purine Biosynthesis in Persistent Methicillin-Resistant Staphylococcus aureus Infection. J Infect Dis. 2018;218(9):1367-77. Epub 2018/06/06. doi: 10.1093/infdis/jiy340. PubMed PMID: 29868791; PMCID: PMC6151072.

149. Sullivan LB, Gui DY, Hosios AM, Bush LN, Freinkman E, Vander Heiden MG. Supporting Aspartate Biosynthesis Is an Essential Function of Respiration in Proliferating Cells. Cell. 2015;162(3):552-63. Epub 2015/08/02. doi: 10.1016/j.cell.2015.07.017. PubMed PMID: 26232225; PMCID: PMC4522278.

150. Birsoy K, Wang T, Chen WW, Freinkman E, Abu-Remaileh M, Sabatini DM. An Essential Role of the Mitochondrial Electron Transport Chain in Cell Proliferation Is to Enable Aspartate Synthesis. Cell. 2015;162(3):540-51. Epub 2015/08/02. doi: 10.1016/j.cell.2015.07.016. PubMed PMID: 26232224; PMCID: PMC4522279.

151. Winstel V, Missiakas D, Schneewind O. Staphylococcus aureus targets the purine salvage pathway to kill phagocytes. Proc Natl Acad Sci U S A. 2018;115(26):6846-51. Epub 2018/06/13. doi: 10.1073/pnas.1805622115. PubMed PMID: 29891696; PMCID: PMC6042115.

152. Thammavongsa V, Kern JW, Missiakas DM, Schneewind O. Staphylococcus aureus synthesizes adenosine to escape host immune responses. J Exp Med. 2009;206(11):2417-27. Epub 2009/10/08. doi: 10.1084/jem.20090097. PubMed PMID: 19808256; PMCID: PMC2768845.

153. Boles BR, Thoendel M, Roth AJ, Horswill AR. Identification of genes involved in polysaccharide-independent Staphylococcus aureus biofilm formation. PLoS One. 2010;5(4):e10146. Epub 2010/04/27. doi: 10.1371/journal.pone.0010146. PubMed PMID: 20418950; PMCID: PMC2854687.

154. Kaito C, Saito Y, Nagano G, Ikuo M, Omae Y, Hanada Y, Han X, Kuwahara-Arai K, Hishinuma T, Baba T, Ito T, Hiramatsu K, Sekimizu K. Transcription and translation products of

the cytolysin gene psm-mec on the mobile genetic element SCCmec regulate Staphylococcus aureus virulence. PLoS pathogens. 2011;7(2):e1001267. doi: 10.1371/journal.ppat.1001267. PubMed PMID: 21304931; PMCID: 3033363.

155. Fey PD, Endres JL, Yajjala VK, Widhelm TJ, Boissy RJ, Bose JL, Bayles KW. A genetic resource for rapid and comprehensive phenotype screening of nonessential Staphylococcus aureus genes. mBio. 2013;4(1):e00537-12. doi: 10.1128/mBio.00537-12. PubMed PMID: 23404398; PMCID: 3573662.

156. Yanisch-Perron C, Vieira J, Messing J. Improved M13 phage cloning vectors and host strains: nucleotide sequences of the M13mp18 and pUC19 vectors. Gene. 1985;33(1):103-19. PubMed PMID: 2985470.

157. Chen J, Novick RP. svrA, a multi-drug exporter, does not control agr. Microbiology. 2007;153(Pt 5):1604-8. doi: 10.1099/mic.0.2007/006247-0. PubMed PMID: 17464075.

158. Bubeck Wardenburg J, Williams WA, Missiakas D. Host defenses against Staphylococcus aureus infection require recognition of bacterial lipoproteins. Proc Natl Acad Sci U S A. 2006;103(37):13831-6. Epub 2006/09/07. doi: 10.1073/pnas.0603072103. PubMed PMID: 16954184; PMCID: PMC1564215.

159. Dunman PM, Murphy E, Haney S, Palacios D, Tucker-Kellogg G, Wu S, Brown EL, Zagursky RJ, Shlaes D, Projan SJ. Transcription profiling-based identification of Staphylococcus aureus genes regulated by the agr and/or sarA loci. J Bacteriol. 2001;183(24):7341-53. Epub 2001/11/22. doi: 10.1128/jb.183.24.7341-7353.2001. PubMed PMID: 11717293; PMCID: PMC95583.

160. Beenken KE, Dunman PM, McAleese F, Macapagal D, Murphy E, Projan SJ, Blevins JS, Smeltzer MS. Global gene expression in Staphylococcus aureus biofilms. J Bacteriol. 2004;186(14):4665-84. Epub 2004/07/03. doi: 10.1128/jb.186.14.4665-4684.2004. PubMed PMID: 15231800; PMCID: PMC438561.

161. Bischoff M, Dunman P, Kormanec J, Macapagal D, Murphy E, Mounts W, Berger-Bachi B, Projan S. Microarray-based analysis of the Staphylococcus aureus sigmaB regulon. J Bacteriol. 2004;186(13):4085-99. Epub 2004/06/19. doi: 10.1128/JB.186.13.4085-4099.2004

186/13/4085 [pii]. PubMed PMID: 15205410; PMCID: 421609.

162. Anderson KL, Roberts C, Disz T, Vonstein V, Hwang K, Overbeek R, Olson PD, Projan SJ, Dunman PM. Characterization of the Staphylococcus aureus heat shock, cold shock, stringent, and SOS responses and their effects on log-phase mRNA turnover. J Bacteriol. 2006;188(19):6739-56. Epub 2006/09/19. doi: 188/19/6739 [pii]

10.1128/JB.00609-06. PubMed PMID: 16980476; PMCID: 1595530.

163. Roberts C, Anderson KL, Murphy E, Projan SJ, Mounts W, Hurlburt B, Smeltzer M, Overbeek R, Disz T, Dunman PM. Characterizing the effect of the Staphylococcus aureus

virulence factor regulator, SarA, on log-phase mRNA half-lives. J Bacteriol. 2006;188(7):2593-603. Epub 2006/03/21. doi: 188/7/2593 [pii]

10.1128/JB.188.7.2593-2603.2006. PubMed PMID: 16547047; PMCID: 1428411.

164. Khodaverdian V, Pesho M, Truitt B, Bollinger L, Patel P, Nithianantham S, Yu G, Delaney E, Jankowsky E, Shoham M. Discovery of antivirulence agents against methicillin-resistant Staphylococcus aureus. Antimicrobial agents and chemotherapy. 2013;57(8):3645-52. doi: 10.1128/AAC.00269-13. PubMed PMID: 23689713; PMCID: 3719762.

165. Bose JL, Fey PD, Bayles KW. Genetic tools to enhance the study of gene function and regulation in Staphylococcus aureus. Appl Environ Microbiol. 2013;79(7):2218-24. Epub 2013/01/29. doi: 10.1128/aem.00136-13. PubMed PMID: 23354696; PMCID: PMC3623228.

166. Chen J, Yoong P, Ram G, Torres VJ, Novick RP. Single-copy vectors for integration at the SaPI1 attachment site for Staphylococcus aureus. Plasmid. 2014;76:1-7. Epub 2014/09/07. doi: 10.1016/j.plasmid.2014.08.001. PubMed PMID: 25192956; PMCID: PMC4346540.

167. Wardenburg JB, Williams WA, Missiakas D. Host defenses against Staphylococcus aureus infection require recognition of bacterial lipoproteins2006. doi: 10.1073/pnas.0603072103.

168. Pattee PA, Neveln DS. Transformation analysis of three linkage groups in Staphylococcus aureus. J Bacteriol. 1975;124(1):201-11. Epub 1975/10/01. PubMed PMID: 1176430; PMCID: PMC235883.

169. Vitko NP, Richardson AR. Laboratory maintenance of methicillin-resistant Staphylococcus aureus (MRSA). Curr Protoc Microbiol. 2013;Chapter 9:Unit 9C.2. Epub 2013/02/15. doi: 10.1002/9780471729259.mc09c02s28. PubMed PMID: 23408135; PMCID: PMC4070006.

170. White MJ, Boyd JM, Horswill AR, Nauseef WM. Phosphatidylinositol-specific phospholipase C contributes to survival of Staphylococcus aureus USA300 in human blood and neutrophils. Infect Immun. 2014;82(4):1559-71. Epub 2014/01/24. doi: 10.1128/iai.01168-13. PubMed PMID: 24452683; PMCID: PMC3993399.

171. Robertson G, Hirst M, Bainbridge M, Bilenky M, Zhao Y, Zeng T, Euskirchen G, Bernier B, Varhol R, Delaney A, Thiessen N, Griffith OL, He A, Marra M, Snyder M, Jones S. Genome-wide profiles of STAT1 DNA association using chromatin immunoprecipitation and massively parallel sequencing. Nat Methods. 2007;4(8):651-7. Epub 2007/06/15. doi: 10.1038/nmeth1068. PubMed PMID: 17558387.

172. Johnson DS, Mortazavi A, Myers RM, Wold B. Genome-wide mapping of in vivo protein-DNA interactions. Science. 2007;316(5830):1497-502. Epub 2007/06/02. doi: 10.1126/science.1141319. PubMed PMID: 17540862.

173. Geng H, Nakano S, Nakano MM. Transcriptional activation by Bacillus subtilis ResD: tandem binding to target elements and phosphorylation-dependent and -independent

transcriptional activation. J Bacteriol. 2004;186(7):2028-37. Epub 2004/03/19. doi: 10.1128/jb.186.7.2028-2037.2004. PubMed PMID: 15028686; PMCID: PMC374413.

174. Zhang X, Hulett FM. ResD signal transduction regulator of aerobic respiration in Bacillus subtilis: ctaA promoter regulation. Mol Microbiol. 2000;37(5):1208-19. Epub 2000/09/06. PubMed PMID: 10972837.

175. Lu S, Killoran PB, Fang FC, Riley LW. The global regulator ArcA controls resistance to reactive nitrogen and oxygen intermediates in Salmonella enterica serovar Enteritidis. Infect Immun. 2002;70(2):451-61. Epub 2002/01/18. doi: 10.1128/iai.70.2.451-461.2002. PubMed PMID: 11796570; PMCID: PMC127680.

176. Scharf B. Summary of useful methods for two-component system research. Current Opinion in Microbiology. 2010;13(2):246--52. doi: 10.1016/j.mib.2010.01.006. PubMed PMID: Scharf2010.

177. Cao S, Huseby DL, Brandis G, Hughes D, Proctor RA, Novick RP. Alternative Evolutionary Pathways for Drug-Resistant Small Colony Variant Mutants in Staphylococcus aureus2017. doi: 10.1128/mBio.00358-17.

178. Proctor RA, von Eiff C, Kahl BC, Becker K, McNamara P, Herrmann M, Peters G. Small colony variants: a pathogenic form of bacteria that facilitates persistent and recurrent infections. Nat Rev Microbiol. 2006;4(4):295-305. Epub 2006/03/17. doi: 10.1038/nrmicro1384. PubMed PMID: 16541137.

179. Thibault D, Wood S, Jensen P, Opijnen Tv. droplet-Tn-Seq combines microfluidics with Tn-Seq identifying complex single-cell phenotypes2018. doi: 10.1101/391045.

180. Jacobsson G, Dashti S, Wahlberg T, Andersson R. The epidemiology of and risk factors for invasive Staphylococcus aureus infections in western Sweden. Scand J Infect Dis. 2007;39(1):6-13. Epub 2007/03/17. doi: 10.1080/00365540600810026. PubMed PMID: 17366006.

181. Engemann JJ, Carmeli Y, Cosgrove SE, Fowler VG, Bronstein MZ, Trivette SL, Briggs JP, Sexton DJ, Kaye KS. Adverse clinical and economic outcomes attributable to methicillin resistance among patients with Staphylococcus aureus surgical site infection. Clin Infect Dis. 2003;36(5):592-8. Epub 2003/02/21. doi: 10.1086/367653. PubMed PMID: 12594640.

182. Befus M, Lowy FD, Miko BA, Mukherjee DV, Herzig CT, Larson EL. Obesity as a Determinant of Staphylococcus aureus Colonization Among Inmates in Maximum-Security Prisons in New York State. Am J Epidemiol. 2015;182(6):494-502. Epub 2015/08/22. doi: 10.1093/aje/kwv062. PubMed PMID: 26292691; PMCID: PMC4564937.

183. Nikoloudi M, Eleftheriadou I, Tentolouris A, Kosta OA, Tentolouris N. Diabetic Foot Infections: Update on Management. Curr Infect Dis Rep. 2018;20(10):40. Epub 2018/08/03. doi: 10.1007/s11908-018-0645-6. PubMed PMID: 30069605.

184. Lavery LA, Peters EJ, Armstrong DG, Wendel CS, Murdoch DP, Lipsky BA. Risk factors for developing osteomyelitis in patients with diabetic foot wounds. Diabetes Res Clin Pract. 2009;83(3):347-52. Epub 2009/01/02. doi: 10.1016/j.diabres.2008.11.030. PubMed PMID: 19117631.

185. Cassat JE, Moore JL, Wilson KJ, Stark Z, Prentice BM, Plas RVd, Perry WJ, Zhang Y, Virostko J, Colvin DC, Rose KL, Judd AM, Reyzer ML, Spraggins JM, Grunenwald CM, Gore JC, Caprioli RM, Skaar EP. Integrated molecular imaging reveals tissue heterogeneity driving host-pathogen interactions2018. doi: 10.1126/scitranslmed.aan6361.

186. Davis KM, Mohammadi S, Isberg RR. Community behavior and spatial regulation within a bacterial microcolony in deep tissue sites serves to protect against host attack. Cell Host Microbe. 2015;17(1):21-31. doi: 10.1016/j.chom.2014.11.008. PubMed PMID: 25500192; PMCID: 4669952.

187. Schrimpe-Rutledge AC, Codreanu SG, Sherrod SD, McLean JA. Untargeted Metabolomics Strategies-Challenges and Emerging Directions. J Am Soc Mass Spectrom. 2016;27(12):1897-905. Epub 2016/11/01. doi: 10.1007/s13361-016-1469-y. PubMed PMID: 27624161; PMCID: PMC5110944.

188. Sugiura Y, Honda K, Suematsu M. Development of an Imaging Mass Spectrometry Technique for Visualizing Localized Cellular Signaling Mediators in Tissues. Mass Spectrom (Tokyo). 2015;4(1). doi: 10.5702/massspectrometry.A0040. PubMed PMID: 26819911; PMCID: 4541036.

189. Toue S, Sugiura Y, Kubo A, Ohmura M, Karakawa S, Mizukoshi T, Yoneda J, Miyano H, Noguchi Y, Kobayashi T, Kabe Y, Suematsu M. Microscopic imaging mass spectrometry assisted by on-tissue chemical derivatization for visualizing multiple amino acids in human colon cancer xenografts. Proteomics. 2014;14(7-8):810-9. Epub 2013/07/03. doi: 10.1002/pmic.201300041. PubMed PMID: 23818158.